POTENTIAL FIELD MODELLING AND INTERPRETATION ALONG THE LITHOPROBE EAST ONSHORE SEISMIC REFLECTION TRANSECTS ACROSS THE NEWFOUNDLAND APPALACHIANS

RONALD E. WISEMAN

INFORMATION TO USERS

This manuscript has been reproduced from the microfilm master. UMI films the text directly from the original or copy submitted. Thus, some thesis and dissertation copies are in typewriter face, while others may be from any type of computer printer.

The quality of this reproduction is dependent upon the quality of the copy submitted. Broken or indistinct print, colored or poor quality illustrations and photographs, print bleedthrough, substandard margins, and improper alignment can adversely affect reproduction.

In the unlikely event that the author did not send UMI a complete manuscript and there are missing pages, these will be noted. Also, if unauthorized copyright material had to be removed, a note will indicate the deletion.

Oversize materials (e.g., maps, drawings, charts) are reproduced by sectioning the original, beginning at the upper left-hand corner and continuing from left to right in equal sections with small overlaps. Each original is also photographed in one exposure and is included in reduced form at the back of the book.

Photographs included in the original manuscript have been reproduced xerographically in this copy. Higher quality 6" x 9" black and white photographic prints are available for any photographs or illustrations appearing in this copy for an additional charge. Contact UMI directly to order.

UMI

A Bell & Howell Information Company
300 North Zeeb Road, Ann Arbor MI 48106-1346 USA
313/761-4700 800/521-0600

Potential field modelling and interpretation along the Lithoprobe East onshore seismic reflection transects across the Newfoundland Appalachians

by

Ronald E. Wiseman

A thesis submitted to the
School of Graduate Studies
in partial fulfilment of the
requirements for the degree of
Master of Earth Sciences
(Geophysics)

Department of Earth Sciences
Memorial University of Newfoundland

April 1994

St. John's Newfoundland

Abstract:

The Canadian Appalachians have been, and continue to be, an area of great geological interest. The island of Newfoundland is an ideal location to study the Appalachian orogen, and a study of Newfoundland geology led to the initial tectono-stratigraphic subdivision of the orogen.

The Lithoprobe East program began an intensive study of the Appalachians in Canada, with much of the geological and geophysical research carried out in Newfoundland. In 1989 three Vibroseis transects across the island were shot. In addition, physical property and Bouguer gravity measurements were carried out along the transects to allow a potential field study.

This thesis consists of a presentation of the potential field data for areas surrounding each of the transects, and application of several processing techniques applied to the data to elucidate the more subtle features of the fields.

Traditional 2½-D potential field modelling is undertaken using constraints from the Vibroseis data and physical property data to develop a model of the crust across the Newfoundland Appalachians. The results from the processing are then used to interpret the crustal structure away from the seismic line.

In general it is found that the major features on the potential field maps can be explained by sources in the

upper crust. Most of the major terrane bounding faults have significant geophysical signatures as the terranes exhibit differing potential field character.

Most of the Appalachian terrane or tectono-stratigraphic boundaries are observed to be northwest-directed thrusts. The Red Indian Line and the Day Cove Thrust appear to be exceptions, in that they exhibit a northwesterly dip.

The Dunnage Zone material consists of oceanic remnants of the Iapatus Ocean which have been thrust upon the continental margin of North America.

The gravity and magnetic processing and modelling are a good supplement to the Vibroseis data for studying the Appalachian Orogen in Newfoundland. These data are able to identify terrane boundaries which are not directly observed on the Vibroseis data due to gaps in the coverage.

Acknowledgements:

I would like to thank the following people: Hugh Miller for all the insight and suggestions he has offered and for the opportunity to work on this data, Gary Quinlan and Brian Roberts for making available the seismic reflection results prior to publication, Brian O'Brien for providing physical property data, Peter Cawood for some geological discussion of western Newfoundland, and Rebecca

Jameison for providing new information on Baie Verte Peninsula geology.

This research was funded in part by a Lithoprobe Supporting Geoscience Grant to a group led by Hugh Miller for the processing and interpretation of potential field data for the areas around the Lithoprobe East onshore seismic reflection lines, and a Newfoundland Offshore Career Development Award to Ron Wiseman.

LIST OF TABLES

LIST OF FIGURES

1.0. INTRODUCTION:

1.1. OBJECTIVES:

The aim of this thesis is to study the gravity and magnetic data for the island of Newfoundland in conjuction with the Lithoprobe East Vibroseis data to assist in the understanding of Appalachian structural evolution.

The gravity and magnetic data can provide data where the Vibroseis data is lacking. This includes several aspects: (1) gravity and magnetic data respond to different physical properties of the subsurface than does the seismic method, (2) the gravity and magnetic data are continuous along the transects and are not subject to the gaps present in the seismic coverage, and (3) gravity and magnetic data is available for all of the island, while the seismic data is avaliable only along the transect itself.

All of these thing allow the gravity and magnetic data to supplement the avaliable seismic by providing additional information which can not be detected by seismic means. Results of the combined geophysical methods may be extended to three dimensions as opposed to the normal two dimensions provided by the seismic method.

1.2. GENERAL GEOLOGY:

Four of the five major tectonic zones of the Appalachian Orogen as defined by Williams (1979) and Williams et al. (1988) are exposed on the island of Newfoundland. This zonal subdivision of the Appalachians is based upon contrasting structure and stratigraphy in Cambro-Ordovician and older rocks. The zones, from west to east, are: the Humber, Dunnage, Gander, and Avalon Zones. The Meguma Zone, is eastward of the Avalon Zone and is not exposed in Newfoundland (Figure 1.1). The Humber Zone is the Appalachian miogeocline, and all the zones to the east are suspect terranes or composite suspect terranes (Williams and Hatcher, 1983; Williams et al., 1988).

The Humber Zone has been interpreted as the paleo-margin of eastern North America (Williams, 1979). Its boundary to the west is defined by the limit of Appalachian deformation, and to the east by the ophiolite occurrences on the Baie Verte Line (BVL) (Figure 1.1).

The Humber Zone is underlain by Grenvillian crystalline basement rocks, which are predominantly unconformably overlain by clastic sediments followed by a Cambro-Ordovician carbonate sequence (Stevens, 1970; Williams, 1979; and St. Julien and Béland, 1982). Above the carbonates are easterly derived clastics, mélanges and allochthonous units including an ophiolite sequence (Bay of Islands Igneous Complex) (Stevens,

1970 and Williams, 1979).

The Humber Zone in Newfoundland is generally characterized by low Bouguer gravity anomalies (-15 to -20 mGal), with some localized highs over basement inliers and ophiolites (Figure 1.2).

Magnetically, the Humber Zone in Newfoundland is rather complex. Magnetic highs occur above ophiolites complexes in the zone, and complex high frequency magnetic patterns are seen above exposed Grenville basement inliers (Figure 1.3).

The Dunnage Zone contains remnants of the Iapetus Ocean (Williams, 1979), and records an extensive history of oceanic volcanism and sedimentation (Williams et al., 1988). The Dunnage Zone rocks are both less deformed and less metamorphosed than the rocks of either the Humber Zone or Gander Zone (St. Julien and Béland, 1982). Dunnage Zone rocks are either on top of continental crust or overthickened oceanic rocks extending to the mantle (Williams et al., 1988).

The Dunnage Zone has been divided into two subzones based upon a number of geological contrasts relating to: (1) stratigraphy, (2) structure, (3) fossil fauna, (4) plutonic rocks, (5) radiogenic lead isotopes in mineral deposits, and (6) gravity and magnetic signatures (Williams et al., 1988). The Notre Dame Subzone makes up the northwest portion of the Dunnage Zone, and the Exploits Subzone lies to the southeast (Williams et al., 1988). The Red Indian Line (RIL), a late

rectilinear fault sometimes marked by mylonites, separates the two subzones (Figure 1.1). The Red Indian Line is coincident with the suture between the Grenville lower crustal block and the Central lower crustal block proposed by Marillier et al. (1989).

The Notre Dame Subzone differs from the Exploits Subzone in Upper Ordovician and Silurian stratigraphy. The Exploits Subzone contains Upper Ordovician and Silurian marine greywackes and conglomerates, as well as Silurian olistostromes and mélanges. All of these are absent in the Notre Dame Subzone (Williams et al., 1988).

The two subzones of the Dunnage Zone are also structurally different. The Notre Dame Subzone has a pre-Silurian or pre-Devonian unconformity which is absent in the northern part of the Exploits Subzone (Williams et al., 1988). Along the Red Indian Line (RIL) the Silurian or Devonian rocks of the Notre Dame Subzone are much less deformed than those of the Exploits Subzone (Williams et al., 1988). The Taconic Orogeny affected all of the Notre Dame Subzone and the Humber Zone, but appears to have affected only parts of the Exploits Subzone (Williams et al., 1988).

Ordovician conodonts found within the Buchans Group of the Notre Dame Subzone have a North American affinity, while Lower to Middle Ordovician brachiopods in the Exploits Subzone are of the Celtic realm and are thought to have evolved on

isolated ocean islands. This suggests that the two subzones were separated during the Early to Middle Ordovician (Williams et al., 1988).

The Exploits and Notre Dame Subzones can also be distinguished on the basis of plutonic rocks. Middle Paleozoic Notre Dame Subzone plutons are large granite batholiths which are commonly alkaline, while plutons within the Exploits Subzone are typically Ordovician tonalites and large Devonian composite batholiths with granitic phases cutting mafic phases (Williams et al., 1988).

Lead isotopes of mineral deposits are different in the Exploits and Notre Dame Subzones. In the Exploits Subzone the lead is relatively radiogenic, while that of the Notre Dame Subzone is relatively non-radiogenic. This suggests that the lead is from different sources and the two subzones may represent different tectonic-stratigraphic environments (Williams et al., 1988).

Different gravity and magnetic signatures characterize the two subzones. The Notre Dame Subzone generally has higher magnetic and Bouguer gravity anomalies than the Exploits Subzone. This reflects the abundance of mafic rocks in the Notre Dame Subzone and the sediments, granites, and metamorphic rocks in the Exploits Subzone (Williams et al., 1988). This is discernible in the gravity (Figure 1.2) and the magnetic (Figure 1.3) maps of the island of Newfoundland.

The next zone to the east is the Gander Zone. The rocks in this zone are predominantly monotonous clastic sedimentary rocks with small amounts of volcanics in the Gander Lake Subzone, and also the metamorphosed equivalents of the Meelpaeg Subzone and Mount Cormack Subzone (Williams et al., 1988). These are interpreted as continental or continental-margin sediments from the eastern side of the Iapetus Ocean (Williams, 1979).

The Dunnage Zone boundary with the Gander Lake Subzone of the Gander Zone is the Gander River Ultrabasic Belt or GRUB Line (GL) (Figure 1.1), which is defined by ophiolite occurrences along much of its length or by faults (Williams et al., 1988). The boundary between the Dunnage Zone and the Meelpaeg Subzone of the Gander Zone is the Noel Pauls Line (NPL), which is interpreted as a fault with a small ultramafic occurrence at one location (Williams et al., 1988).

The Gander Zone appears on the gravity map as a gravity low (Figure 1.2). Bouguer gravity values are typically between -10 to -20 mGal, except over the Meelpaeg Subzone where values plunge to less than -45 mGal.

Magnetic anomalies over the Gander Lake Subzone are quite high in the eastern half of the subzone and often exceed 375 nT (Figure 1.3), while those of the western Gander Lake Subzone, Meelpaeg Subzone, and Mount Cormack Subzone are generally less than -350 nT. The magnetic pattern over the

Gander Lake Subzone may reflect the metamorphic gradient across the subzone. Metamorphism increases eastward across the Gander Lake Subzone (Williams et al., 1988), and may cause the increased magnetism to the east.

The Avalon Zone is the most easterly Appalachian tectonic-stratigraphic zone present in Newfoundland (Figure 1.1). This zone consists mainly of late Precambrian volcanic and sedimentary rocks which are relatively unmetamorphosed and undeformed compared to the nearby Gander Zone rocks (Williams, 1979). Above these Precambrian units are white quartzite, followed by lower Cambrian fossiliferous shales with Atlantic trilobite faunas, and locally these are covered by Ordovician and younger rocks (Williams, 1979). Keppie (1985) and Keppie et al. (1989) suggest that the Avalon Zone is a composite terrane which was accreted together before accreting to the rest of the orogen.

The potential fields signature of the Avalon Zone consists of a series of repeating arcuate bands of positive gravity and magnetic anomalies, separated by lows. The gravity and magnetic highs correspond with mapped Precambrian volcanics exposed on the island of Newfoundland (Miller, 1990).

The Meguma Zone is recognized on land in Canada only in Nova Scotia (Figure 1.1) (Williams, 1979). It consists mainly of a 13 km thick conformable succession of Cambro-Ordovician

sediments comprised of a lower greywacke unit overlain by shale. This is in turn conformably overlain by mixed sedimentary and volcanic rocks, and finally by Devonian sediments (Williams, 1979). This zone either represents the ancient continental embankment of Northwest Africa or the marine fill of a graben developed within the Avalon Zone (Williams, 1979).

The Meguma Zone is characterized by negative Bouguer gravity and magnetic anomalies (Miller, 1990).

1.3. PREVIOUS GEOPHYSICS:

The northern Appalachians in Canada has been of great interest to the geological community. The Lithoprobe East project has provided the most extensive seismic coverage of the Canadian Appalachians.

Since 1984 the Lithoprobe East project began acquiring a series of deep seismic reflection lines across the northern Appalachians near Newfoundland. The deep seismic reflection program consists of marine air gun surveys carried out by the Atlantic Geoscience Centre (1984 - 1986) (Keen et al., 1987; Marillier et al., 1989; Hall et al., 1990) and several onland Vibroseis transects on the island of Newfoundland (1989) (Quinlan et al., 1992). Gravity measurements at 1 km intervals, rock sample density and magnetic susceptibility measurements, and some remanent magnetization determinations

(Appendix A), were also made along the onshore Vibroseis transects in 1989. These results are used for the potential field modelling included later, and will be discussed in the chapters dealing with each of the three transects.

In 1991 Lithoprobe East carried out a combined land and marine seismic refraction experiment on and around Newfoundland (Roberts et al., 1991; Marillier and Louden, 1991), as well as began a series of magnetotelluric depth soundings (Wright et al., 1991).

Miller (1990) published a summary of potential field terrane analysis results for the Canadian Appalachians, drawing on a number of previous studies and newly available data. This approach has aided in identification and correlation of the various terranes throughout the Appalachians.

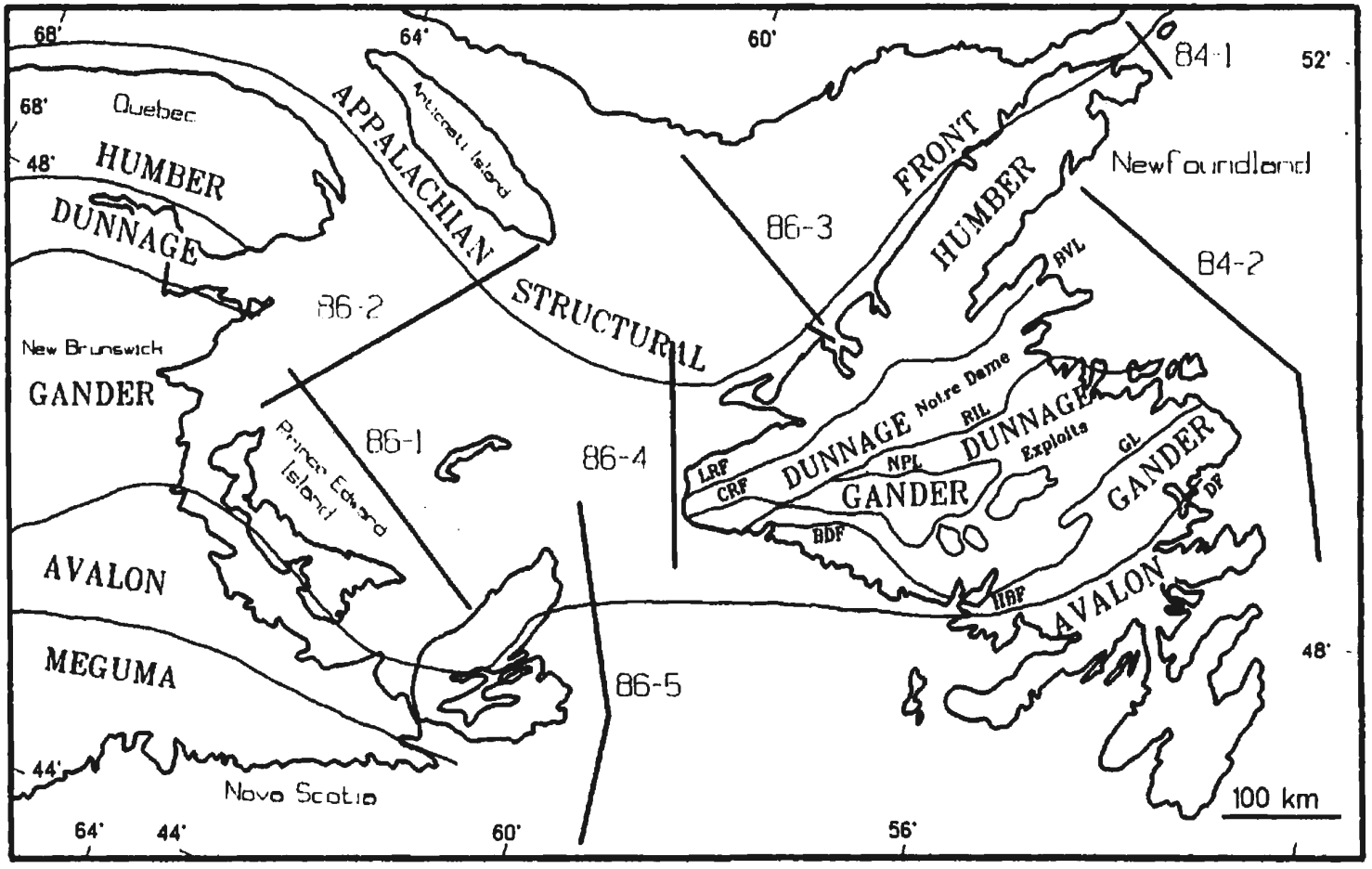

Figure 1.1: Tectono-stratigraphic zones of the northern Appalachians in Canada (after Marillier et al., 1989). Also shown are the locations of the Lithoprobe East marine seismic reflection lines in the area shot between 1984 and 1986.

Legend: BDF – Bay D'Est Fault, BVL – Baie Verte Line, CRF – Cape Ray Fault, DF – Dover Fault, GL – GRUB Line, HBF – Hermitage Bay Fault, LRF – Long Range Fault, NPL – Noel Pauls Line, RIL – Red Indian Line.

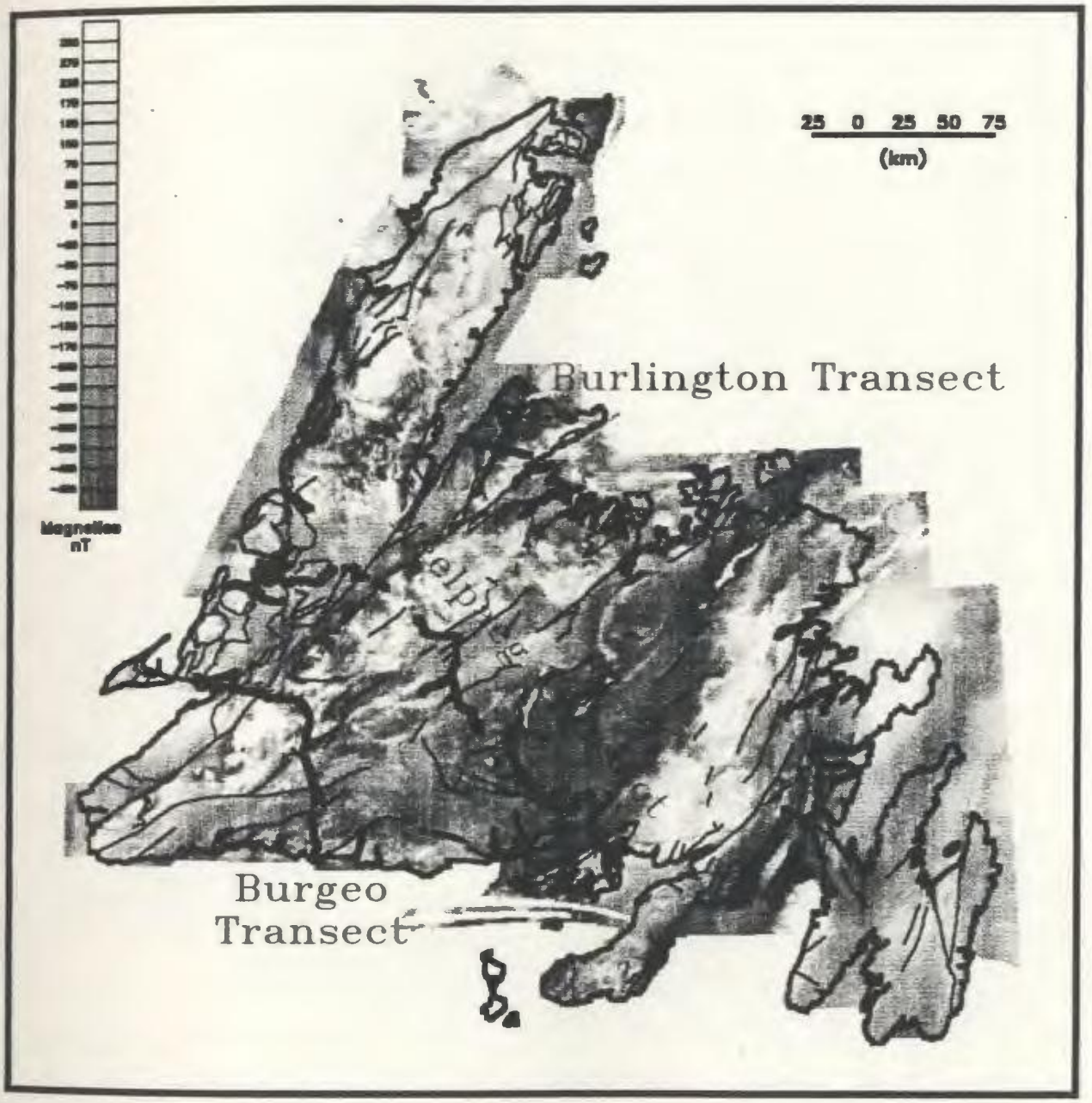

Figure 1.3: Newfoundland. Total field magnetic map of the Island of Otherwise the same as Figure 1.2.

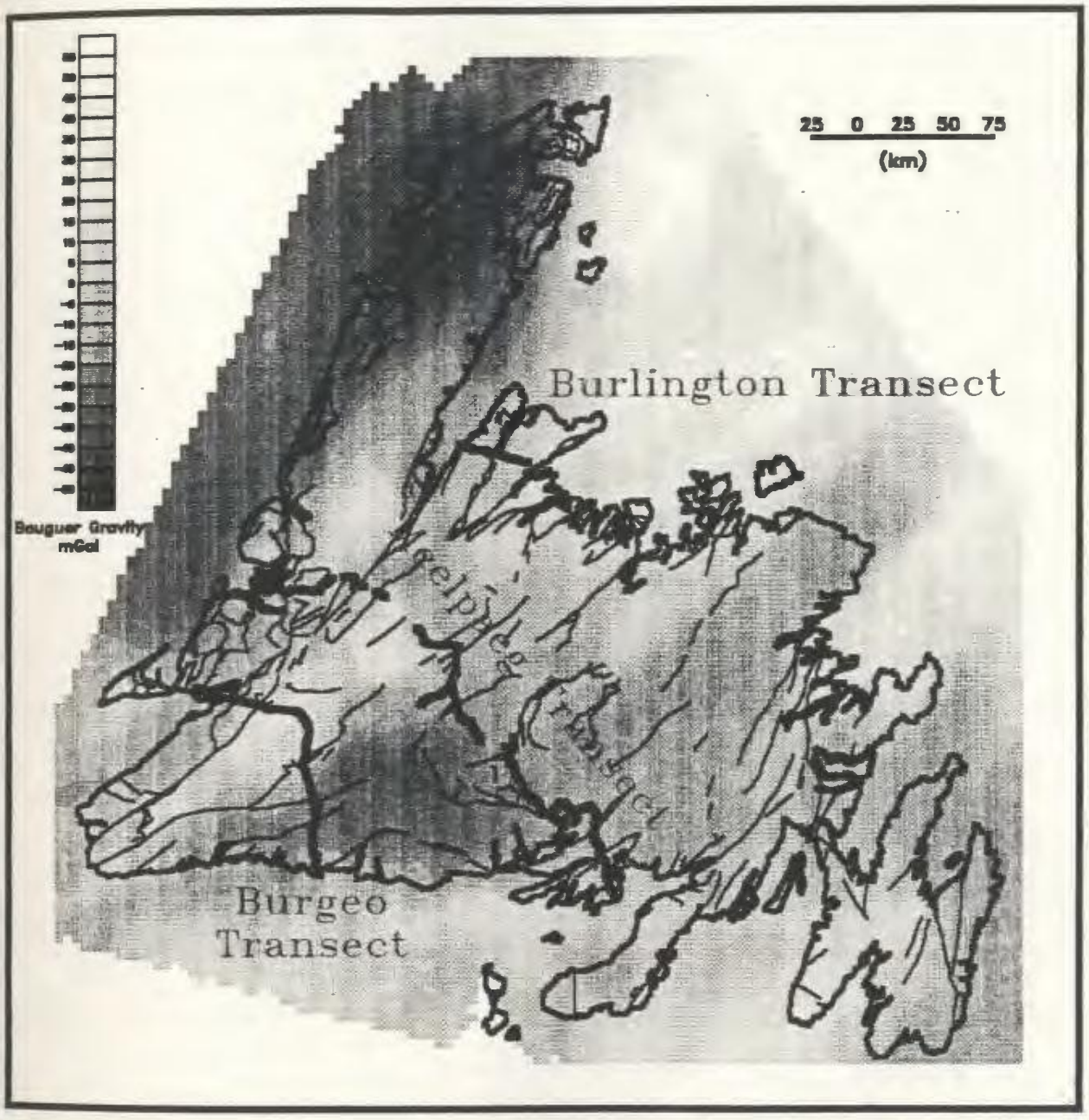

Figure 1.2: Gravity map of the Island of Newfoundland showing the location of the three Lithoprobe East on-shore Vibroseis transects shot in 1989 (thick lines). The thin lines show the locations of major faults taken from Colman-Sadd et al. (1990).

2.0. GEOPHYSICAL THEORY:

2.1. POTENTIAL FIELD MAP PROCESSING:

Map processing techniques have become an important tool for interpretation of potential field data since the wide-spread use of computers. The speed of today's microcomputers allows one to apply numerical filters in the space or wavenumber domain and nearly instantly see the results on the video screen.

Image processing using digital filtering requires that the areal data be equally spaced upon a regular two-dimensional grid of data points. This allows calculation of the discrete two-dimensional Fourier transform of the map data. Normally potential field data don't meet the regular spacial requirement, and therefore they must be passed through a gridding algorithm.

All the potential field maps presented here were produced using the GEOSOFT mapping system on a PC under MS-DOS. The gravity data were extracted from the Geological Survey of Canada (GSC) data base and were augmented with some data compiled by Dr. Hugh Miller of Memorial University of Newfoundland from various sources. The gravity coverage was gridded to a 5 kilometer cell size. The magnetic data (Kilfoil and Bruce, 1991) were regridded to a 500 meter cell size from the original 200 meter cell size to reduce processing time and disk storage requirements.

The GEOSOFT gridding program utilizes a minimum curvature surface fit to the original data by using an inverse distance average of data points within a specified search radius about the grid point (Briggs, 1974). An internal tension parameter may be specified to reduce overshooting in areas of poor observational spatial coverage (Smith and Wessel, 1990). Regridding of the 200 meter aeromagnetic data is accomplished by calculating a bicubic spline of the data and resampling the calculated surface at 500 meter spacing.

After gridding to a regular two-dimensional grid, the maps are then transformed to the Fourier domain using a discrete fast Fourier transform algorithm. Once in the Fourier domain, many filtering options are available which may be applied to the maps.

Potential field maps may be presented in several manners. The data may be presented as line contour maps, or colour maps where ranges of data values are assigned a particular colour. These colours may be grey shades or true spectral colours usually ranging from blue (lows) to violet (highs). Colour divisions are typically chosen in one of two manners: (1) linear scaling, in which equal ranges of data are used for each colour, or (2) equal area scaling in which ranges are determined by equalization of the data histogram so that each colour appears on the map with approximately the same area as all the others. Equal area colour scaling is especially

useful for presentation of data with a large dynamic range.

2.1.1. REDUCTION TO THE POLE:

As a first step in processing the aeromagnetic data, the maps have been reduced or rotated to the north magnetic pole. This procedure removes the effect of an inclined magnetic field direction by simulating the effect of vertical magnetization.

Reduction to the north magnetic pole is easily carried out in the Fourier domain by the following relation (Bhattacharyya, 1965):

$$F[f_p] = \frac{F[f]k_r^2}{(\hat{B}\cdot\vec{G})(\hat{M}\cdot\vec{G})} \qquad (1)$$

$$\vec{G} = \left(ik_x, ik_y, -\sqrt{k_x^2+k_y^2}\right)$$

Here, F is the Fourier Transform operation, f_p is the reduced to the pole field, f is the original gridded field, k_r is the radial wavenumber, k_x is the x-wavenumber, k_y is the y-wavenumber, $\hat{B}$ is the unit vector along the geomagnetic field, and $\hat{M}$ is the unit vector along the crustal magnetization.

Quite often it is assumed that all the body magnetizations are nearly parallel to the Earth's geomagnetic field direction in the area. The process of reduction to the pole ideally results in a symmetrical anomaly directly above

the causative body. This results in easier visual interpretation, as anomalies may be directly correlated with geological bodies. In Newfoundland, since the inclination of the geomagnetic field is approximately 70° everywhere due to its high latitude, reduction to the north magnetic pole has only a small effect. Its major effect is to remove the lows typically found to the northwest of a body caused by the -25° magnetic declination on the island of Newfoundland.

2.1.2. REGIONAL-RESIDUAL SEPARATION:

One of the most important aspects of gravity field analysis is the concept of regional-residual separation. Typically gravity maps are comprised of a superposition of anomalies of widely varying wavelengths. In general, the longer wavelength anomalies have sources which are deeper than the shallow sources which typically produce short wavelength anomalies. Quite often anomalies are present on the gravity map of such a long wavelength that they appear as smooth trends over the whole map. These trends can sometimes obscure the more subtle short wavelength anomalies. The longer wavelength anomalies are called the regional field while the shorter wavelength anomalies, once isolated from the regional field, are called the residual anomalies. Criteria for separating long and short wavelength components of the field should be chosen based upon the scale of the survey and the

size of the target of interest.

A simple method of regional-residual separation is to calculate a best fitting N'th order polynomial surface from the observed data which is taken as the regional field. This is then subtracted from the total field to produce the residual anomaly map. Other methods of regional-residual separation involve the use of various numerical wavelength filters applied in the Fourier domain.

2.1.3. SHADED RELIEF MAPS:

One procedure used to emphasize anomaly patterns on potential field maps is the shaded relief technique (Horn and Bachman, 1978). This consists of artificially illuminating the anomalies from any chosen azimuth (θ) and elevation angle (ϕ). The light intensity at each grid point is taken to be proportional to the angle between the surface normal vector and the light source direction vector (λ), which is given by the following equation (Dods et al., 1985):

$$\cos\lambda = \frac{-S\frac{\partial z}{\partial x}\cos\theta\cos\phi - S\frac{\partial z}{\partial y}\sin\theta\cos\phi - \sin\phi}{\sqrt{S\left(\frac{\partial z}{\partial x}\right)^2 + S\left(\frac{\partial z}{\partial y}\right)^2 + 1}} \qquad (2)$$

Here, S is a scale factor chosen to be applied to the horizontal partial derivatives to correct for the difference

in horizonal units (distance) and vertical units (either nT or mGal). This calculation results in a reflection intensity map which can be shaded to give the appearance of shadows cast by the anomalies. These tend to emphasize features trending normal to the illumination direction and subdue features parallel to the illumination direction (Broome, 1986).

2.1.4. VERTICAL DERIVATIVE MAPS:

Vertical derivative maps tend to sharpen the edges of anomalies by enhancing near-surface effects at the expense of deeper sources. This is a form of regional-residual separation which makes identification of individual shallow source anomalies much easier. In the Fourier domain, N'th order vertical derivatives are very easy to calculate using the following formula:

$$\frac{\partial^N f}{\partial z^N} = F^{-1}\left[k_r^N \cdot F[f]\right] \qquad (3)$$

Here, f is the potential field of interest, F is the Fourier transform operation, F^{-1} is the inverse Fourier transform operation, and k_r is the radial wavenumber. Normally, only the first or second order vertical derivative is calculated, because the derivative process also enhances the noise inherent in the observed field.

Second vertical derivative maps of the gravity field

often delineate lithological contacts if the density contrast is significant enough. Such contacts are reflected in the gravity field by inflection points, which correspond to the zero contour level of the second vertical derivative (Gupta and Ramani, 1982).

These maps often require smoothing to suppress the noise. Smoothing of the resultant grid can be carried out by single or multiple passes of a moving window Hanning filter. The 9-point Hanning filter looks like this:

$$\begin{matrix} 0.06 & 0.10 & 0.06 \\ 0.10 & 0.36 & 0.10 \\ 0.06 & 0.10 & 0.06 \end{matrix} \qquad (4)$$

2.1.5. HORIZONTAL DERIVATIVE MAPS:

Horizontal derivatives of gridded maps in the x- and y-directions are easily estimated by finite differences using the following equations:

$$\frac{\partial f}{\partial x} = \frac{f_{x+1} - f_{x-1}}{2\Delta x}$$
$$\frac{\partial f}{\partial y} = \frac{f_{y+1} - f_{y-1}}{2\Delta y} \qquad (5)$$

or in the Fourier domain by:

$$\frac{\partial f}{\partial x} = F^{-1}[ik_x F[f]]$$
$$\frac{\partial f}{\partial y} = F^{-1}[ik_y F[f]] \qquad (6)$$

Here, Δx is the grid spacing in the x-direction, Δy is the grid spacing in the y-direction, k_x is the wavenumber in the x-direction, and k_y is the wavenumber in the y-direction.

A horizontal derivative of the field may be calculated for any arbitrary direction (θ) using the following equation:

$$\cos\left(\frac{\partial f}{\partial \theta}\right) = \frac{-\frac{\partial f}{\partial x}\cos\theta - \frac{\partial f}{\partial y}\sin\theta}{\sqrt{\left(\frac{\partial f}{\partial x}\right)^2 + \left(\frac{\partial f}{\partial y}\right)^2}} \qquad (7)$$

Due to the directional nature of the horizontal derivatives, maps of the amplitude of the horizontal gradient are more commonly produced using the following equation:

$$\left|\frac{\partial f}{\partial \theta}\right| = \sqrt{\left(\frac{\partial f}{\partial x}\right)^2 + \left(\frac{\partial f}{\partial y}\right)^2} \qquad (8)$$

Here θ is the direction of maximum horizontal gradient and is given by:

$$\tan\theta = \frac{\frac{\partial f}{\partial y}}{\frac{\partial f}{\partial x}} \qquad (9)$$

Horizontal gradient maps are constructed predominantly for gravity maps. Maximum magnitudes of horizontal gravity gradients generally occur above lithologic contacts (Hildenbrand, 1985). In the case of non-vertical boundaries or when several boundaries lie in proximity the maximum may be shifted somewhat (Grauch and Cordell, 1987).

2.1.6. CONTINUATION OF POTENTIAL FIELDS:

Potential field strength may be calculated on any arbitrary surface outside of the source using the measured data taken on the plane of observation. This process is called continuation. Downward continuation involves calculating the expected field at a level closer to the source than the plane of observation, while upward continuation involves calculating the expected field at a level further away from the source than the surface of observation.

Continuation of potential field data from one horizontal plane to another, either upwards or downwards, is simple in the Fourier domain:

$$F[f_c] = F[f] \cdot e^{hk_r} \qquad (10)$$

Here h is the vertical distance in grid cell units to the plane of continuation (+'ve for downward continuation, -'ve for upward continuation), and f_c is the calculated field at the new plane of observation. Downward continuation suffers greatly from enhancement of high-frequency noise, and is inherently an unstable process (Broome, 1986).

One important application of continuation is to merge different aeromagnetic surveys which were flown at different elevations. These may be merged once one is continued to the elevation level of the other.

Downward continuation is often used to enhance the high-frequency near-surface anomalies at the expense of the longer wavelength regional anomalies, while upward continuation can be used to enhance the longer wavelength anomalies at the expense of the short wavelength anomalies (Broome, 1986). Continuation is therefore another method of regional-residual separation (Jacobson, 1987).

Using a sandwich source distribution consisting of N thin-sheet random sources, Jacobson (1987) has shown that the regional field (f_{reg}) taken as originating below depth h is given by:

$$F[f_{reg}] = F[f] \cdot e^{-2k_r h} \qquad (11)$$

which is the upward continuation of the total field to a height of 2h above the plane of observation. Jacobson (1987) has also shown that the field originating from a depth interval between h_1 and h_2 is given by:

$$F[f_{slab}] = F[f]\left\{e^{-2k_r h_1} - e^{-2k_r h_2}\right\} \qquad (12)$$

which is equivalent to taking the difference between upward continuations to the heights $2h_1$ and $2h_2$. This is an effective method of layer stripping to separate sources that lie in different depth ranges.

2.1.7. DIRECTIONAL FILTERING:

Directional filtering may be employed to help emphasize or eliminate linear trends in potential field data (Fuller, 1967; Thorarinsson et al., 1988). A particular direction observed on a gravity or magnetic map may be enhanced by applying a directional cosine or pie-slice filter to the 2-D power spectrum which passes the chosen direction. This can make subtle linear trends much more obvious, but care must be taken to not interpret false anomaly trends which may be created (Thorarinsson et al., 1988). A directional reject filter can be used to eliminate or reduce linear trends which may be obscuring other important trends in the observed potential field map.

Another use for directional filtering is to reduce levelling problems in surveys conducted along lines. Examples are aeromagnetic surveys where the plane's elevation may vary slightly from line to line, or surveys where instrument drift has occurred.

2.2. POTENTIAL FIELD MODELLING:

Computer modelling of potential field data can be divided into three main applications: two-dimensional (2-D) modelling, two-and-a-half-dimensional (2½-D) modelling, or three-dimensional (3-D) modelling.

2-D modelling of gravity (Talwani et al., 1959) and magnetic (Talwani et al., 1964) anomalies requires that the geological structure to be modelled is approximately linear and continues to infinity perpendicular to the line of the profile. In general this is not the case, but if the length to width ratio of the anomaly on the potential field map is 5:1 or greater 2-D modelling may be applied with minimal error (Miller, pers. comm.).

Two-dimensional (2-D) modelling requires data along a single profile roughly perpendicular to the strike of the anomaly. Modelling is carried out by calculating the expected anomaly from a constructed N-sided polygon which is assumed to extend to infinity in both directions perpendicular to the line profile of observations. This calculated anomaly is then

compared to the observed anomaly and adjustments are made to the polygon and/or its physical properties to minimize the difference between the two anomalies.

In the case where the minimum 5:1 length to width ratio required for 2-D modelling is not satisfied, 3-D or 2½-D modelling should be employed. Three-dimensional modelling generally requires a two-dimensional coverage of surface observations. The modelled bodies can be created as an amalgamation of cubic blocks (Mufti, 1975), regular prisms (Nagy, 1966; Cordell and Henderson, 1968), stacked polygonal lamina (Talwani and Ewing, 1960; Talwani, 1965), or three-dimensional polyhedra (Paul, 1974; Coggon, 1975; Barnett, 1976). The effect of the body is then calculated for each grid point and compared with the observed anomaly. Three-dimensional (3-D) modelling requires that the user enter a large number of data points to define the bodies, and is often quite difficult to visualize and present.

Rasmussen and Pedersen (1979) coined the term two-and-a-half-dimensional (2½-D) modelling for 2-D modelling in which end corrections are applied to the anomaly calculated for the 2-D polygon to allow for the finite extent in both directions away from the profile. This approach is often sufficient for many anomalies, and greatly reduces the numerical load required of 3-D modelling.

Modelling, whether it be in 2-D, 2½-D, or 3-D, can be

carried out in two modes: forward, or inverse. Forward modelling requires that the user create the initial model and then compare the calculated anomaly with the observed anomaly. Any subsequent changes to the model must be decided on and implemented by the user. Inverse modelling is an automatic modelling procedure in which a statistical comparison is made between the calculated and observed anomalies and the computer changes the model automatically to improve the 'goodness of fit' of the calculated anomaly. Inverse modelling may or may not require the user to input a starting model depending on the method used, but often some assumptions about the causative body need to be given.

All of the modelling presented here was carried out using the MS-DOS based gravity and magnetic modelling program GM-SYS. This program allows simultaneous forward modelling of gravity and magnetic data in 2½-D and does not require that the bodies trend perpendicular to the strike of the profile.

3.0. BURLINGTON TRANSECT:

3.1. GEOLOGY:

The Burlington transect (LE89-13) crosses the Baie Verte Peninsula, northern Newfoundland, from Western Arm in the west to the town of Burlington in the east (Figure 3.1).

This transect crosses the Baie Verte Line, which is considered to be the surface boundary between the Humber Zone to the west and the Dunnage Zone to the east (St. Julien et al., 1976; Williams and St. Julien, 1978; Williams, 1979). This contact is a steeply faulted structural zone characterized by ophiolite occurrences on the east side.

The Baie Verte Line trends roughly NNE through the Baie Verte Peninsula. At Baie Verte, the line assumes an eastward orientation and continues offshore (Hibbard, 1983). Williams (1979) and Williams and Hatcher (1982) continue the Baie Verte Line southward to join the Long Range Fault in southwestern Newfoundland. The east-west portion of the Baie Verte Line has a significantly different character from the rest of the Line: here it forms a wide polytectonized structural zone intruded by granite (Hibbard, 1983).

The Humber Zone rocks on the Baie Verte Peninsula, west of the Baie Verte Line, are comprised of three main lithic elements: (1) local structural basement, (2) a metaclastic cover sequence, and (3) post-kinematic granitoid intrusives (Hibbard, 1983).

The structural basement is composed of migmatites, banded gneisses, and psammitic and semipelitic schists. These are in tectonic contact, in many places, with the cover sequence, although locally the contact appears gradational (Hibbard, 1983). There is some debate whether these rocks are part of the Grenville basement (de Wit, 1972 and de Wit, 1980), or are a deeper more deformed part of the cover sequence immediately above the Grenville basement (Hibbard, 1983).

The cover sequence rocks (East Pond Metamorphic Suite - **EPM**, and Old House Cove Group - **OHC**) consist mainly of psammitic, semipelitic and graphitic schists, marble, amphibole-chlorite-epidote schists, and amphibolite. In places these units are deposited conformably upon Grenville basement, while the contact is tectonic in other areas (Hibbard, 1983).

Both the structural basement and cover sequence have been post-tectonically intruded by a muscovite-bearing granite batholith.

Immediately to the east of the Baie Verte Line lie rocks of the Dunnage Zone. These are composed of: (1) ophiolite suites and volcanic cover sequences, and (2) intrusives. The Dunnage Zone rocks on the Baie Verte Peninsula are stratigraphically and geochemically different from those in other parts of the Dunnage Zone (Hibbard, 1983).

The four ophiolitic units on the Baie Verte Peninsula

(Advocate Complex (AC, FWP), Point Rousse Complex (PRC), Betts Cove Complex (BCC), and the Pacquet Harbour Group (PHG)) are considered mutually correlative although they are geographically separated, and are structurally different. Only mafic and felsic lavas have been observed in the Pacquet Harbour Group suggesting that it consists only of the uppermost portion of an ophiolite assemblage. The Advocate and Betts Cove Complexes contain nearly all the components of an ophiolite sequence from ultramafic members to the overlying cover sequence, with various degrees of completeness. The Advocate Complex lacks a pillow lava member, while the Betts Cove Complex lacks a noncumulate ultramafic layer at the base. Only the Point Rousse Complex is complete (Hibbard, 1983).

Ordovician and Silurian-Devonian intrusives cut the ophiolites and cover sequences throughout the Baie Verte Peninsula. Most notable of the Ordovician intrusions is the Burlington Granodiorite (BG), which covers much of the exposed area east of the Baie Verte Line. The Cape Brule Porphyry (CBP) is a large Silurian-Devonian intrusion cutting the Burlington Granodiorite and older rocks, including the Pacquet Harbour Group (Hibbard, 1983).

3.2. GEOPHYSICS:

3.2.1. Seismic Reflection:

The seismic reflection line across the Baie Verte Peninsula, Lithoprobe East Line LE89-13, is approximately 37.5 km long, and relatively straight (Figure 3.1). The profile crosses the Flat Water Pond (**FWP**) ultramafic body of the Advocate Complex at the Baie Verte Line. To the east it crosses the Burlington Granodiorite (**BG**), and to the west the many metasedimentary units of the Humber Zone in this area. A line drawing of the seismic reflection data modified from Quinlan et al. (1992) is presented in Figure 3.2.

Although the Baie Verte Line has been geologically interpreted as a near-vertical major tectonic boundary between the Humber Zone and Dunnage Zone, it does not manifest itself in this manner on the seismic data. Here, the Baie Verte Line (**BVL**) appears to be a shallow (~30°) east-dipping reflector, but cannot be directly tied to the surface due to a lack of coherent reflections between 0.0 seconds and 0.2 seconds two way travel time.

There are many shallow east-dipping reflectors (**E**), predominantly in the upper part of the section. These terminate at deep crustal west-dipping reflectors (**W**) that appear to cross the entire section and may also cut the Moho (**M**). Another west-dipping reflector (**A**) occurs in the upper part of the section, and appears to cut the Baie Verte Line

(BVL). This reflector, although it cannot be traced to the surface, is coincident with some small-scale faulting in the Burlington Granodiorite (BG) and Cape Brule Porphyry when projected to the surface. These small-scale faults may represent some late movement on this crustal-scale fault.

There is a near horizontal reflector at 0.5 seconds two way travel time (B) in the eastern part of the section, which may represent the base of the Burlington Granodiorite.

The Moho (M) dips west between 12-13 seconds two way travel time in the eastern portion of the seismic profile, but is not imaged near the center of the profile.

3.2.2. Magnetics:

The Baie Verte Line appears on the total field magnetic map (Figure 3.3) as a strong linear NNE-SSW trending relative magnetic high with a series of discrete very high anomalies over exposed ultramafic bodies of the Advocate Complex (e.g. the Flat Water Pond body). The lower amplitude magnetic high along the Baie Verte Line between the ultramafic bodies correlates with the location of graphitic schist units exposed there. As a first step in map processing, the total field magnetic map (Figure 3.3) was reduced to the magnetic pole. The resulting map is shown in Figure 3.4. Reduction to the magnetic pole results in removal of anomaly asymmetry due to the magnetic inclination and declination of the Earth's

magnetic field in the area of interest, and places the anomaly directly above the causative body. This allows easier interpretation of the map anomaly patterns.

Two shaded relief maps were produced for the Baie Verte Peninsula. One was produced with a false sun located at an azimuth of 125° and inclination of 45° (Figure 3.5a) which is roughly perpendicular to the Baie Verte Line, and the other has an illumination angle of 40° azimuth and 45° inclination (Figure 3.5b). These are very useful for enhancing the detail within anomaly patterns.

Upward continuation maps (Figures 3.6a,b,c,d) and the depth separation filtering method of Jacobson (1987) (Figures 3.7a,b,c,d) suggest that anomalies associated with the Baie Verte Line arise from a shallow feature, predominantly within the upper 5 km. In the equivalent source maps of depths greater than this, the anomaly associated with Baie Verte Line is not observed. This is consistent with the seismic reflection data (Figure 3.2). It is possible that the magnetic anomaly is simply not resolved at the heights of upward continuation used to produce the layer stripped maps (Figures 3.7a,b,c,d), resulting in an erroneous conclusion about the source depth.

There is a large positive magnetic anomaly coincident with Baie Verte, roughly outlined by the coastline in this area (Figure 3.3). This, combined with observed peridotite

exposure on islands in the bay, suggests that the bay is underlain by ophiolitic rocks.

Along the whole eastern margin of the Baie Verte Peninsula is a large irregular magnetic high (Figure 3.3). There appears to be a change in character of this anomaly pattern from north to south at roughly 5520 km N. Towards the north, the anomaly is higher amplitude and more continuous than the anomaly in the south. The anomaly appears to terminate abruptly on its eastern edge at the coast of the peninsula (Green Bay Fault). On its western edge, this anomaly doesn't correlate with any geologic boundary on the geology map produced by Hibbard (1983). This anomaly does include the area of the Betts Cove Complex.

Examining the magnetic shaded relief map with illumination azimuth of 125° (Figure 3.5a), we can see that the Betts Cove Complex is responsible for a positive magnetic anomaly superimposed upon part of this larger anomaly. This is evident from the shadow cast along the western edge of the Betts Cove Complex.

Within this anomaly pattern there is a distinct step in the magnetic anomaly amplitude (about 300 nT) at about 25 km eastward along the seismic line (Figure 3.2 and 3.3). It is also highlighted quite distinctly by a shadow on the magnetic shaded relief map with false sun illumination angle of 125° (Figure 3.5a). This is coincident with the location of the

west-dipping reflector that appears to cut the Baie Verte Line on the seismic data (reflector 'A' on Figure 3.2). This diagnostic step in the magnetics can be used on the magnetic map (Figure 3.3) to trace this feature in the subsurface away from the control of the seismic data.

Also visible in the total field magnetic map (Figure 3.3), and even more so on the layer strip map for sources between the surface and 1.5 km depth (Figure 3.7a), is a series of arcuate magnetic highs which follow the edges of the Pacquet Harbour Group. These trends can be traced into a linear magnetic high which crosses Notre Dame Bay to the east, and can be traced further north than the areal extent of the Pacquet Harbour Group (PHG). They are also indicated by shadows on the magnetic shaded relief maps (Figures 3.5a,b). These trends are highlighted on the maps with the dashed black line.

3.2.3. Gravity:

The gravity field in this area (Figure 3.8) shows a general regional trend from high in the southeast to low in the northwest. There appears to be a high over much of the Pacquet Harbour Group (PHG) as well, but low station density makes the areal extent of this anomaly uncertain. There is also a gravity high above the Baie Verte Line to the south of the Flat Water Pond body, but the low station density makes

its definition poor.

When the regional gravity field is subtracted from the total field, the residual field remains. This was determined by two methods: subtraction of a planar trend (Figure 3.9a), and by a Gaussian regional/residual filter with 0.025 cycles/km central wavenumber (Figure 3.9b). These two residual gravity field maps are very similar in appearance.

The most noticeable feature in the residual gravity maps for the Baie Verte Peninsula, is the distinct gravity high over the Betts Cove Complex (**BCC**), which continues towards the southwest under Notre Dame Bay. This indicates that the rocks of the Betts Cove Complex are denser than the surrounding rocks. This is to be expected, as the Betts Cove Complex is composed of dense ultramafic and mafic volcanic rocks and the surrounding rocks are the lower density Cape Brule Porphyry (**CBP**) and Snooks Arm Group (**SAG**) volcanics and sediments.

Another interesting feature on the residual gravity maps is a roughly linear NNW trending high which covers the area of the Pacquet Harbour Group (**PHG**) and crosses the Baie Verte Line. This occurs where the location of the Baie Verte Line becomes questionable and its character appears to change. It is near this location that Hibbard (1983) noted that the Baie Verte Line turns sharply east.

3.2.4. The Model:

In order to ascertain the correlation between the seismic section and the gravity and magnetic field data the potential field data along the Lithoprobe East line 89-13 were modelled using a 2½-D modelling package. The physical property data presented in Appendix A were used to assign density contrasts and magnetic susceptibilities to the bodies identified on the seismic section. Gravity and magnetic modelling were carried out simultaneously to develop a model which agreed with both potential fields. No regional trend was removed from the data prior to modelling.

The potential field 2½-D model along with the seismic line drawing modified from Quinlan et al. (1992) is shown in Figure 3.2. Essentially all of the observed gravity and magnetic anomalies along LE89-13 can be explained by shallow depth bodies within the upper 10 km.

The Flat Water Pond body (FWP) of the Advocate Complex is responsible for the gravity and magnetic high near the center of the profile, and defines the potential field response of the Baie Verte Line on the profile. For modelling purposes, this layered harzburgite/dunite body was required to have an assigned density contrast of 0.21 g/cm^3 relative to 2.67 g/cm^3 and a magnetic susceptibility of 4.70 x 10^{-3} c.g.s. units. The density contrast is at the upper limit of the measured density data (Appendix A), but at greater depths in the body

serpentinization may be less extensive than that near the surface. The effect of this would be higher densities with depth, so the modelling density contrast is not considered excessive. The required magnetic susceptibility for this body is higher than the average value presented in Appendix A, but it should be noted that the tabulated value includes many talc and magnesite-talc alteration samples which only comprise a small percentage of the exposed Flat Water Pond body. This type of alteration consumes magnetite (Wiseman, 1991) and biases the average susceptibility towards low values. The true average magnetic susceptibility is likely considerably higher.

Although the Flat Water Pond body has been interpreted geologically as an ophiolite body bounded by near vertical faults which parallel the Baie Verte Line, both the seismic data and the gravity and magnetic modelling insist that it and the Baie Verte Line, in fact, dip to the east.

The other major feature modelled on LE89-13 is a near-horizontal block of high density ($\Delta\rho$=0.09) and high magnetic susceptibility (6.20 x 10^{-3} c.g.s. units) beneath the Burlington Granodiorite (BG). The western edge of this body coincides with the step in the both the gravity and magnetic profiles, and with a west dipping reflector on the seismic reflection profile (A). Since this body is not exposed at the surface, there is no control for the magnetic susceptibility

and density contrast assigned to it except by the geometry and amplitude of the observed anomalies.

Other anomalies are seen to correlate with surface lithologies and their respective density and magnetic susceptibility variations. The Flat Water Pond Group (**FPG**) rocks between the Burlington Granodiorite (**BG**) and the Flat Water Pond body (**FWP**) were assigned a density contrast of 0.07 g/cm^3 and a magnetic susceptibility of 1.00 x 10^{-9} c.g.s. units which is typical of mafic volcanics (Telford et al., 1976) as no specific data was available.

West of the Baie Verte Line, gravity and magnetic anomalies correlate with exposed geological units. The East Pond Metamorphic Suite (**EPM**) is modelled as a shallow wedge-shaped body of metamorphosed sediments in the upper 2 km with a density contrast of -0.03 g/cm^3 and a magnetic susceptibility of 2.50 x 10^{-5} c.g.s. units. Its physical properties match those measured for rock samples for this group (Appendix A).

There was no physical property data available for the Old House Cove Group (**OHC**). Although the body was modelled with a density contrast of 0.15 g/cm^3 and a magnetic susceptibility of 1.30 x 10^{-3} c.g.s. units to match the observed gravity and magnetic profile, this may not reflect the true geology. Examination of the gravity map (Figure 3.8) reveals that the observed gravity anomaly above **OHC** may in fact be related to

the generally higher Bouguer anomalies observed south of LE89-13 originating from another source. The OHC body was included merely to fit the observed profile.

Beneath the whole western half of the profile there was a 6 km thick relatively dense body required ($\Delta\rho$=0.01 g/cm^3) to raise the calculated gravity anomalies to the level of 4-5 mGal which is observed to the west of the Baie Verte Line. A body of similar dimensions appears to be defined on the Vibroseis data (Figure 3.2). Alternatively, the crust may become gradationally denser with depth.

3.3. INTERPRETATION:

The Vibroseis data indicate that the Baie Verte Line is a shallow east-dipping fault. Potential field processing and modelling indicates that the Flat Water Pond ultramafic body, which reflects the orientation of the Baie Verte Line, is confined to the upper 5 km of the Earth's crust and has an easterly dip.

The magnetic and gravity highs on the eastern half of the Baie Verte Peninsula are interpreted to be due to the subsurface extent of an ophiolite thrust slice. This is consistent with local geology, where ultramafic inclusions are found within the Cape Brule Porphyry (Hibbard, 1983). This porphyry must have been intruded into the previously emplaced ophiolite sheet. This allows us to date the thrusting at pre-

Silurian, knowing the age of the Cape Brule Porphyry.

The base of this ophiolite body is defined on the seismic section as a reflector (Figure 3.2) which is interpreted to be a continuation of the Baie Verte Line (**BVL**) (Quinlan et al., 1992). If this interpretation is correct, this suggests that both this body and the Advocate Complex (**FWP**) were emplaced simultaneously from the east by thrusting along the Baie Verte Line.

Since this gravity and magnetic high does not continue all the way westward to the surface exposure of the Baie Verte Line, the ultramafic rocks which form the Flat Water Pond body and other bodies of the Advocate Complex must be dismembered slivers of ophiolite separated from the rest of the thrust sheet. This could have happened by internal dismemberment of the thrust sheet during emplacement, or by later extensional and strike-slip faulting throughout the region (Jamieson et al., 1993).

The arcuate magnetic anomalies tracing the edge of the Pacquet Harbour Group, as mentioned previously, are interpreted as defining the fault boundaries of the thrust sheet emplacing this ophiolite unit and possibly also the Point Rousse Complex, although these are considered separate ophiolites (Hibbard, 1983). Hibbard (1983) states that the lavas of the Pacquet Harbour Group are chemically correlative with equivalent lavas of the Betts Cove Complex and the Point

Rousse Complex, so it is not unreasonable to link them as being part of the same thrust sheet.

A possible geological evolution of the Burlington Transect is shown in Figure 3.10. The ophiolites of the peninsula were emplaced by imbricate thrusting from the east. The Baie Verte Line is the sole thrust of the emplaced complex. The thrust sheets contain variable thicknesses of the various ophiolite units, and in some places the gabbro and ultramafic sections are completely missing. This explains the absence of strongly magnetic material in places between the surface exposure of the Baie Verte Line and the areas further east beneath the Burlington Granodiorite.

Towards the northern part of the Baie Verte Peninsula, the geometry is thought to be similar to that of the Burlington Transect, but another thrust sheet has been thrust over the sequence forming a duplex structure. The western and southern boundaries of this upper thrust sheet are defined on the magnetic maps as the arcuate highs on the edge of the Pacquet Harbour Group which were mentioned previously.

Following emplacement of the ophiolite, a period of strike-slip motion along the Baie Verte Line and other faults occurred. Some slight extension also occurred.

In the Ordovician, the Burlington Granodiorite was intruded through the previously emplaced ophiolite units followed by the Cape Brule Porphyry in the Silurian-Devonian.

This process truncated the top of the ultramafic member of the ophiolite, forming the lateral discontinuity identified by the step on the gravity and magnetic data.

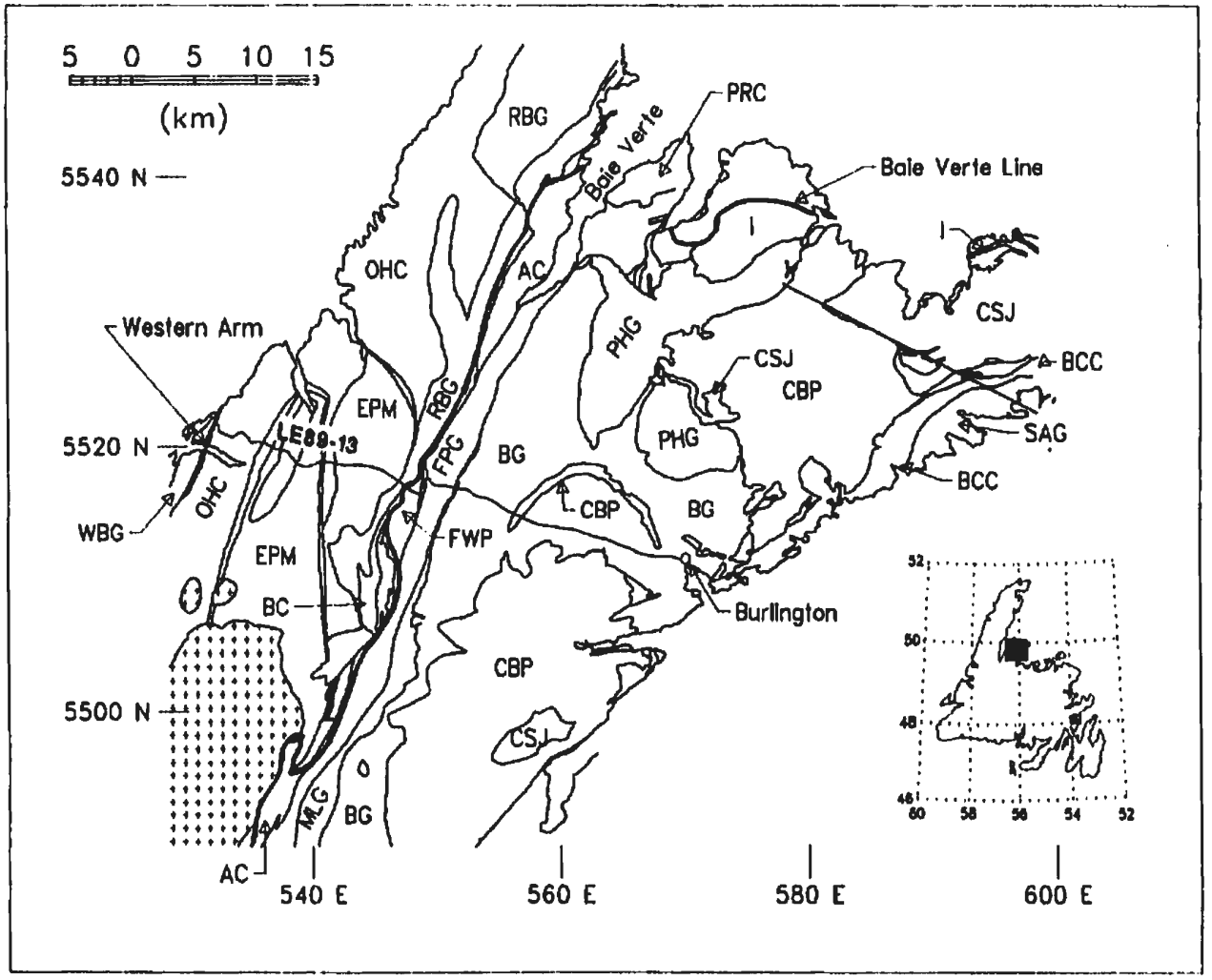

Figure 3.1: Geology map of the Baie Verte Peninsula (after Hibbard, 1983). The location of LE89-13 is shown, as well as the location of the Baie Verte Line. Coordinates are in UTM Zone 21 kilometers. Legend: AC – Advocate Complex, BC – Birchy Complex, BCC – Betts Cove Complex, BG – Burlington Complex, CBP – Cape Brule Porphyry, CSJ – Cape St. John Gp., EPM – East Pond Metamorphic Suite, FPG – Flat Water Pond Gp., FWP – Flat Water Pond body, I – Silurian–Devonian intrusives, MLG – Micmac Lake Gp., OHC – Old House Cove Gp., PHG – Pacquet Harbour Gp., PRC – Point Rousse Complex, RBG – Rattling Brook Gp., SAG – Snooks Arm Gp., WBG – White Bay Gp.

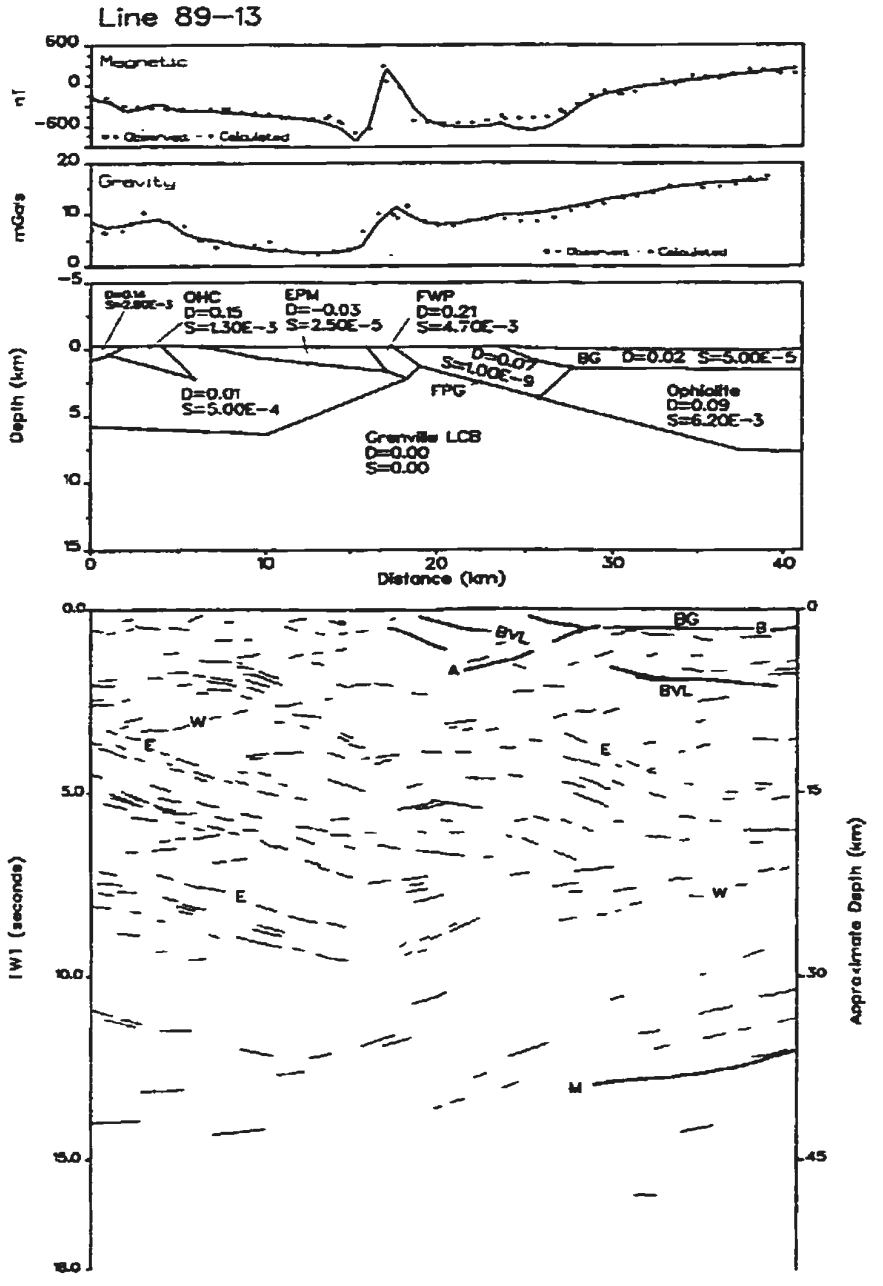

Figure 3.2: Seismic line drawing and 2 1/2–D gravity and magnetic model for the Burlington Transect. Legend: A – west–dipping reflector mentioned in the text, B – base of the Burlington Granodiorite, BG – Burlington Granodiorite, BVL – Baie Verte Line, D – density contrast relative to 2.67 g/cc, E – east–dipping reflectors, EPM – East Pond Metamorphic Suite, FPG – Flat Water Pond Gp., FWP – Flat Water Pond body, M – Moho, OHC – Old House Cove Gp., S – magnetic susceptibility in c.g.s. units, W – west–dipping reflectors.

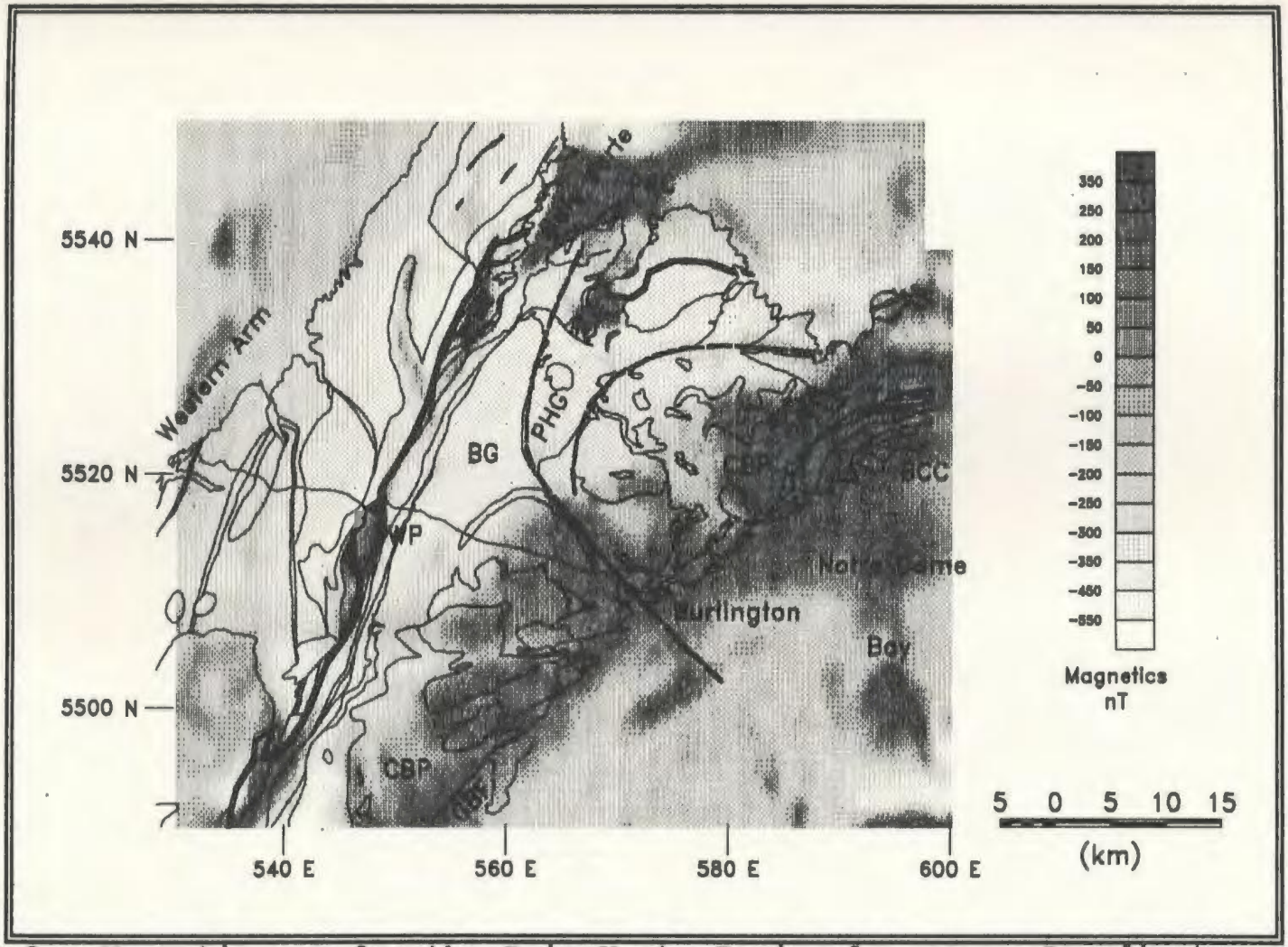

Figure 3.3: Magnetic map for the Baie Verte Peninsula area. Coordinates are in UTM Zone 21 kilometers. The geology (Hibbard, 1983) is shown by solid black lines. The Baie Verte Line is expressed by the thick solid black line. The thick dashed line is the magnetically defined fault boundary of the thrust sheet emplacing the Pacquet Harbour Group. The legend follows that of Figure 3.1.

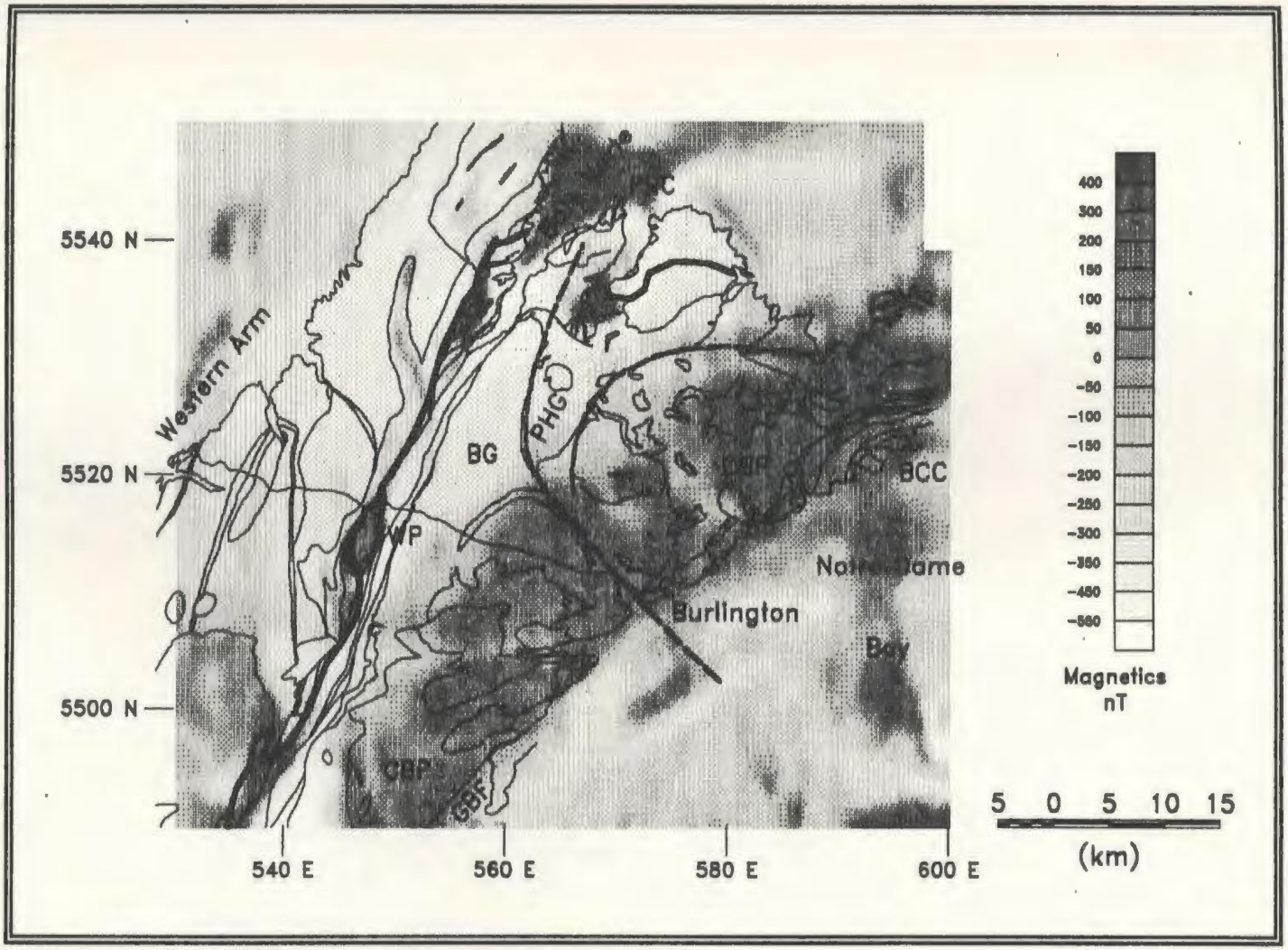

Figure 3.4: Total field magnetic map for the Baie Verte Peninsula after rotation to the north magnetic pole. The legend is the same as that for Figure 3.1.

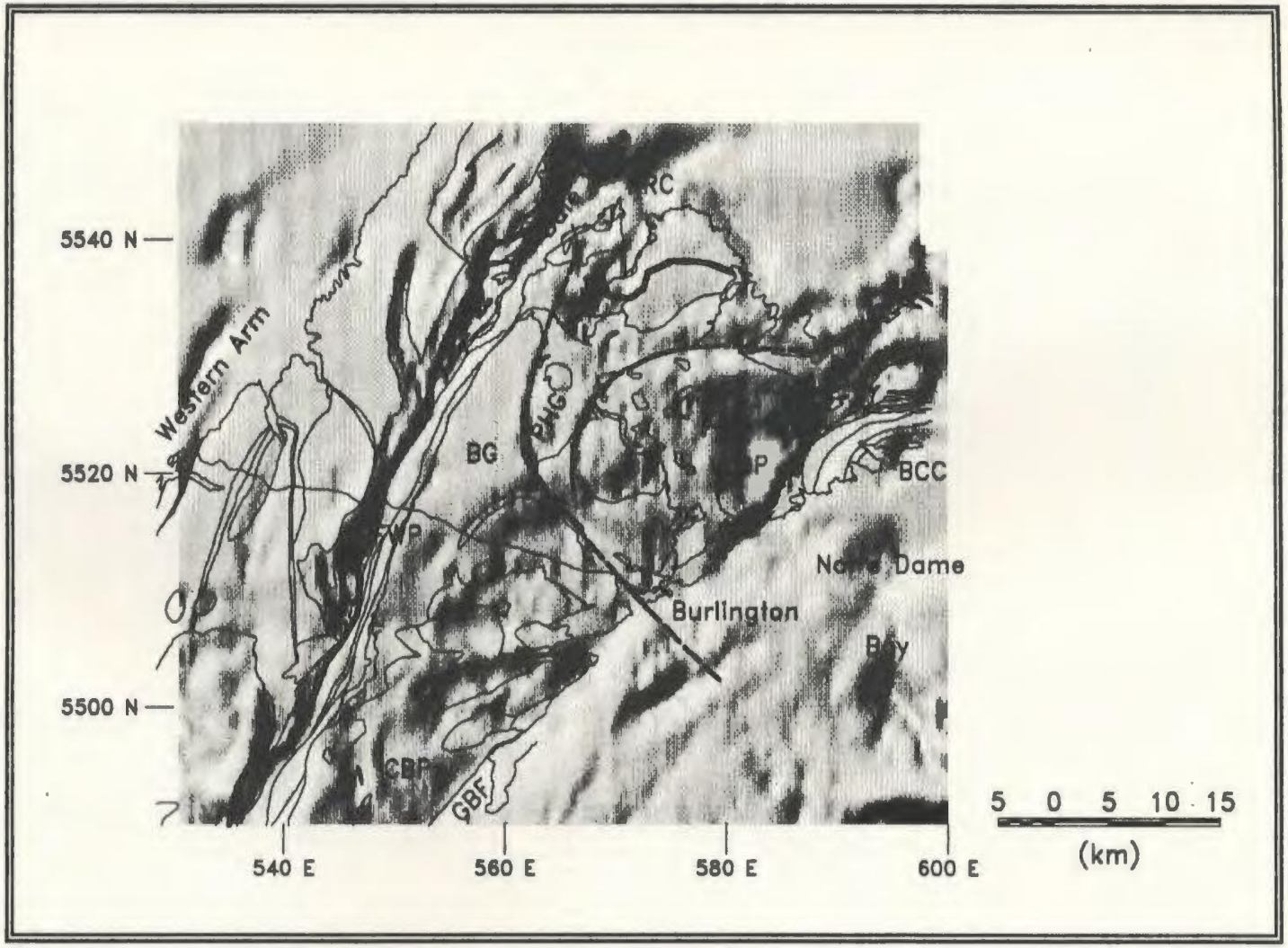

Figure 3.5(a): Shaded relief image of the Baie Verte Peninsula magnetic map with illumination angle A=125°, I=45°. Legend follows that of Figure 3.1.

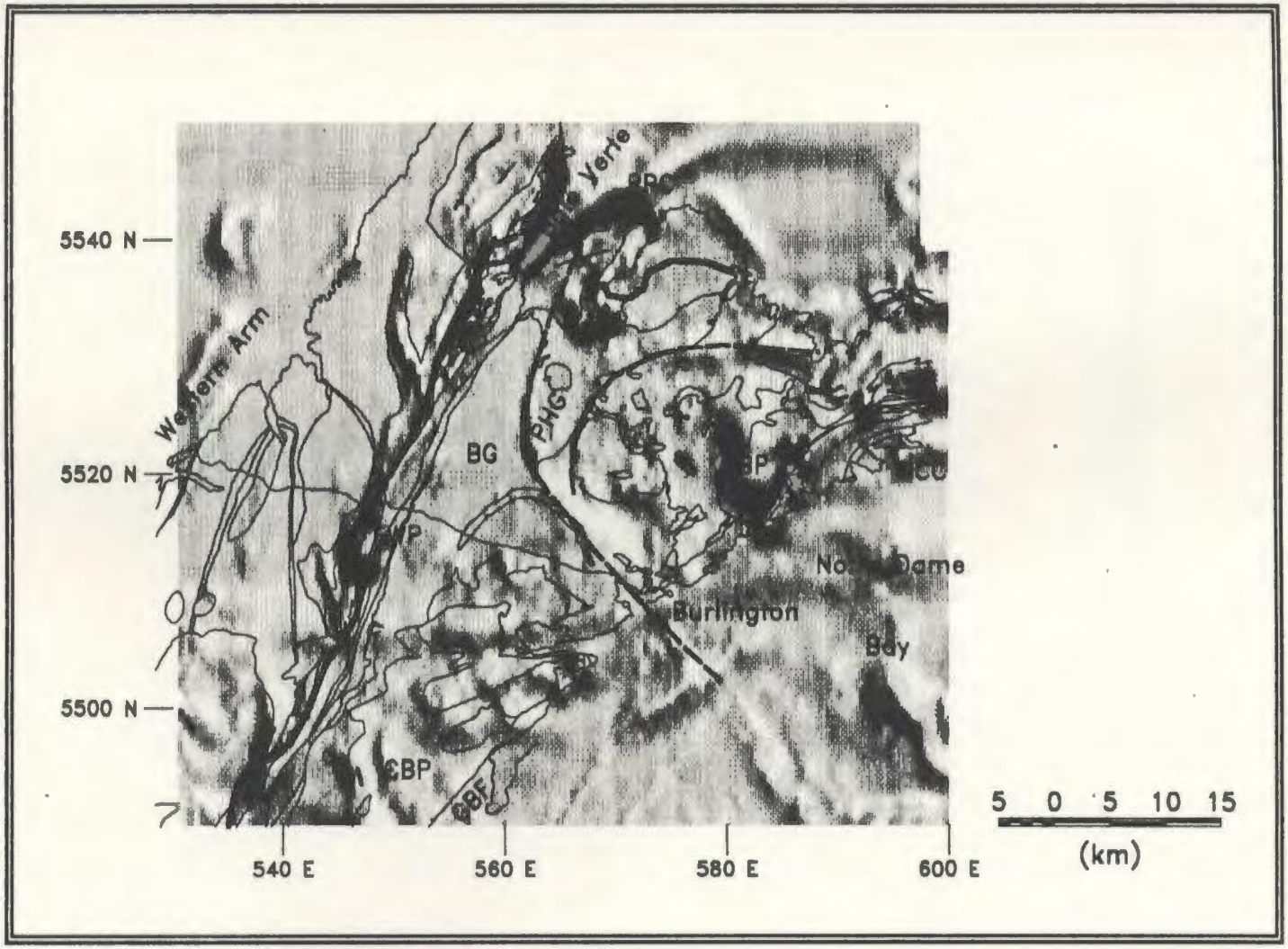

Figure 3.5(b): Shaded relief image of the Baie Verte Peninsula magnetic map with illumination angle A=40° , I=45°. Legend follows that of Figure 3.1.

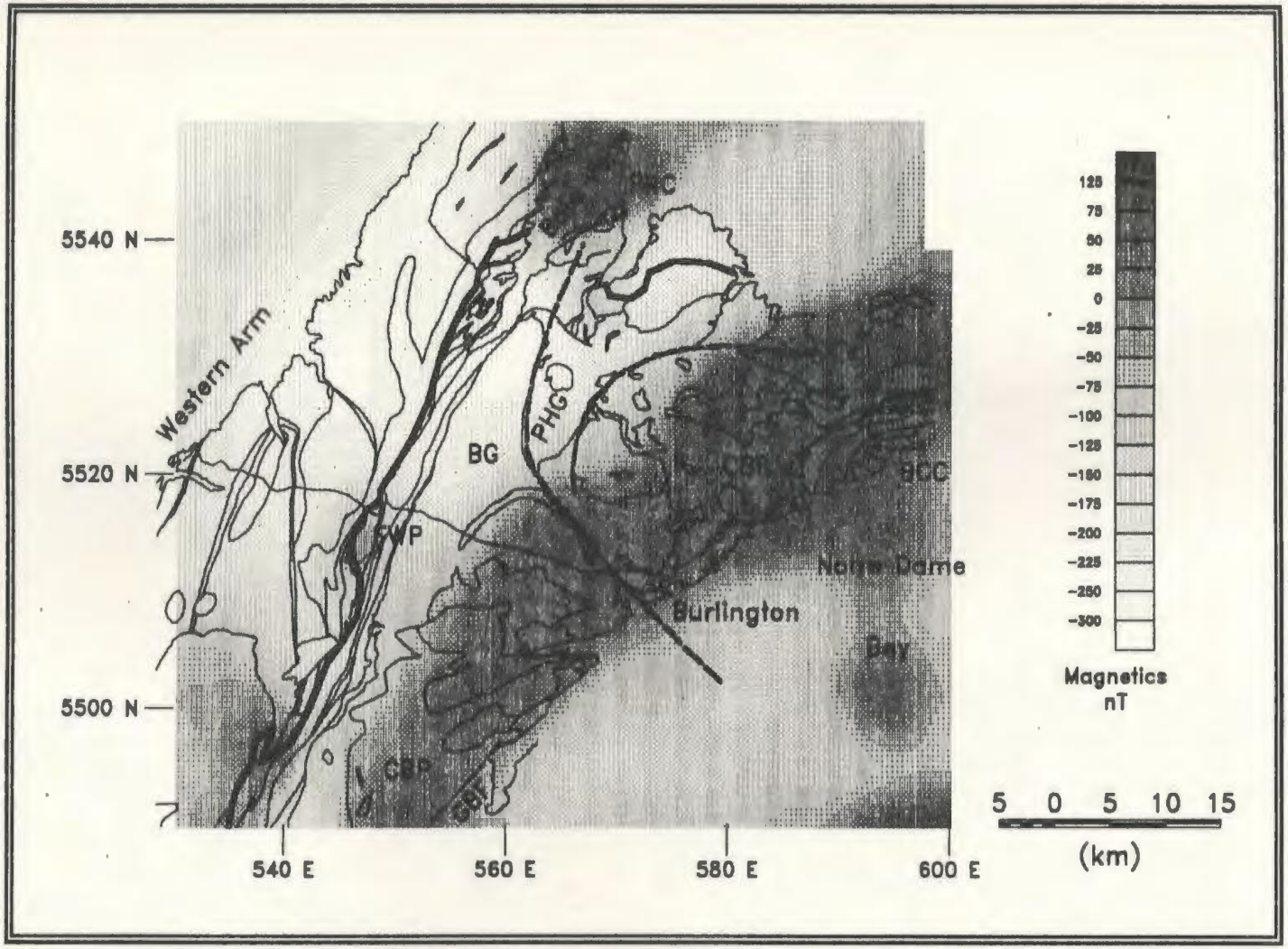

Figure 3.6(a): Magnetic field map of the Baie Verte Peninsula continued upward 3 km. The legend follows that of Figure 3.1.

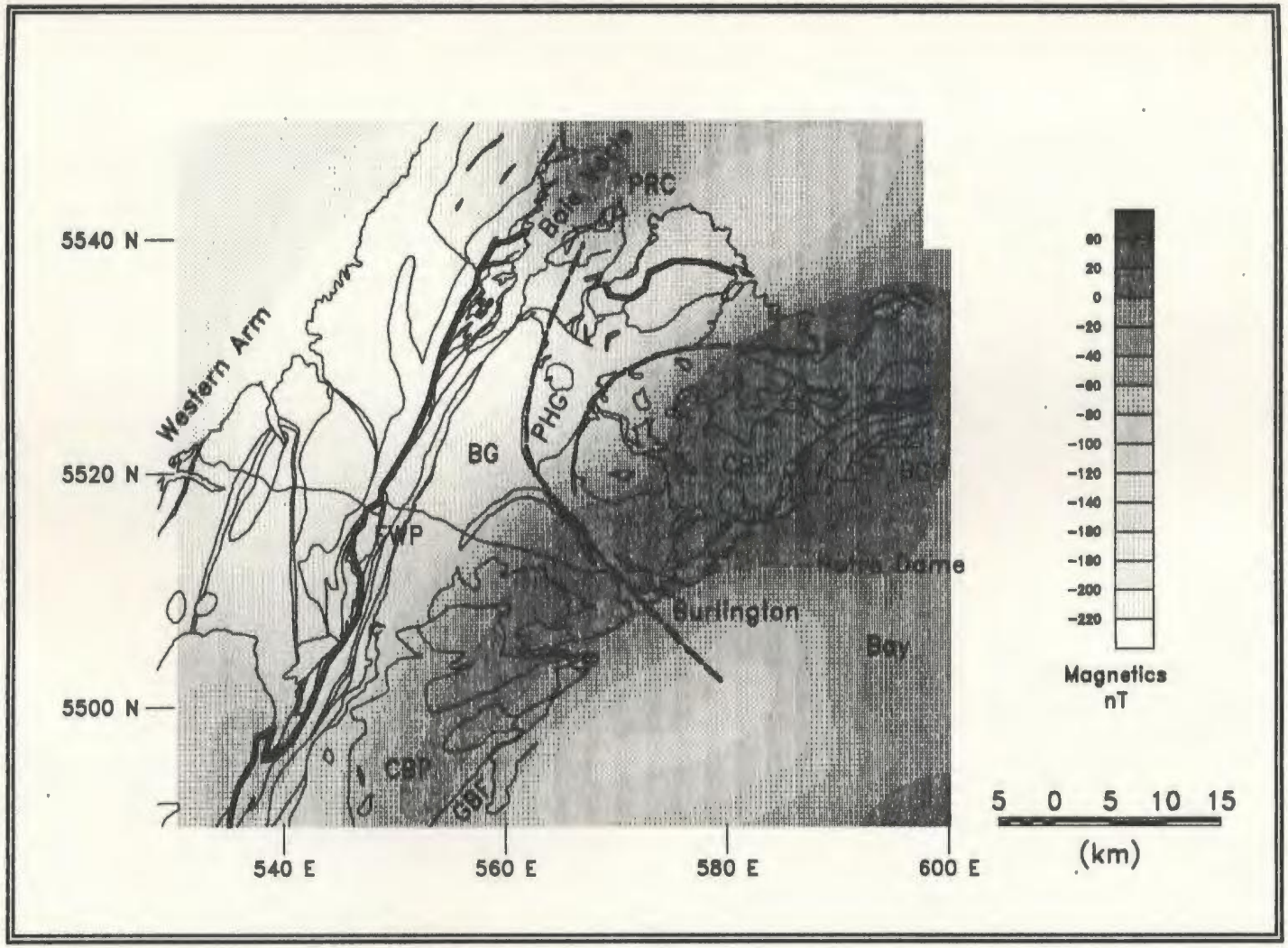

Figure 3.6(b): Magnetic field map of the Baie Verte Peninsula continued upward 6 km. The legend follows that of Figure 3.1.

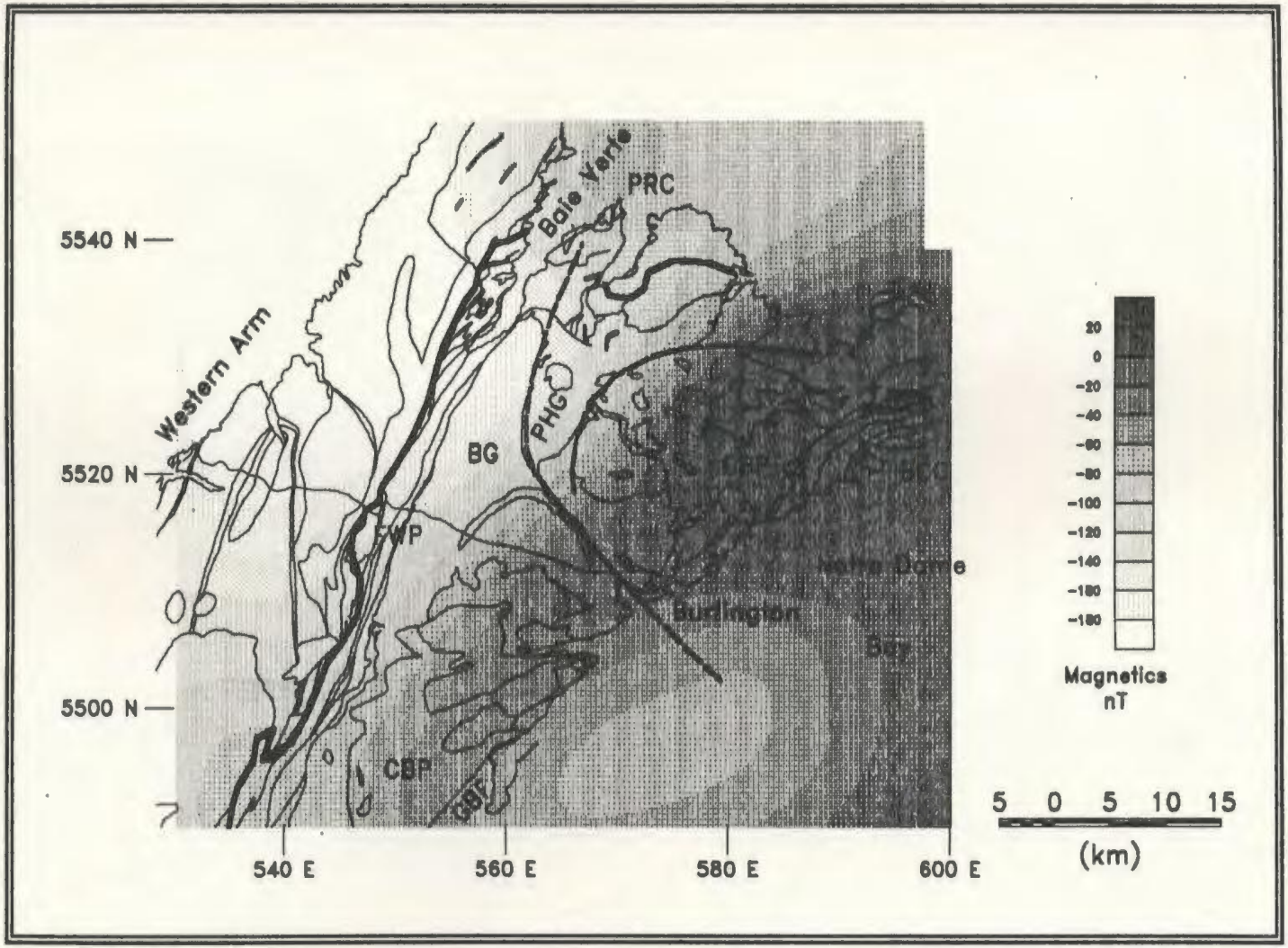

Figure 3.6(c): Magnetic field map of the Baie Verte Peninsula continued upward 10 km. The legend follows that of Figure 3.1.

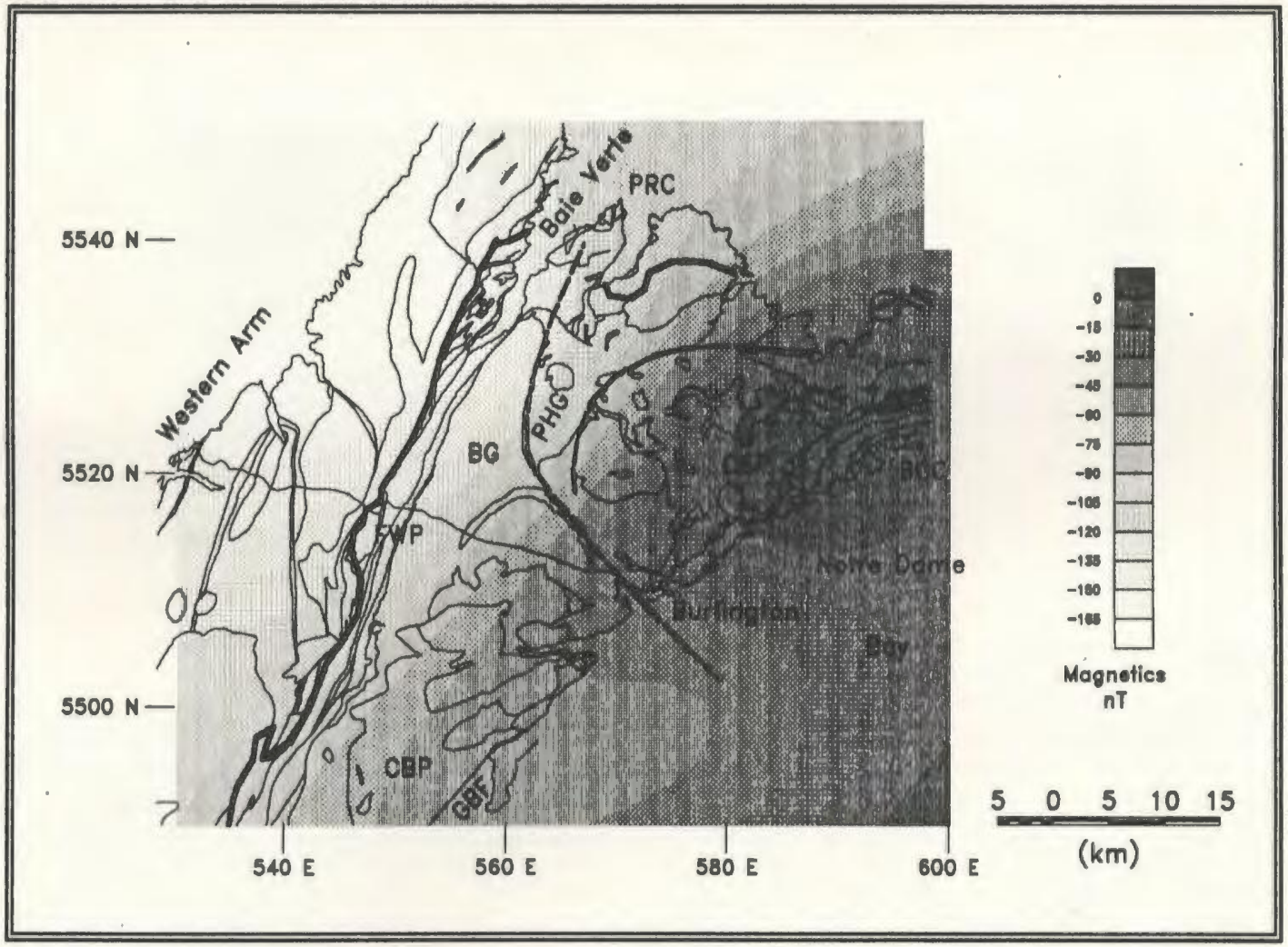

Figure 3.6(d): Magnetic field map of the Baie Verte Peninsula continued upward 15 km. The legend follows that of Figure 3.1.

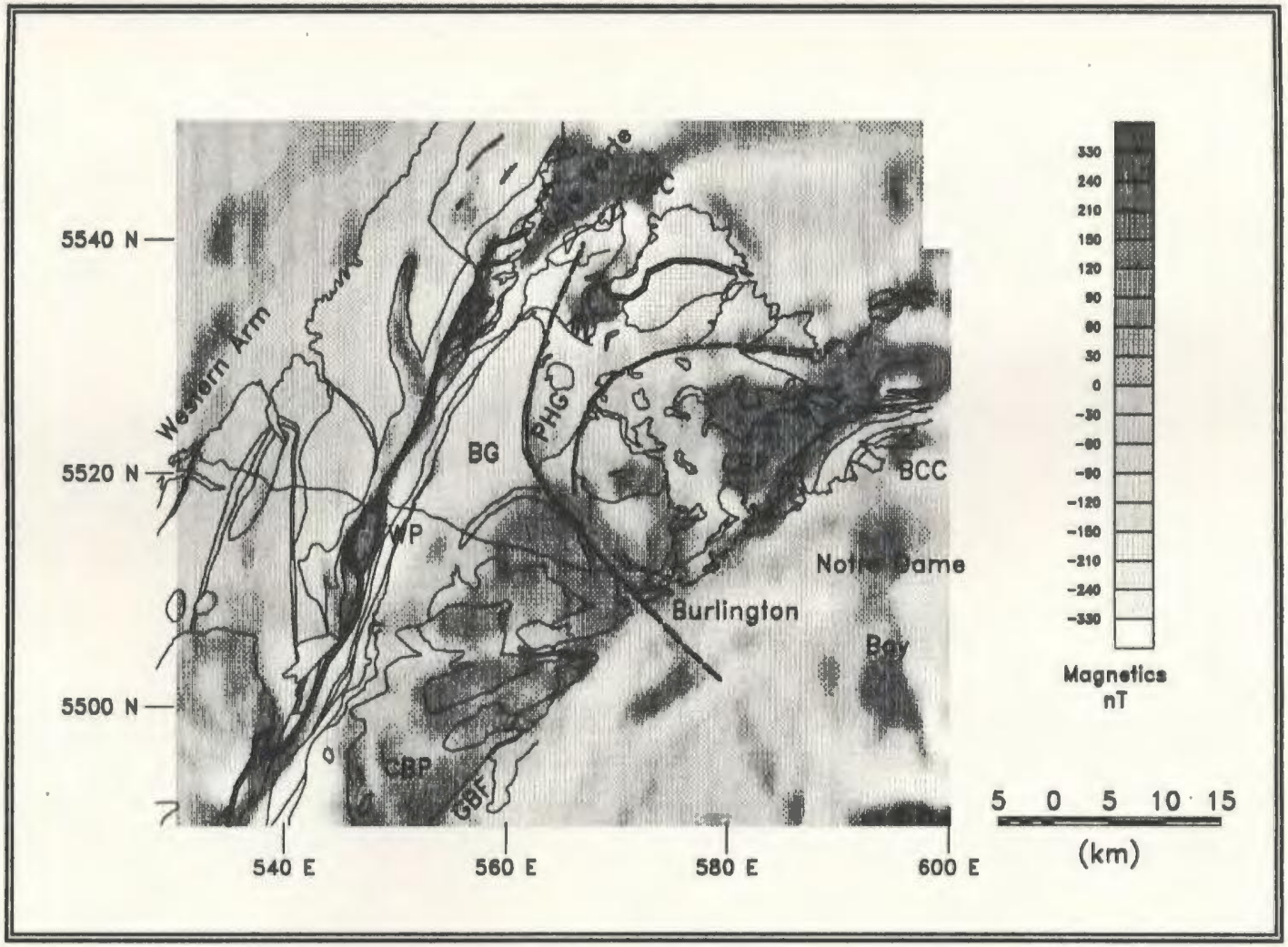

Figure 3.7(a): Magnetic Layer strip map (Jacobson, 1987) for sources within the upper 1.5 km. The legend follows that of Figure 3.1.

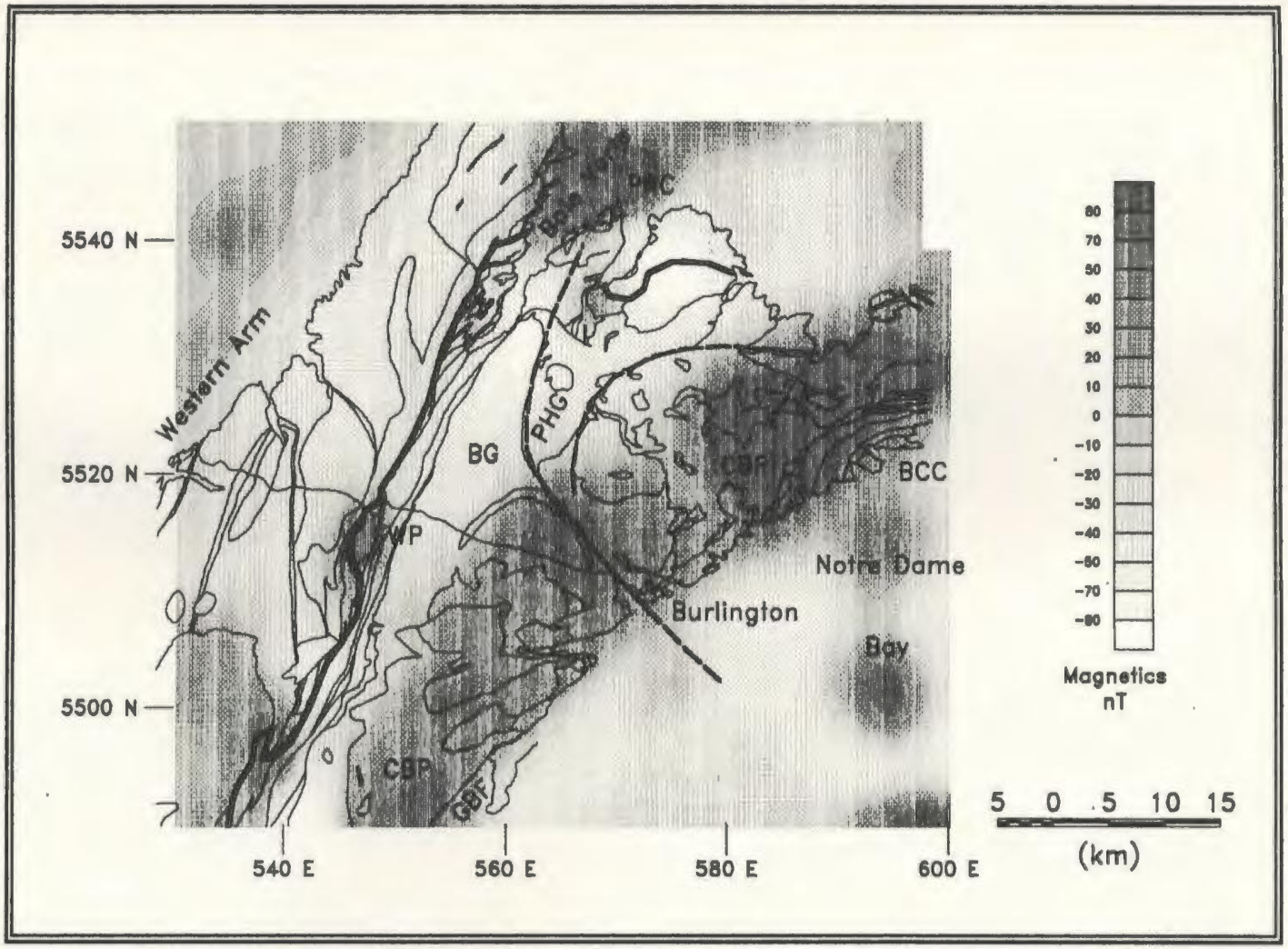

Figure 3.7(b): Magnetic Layer strip map (Jacobson, 1987) for sources between 1.5 and 3 km depths. The legend follows that of Figure 3.1.

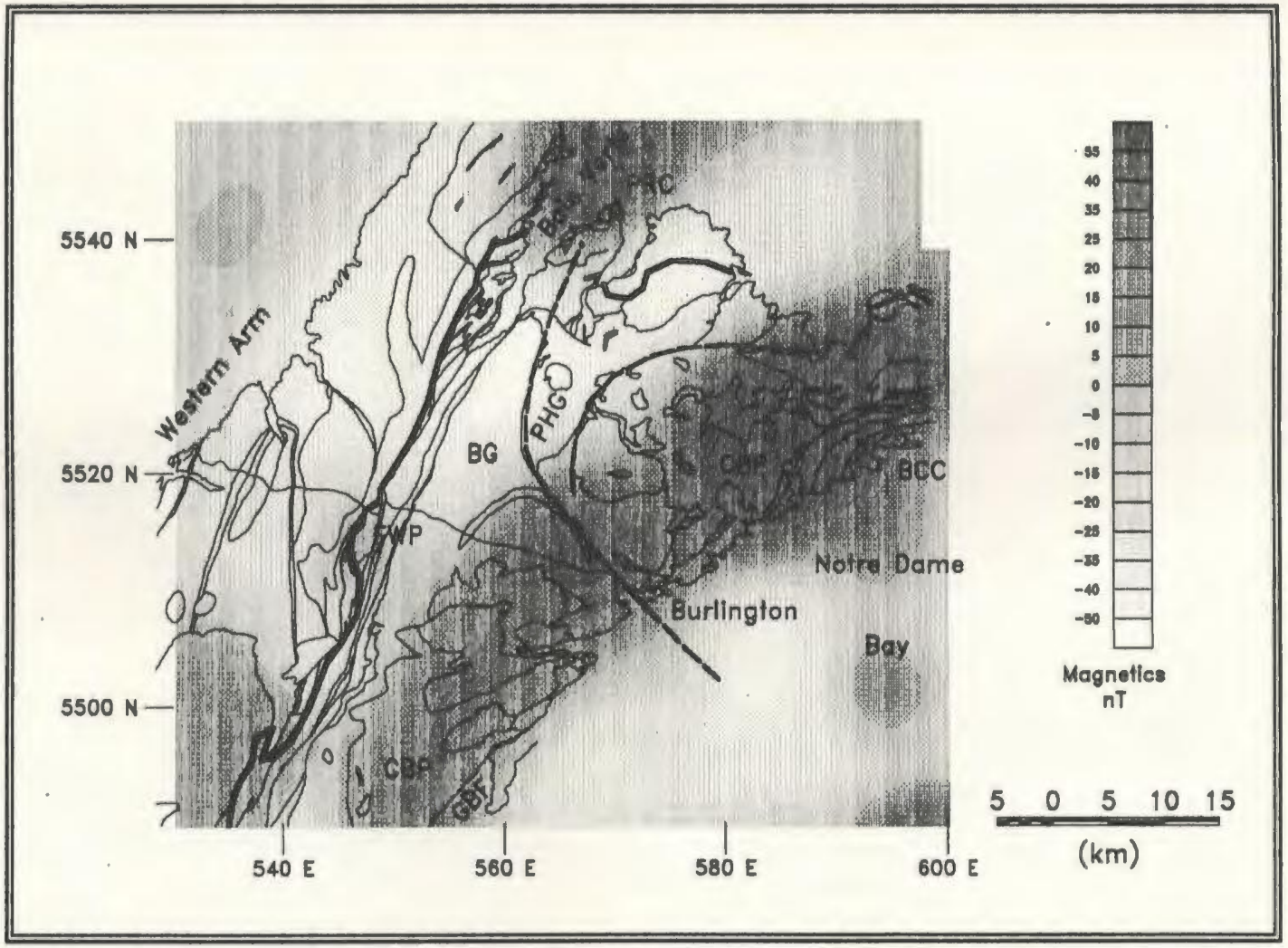

Figure 3.7(c): Magnetic Layer strip map (Jacobson, 1987) for sources between 3 and 5 km depths. The legend follows that of Figure 3.1.

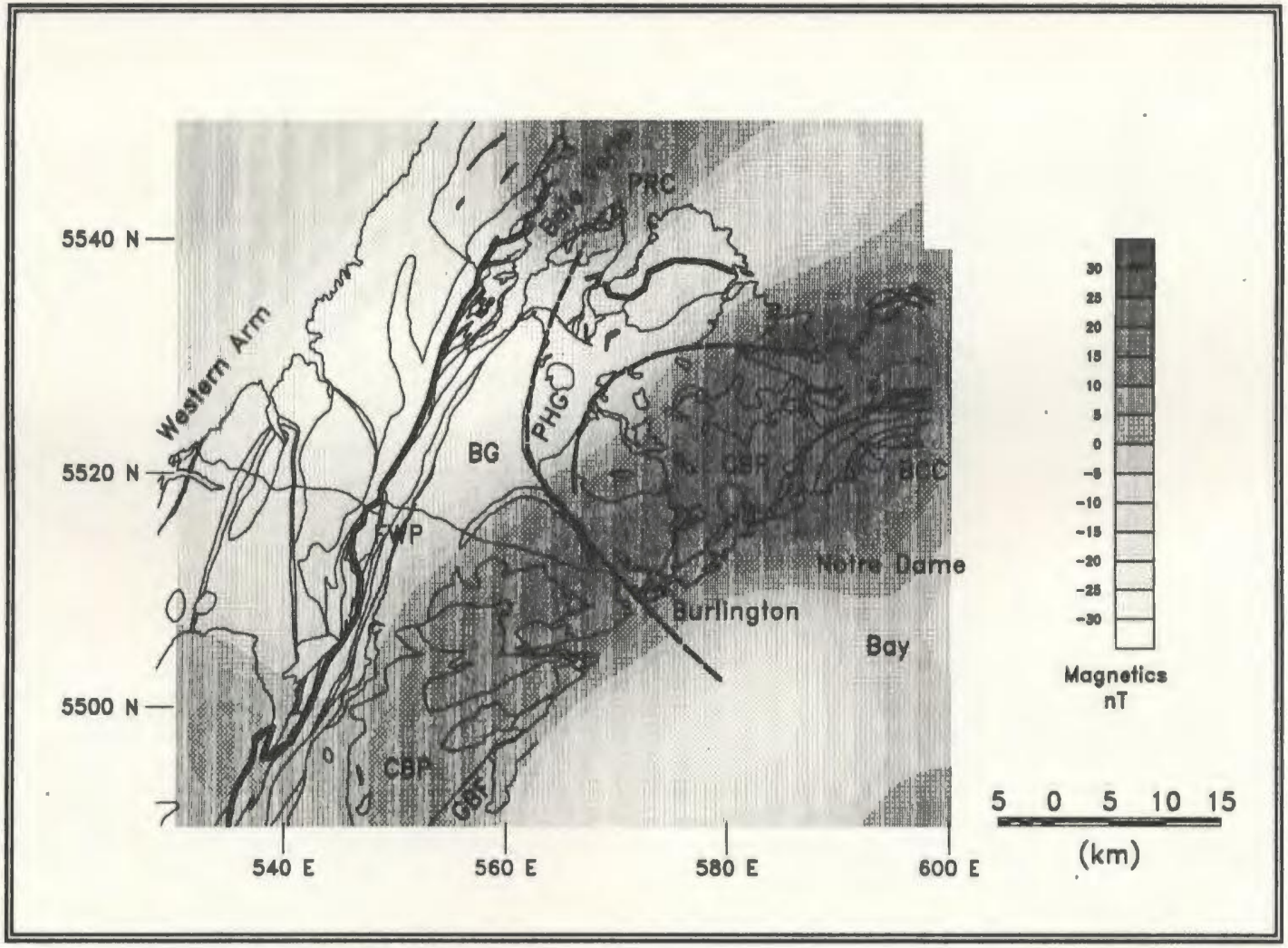

Figure 3.7(d): Magnetic Layer strip map (Jacobson, 1987) for sources between 5 and 7.5 km depths. The legend follows that of Figure 3.1.

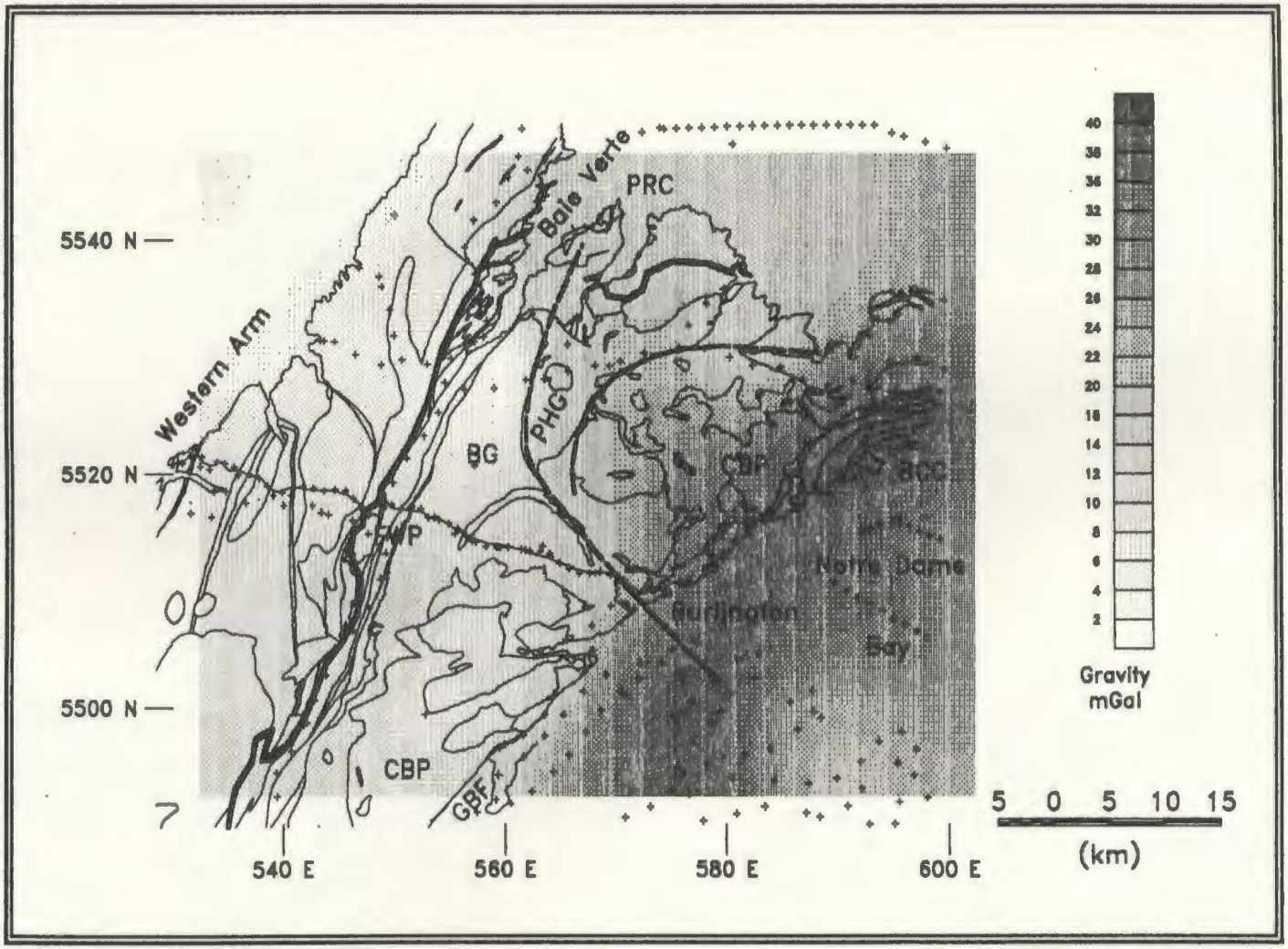

Figure 3.8: Gravity map for the Baie Verte Peninsula. The small plus signs indicate the location of gravity stations. The other symbols follow the legend of Figure 3.1.

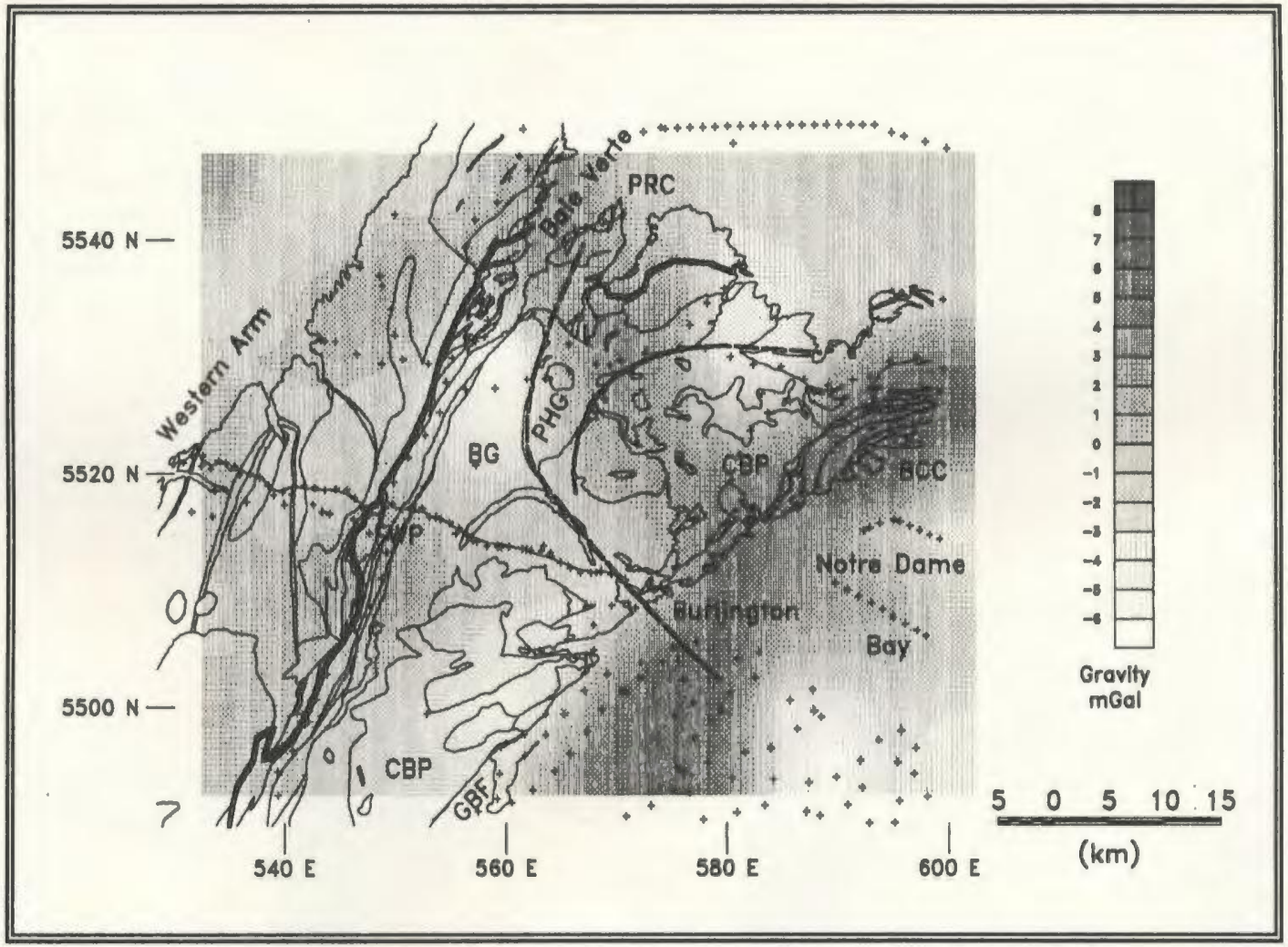

Figure 3.9(b): Residual gravity map calculated by subtraction of a high pass gausian filter with central peak at 0.025 cycles/km. The legend follows that of Figure 3.8.

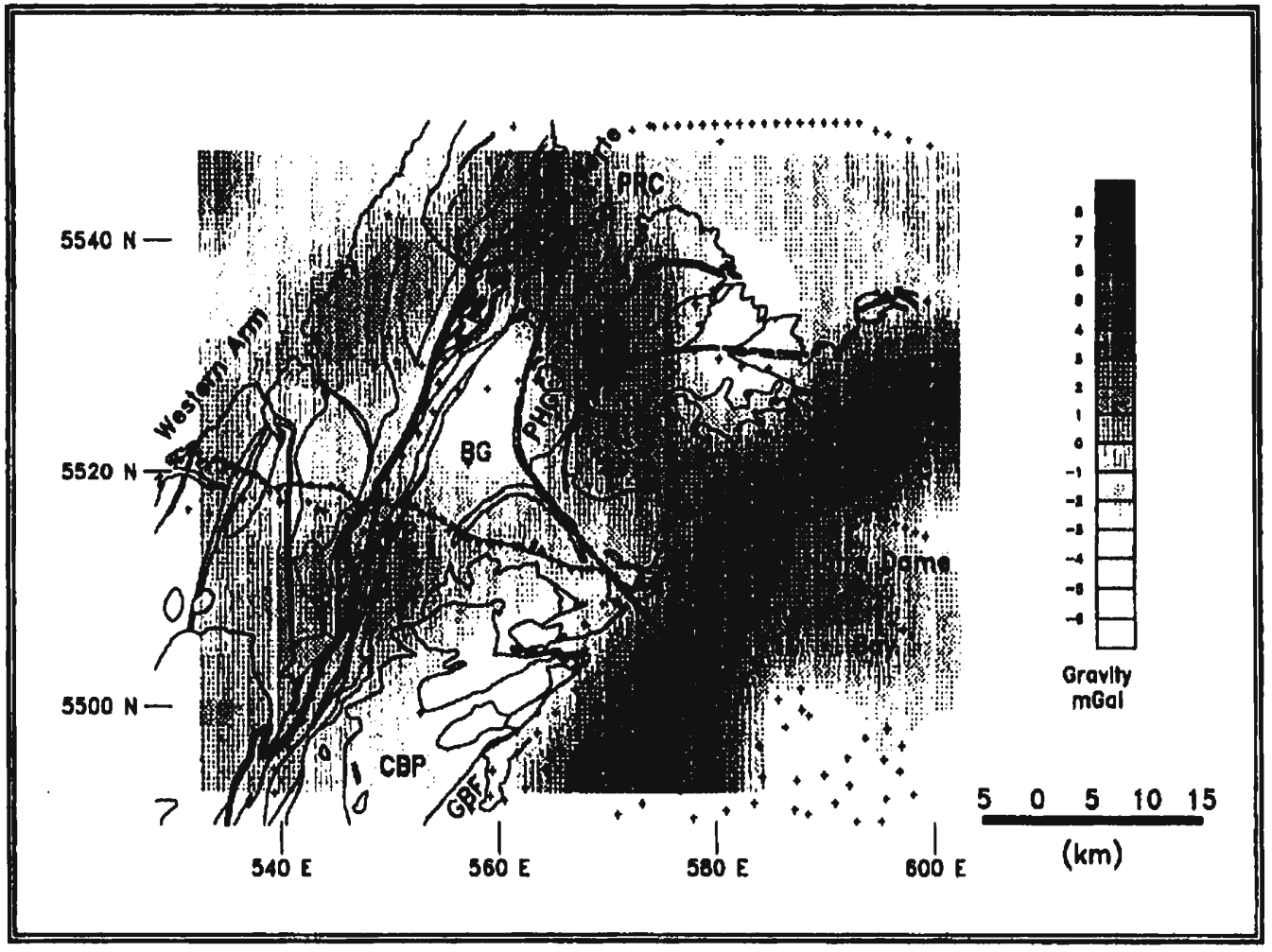

Figure 3.9(b): Residual gravity map calculated by subtraction of a high pass gaussian filter with central peak at 0.025 cycles/km. The legend follows that of Figure 3.8.

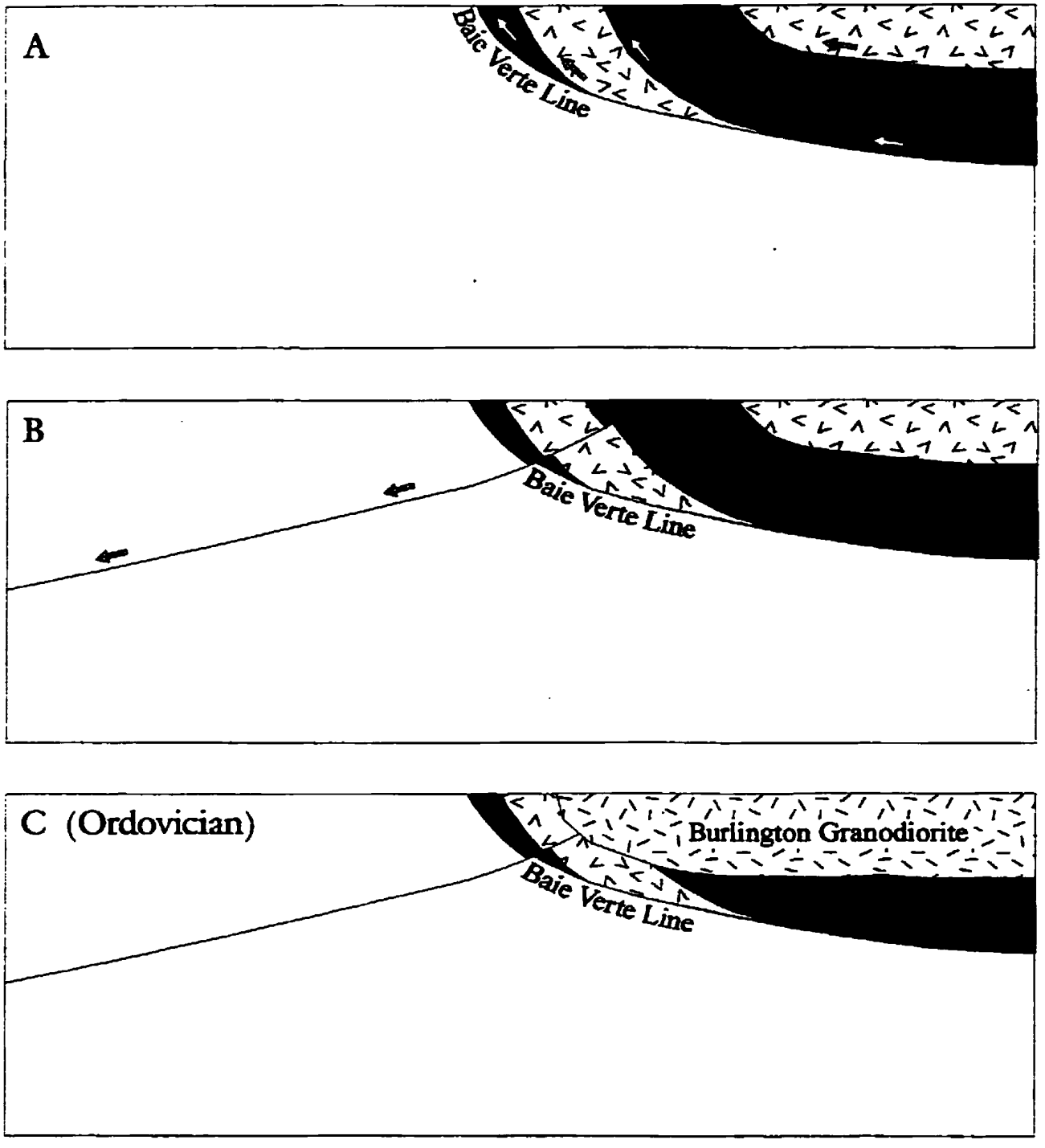

Figure 3.10: Geological evolution of the Burlington Transect (LE89-13). The current structure can be explained by three stages: (A) emplacement of ophiolite units by imbricate thrusting towards the west, (B) a stage of strike-slip motion with slight extension, and (C) emplacement of late-tectonic intrusives.

4.0. BURGEO ROAD TRANSECT:

4.1. GEOLOGY:

The Burgeo Road Transect, in southwestern Newfoundland, as discussed here, includes Lithoprobe East Vibroseis lines LE89-11 and LE89-12. Line LE89-12, the western part of the Burgeo Road Transect, covers part of the Port au Port Highway and part of the Trans Canada Highway. Line LE89-11, the eastern and southern part of the transect, follows the Burgeo Road from its intersection with the Trans Canada Highway to the town of Burgeo on the south coast of Newfoundland (Figure 4.1).

The Burgeo Road Transect crosses several surface structural zone boundaries as defined by Williams (1979) and Williams et al. (1988). From west to east the transect crosses the Long Range Fault (**LRF**), the Lloyd's River Fault (**LLRF**), the Victoria River Fault (**VRF**), the Cape Ray Fault (**CRF**), and the Bay D'Est Fault Zone (**BDF**) (see Figures 4.1 and 4.2).

The Long Range Fault (**LRF**), the surface boundary between the Humber Zone to the northwest and the Dunnage Zone to the southeast, is considered to be equivalent to the Baie Verte Line (Williams, 1979; Williams et al., 1988) (Figure 4.2).

Part of the Lloyd's River Fault (**LLRF**), which joins the Cape Ray Fault (**CRF**) to the south, is the boundary between the Dunnage Zone to the northwest and the Gander Zone to the

southeast (Williams, 1979; Williams et al., 1988) (Figure 4.2) and part is the northwestern boundary of the Annieopsquotch ophiolite complex (AC) (Figure 4.1) which also marks the junction of the Notre Dame and Exploits subzones of the Dunnage Zone (Figure 4.2). This fault is considered to be part of the Red Indian Line, which divides the Notre Dame subzone of the Dunnage Zone from the Exploits subzone of the Dunnage Zone (Williams et al., 1988) (Figure 1.1).

West of where the Lloyd's River Fault (LRF) converges with it, the Cape Ray Fault (CRF) serves as the division between Notre Dame subzone rocks to the northwest and Exploits subzone rocks to the southeast (Figure 4.2). East of this position, the Cape Ray Fault (CRF) separates Gander Zone rocks to the north from Dunnage Zone rocks to the south (Williams et al., 1988) (Figure 4.2).

The Bay D'Est Fault zone (BDF) separates Dunnage Zone rocks to the north from Gander Zone rocks to the south (Williams et al., 1988) (Figure 4.2).

The Humber Zone rocks west of the Long Range Fault in this area consist of Grenville basement exposed in the Indian Head Inlier (IHI) and Steel Mountain Anorthosite (SMA) (van Berkil et al., 1985). This basement includes anorthosite (Steel Mountain Anorthosite), tonalite-diorite, norite, and hornblende-biotite gneiss. These are overlain by low grade pelitic and calcareous schists, followed by Cambro-Ordovician

carbonate units found towards the northwest. Towards the east margin of Bay St. George (BSG) are Carboniferous sedimentary rocks (CB) unconformably overlying the Grenville basement (van Berkil et al., 1985).

The Dunnage Zone rocks between the Long Range Fault (LRF) and Lloyd's River Fault (LLRF) consist of migmatized psammitic, pelitic and calcareous gneiss of the Central Gneiss Terrane. These rocks contain thin strips of foliated and partially chloritized serpentinites, which appear to be of much lower metamorphic grade than their host (van Berkil et al., 1985). Intruded into these gneisses are many large plutons of late-tectonic granite and granodiorite (van Berkil et al., 1985).

The Lower Ordovician Annieopsquotch ophiolite complex (AC), also part of the Dunnage Zone, lies between the Lloyd's River Fault (LLRF) and the Victoria River Fault (VRF). This complex contains the complete ophiolite stratigraphy from the layered cumulates through to high-level gabbro and sheeted dykes, to pillow lavas, all dipping to the southeast (Dunning and Herd, 1980; Dunning, 1981; Dunning and Chorlton, 1985). This complex is considered to be part of the broader Annieopsquotch ophiolite belt which consists of ophiolite fragments stretching from southwest Newfoundland to the Buchans area in central Newfoundland (Dunning, 1981; Dunning and Chorlton, 1985).

The Gander Zone (Meelpaeg subzone) rocks southeast of the Victoria River Fault (VRF) and north of the Cape Ray Fault (CRF) consist of metaclastics intruded by large, foliated and locally mylonitic granites (van Berkil et al., 1985; Williams et al., 1988).

Between the Cape Ray Fault (CRF) and the Bay D'Est Fault Zone (BDF) lie Dunnage Zone (Exploits subzone) rocks. Here, these rocks are metamorphosed submarine volcanics and marine siliciclastic sediments, intruded by mid-Paleozoic granitoids (Chorlton, 1980).

South of the Bay D'Est Fault Zone (BDF) are metasediments intruded by many large, foliated to mylonitic granitoids (Williams et al., 1988; O'Brien and O'Brien, 1989).

4.2. GEOPHYSICS:

4.2.1. Seismic Reflection:

The Burgeo Road Transect, as defined here, consists of two Lithoprobe East Vibroseis lines (LE89-11 and LE89-12) forming an arcuate transect approximately 160 km long across the southwestern tip of the island of Newfoundland (Figures 1.2 and 4.1). Seismic lines LE89-11 and LE89-12 were modelled separately. Only the part of LE89-12 which runs perpendicular to regional geology is examined by potential field methods here; the section running parallel to regional geology was not modelled. Line drawings modified from Quinlan et al. (1992)

of the migrated seismic reflection data for portions of LE89-11 and LE89-12 corresponding to the potential field transects are presented in Figures 4.3 and 4.4 respectively.

It should be noted that seismic line LE89-11 cuts major geologic trends obliquely, and out-of-the-plane reflections are to be expected. This probably explains the noisy character of this line.

The Vibroseis data shows two predominant reflector trends, particulary for Line 89-11. In the upper part of the profile, the reflection data is dominated by southeast-dipping reflectors (E), while northwest-dipping reflectors (W) appear to dominate middle to lower depths (Figure 4.4). In most cases the northwest-dipping reflectors (W) cut the southeast-dipping reflectors (E) (Quinlan et al., 1992).

A notable exception to this generalization is the southeast-dipping reflector (A) in the southeastern end of LE89-11 (Figure 4.4). This reflector clearly cuts several northwest-dipping reflectors (W). This reflector is interpreted to be the Cape Ray Fault (CRF), and the latest motion along this fault is more recent than motion along the other faults (Quinlan et al., 1992).

The Moho (M) occurs at about 12 seconds TWT on much of LE89-11 and LE89-12, but appears to deepen at the southeastern end of LE89-11 (Figure 4.4). Here, it appears to be offset by some of the northwest-dipping reflectors.

4.2.2. Magnetics:

The most obvious feature on the total field magnetic map (Figure 4.5) and the reduced to the magnetic pole map (Figure 4.6) is the large magnetic high over much of the Central Gneiss Terrane near the centre of the map. Comparing the areal extent of this anomaly with the geology compiled by Colman-Sadd et al. (1990) (black lines on Figure 4.5) and a more detailed compilation by van Berkil and Currie (1986), it is obvious that in general the areas of high magnetic values correlate with the surface exposure of foliated granitoid orthogneisses (go - Figure 4.1) containing a hornblende+biotite+magnetite assemblage (van Berkil, Johnston, and Currie, 1985). The other areas of the Central Gneiss Terrane contain paragneisses (gp - Figure 4.1) with a gedrite+pyrite assemblage (van Berkil et al., 1985) and have no associated magnetic high.

The northeastern edge of this anomaly appears as a straight line trending NW-SE (Figure 4.5) and does not correlate with any mapped geologic boundary. The straight character of this edge suggests that the boundary may be fault controlled. Although there is no geologic evidence to support this suggestion, the topography and stream orientations in this region do reflect this linear trend. Also, many of the mapped boundaries by van Berkil and Currie (1986) are not observed crossing this region.

Examining the shaded relief images (Figures 4.7a,b), the complex internal structure of the Central Gneiss Terrane anomaly becomes apparent, especially when the false sun azimuth is at 40° (Figure 4.7b). This reflects the structurally complex geology as mapped by van Berkil and Currie (1986) found within the Central Gneiss Terrane. This complexity is also enhanced in the horizontal gradient map (Figure 4.8) and the second vertical derivative map (Figure 4.9). This type of pattern is typical of metamorphic terranes where strong metamorphism and deformation have occurred.

Upward continuation maps (Figures 4.10a,b,c,d) and depth separation maps following the method of Jacobson (1987) (Figures 4.11a,b,c,d) indicate that the long wavelength part of this Central Gneiss Terrane anomaly originates from magnetic material at depths exceeding 5 km.

Many of the mapped faults shown on Figure 4.1 correspond with magnetic lows. The Long Range Fault (**LRF**) appears as a magnetic low between the high of the Central Gneiss Terrane and the magnetic high over the Steel Mountain Anorthosite (**SMA**) (Figure 4.5). The Lloyd's River Fault (**LLRF**) and Victoria River Fault (**VRF**) appear as magnetic lows around the edge of the Annieopsquotch Complex (**AC**) (Figure 4.5). The Cape Ray Fault (**CRF**), along much of its extent in this area, divides the magnetic high of the Central Gneiss Terrane from the lower amplitude anomalies to the south (Figure 4.5).

The Annieopsquotch Complex (AC) is characterized by a significant magnetic high over the northwestern part of the complex comprised of gabbro and diabase, while the other rock types found along the southern half of the complex appear to have little or no anomaly associated with them (Figure 4.5). Although there are no specific rock magnetic susceptibility data available for the Annieopsquotch Complex, gabbro and diabase typically have higher magnetic susceptibilities than mafic volcanics and sediments. The layer stripping maps (Figures 4.11a,b,c,d) suggest that the anomaly associated with the Annieopsquotch Complex has a significant component derived from depths exceeding 5 km. Whether this is due to the ophiolite itself or something else beneath it, is unresolvable by this method. Magnetic modelling, however, can be used to resolve this dilemma.

Other magnetic highs occur above the exposures of Grenville basement, such as the Steel Mountain Anorthosite (SMA), Indian Head Inlier (IHI), and the small anorthosite exposure in the Flat Bay Anticline (FBA) east of Bay St. George (BSG) (Figure 4.5).

The anomaly associated with the Steel Mountain Anorthosite (SMA) consists of several short-wavelength linear trends oriented roughly in a NE-SW direction (Figure 4.5). These are highlighted well on the shaded relief image with false sun illumination azimuth of 115° (Figure 4.7a), the

magnetic horizontal derivative map (Figure 4.8), and the magnetic second vertical derivative map (Figure 4.9). These linear anomalies appear to be predominantly shallow sourced (Figure 4.11a) and appear to correlate with gabbroic portions of the body (van Berkil and Currie, 1986). The layer stripping method (Jacobson, 1987) also shows a more subtle longer wavelength anomaly (Figure 4.11b) associated with this body which indicates that it extends to significant depths.

The Indian Head Inlier (IHI) anomaly covers the whole extent of the surface exposure of the body (Figure 4.5). Layer stripping (Jacobson, 1987) indicates the Indian Head Inlier is a shallow body within the upper 3 km (Figures 4.11a,b,c,d). Below this depth, the peak amplitude of the anomaly is not significant being less than 15 nT (Figures 4.11c,d).

The anomaly associated with the small exposure of basement in the Flat Bay Anticline (FBA) in the Carboniferous basin (CB) is much larger in areal extent than the exposure itself (Figure 4.5). Since the sediments have insignificant magnetic susceptibility values (Miller et al., 1990), the magnetic basement likely extends beneath the basin in this location. Since this structure is mapped as an anticline (Knight, 1983), this is not surprising. Layer stripping maps (Jacobson, 1987) indicate that the basement beneath the basin is magnetic to depths exceeding 7.5 km (Figures 4.11a,b,c,d).

The Flat Bay Anticline (FBA) magnetic anomaly on these maps also shifts to the east as we progressively look at deeper layers. This suggests that the basement dips and the basin deepens to the east, which also correlates well with the anticlinal structure of the Flat Bay Anticline (FBA).

4.2.3. Gravity:

It is clear, looking at the Bouguer gravity map (Figure 4.12), that many of the major faults appear to be significant density boundaries. These include the Long Range Fault (LRF), the Cape Ray Fault (CRF), and the Victoria River Fault (VRF). When a second order regional trend is removed from the Bouguer field map (Figure 4.13), other density boundaries are enhanced. In addition to the faults mentioned above, the Bay D'Est Fault (BDF) and possibly the Lloyd's River Fault (LLRF) also appear to be density boundaries (Figure 4.13). The second vertical derivative of gravity map (Figure 4.14), and particularly the zero contour level of the smoothed second vertical derivative of gravity map (Figure 4.15), support the claim of the Bay D'Est Fault (BDF) being a subtle density boundary. The zero level contour, which should outline density boundaries (Gupta and Ramani, 1982), follows approximately the surface trace of the Long Range Fault (LRF), part of the Cape Ray Fault (CRF), and the Victoria River Fault (VRF). The horizontal gravity gradient map (Figure 4.16)

which should have maxima over density boundaries also highlights the Victoria River Fault (VRF), Cape Ray Fault (CRF), and the Long Range Fault (LRF). However the high gradient associated with the Long Range Fault appears to be shifted to the western side of the fault, indicating that the density boundary may be further to the west or that the boundary is dipping to the west. Modelling and seismic reflection data (Figure 4.3) indicate that the boundary dips to the east, so the first case is considered more likely. It should be noted that the resolution of the gravity anomalies is quite coarse, so some deviation from the true density boundaries is to be expected.

The Bouguer anomaly over most of the region is largely negative while the Central Gneiss Terrane and Topsail Terrane of the Notre Dame Subzone (Figure 4.2) exhibit a large positive anomaly locally exceeding 30 mGal (Figure 4.12).

In the Central Gneiss Terrane, the larger positive gravity anomalies appear to correlate with the regions of granitoid orthogneiss exposure (go - Figure 4.1). This is exhibited more clearly when a second order trend is removed from the Bouguer anomaly map (Figure 4.13). The second vertical derivative of the gravity map (Figure 4.14) also has the largest anomalies over the granitoid orthogneisses (go - Figure 4.1), although the whole western edge of the Central Gneiss Terrane appears as a relative high. This suggests that

the orthogneiss is denser than the paragneiss, which is a useful constraint for modelling as no rock density data for the Central Gneiss Terrane was available.

The Annieopsquotch Complex (AC) appears on the Bouguer gravity map (Figure 4.12) as a gravitational high. This is further emphasized when the second order regional trend is removed (Figure 4.13), and also on the second vertical derivative map (Figure 4.14).

The Indian Head Inlier (IHI) and Flat Bay Anticline (FBA), although not associated with distinctive Bouguer gravity anomalies (Figure 4.12), do have a signature on the second vertical derivative map (Figure 4.14). Furthermore, the two appear to both be linked as part of a NE-SW trending anomaly pattern on the second vertical derivative map (Figure 4.14). This link is particularly well demonstrated on the zero contour level of the second vertical derivative (Figure 4.15).

4.2.4. The Models:

The potential field 2½-D models for the Burgeo Road Transect are shown in Figures 4.3 and 4.4 along with the corresponding line drawings modified from Quinlan et al. (1992). As mentioned previously, two transects were modelled for this line. In each case, the horizontal and vertical scales of both the seismic profile and the potential field

model are the same. The horizontal scale drawn on the potential field model applies to both the model and the seismic section. In the case of LE89-12 (Fig. 4.3) only the western 23 kilometers, the section running perpendicular to regional geology, are modelled.

No regional trend was removed from the gravity or magnetic data prior to modelling.

Unfortunately, no samples for magnetic susceptibility and density measurements were collected specifically along the Burgeo Road Transect, so some previously published values (Miller et al. 1990) for the Bay St. George area were used as well as a limited set of magnetic susceptibility and density measurements for the southern end of this line (Table 1). The Annieopsquotch Complex was assigned a density and magnetic susceptibility similar to other Dunnage Terrane ophiolites from other parts of Newfoundland (Miller and Wiseman 1993; Miller and Deutsch 1976). Other units were assigned physical property values using tables of physical properties for various rock types (Telford et al. 1976).

The predominant modelled features causing gravity anomalies along the Burgeo Road Transect are low density ($\Delta\rho$=-0.04 g/cm^3) sediments in the Carboniferous basin (CB), high density gneisses ($\Delta\rho$=0.04 to 0.23 g/cm^3) within the Central Gneiss Terrane, and low density granites towards the southern end of the transect (Figure 4.3). Gravity modelling suggests

that the low density sediments ($\Delta\rho$=-0.04 g/cm^3) in the Carboniferous basin (CB) are approximately 2.5 km thick where the profile crosses (Figure 4.3).

The Central Gneiss Terrane is required to have zones of different density contrast ($\Delta\rho$=0.04 g/cm^3 primarily, with a zone of $\Delta\rho$=0.23 g/cm^3) to explain the observed Bouguer field. The anomalous density zone within the Central Gneiss show different reflectivity patterns on the Vibroseis data from the rest of the terrane. The high density block ($\Delta\rho$=0.23 g/cm^3) along the western edge of the Central Gneiss Terrane corresponds to a non-reflective zone (N) on the seismic data, while the other high density block ($\Delta\rho$=0.20 g/cm^3) along the eastern edge, corresponds to a zone of high seismic reflectivity (R) (Figure 4.4). The Central Gneiss is modelled with a uniform magnetic susceptibility of 0.00 c.g.s. except for numerous shallow mafic intrusions with varying magnetic susceptibilities (Figure 4.4).

Towards the south end of the Burgeo Road Transect, the various low density granites and sediments are responsible for the negative Bouguer anomalies (Figure 4.4).

The Annieopsquotch Complex (AC) is modelled as an east-dipping body with a modelled density contrast of 0.27 g/cm^3 and magnetic susceptibility of 3.50 x 10^{-3} c.g.s.

In general, the bodies modelled for the gravity and magnetic profiles corresponding to the Burgeo Road Transect

are in agreement with the location of seismic reflectors. Units are seen to dip southeast in the upper part of the crust, and in the deeper part they dip northwest. Gravity and magnetic anomalies in the Burgeo Road region arise from sources within the upper 15 km of the crust. Deeper anomalous density or magnetic susceptibility regions are not required to fit the observed data.

4.3. INTERPRETATION:

Seismic data indicates that all the major faults within the Burgeo Road region are dipping to the southeast. This is supported by the potential field modelling for the Burgeo Road Transect. For the most part, motion along the northwest dipping faults postdates motion along southeast dipping faults (Figure 4.4). An exception to this generalization is the southeast dipping Cape Ray Fault (reflector A) for which motion obviously occurred later than the northwest dipping faults it cuts (Figure 4.4).

The rocks of the Notre Dame Subzone of the Dunnage Zone (Central Gneiss Terrane and Topsail Terrane) are notably higher density than rocks of the other zones in this region. Therefore, the fault boundaries of the Notre Dame Subzone are significant density boundaries. These include the Long Range Fault (LRF), the Lloyd's River Fault (LLRF), and the Cape Ray Fault (CRF). The Annieopsquotch Complex (AC) also has a

significantly high density due to mafic and ultramafic components, and also dips to the southeast.

Magnetic anomalies over the region are predominantly controlled by shallow gabbro intrusions, although gabbro, diabase, and anorthosite of the Grenville basement have high magnetic susceptibility values. Part of the Annieopsquotch Complex (AC) also has a high magnetic susceptibility, as is obvious from the magnetic anomaly associated with it.

A possible geological evolution of the structure along the Burgeo Road Transect is presented in Figure 4.17. Allochthonous Dunnage and Gander Zone material is emplaced upon continental crust by thrusting from the east during the closing of the Iapetus Ocean.

Tectonic compression was followed by a period of crustal extension. Movement during this stage occurred predominantly along shallow northwest-dipping normal faults.

Following this, the region underwent another stage of compression with northwest directed thrusting in the eastern portion of the Orogen (Cape Ray Fault).

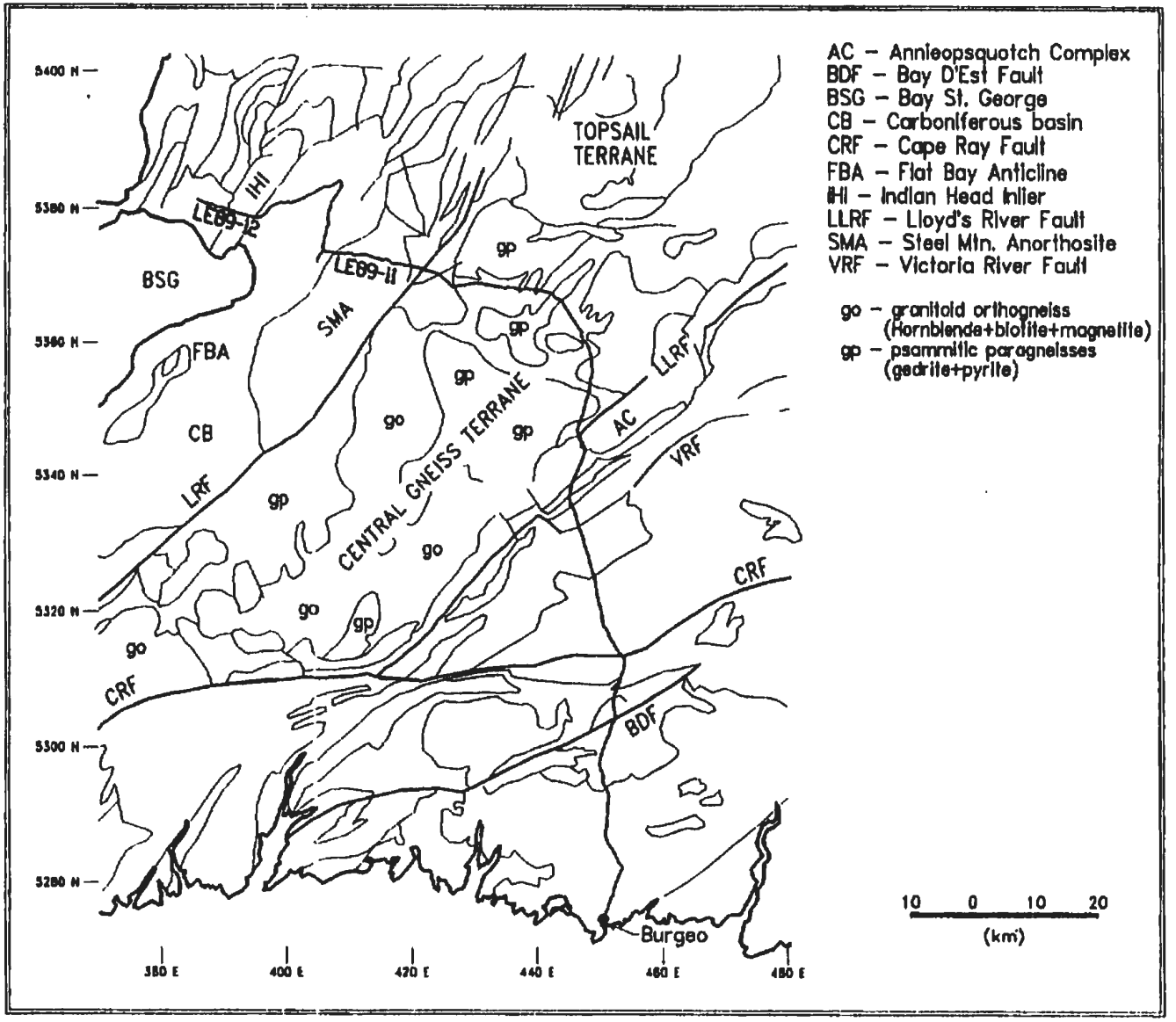

Figure 4.1: Geology map of the Burgeo Road region (after Colman-Sadd et al., 1990). The location of lines LE89-11 and LE89-12 are shown. Coordinates are in UTM Zone 21 kilometers. The legend is shown in the upper right.

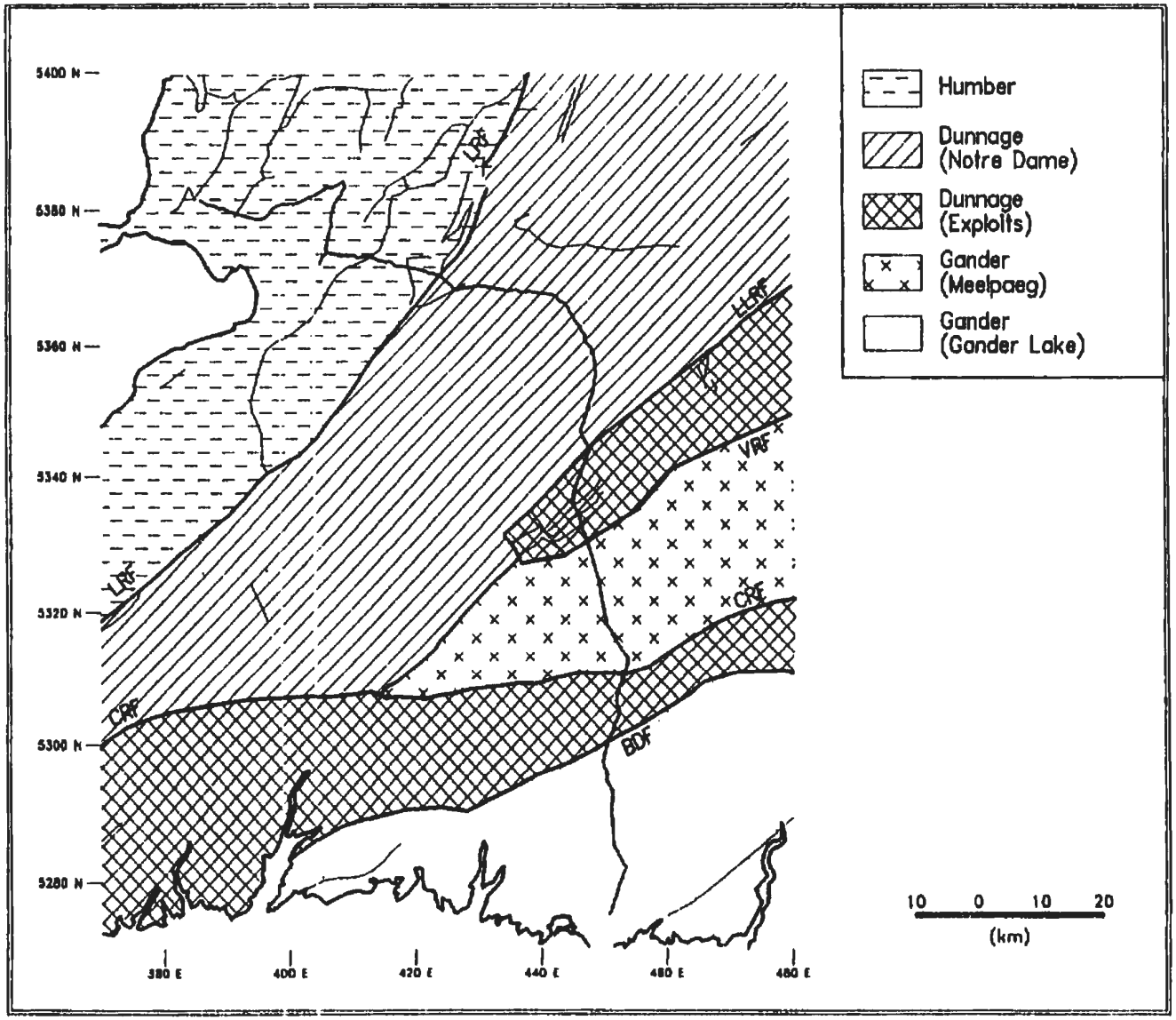

Figure 4.2: Tectono-stratigraphic zones for the Burgeo Road region, and the location of Lithoprobe East lines LE89-11 and LE89-12. The legend follows that of Figure 4.1.

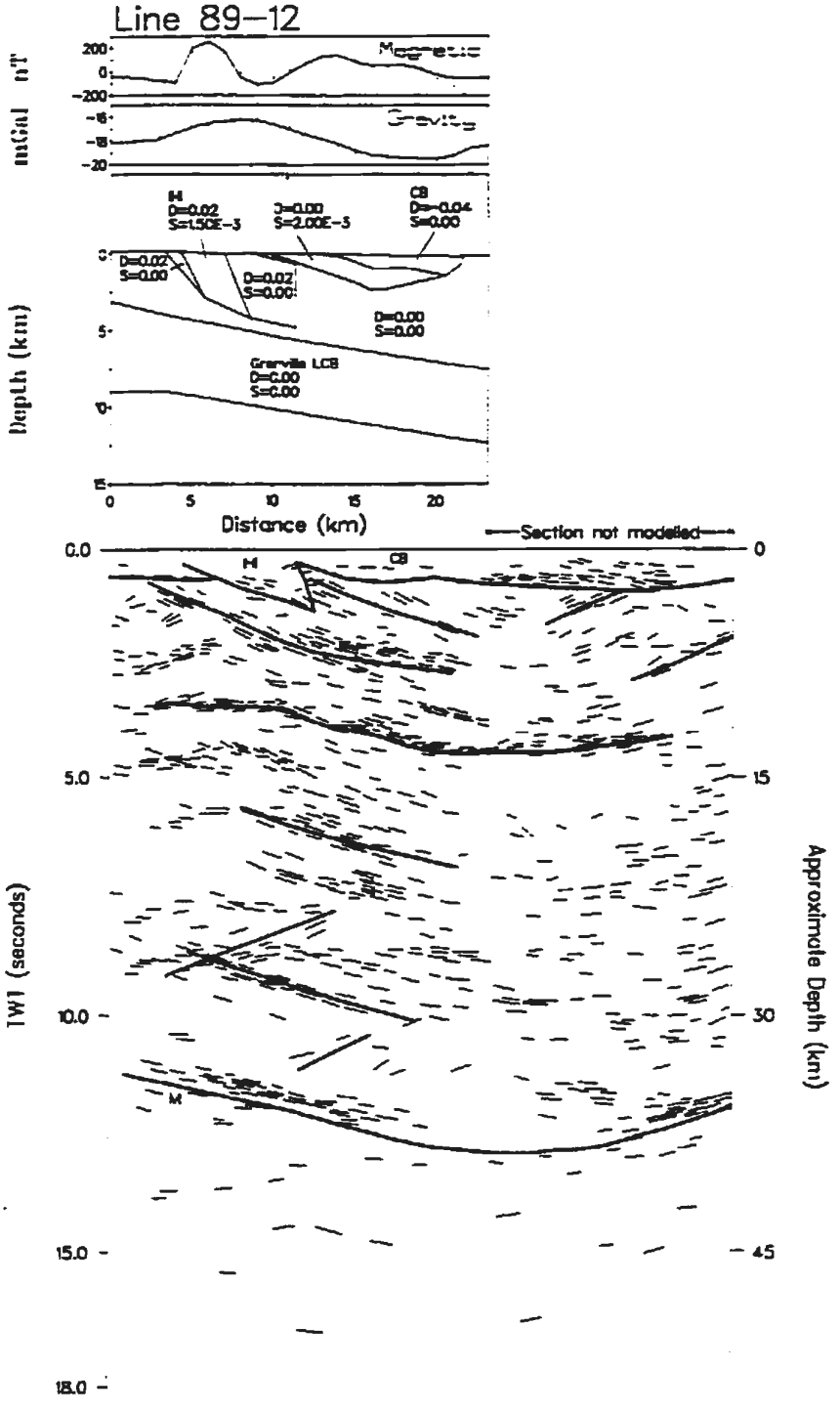

Figure 4.3: Seismic line drawing and 2 1/2–D gravity and magnetic model for LE89–12. Legend: CB – Carboniferous basin, D – density contrast relative to 2.67 g/cc, IHI – Indian Head Inlier, M – Moho, S – magnetic susceptibility in c.g.s. units.

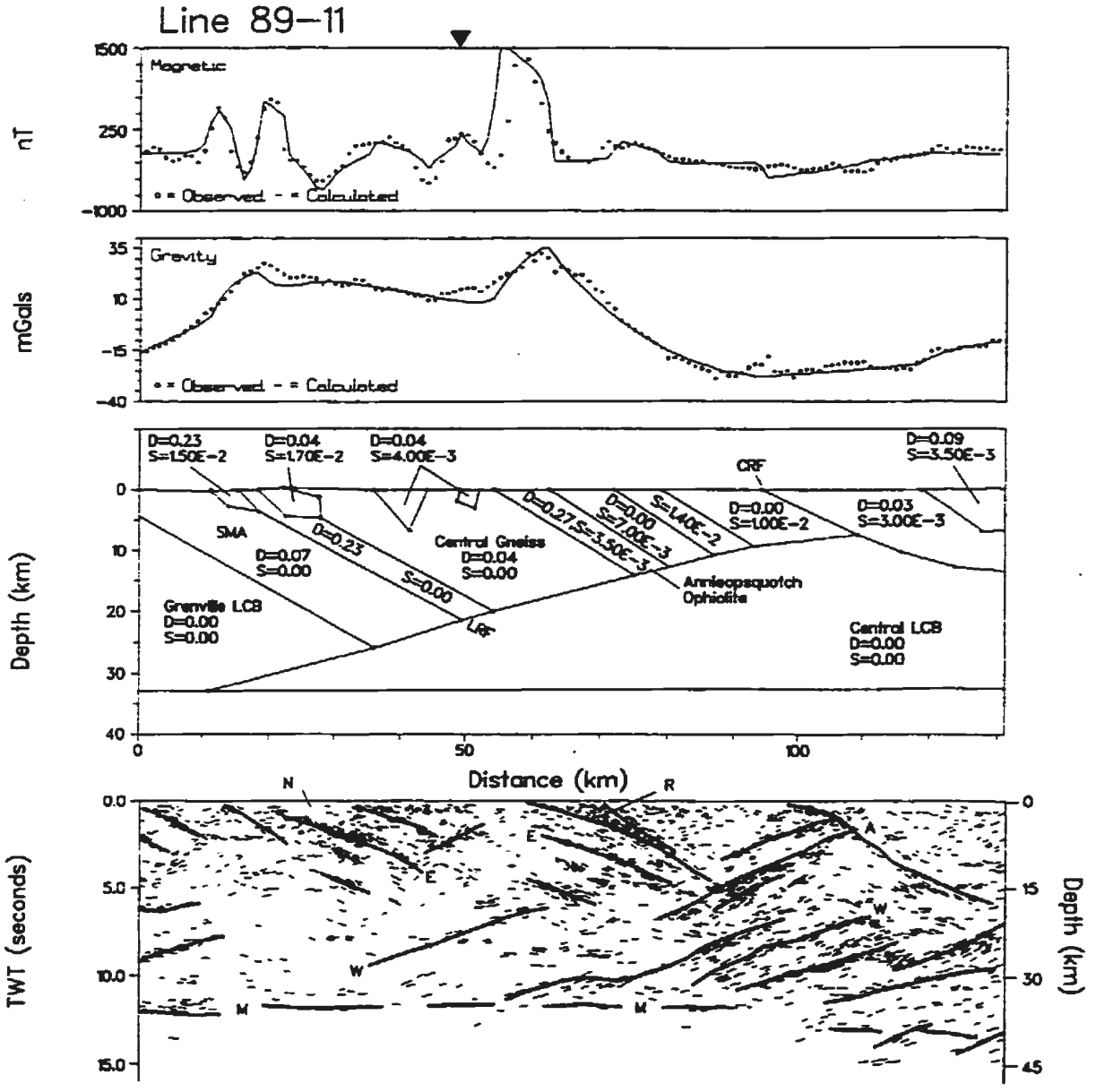

Figure 4.4: Seismic line drawing and 2 1/2–D gravity and magnetic model for LE89–11. The triangle marker shows the approximate location of the bend in the line. Legend: A – reflector referred to in the text, CRF – Cape Ray Fault, D – density contrast relative to 2.67 g/cc, E – east–dipping reflectors, LRF – Long Range Fault, M – Moho, S – magnetic susceptibility in c.g.s. units, SMA – Steel Mountain Anorthosite, W – west–dipping reflectors.

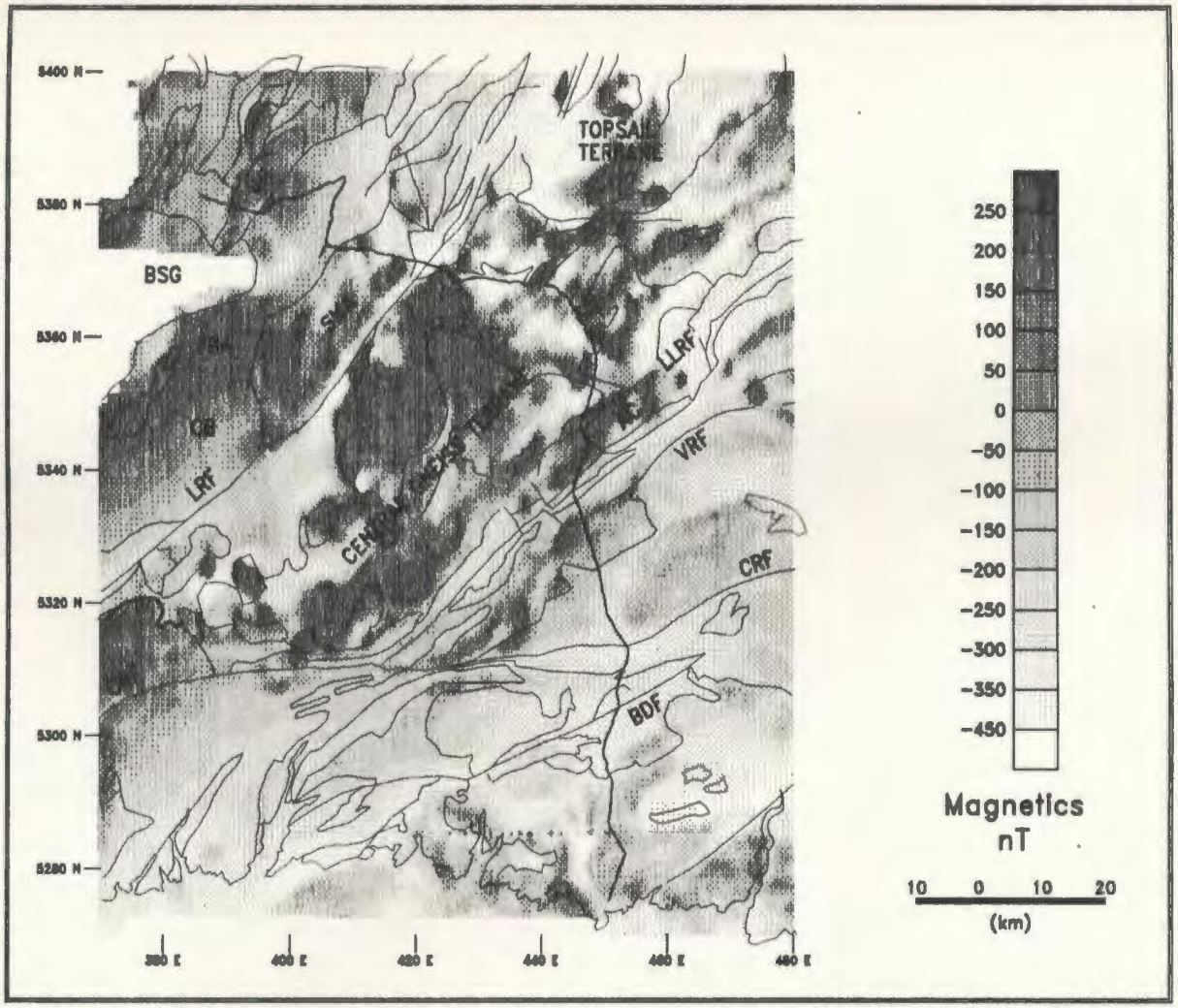

Figure 4.5: Magnetic anomaly map with equal area color scaling for the Burgeo Road area. Coordinates are in UTM Zone 21 kilometers. The geology (Colman-Sadd et al., 1990) is overlain on the grid and is shown by the black lines. The legend follows that of Figure 4.1. Also shown are the locations of LE89-12 and LE89-11.

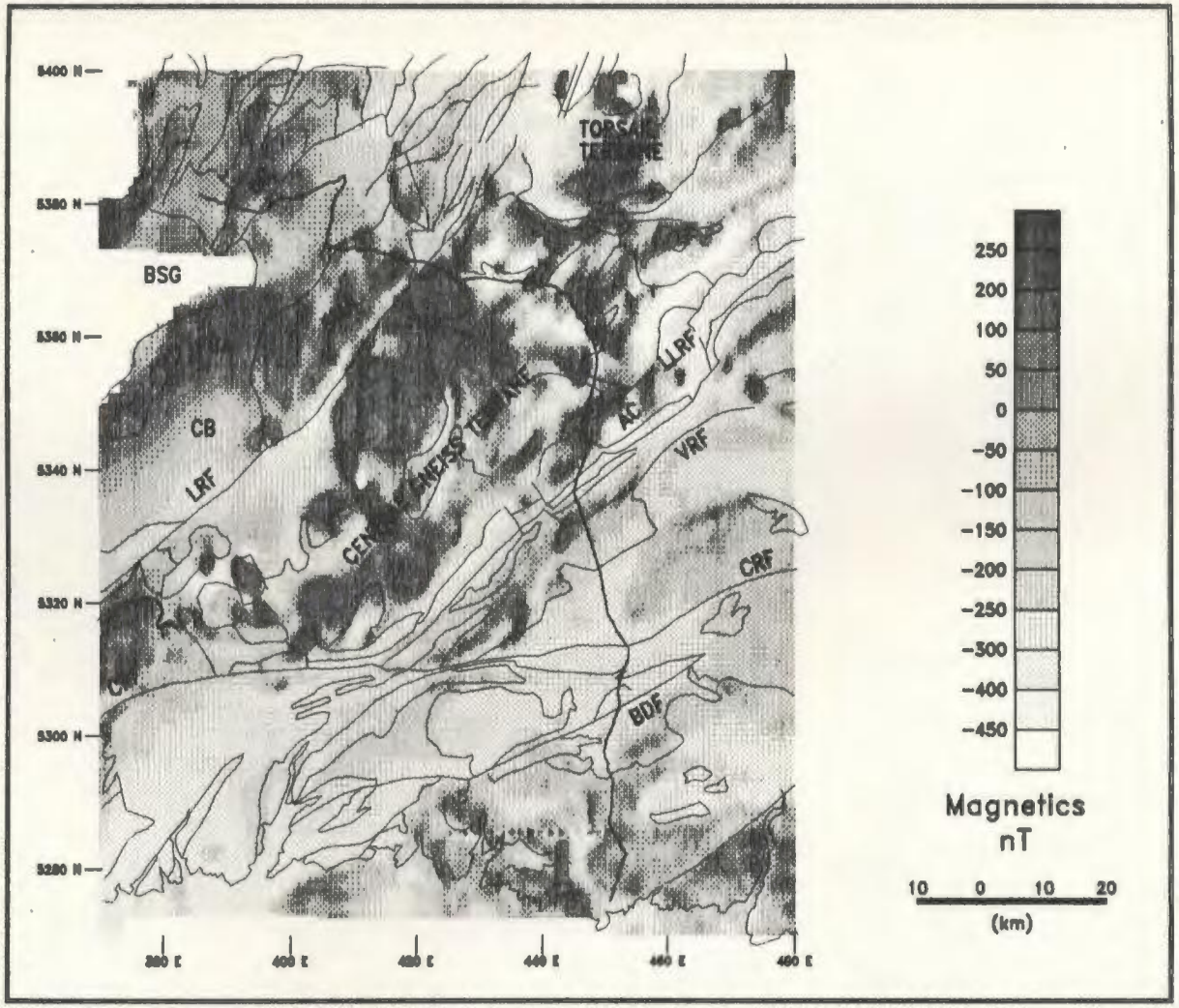

Figure 4.6: Total field magnetic map for the Burgeo Road area after rotation to the north magnetic pole. The legend follows that of Figure 4.1.

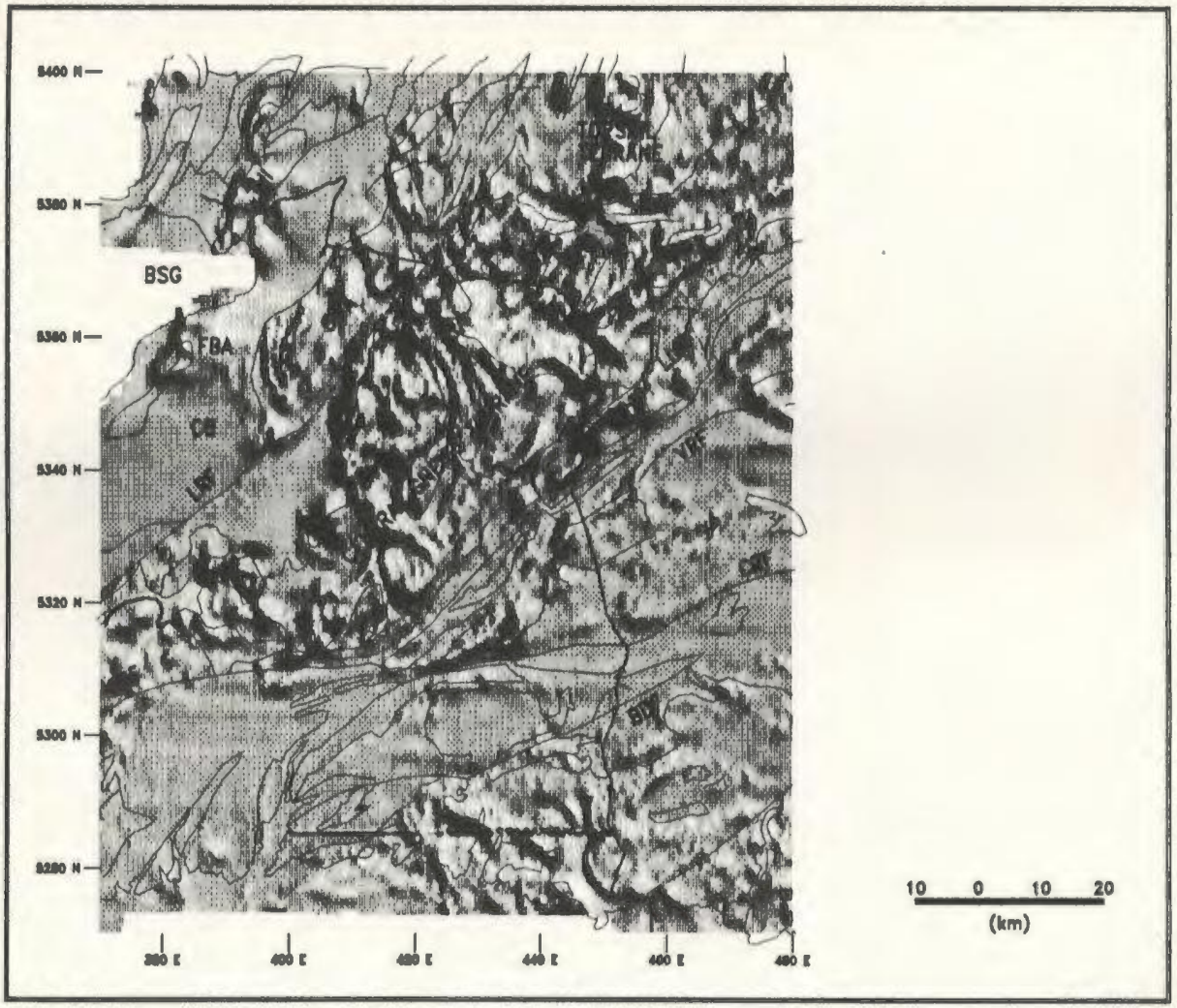

Figure 4.7(b): Shaded relief image of the magnetic map of the Burgeo Road region with illumination angle A=40°, I=45°. Legend follows that of Figure 4.1.

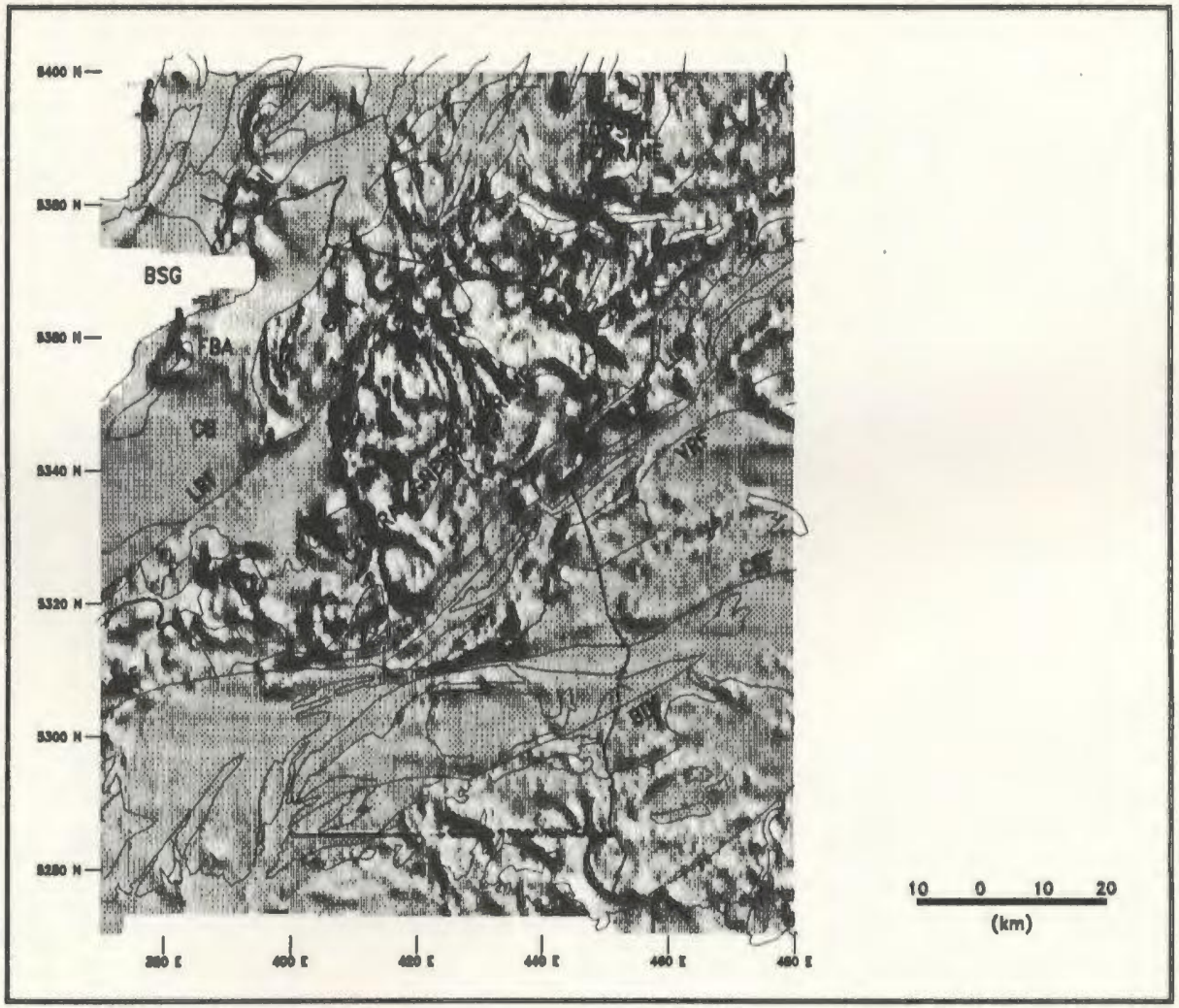

Figure 4.7(b): Shaded relief image of the magnetic map of the Burgeo Road region with illumination angle A=40°, I=45°. Legend follows that of Figure 4.1.

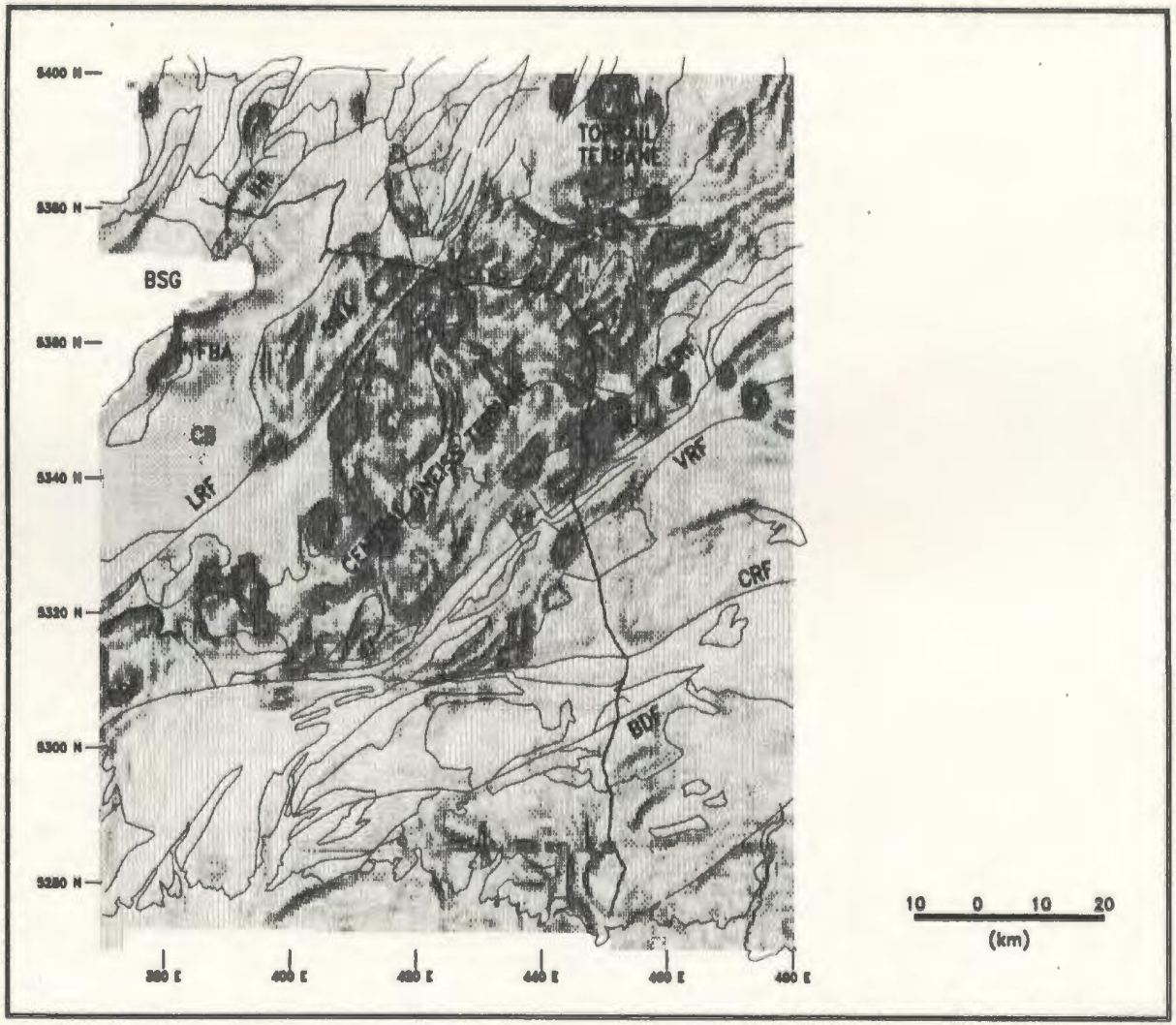

Figure 4.8: Horizontal gradient map of the magnetic field for the Burgeo Road area. The legend is the same as that for Figure 4.1.

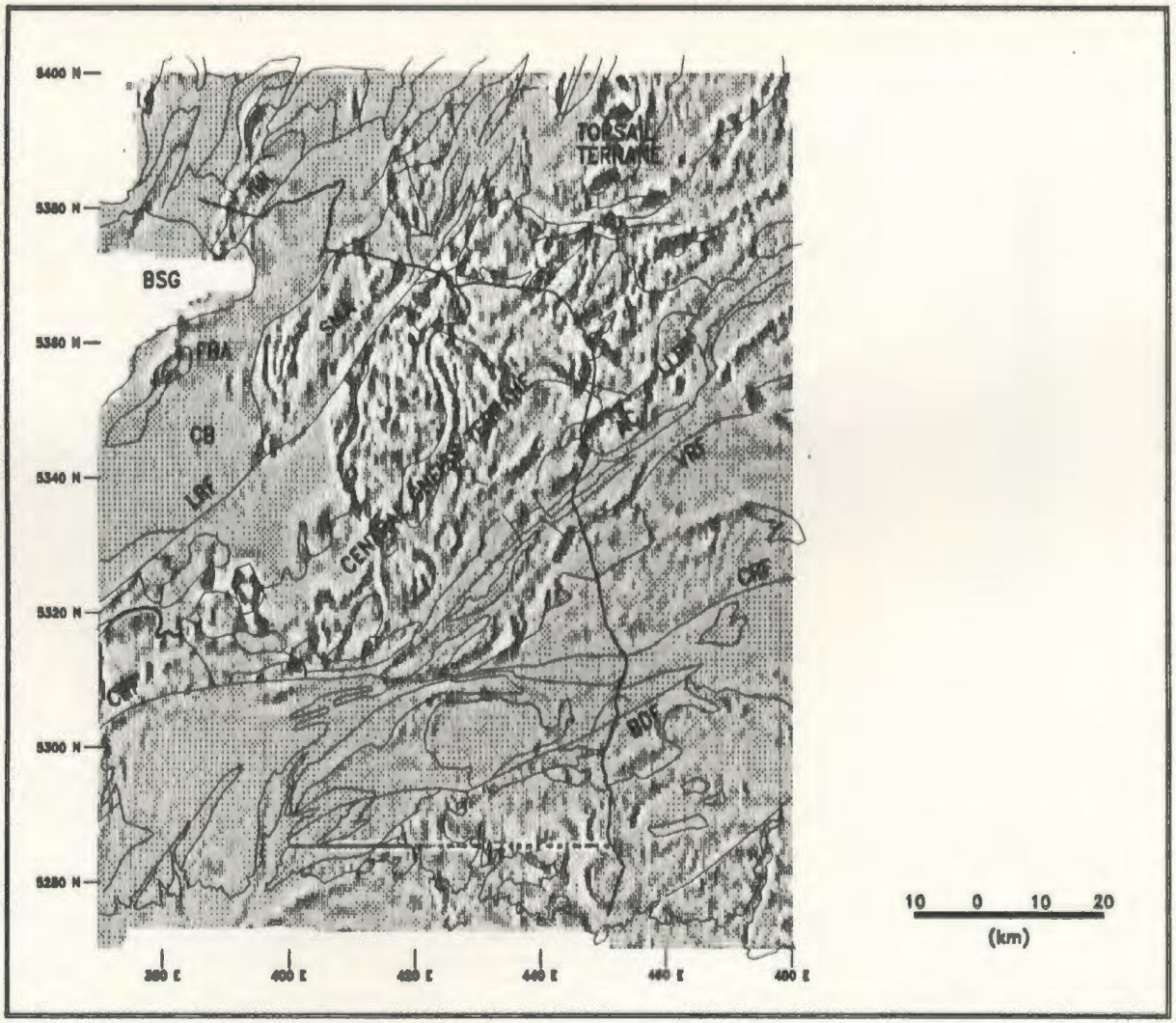

Figure 4.9: Second vertical derivative map of the magnetic field for the Burgeo Road region. The legend follows that of Figure 4.1.

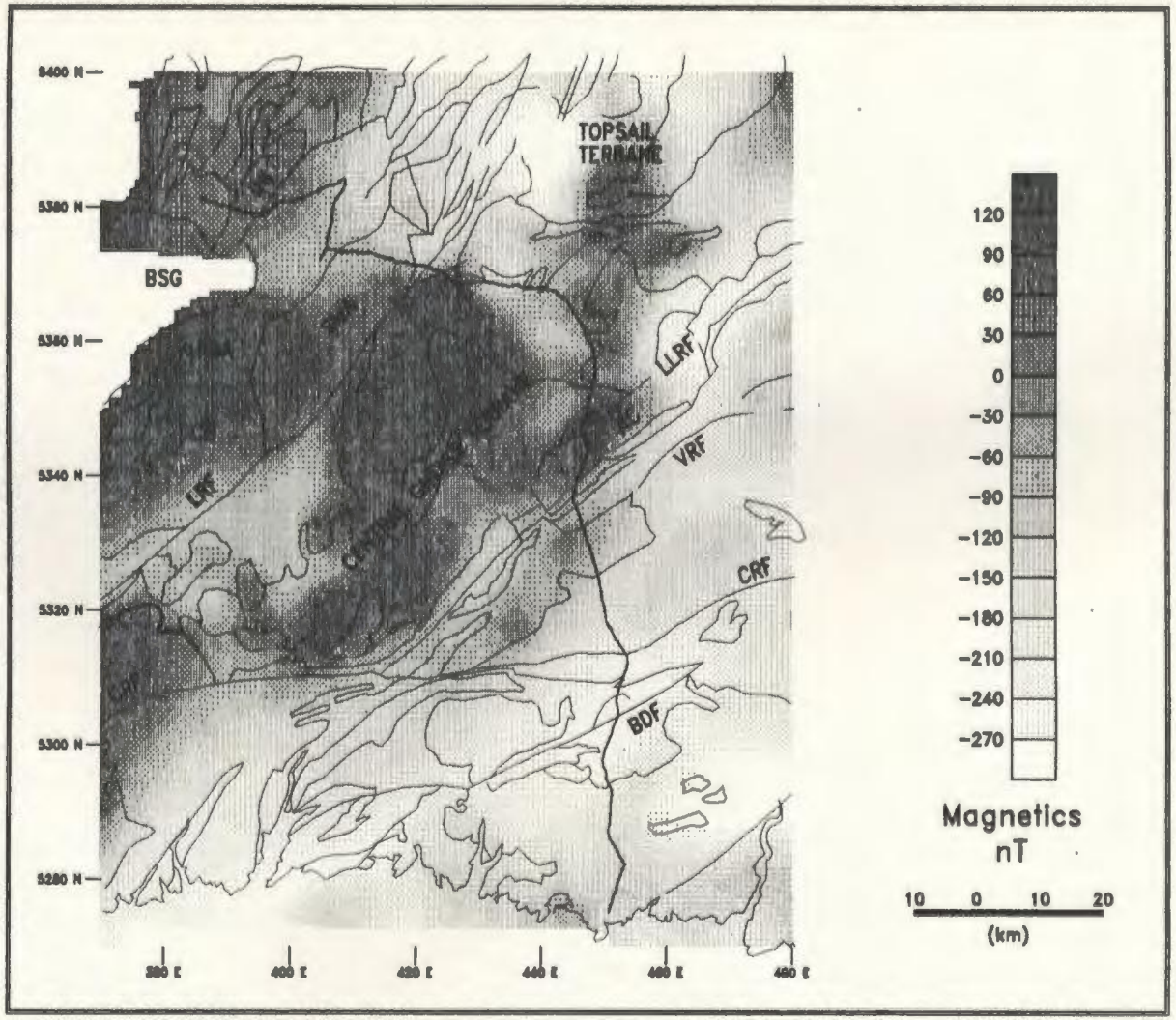

Figure 4.10(a): Magnetic map of the Burgeo Road area continued upward 3 km. The legend is the same as that for Figure 4.1.

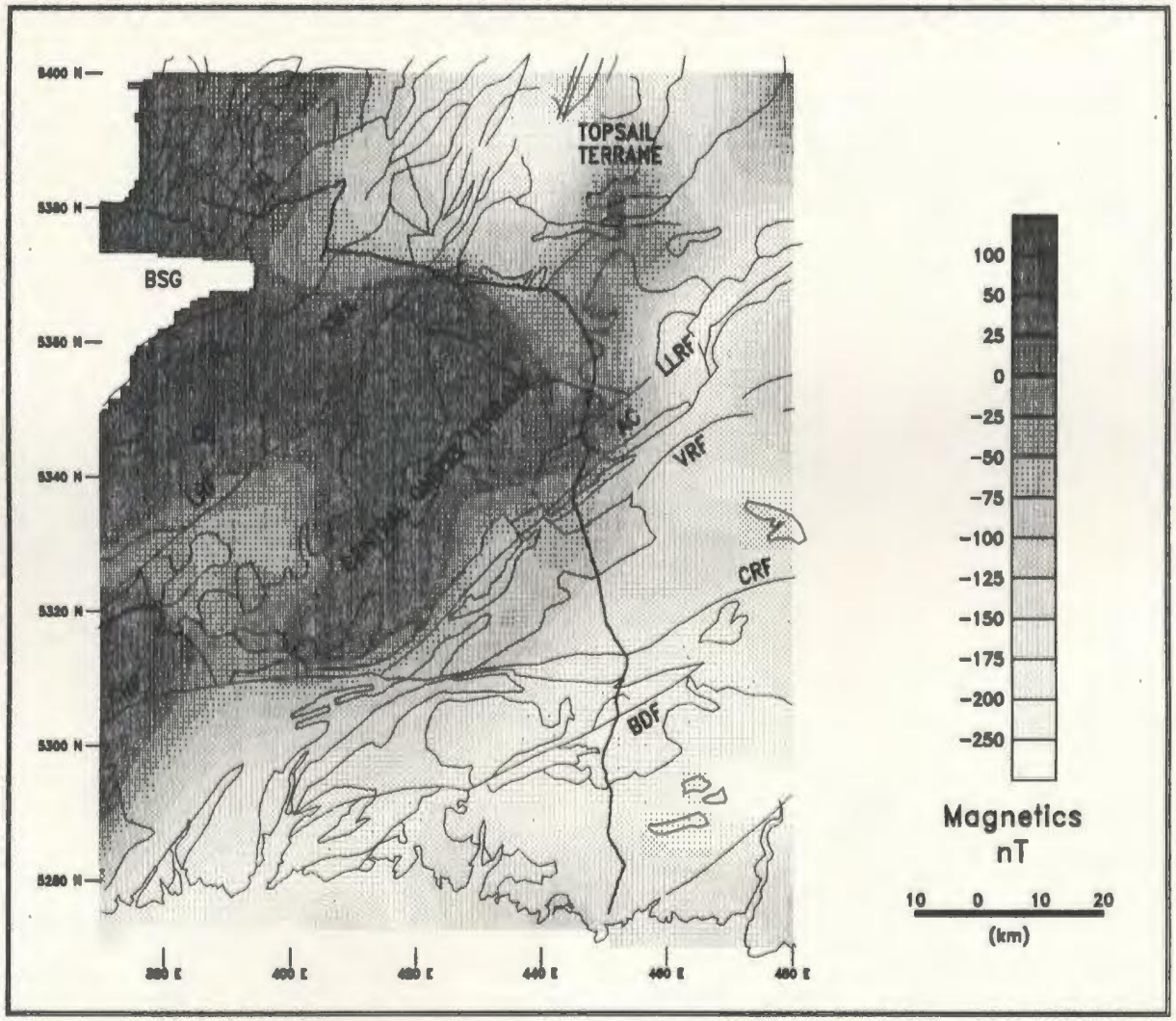

Figure 4.10(b): Magnetic map of the Burgeo Road area continued upward 6 km. The legend is the same as that for Figure 4.1.

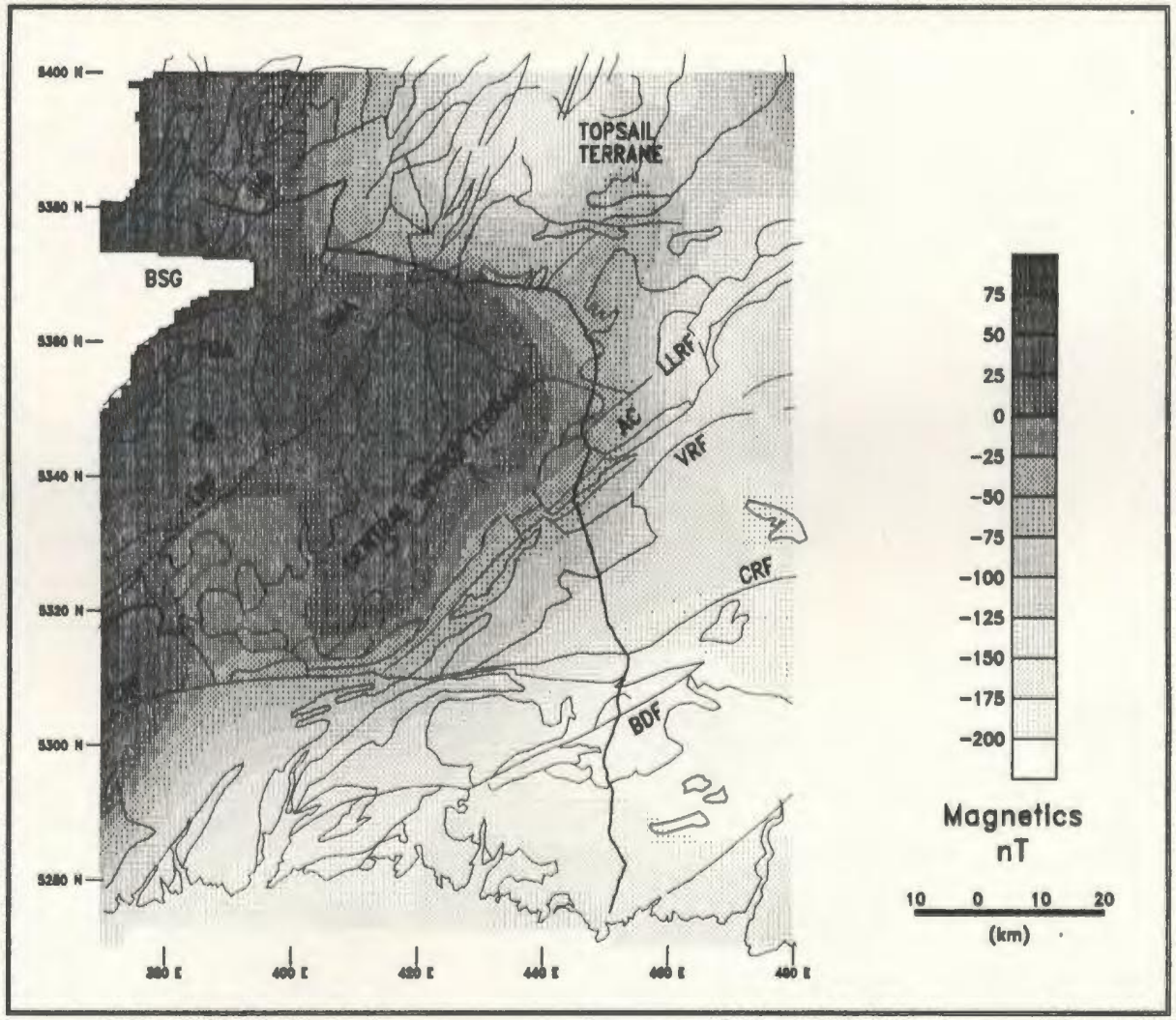

Figure 4.10(c): Magnetic map of the Burgeo Road area continued upward 10 km. The legend is the same as that for Figure 4.1.

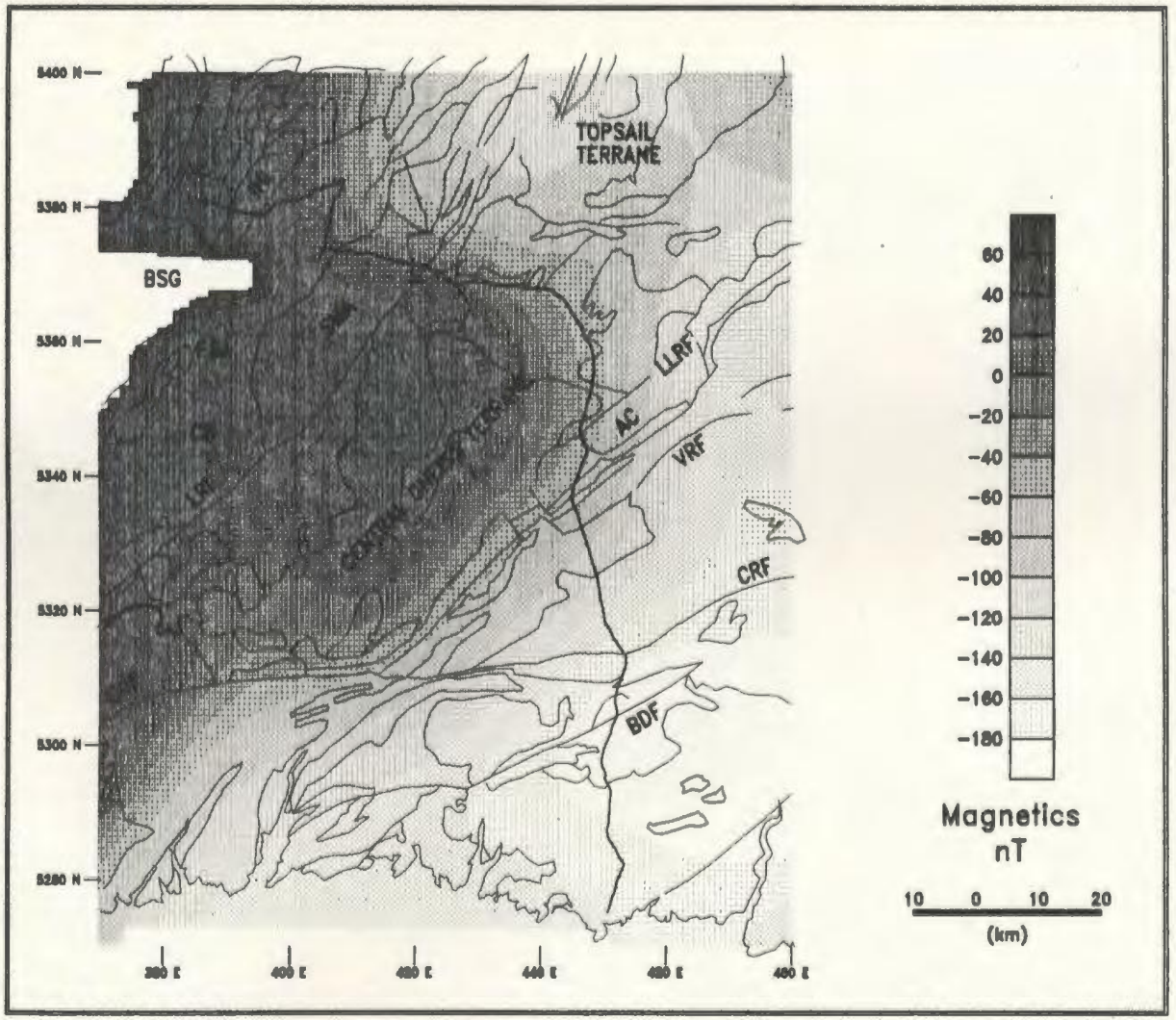

Figure 4.10(d): Magnetic map of the Burgeo Road area continued upward 15 km. The legend is the same as that for Figure 4.1.

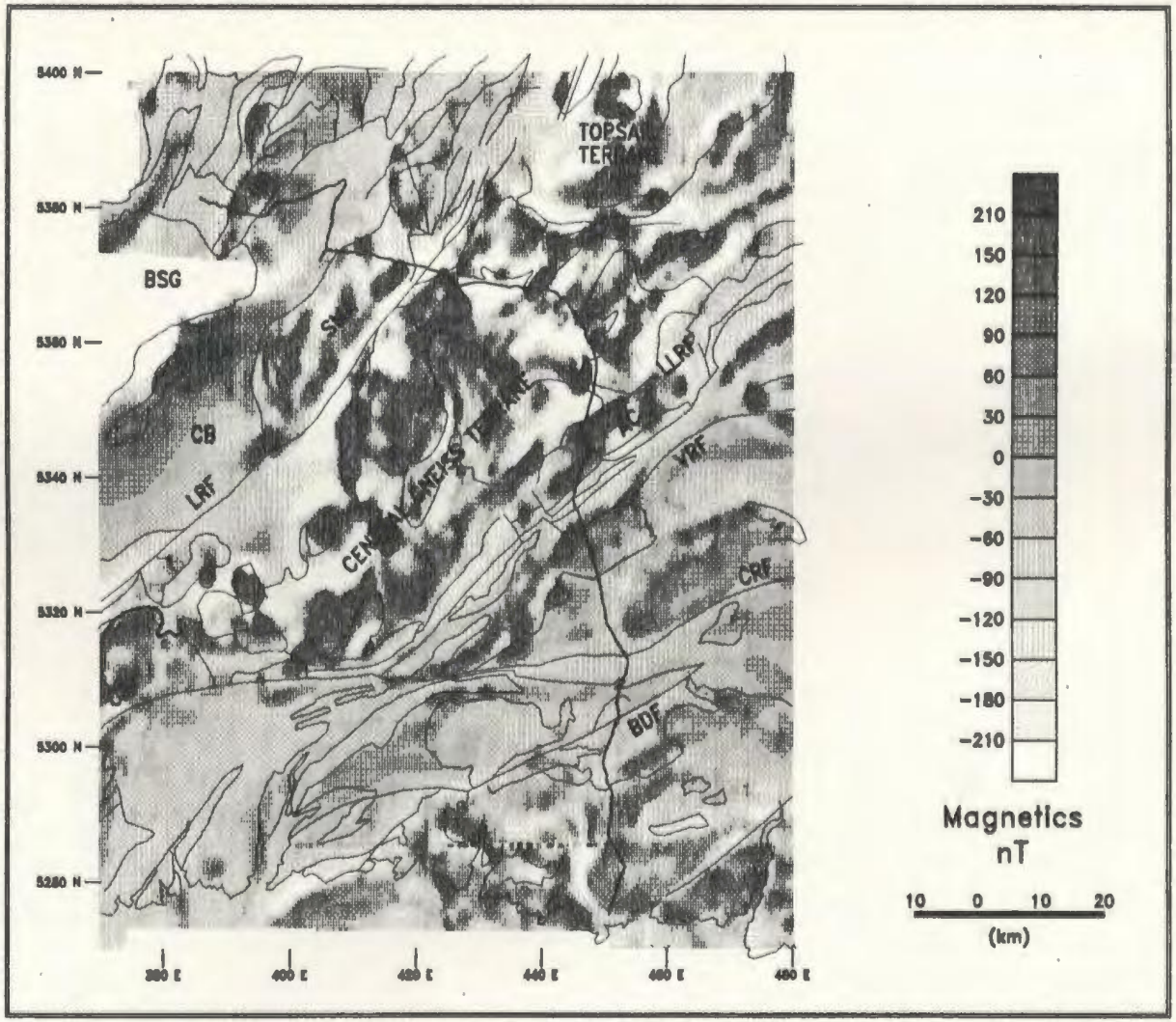

Figure 4.11(a): Magnetic layer strip map (Jacobson, 1987) for sources within the upper 1.5 km. The legend is the same as Figure 4.1.

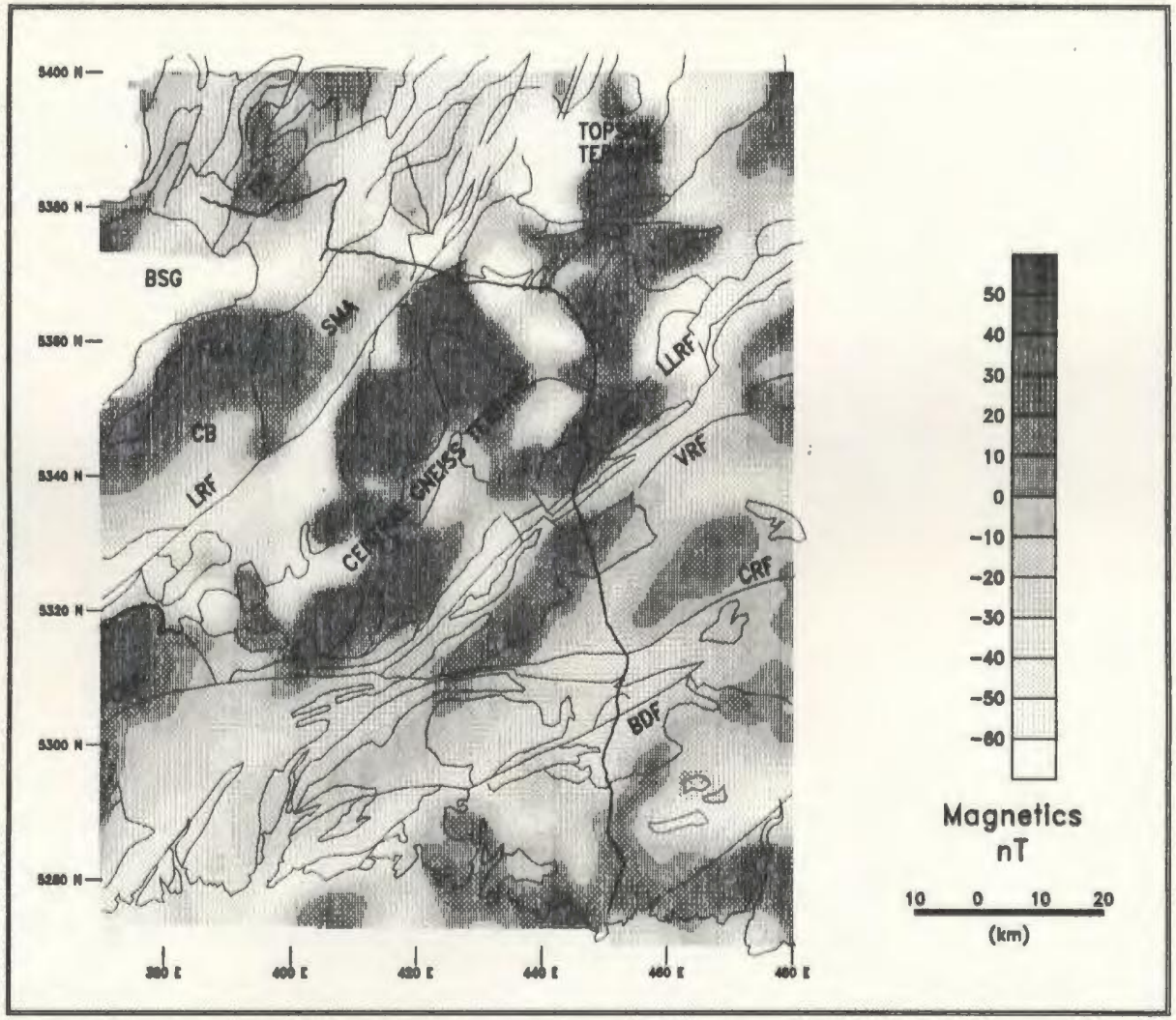

Figure 4.11(b): Magnetic layer strip map (Jacobson, 1987) for sources between 1.5 and 3 km depths. The legend is the same as Figure 4.1.

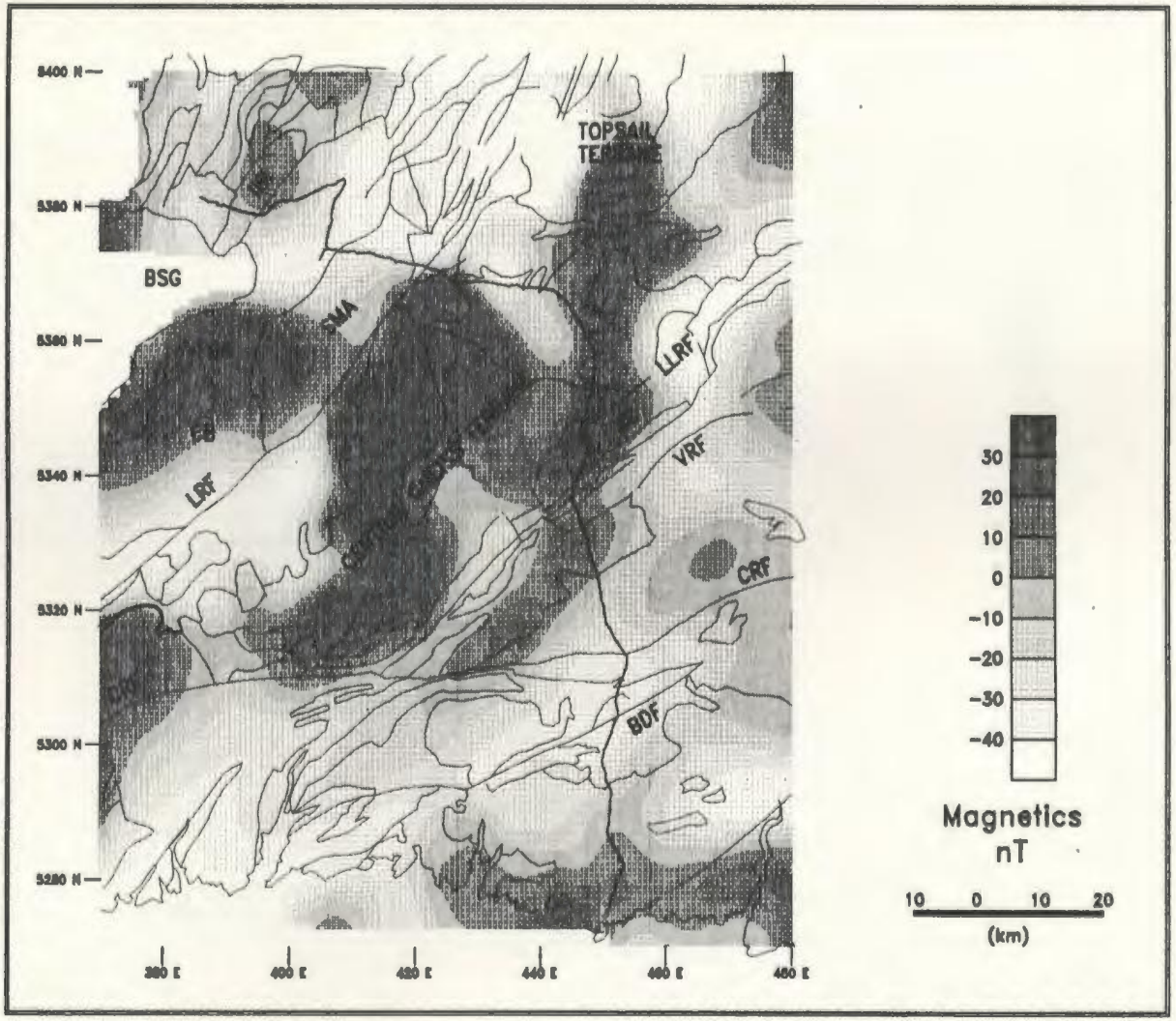

Figure 4.11(c): Magnetic layer strip map (Jacobson, 1987) for sources between 3 and 5 km depths. The legend is the same as Figure 4.1.

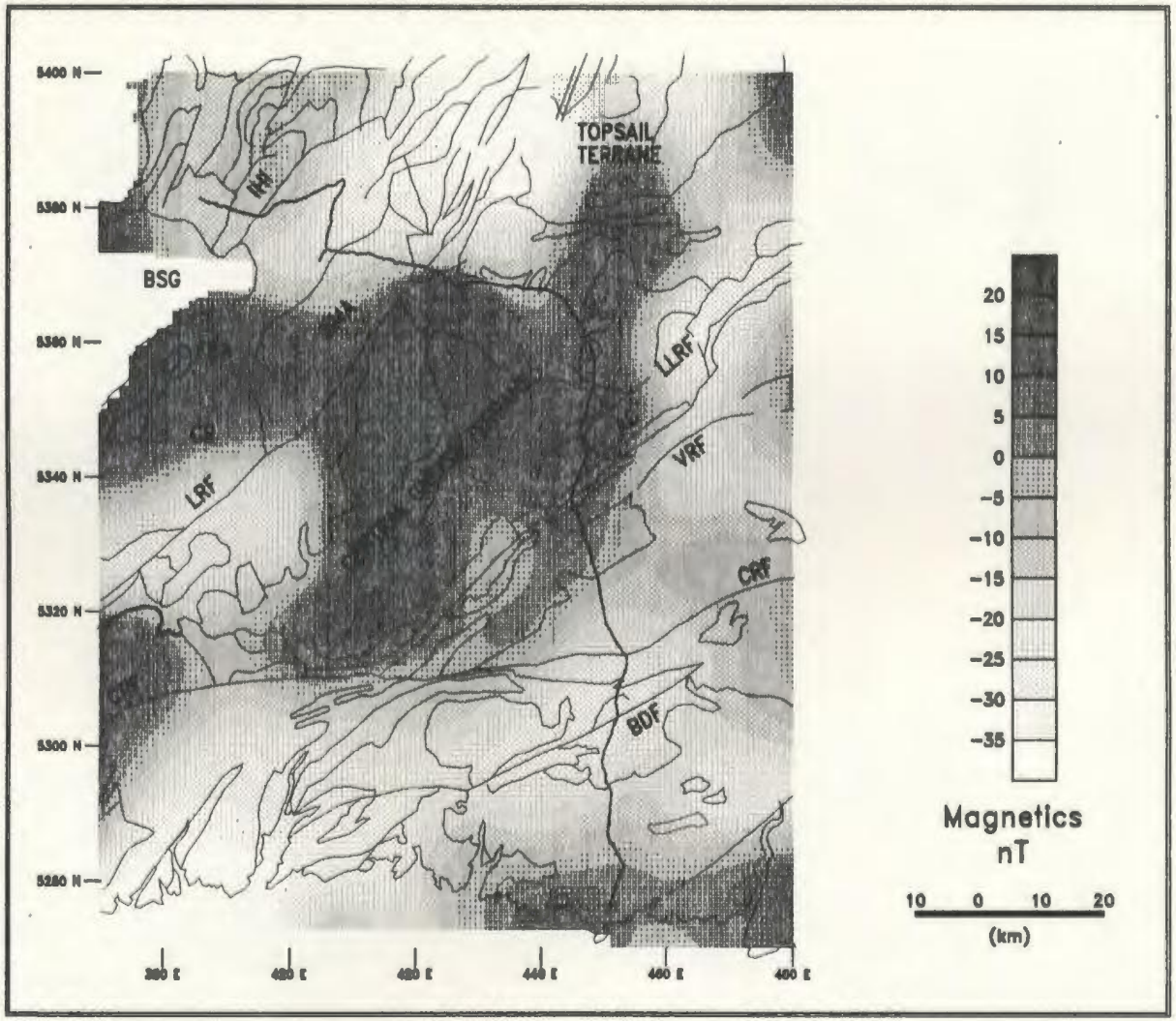

Figure 4.11(d): Magnetic layer strip map (Jacobson, 1987) for sources between 5 and 7.5 km depths. The legend is the same as Figure 4.1.

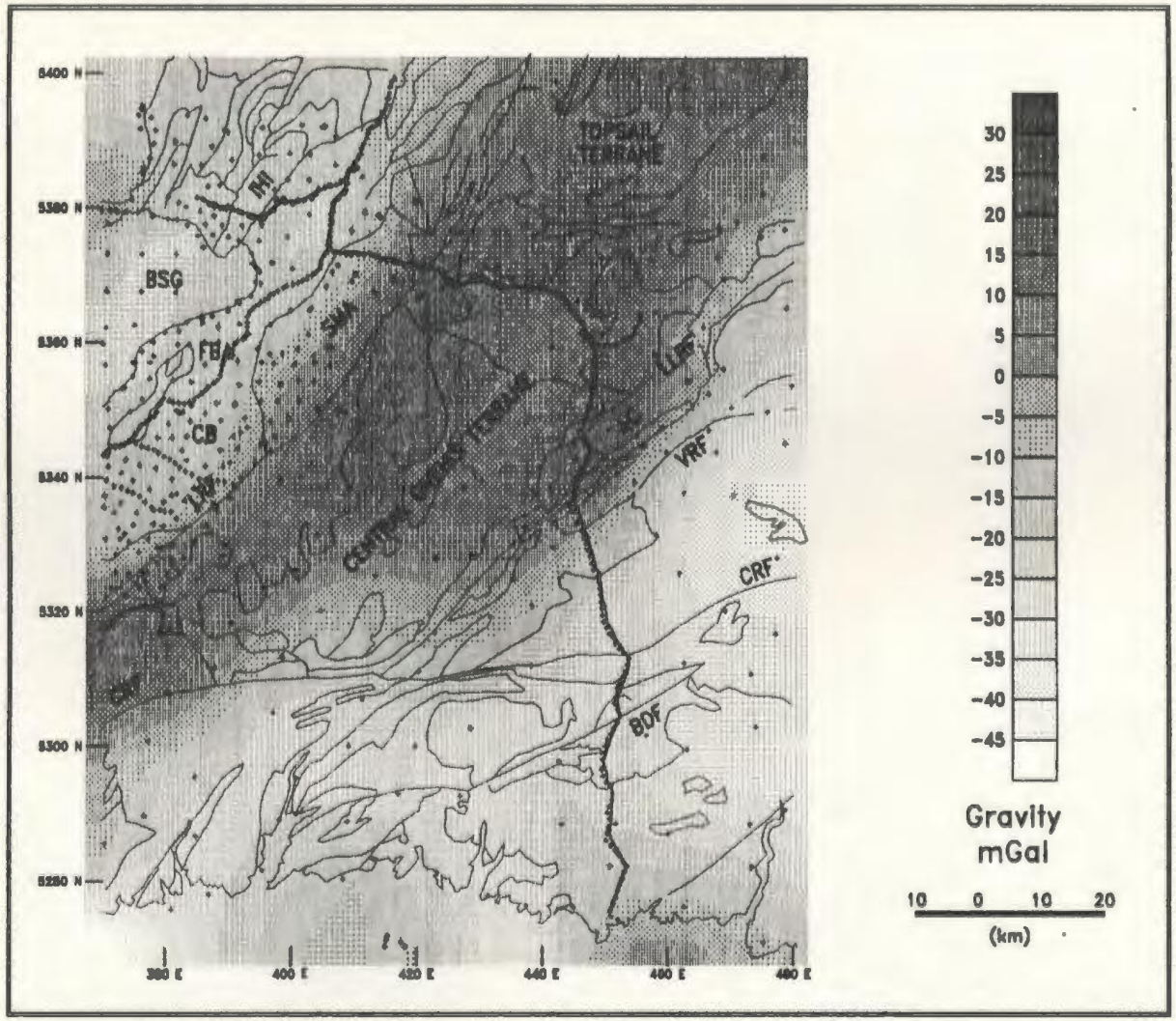

Figure 4.12: Gravity map for the region around the Burgeo Road. The small plus symbols indicate the gravity station locations. The legend follows that of Figure 4.1.

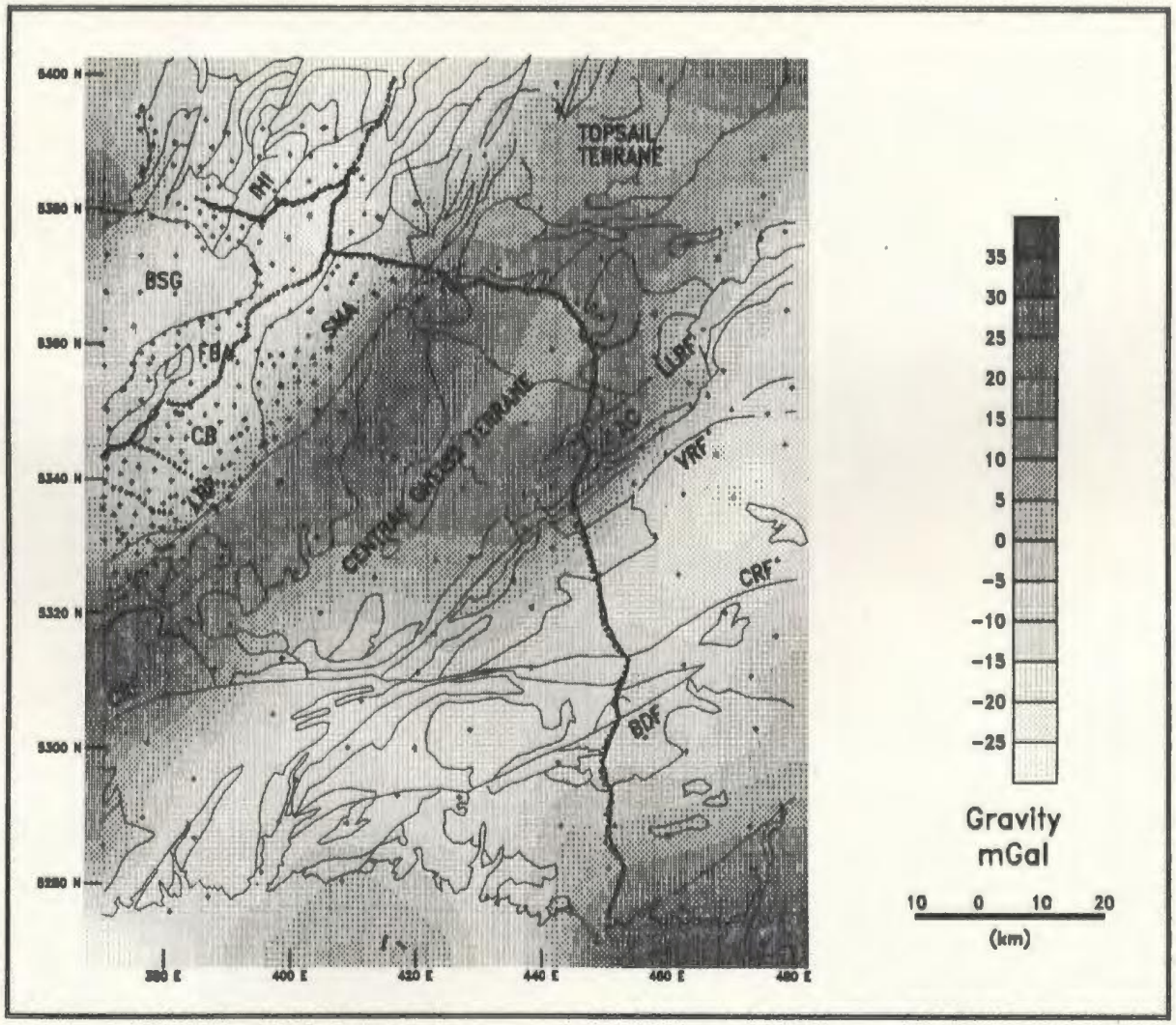

Figure 4.13: Residual gravity map for the Burgeo Road region resulting from subtraction of a best fitting second order polynomial surface. The legend follows that of Figure 4.12.

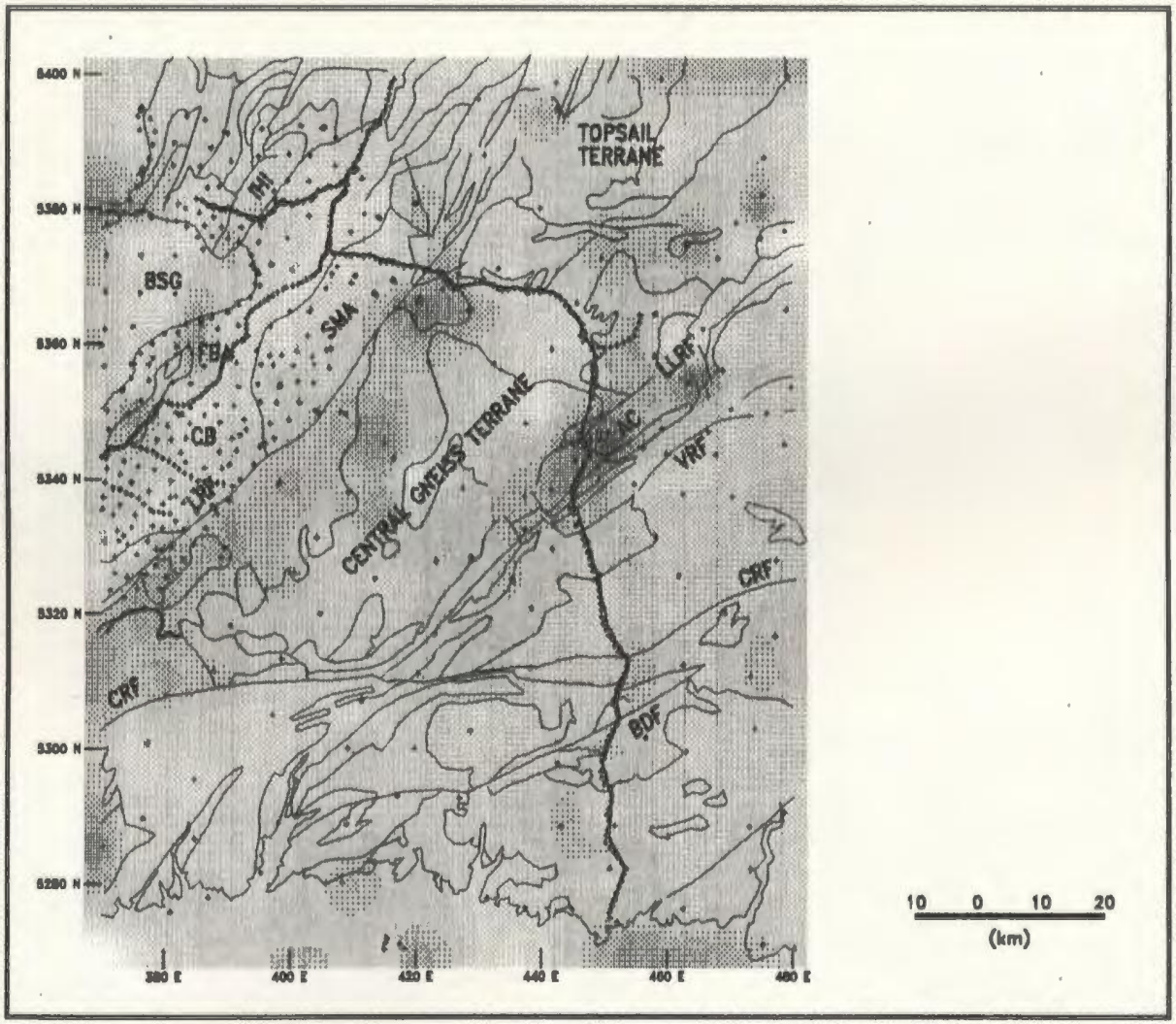

Figure 4.14: Second vertical derivative of gravity for the Burgeo Road area. The legend is the same as that of Figure 4.12.

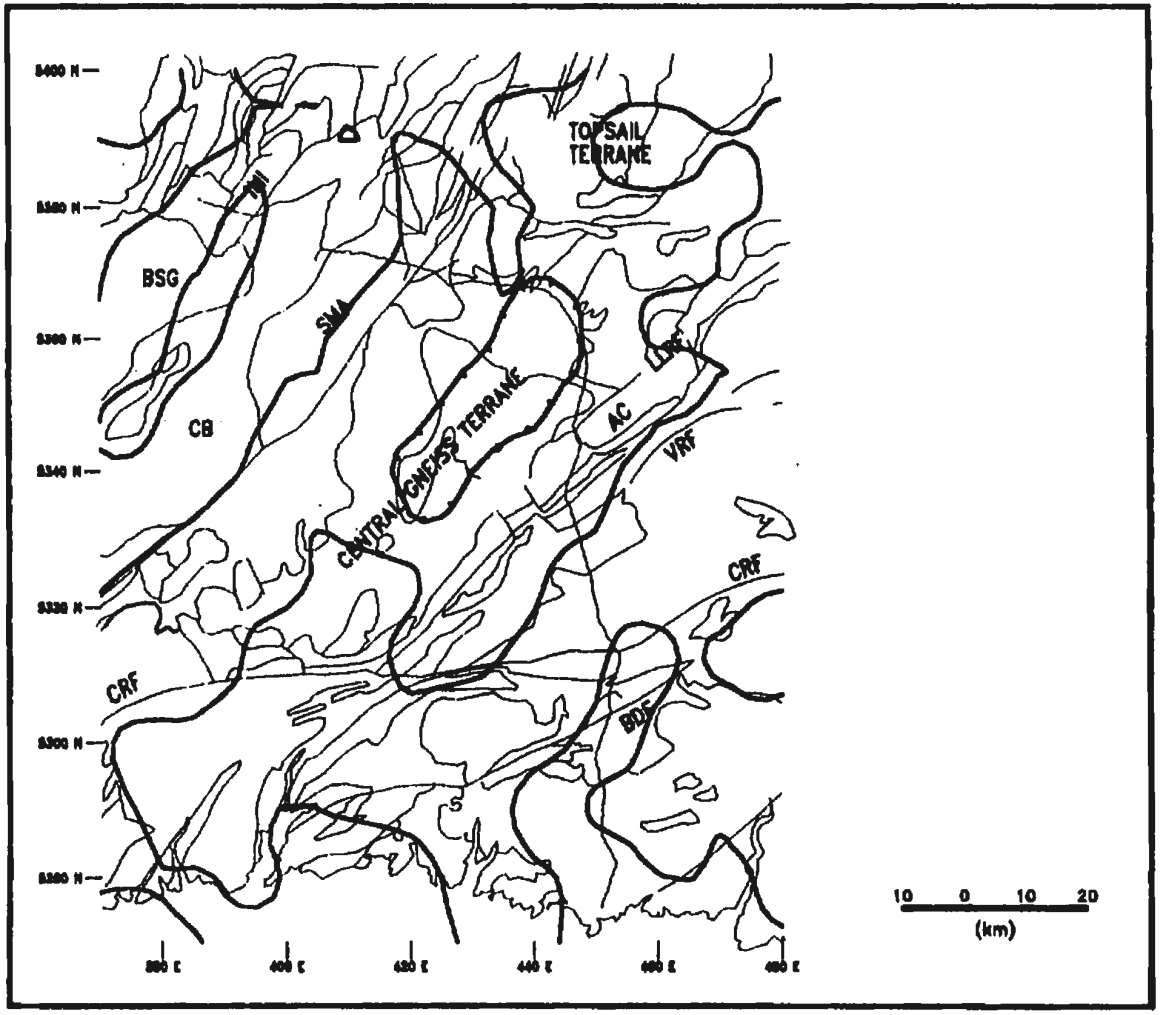

Figure 4.15: Map showing the zero level contour (red) of the second vertical derivative of gravity for the Burgeo Road area. The legend follows that of Figure 4.12.

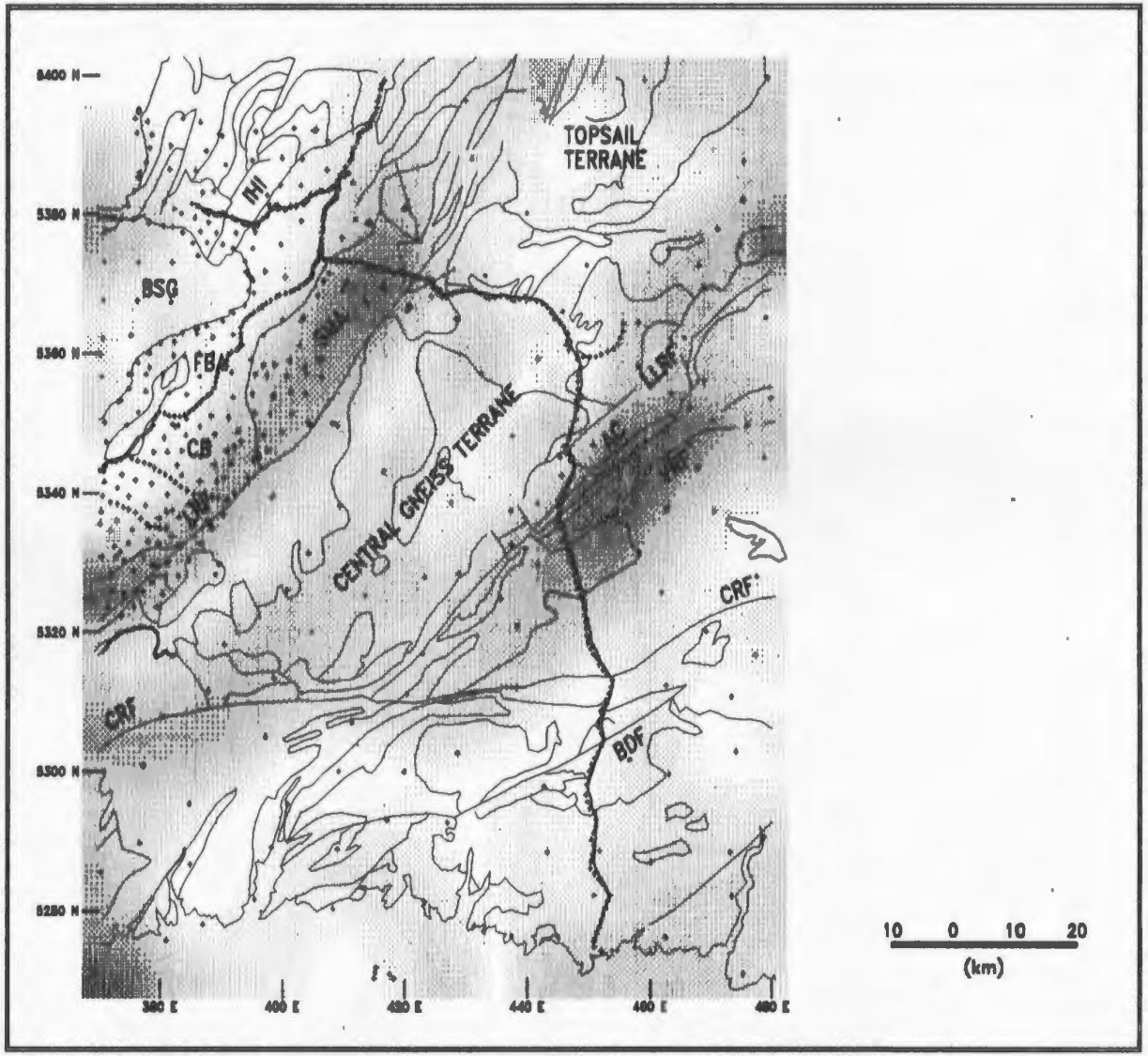

Figure 4.16: Horizontal gradient map of the gravity field for the Burgoe Road area. Legend follows that of Figure 4.12.

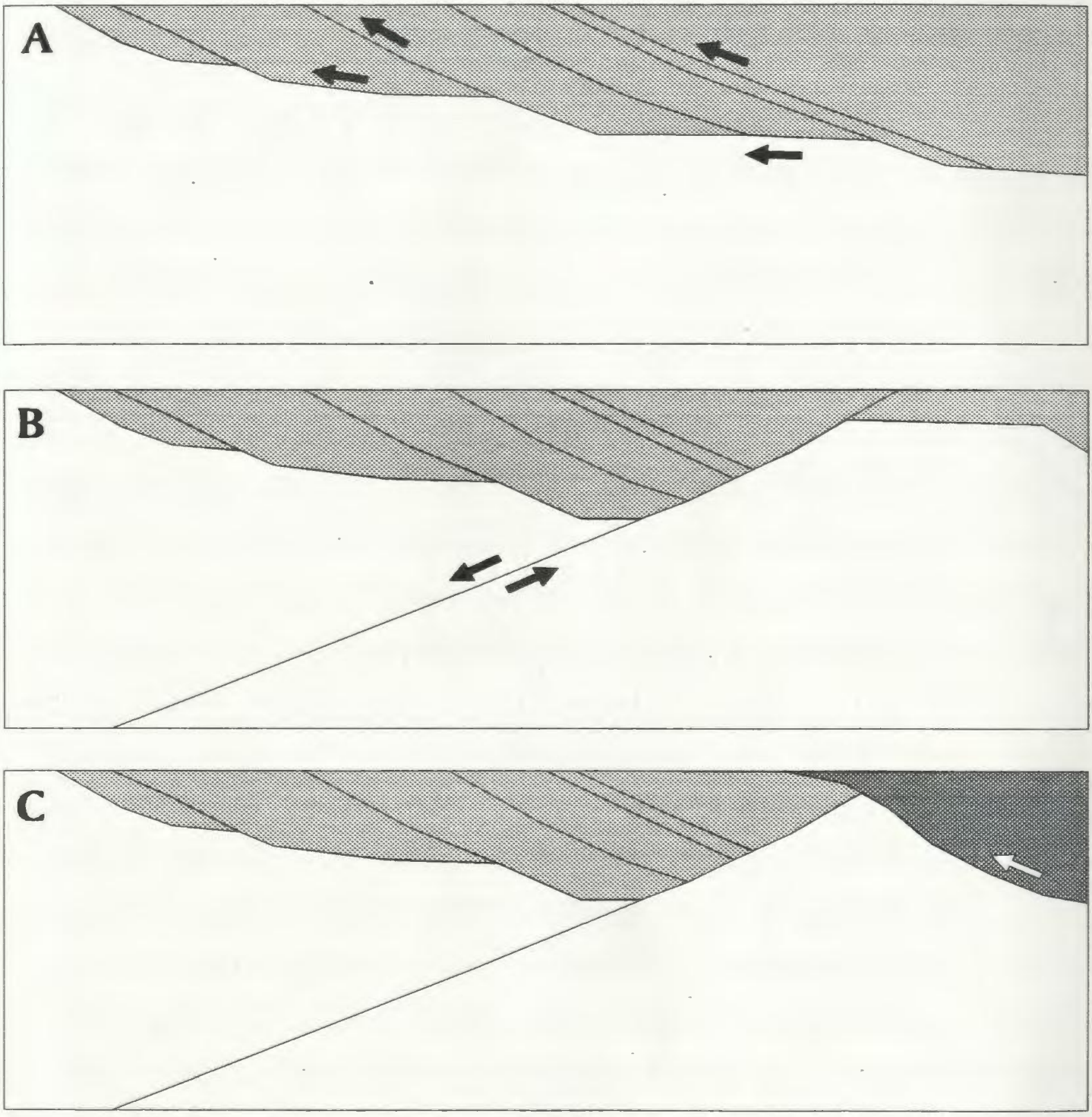

Figure 4.17: Geological evolution of the Burgeo Road Transect (LE89-11 & LE89-12). The current structure can be explained by three stages: (A) thrusting of allochthonous units from the east, (B) a stage of crustal extension, and (C) a later stage of west directed thrusting.

5.0. MEELPAEG TRANSECT:

5.1. GEOLOGY:

The LITHOPROBE East Meelpaeg Transect (LE89-1, LE89-2, LE89-3, LE89-4, LE89-5, LE89-6, and LE89-9) crosses the center of the island of Newfoundland, from the Bay of Islands in the west to Fortune Bay in the south (Figures 1.2 and 1.3). To facilitate map processing techniques, which require square grids of data for transformation to and from the Fourier domain, the transect was separated into three segments: a West segment (LE89-1, LE89-2, LE89-3, and LE89-4), a Central segment (LE89-5 and LE89-6), and an East segment (LE89-9).

The Meelpaeg Transect crosses several tectono-stratigraphic zone boundaries as defined by Williams (1979) and Williams et al. (1988) (Figures 1.1, 5.2, 5.4, and 5.6). From west to east the transect crosses the Long Range Fault (LRF), the Red Indian Line (RIL), the Noel Pauls Line (NPL), the Day Cove Thrust (DCT), and the Hermitage Bay Fault (HBF).

The Long Range Fault (LRF) is interpreted to be equivalent to the Baie Verte Line defined further to the north on the Baie Verte Peninsula (Williams, 1979; Williams et al, 1988), and is the surface boundary between the Humber Zone rocks to the west and the Dunnage Zone (Notre Dame Subzone) rocks to the east (Figures 5.1 and 5.2). It occurs beneath Grand Lake (GL) along the Meelpaeg Transect, and thus its surface exposure is between lines LE89-3 and LE89-4 (Figure

5.1).

The Red Indian Line (RIL) is the surface boundary between the Notre Dame Subzone of the Dunnage Zone to the west and the Exploits Subzone of the Dunnage Zone to the east (Williams, 1979; Williams et al, 1988) (Figures 5.3 and 5.4). Along the Meelpaeg Transect the surface trace of this fault occurs just to the east of Red Indian Lake (RI), placing it on the western end of line LE89-6 (Figure 5.3).

Noel Pauls Line (NPL), the surface boundary between the Exploits Subzone of the Dunnage Zone to the northwest and the Meelpaeg Subzone of the Gander Zone to the southeast (Williams, 1979; Williams et al, 1988) (Figures 5.3 and 5.4), has its surface trace exposed near the midpoint of line LE89-6 (Figure 5.3).

The Day Cove Thrust (DCT) is the surface boundary between the Dunnage Zone (Exploits Subzone) to the northwest and the Gander Zone (Gander Lake Subzone) to the southeast (Williams, 1979; Williams et al, 1988) (Figures 5.5 and 5.6). This thrust is exposed within the southern part of line LE89-9 (Figure 5.5).

The Hermitage Bay Fault (HBF), the equivalent of the Dover Fault further northeast, is the surface boundary between the Gander Zone (Gander Lake Subzone) to the northwest and the Avalon Zone to the southeast (Williams, 1979; Williams et al, 1988) (Figures 5.5 and 5.6). It is exposed near the southern

end of line LE89-9 (Figure 5.5).

West of the Long Range Fault (LRF), the Humber Zone rocks consist of Grenville Basement composed of anorthosite, tonalite-diorite, norite, and hornblende-biotite gneiss. These are exposed to the north in the Long Range Inlier (LRI), and to the south in the Indian Head Inlier and Steel Mountain Anorthosite (van Berkil et al., 1985; Williams and Cawood, 1989). Along the Meelpaeg Transect, basement is not exposed. Grenville Basement is overlain by Lower Cambrian metaclastic sequences consisting of psammitic and pelitic schist, metagreywacke, and conglomerate, followed by Cambro-Ordovician carbonate sequences, and Middle Ordovician transgressive sandstones and carbonate breccia (Williams and Cawood, 1989).

Emplaced on top of these autochthonous units is the Humber Arm Allochthon. The allochthon consists of several structural slices separated by mélanges. The lower structural slices consist of sedimentary rocks including shale, sandstone, limestone and limestone breccia. The intermediate structural slices consist of shale, sandstone and conglomerate, with pillow lavas, trachyte, and volcanic breccia at the top. The upper structural slices consist of minor sediments and ophiolitic rocks including the Bay of Islands Complex (**BMD** - Blow Me Down Massif, **LH** - Lewis Hills Massif, **NA** - North Arm Massif, and **TM** - Table Mountain Massif) (Figure 5.1 and 5.2) (Williams and Cawood, 1989).

Along the Meelpaeg Transect the oldest exposed Notre Dame Subzone rocks to the east of the Long Range Fault (LRF) and to the west of the Red Indian Line (RIL) consist of Ordovician gabbro to granite intrusions with inclusions of mafic to ultramafic material in the Hungry Mountain Complex (HMC). Deposition of the Buchans Group (BG), which consists of basalt, rhyolite, tuff breccia, and minor conglomerate, occurred later. This was then followed by the emplacement of gabbro, diorite, and granodiorite making up the Rainy Lake Complex (RLC). The Springdale Group (SG), consisting of flow-banded rhyolite, rhyolite breccia, and tuff, was deposited in the Silurian, followed by emplacement of granite, rhyolite, and minor basalt of the Topsails Intrusive Suite (TG) (Whalen and Currie, 1988; Kean et al., 1981) (Figure 5.3).

The Deer Lake Basin (DLB) consists of Carboniferous sediments deposited unconformably upon Lower Cambrian metasediments of the Humber Zone (Williams and Cawood, 1989) and the Notre Dame Subzone rocks (Whalen and Currie, 1988) (Figures 5.1 and 5.3).

The Exploits Subzone rocks between the Red Indian Line (RIL) and Noel Pauls Line (NPL) have a similar stratigraphy to the Notre Dame Subzone rocks to the west (Williams et al., 1988). However, only tuff and slate of the Victoria Lake Group (VLP and VLS) and the Tally Pond Volcanics (TPV) of the Victoria Lake Group are exposed. This group is covered

partially by Ordovician conglomerate (OC) (Kean et al., 1981) (Figure 5.3), which is not found in the Notre Dame Subzone (Williams et al, 1988).

South of Noel Pauls Line (NPL), the Meelpaeg Transect crosses the Meelpaeg Subzone of the Gander Zone. Along LE89-6, this subzone has exposed Ordovician phyllite, siltstone and sandstone (OS) units intruded by numerous Devonian granitoids (DG) (Kean et al., 1981) (Figure 5.3).

Southeast of the Meelpaeg Subzone, line LE89-9 of the Meelpaeg Transect crosses more Exploits Subzone rocks. These are almost exclusively Lower to Middle Ordovician marine sediments of the Bay D'Espoir Group (BDG), consisting of sandstone and siltstone, psammite, semipelite, pelite, and tuff with minor limestone and migmatite. These have been intruded by Devonian granitoids (Dickson, 1990; Colman-Sadd, 1976) (Figures 5.3 and 5.5).

To the southeast of the Day Cove Thrust, the Meelpaeg Transect crosses Gander Zone (Gander Lake Subzone) rocks. These are predominantly Silurian-Devonian granites of the Northwest Brook Complex (NBC) intruded into the Middle Ordovician or older psammitic and semipelitic gneisses and schists of the Little Passage Gneiss (LPG) (Dickson, 1990; Colman-Sadd, 1976) (Figure 5.5).

Avalon Zone rocks are crossed along the Meelpaeg Transect southeast of the Hermitage Bay Fault (HBF). These consist of

Precambrian volcanics and sediments comprising the Connaigre Bay Group (CBG), Ordovician diorite and granite cut by mafic and felsic dykes comprising the Hermitage Bay Complex (HBC). Intrusions of Devonian granitoids (DG) cut both earlier units (Colman-Sadd et al., 1979).

5.2. GEOPHYSICS:

5.2.1. Seismic Reflection:

Seismic data for the western and central segments of the Meelpaeg Transect have reflector patterns similar to that of the Burgeo Road Transect. The upper and middle crust has predominantly east-dipping reflectors (E), cut by deeper west-dipping reflectors (W) (Figures 5.7 and 5.8). Shallow reflectors are seen on the western segment, probably related to the Humber Arm Allochthon and Deer Lake Basin (DLB). The Moho (M) appears to dip to the west in this area (Quinlan et al., 1992).

The eastern segment of the Meelpaeg Transect differs from rest of the transect, in that it nearly exclusively consists of northwest-dipping reflectors (W) throughout the whole crust. These appear to be cut near the midpoint of LE89-9 by a southeast-dipping reflector (A) (Quinlan et al, 1992) (Figure 5.9). The surface projection of reflector 'A' is coincident with the location of the Salmon River Fault, a near vertical fault within the Bay D'Espoir Group (BDG) sediments.

The Day Cove Thrust (DCT) appears as a northwest-dipping reflector in the upper part of the section (Figure 5.9).

5.2.2. Magnetics:

Total field aeromagnetic maps for areas along the three segments of the Meelpaeg Transect are presented in Figures 5.10, 5.11, and 5.12, and the equivalent maps reduced to the magnetic pole are presented in Figures 5.13, 5.14, and 5.15.

Large magnetic anomalies occur over the separate massifs of the Bay of Islands Complex (TM, NA, BMD, and LH) and also over Bay of Islands (BI) (Figures 5.10 and 5.13). The anomalies exhibit some internal structure, indicating that not all parts of the Bay of Islands Complex have the same magnetic susceptibility. The internal complexity of these anomalies is emphasized in the shaded relief images (Figures 5.16a,b) and particularly well in the second vertical derivative map (Figure 5.19).

Upward continuation (Figures 5.22a,b,c,d) and layer stripping (Jacobson, 1987) (Figures 5.25a,b,c,d) suggest that the Bay of Islands Complex is thin. The magnetic anomalies associated with the Bay of Islands Complex are retained on the upward continuation maps to heights greater than 10 km (Figures 5.22a,b,c,d) as a small amplitude magnetic ridge parallel to the west coast of Newfoundland, but this is considered an artifact of the processing. The thin source

interpretation is consistent with local geology (Williams and Cawood, 1989). These maps also suggest that the massifs to the north of Bay of Islands (**TM** and **NA**) have less depth extent than those to the south of Bay of Islands (**BMD** and **LH**). The anomaly beneath Bay of Islands appears to extend to the greatest depth extent, exceeding 7.5 km.

The exposed Grenville basement in the Long Range Inlier (**LRI**) has a complex magnetic anomaly pattern associated with it (Figures 5.10 and 5.13). In general there is a pattern of irregular high frequency NW-SE lineaments throughout the Long Range Inlier (**LRI**). These are enhanced very well in the shaded relief map with false sun azimuth set at 45° (Figure 5.16a) and also on the second vertical derivative map (Figure 5.19). Longer wavelength positive magnetic anomalies found over parts of the Long Range Inlier (**LRI**) are associated with Grenvillian granitoids intruded into the basement gneisses (Figures 5.10 and 5.13).

Upward continuation (Figures 5.22a,b,c,d) and depth separation filtering (Jacobson, 1987) (Figures 5.25a,b,c,d) indicates that the linear magnetic pattern in the Long Range Inlier (**LRI**) is a shallow feature, while the Grenvillian granitoid intrusions may extend to significant depths.

Much of the Humber Zone, west of the Long Range Fault, consists of sedimentary units aside from the Long Range Inlier (**LRI**) and the Bay of Islands Complex (**TM**, **NA**, **BMD**, and **LH**)

mentioned above. These sedimentary units, as well as the Carboniferous Deer Lake Basin (DLB) have very little in the way of magnetic anomalies (Figures 5.10 and 5.13). Long wavelength, low amplitude anomalies occur over some of these areas and is likely due to magnetic basement beneath the sediments. The differing character of the sedimentary and igneous units is emphasized very well on the second vertical derivative map (Figure 5.19).

Several large magnetic highs occur over the granitoids of the Topsails Igneous Terrane (**TG**, **HBG**, and **HMC**) between the Deer Lake Basin (**DLB**) and the Red Indian Line (**RIL**). In places, anomalies associated with the granitoids extend beneath the sediments of the Springdale Group (**SG**) and the Buchans Group (**BG**), suggesting that the granitoids underlie the sediments (Figures 5.10, 5.11, 5.13, and 5.14). Some of the granitoid intrusions obviously do not have associated magnetic highs (Figures 5.10, 5.11, 5.13, and 5.14).

Layer stripping (Jacobson, 1987) of the magnetic field (Figures 5.25a,b,c,d and 5.26a,b,c,d) shows that there is a wide range of magnetic anomaly wavelengths associated with the Topsails Igneous Terrane. These maps suggest that the causative bodies in the Topsails Igneous Terrane may extend to depths beyond 5 km.

There are several linear magnetic anomalies within the Victoria Lake Group (**VLT** and **VLS**) and Tally Pond Volcanics

(TPV) between the Red Indian Line (RIL) and Noel Pauls Line (NPL) (Figures 5.11 and 5.14). These are orientated parallel to regional structural trends in the area, but do not correlate with the mapped geology except for one anomaly obviously associated with an exposed quartz porphyry (QP) intrusion. The other anomalies may reflect unexposed shallow intrusions of similar composition. The shaded relief map with false sun illumination angle of 315° (Figure 5.17b) highlights the southeast edge of these anomalies.

Upward continuation (Figures 5.23a,b,c,d) and layer stripping (Jacobson, 1987) (Figures 5.26a,b,c,d) suggest that these anomalies have significant contributions from depths below 5 km.

Southeast of Noel Pauls Line (NPL) the magnetic field is predominantly negative until the Hermitage Bay Fault (HBF), the Gander-Avalon boundary, is reached (Figures 5.11, 5.12, 5.14, and 5.15). The Pipestone Pond (PP) ultramafic body on the western edge of the Mount Cormack Subzone has a large amplitude magnetic high associated with it (Figures 5.11 and 5.14). The Pipestone Pond (PP) anomaly is highlighted on both of the shaded relief maps (Figures 5.17a,b), and also on the second vertical derivative of the magnetic field (Figure 5.20).

Layer stripping (Jacobson, 1987) indicates that the Pipestone Pond (PP) causative body extends to depths greater

than 5 km (Figures 5.26a,b,c,d).

The North Bay Granite (NBG) appears to have an overall low amplitude magnetic high associated with it (Figures 5.12 and 5.15), much of which appears to comprise short wavelength components, as is indicated by the layer stripping (Jacobson, 1987) maps (Figures 5.27a,b,c,d). This indicates that the North Bay Granite (NBG) anomalies are related to shallow sources, but it is possible that the anomaly due to the deeper part of this body is not discerned because of its very small amplitude.

The Ackley Granite (AG) and an area beneath Fortune Bay (FB) contain the most significant magnetic anomalies near the southern part of the Meelpaeg Transect (Figures 5.12 and 5.15). The shaded relief images (Figures 5.18a,b) and second vertical derivative map (Figure 5.21) highlight the internal structure of these anomalies which is not obvious in the original magnetic field map (Figure 5.12).

Upward continuation (Figures 5.24a,b,c,d) and depth separation filtering (Jacobson, 1987) (Figures 5.27a,b,c,d) suggest that the Ackley Granite (AG) continues to depths exceeding 7.5 km, which is consistent with 3-D gravity inversion results (Miller, 1988) which places the base of the Ackley Granite at depths greater than 8 km. The anomaly beneath Fortune Bay (FB) has little shallow contribution (Figures 5.27a,b,c,d), which is to be expected due to the

presence of the water column above the body.

5.2.3. Gravity:

The Bouguer gravity maps for regions along the Meelpaeg Transect are presented in Figures 5.28, 5.29, and 5.30.

It should be noted that the gravity coverage is extremely thin over most of the Bay of Islands Complex and marginal areas, and consequently the associated Bouguer anomalies are ill-defined for the west segment of the Meelpaeg Transect. This poor definition is retained in the derived maps, and therefore, the conclusions drawn for this region are tenuous.

The west coast of Newfoundland in the area of Bay of Islands has a strong gravity gradient associated with it. This is obvious on Figures 1.2 and 5.28, where the Bouguer gravity values are seen to become more negative towards the west. When a third order polynomial surface is removed from the Bouguer gravity map to produce a residual gravity map (Figure 5.31), this trend is still present, but now we can see it is in part due to the presence of a high density body running parallel to the coastline which likely corresponds to the Bay of Islands Complex (**TM**, **NA**, **BMD**, and **LH**). The gradient is highlighted effectively on the horizontal gradient map (Figure 5.34).

Only the North Arm Massif (**NA**) of the Bay of Islands Complex appears to have an associated gravity high (Figure

5.28). When a third order polynomial surface is removed (Figure 5.31) from the Bouguer gravity map, all of the Bay of Islands Complex can be seen to exhibit a slight gravity high. The edge of the North Arm Massif (**NA**) is highlighted on the horizontal gradient map (Figure 5.34), while the other massifs of the Bay of Islands Complex are not. All parts of the complex (**TM**, **NA**, **BMD**, and **LH**) are highlighted on the second vertical derivative map (Figure 5.37), and are picked by the zero contour of the second vertical derivative (Figure 5.40), which ideally corresponds to density boundaries.

The eastern portion of the Long Range Inlier (**LRI**) has a gravity high associated with it (Figure 5.28), which remains on the residual gravity map (Figure 5.31). This anomaly becomes separated into several distinct anomalies on the second vertical derivative map (Figure 5.37), and the zero level contour of the second vertical derivative (Figure 5.40) appears to follow the southeastern edge of the Long Range Inlier (**LRI**) indicating that it is a density boundary.

The Notre Dame Subzone rocks east of the Long Range Fault (**LRF**) have significantly higher Bouguer gravity values than the Humber Zone rocks to the west (Figure 5.28). Looking at the horizontal gradient of gravity (Figure 5.34), it appears that the density boundary separating these two regions is somewhat to the southeast of the Grand Lake Fault (**GLF**). The second vertical derivative of gravity (Figure 5.37) and the

zero level contour of the second vertical derivative (Figure 5.40) also place the density boundary to the southeast of the Grand Lake Fault (GLF). The Grand Lake Fault (GLF), which is not observed on the seismic data, may be the density boundary if it is southeast dipping.

Bouguer gravity maps (Figure 5.29 and 1.2) indicate that the Notre Dame Subzone rocks south of the Meelpaeg Transect are denser than those to the north. This contrast is emphasized when a first order regional trend is removed from the Bouguer map (Figure 5.32). This indicates a density boundary running from 490 E, 5430 N to 510 E, 5400 N, nearly parallel to the Meelpaeg transect which is coincident with it at this location. This boundary is highlighted on the horizontal gradient map (Figure 5.35) which shows a high gravity gradient crossing the Meelpaeg transect between LE89-4 and LE89-5 at an angle of about 15° with the transect. It is also picked up by the zero contour of the second vertical derivative (Figure 5.41). This boundary appears to cross the entire Notre Dame Subzone in this area. Geologically, it is unknown what is causing this boundary.

Although not obvious from the Bouguer gravity map (Figure 5.29), the Red Indian Line (RIL) does have a gravity signature. The Red Indian Line (RIL) gravity signature is only identified on the second vertical derivative map (Figure 5.38) and its corresponding zero contour (Figure 5.41), where

the correlation is very good. This is a prime example of how the derived map provides information not observed in the original Bouguer map.

Noel Pauls Line (NPL) is exhibited on the Bouguer gravity map (Figure 5.29) as a boundary between higher density rocks to the northwest and lower density rocks to the southeast. This relation is made more obvious when a first order polynomial surface is removed from the Bouguer map (Figure 5.32). Noel Pauls Line (NPL) has a large horizontal gradient associated with it towards the southwest, indicating it is a significant density boundary, but the gradient decreases towards the northeast (Figure 5.35).

The Bouguer gravity map (Figure 5.29) and the residual gravity map (Figure 5.32) both show a noticeable positive anomaly over the Pipestone Pond ultramafic body (PP). This also appears on the second vertical derivative map (Figure 5.38).

There is a density boundary just to the east of the Middle Ridge Granite (MRG) indicated by the Bouguer gravity map (Figure 5.30), apparently coincident with a linear trend of small ultramafic bodies and mafic volcanics exposed there. The gravity high to the east of this is bounded on the eastern side by the Mount Sylvester Granite (MSG) and the Northwest Brook Complex (NBC). This anomaly is better defined on the residual gravity map (Figure 5.33). The northwest and

southeast boundaries of this anomaly are highlighted on the horizontal gradient map (Figure 5.36), as well as the second vertical derivative (Figure 5.39) and the corresponding zero contour (Figure 5.42). A dense body within or beneath the Bay D'Espoir Group (BDG) sediments in this area is indicated.

The Hermitage Bay Fault (HBF) separates lower density Gander Zone rocks from higher density Avalon rocks to the south in this area (Figures 5.30 and 5.33). This Gander-Avalon boundary has a horizontal gradient high (Figure 5.36) associated with it, which is particularly strong towards the southwest. The second vertical derivative map (Figure 5.39) shows that the Avalon Zone has a different gravity character than the Gander Lake and Exploits Subzones in this area. The Gander Lake and Exploits Subzones have a smoother varying Bouguer field than does the Avalon Zone. The Hermitage Bay Fault (HBF) is picked by the zero contour of the second vertical derivative (Figure 5.42).

5.2.4. The Models:

The potential field 2½-D models for the Western, Central, and Eastern Segments of the Meelpaeg Transect are presented in Figures 5.7, 5.8, and 5.9 respectively along with the corresponding seismic line drawings. For modelling purposes, gravity and magnetic data for each segment were extracted on straight lines roughly corresponding to the path of the

seismic profiles. It was then scaled lengthwise to match the length of the seismic profile to facilitate easy visual comparison of the model and seismic data.

For all three segments of the Meelpaeg Transect, physical property data (Appendix A) were used to constrain the density and magnetic susceptibility of modelled units.

In the West Segment of the Meelpaeg Transect (Figure 5.7), the predominant features governing the Bouguer gravity response are the package of relatively low density ($\Delta\rho$=0.02 g/cm^3) sediments of the Humber Arm Allochthon, and the very low density ($\Delta\rho$=-0.12 g/cm^3) Carboniferous sediments in the Deer Lake Basin (DLB). Magnetic anomalies appear to be controlled by parts of the Bay of Islands Complex (k=5.00 x 10^{-4} and k=1.00 x 10^{-3}) in the upper part of the Humber Arm Allochthon, a magnetic layer (k=3.00 x 10^{-3}) beneath the Humber Arm Allochthon, magnetic Grenville basement (k=9.00 x 10^{-4}), and a magnetic layer (k=3.00 x 10^{-3}) beneath the Deer Lake Basin (DLB).

The Central Segment Bouguer gravity profile (Figure 5.8) detects the west-dipping modelled boundary between the Springdale Group (SG) sediments ($\Delta\rho$=0.01 g/cm^3) and the dense ($\Delta\rho$=0.15 g/cm^3) intrusives in the Topsails Igneous Terrane. The Red Indian Line is also modelled as a west-dipping boundary between the denser Topsails Terrane rocks and the lighter ($\Delta\rho$=0.10 g/cm^3) rocks to the east. This is consistent

with the contrasting Bouguer values between the Notre Dame and Exploits Subzones noted in Chapter 1. It should be noted that this boundary appears to be shifted westward with respect to its location on the seismic reflection profile. This discrepancy can be reconciled by considering the different geometric paths of the extracted potential field straight line transect and the meandering seismic transect. The potential field transect crosses the Red Indian Line (RIL) about 7 km northwest of where LE89-6 crosses it.

Noel Pauls Line (NPL) is also modelled as a gravity boundary on the Central Segment of the Meelpaeg Transect. It is modelled as a southeast-dipping contact between lower density ($\Delta\rho$=0.01 g/cm^3) metasediments of the Meelpaeg Subzone to the southeast and the higher density ($\Delta\rho$=0.10 g/cm^3) Exploits Subzone rocks to the northwest.

Magnetic anomalies along the Central Segment are modelled as shallow intrusions of various magnetic susceptibilities. These are likely gabbroic intrusions within the Topsails Terrane, and a buried equivalent of the quartz porphyry (QP) mapped on Figure 5.3.

Along the East Segment of the Meelpaeg Transect (Figure 5.9), the major feature modelled affecting the Bouguer gravity profile is the northwest-dipping contact between lower density ($\Delta\rho$=0.09 g/cm^3) crust to the northwest and higher density ($\Delta\rho$=0.10 g/cm^3) crust to the southeast. The Bouguer anomaly

caused by this major feature is relatively small due to the small density contrast across the boundary. Some low density granitoids towards the northern end of the East Segment also locally affect the Bouguer field by producing relative lows.

The most significant magnetic anomaly on the East Segment of the Meelpaeg Transect is related to the difference in character of the crust as the Hermitage Bay Fault (HBF) is crossed (Figure 5.9). Modelling suggests the difference occurs within the upper 5 km, but the orientation of the boundary is unclear.

5.3. INTERPRETATION:

Seismic data indicates that much of the Meelpaeg Transect has a similar character as the Burgeo Road Transect, with shallow southeast-dipping reflectors and northwest-dipping reflectors present in the middle and lower crust. For the most part northwest-dipping reflectors cut southeast-dipping reflectors. At the southern end, however, the transect is dominated by northwest-dipping reflectors that appear to sole into the Moho (Quinlan et al., 1992).

Major faults or terrane boundaries along the Meelpaeg Transect are not well defined on the seismic data. Some run through gaps in the transect: the Baie Verte Line or Long Range Fault runs beneath Grand Lake between lines LE89-3 and LE89-4, and the Red Indian Line runs very near the gap between

lines LE89-5 and LE89-6. Red Indian Line, Noel Pauls Line, and the Hermitage Bay Fault are not observed as seismic reflectors.

Bouguer gravity values appear to be the best method for modelling the terrane boundaries along the Meelpaeg Transect. Both the Red Indian Line and Noel Pauls Line are modelled as significant density boundaries. Magnetic anomalies are more useful for mapping near-surface rock units and intrusives on a more detailed scale, but is the only geophysical method that can detect the surface location of the Hermitage Bay Fault with confidence.

The structure of the crust along the Meelpaeg Transect can be explained by three main stages of deformation (Figure 5.43). These are: (1) thrusting of allochthonous Dunnage material from the east, (2) a stage of crustal extension, and (3) emplacement of Avalon Zone rocks by strike-slip motion.

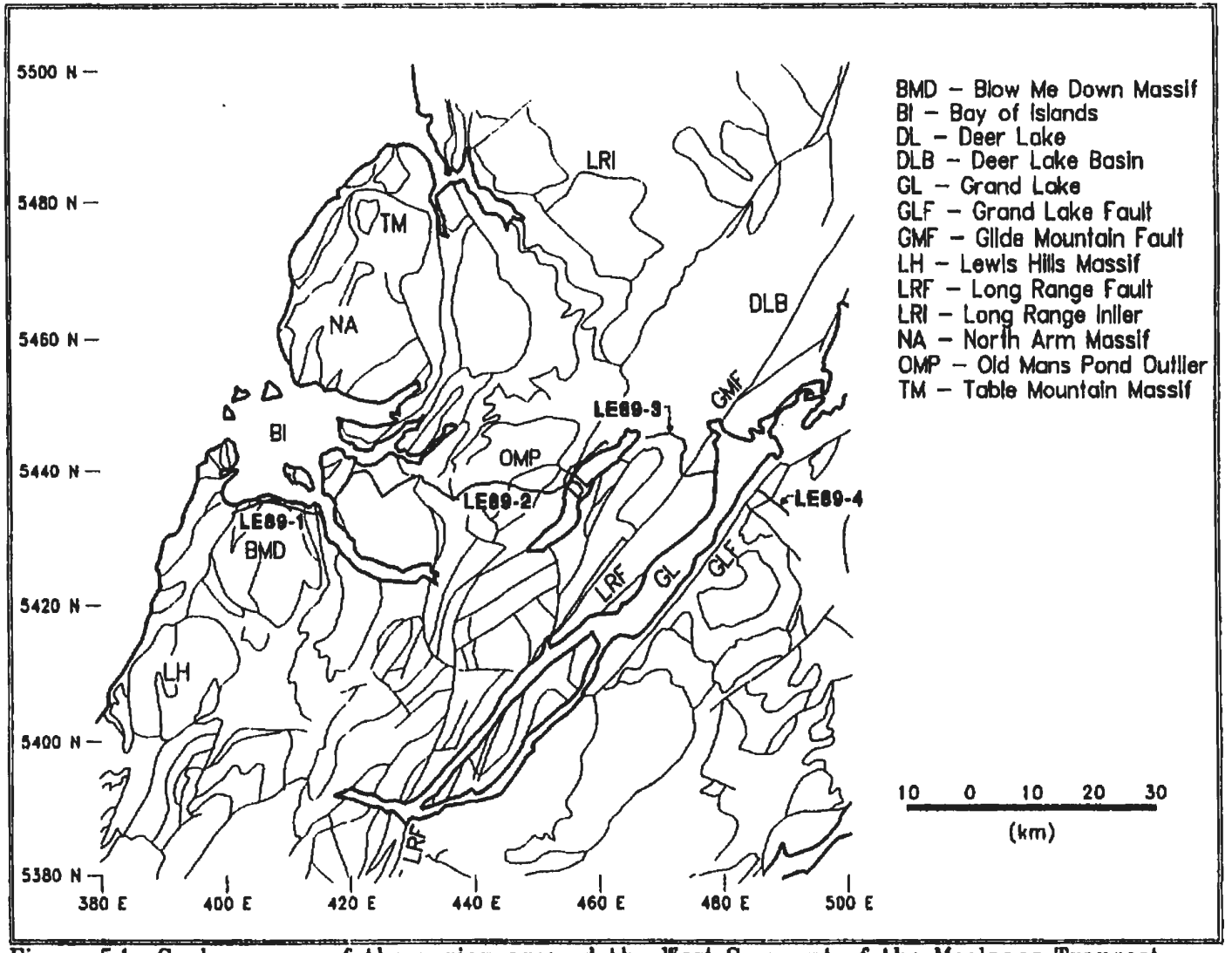

Figure 5.1: Geology map of the region around the West Segment of the Meelpaeg Transect after Colman-Sadd et al. (1990). The coordinates are in UTM Zone 21 kilometers. The legend is presented in the upper right.

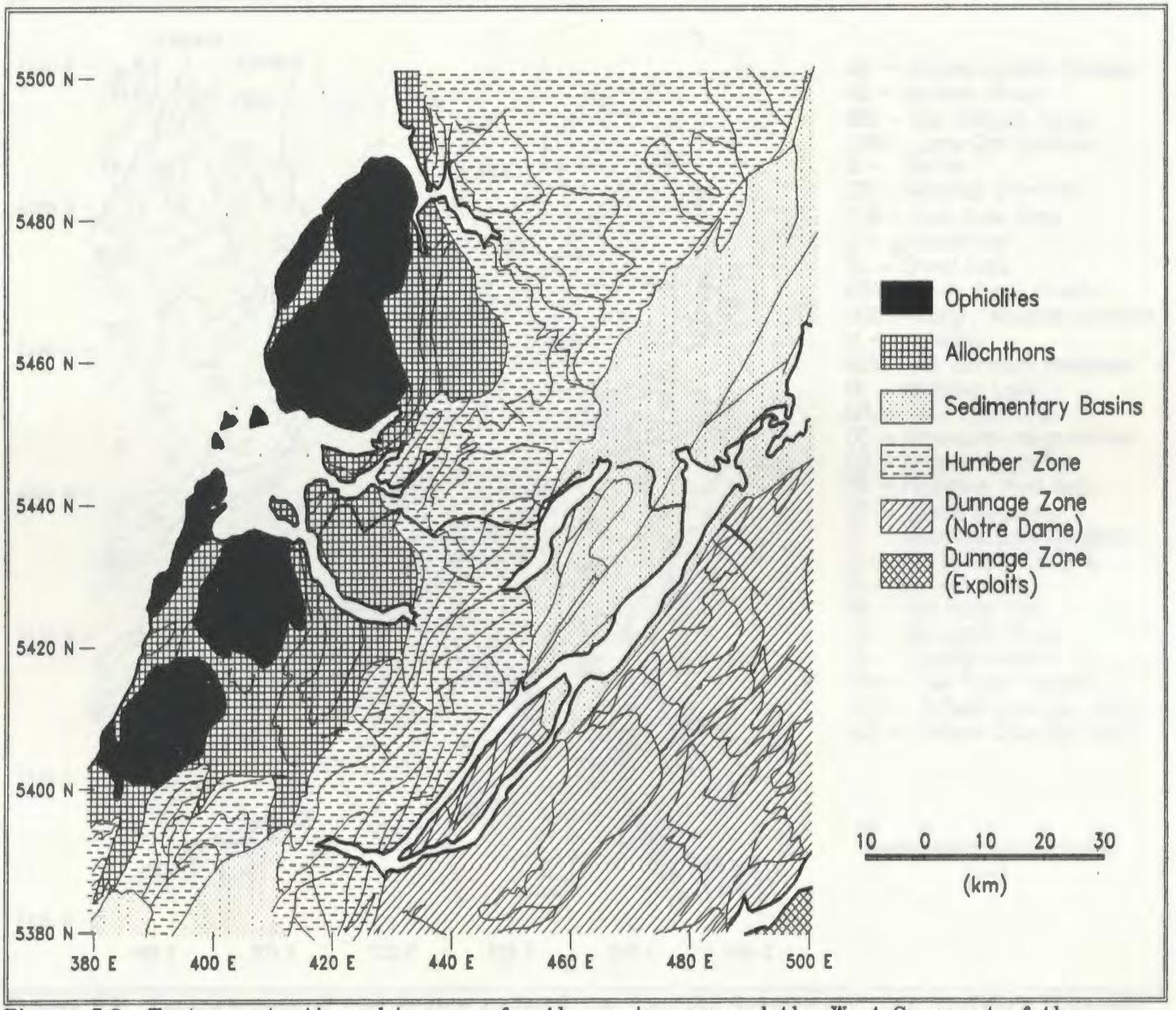

Figure 5.2: Tectono-stratigraphic zones for the region around the West Segment of the Meelpaeg Transect. Coordinates are in UTM Zone 21 kilometers.

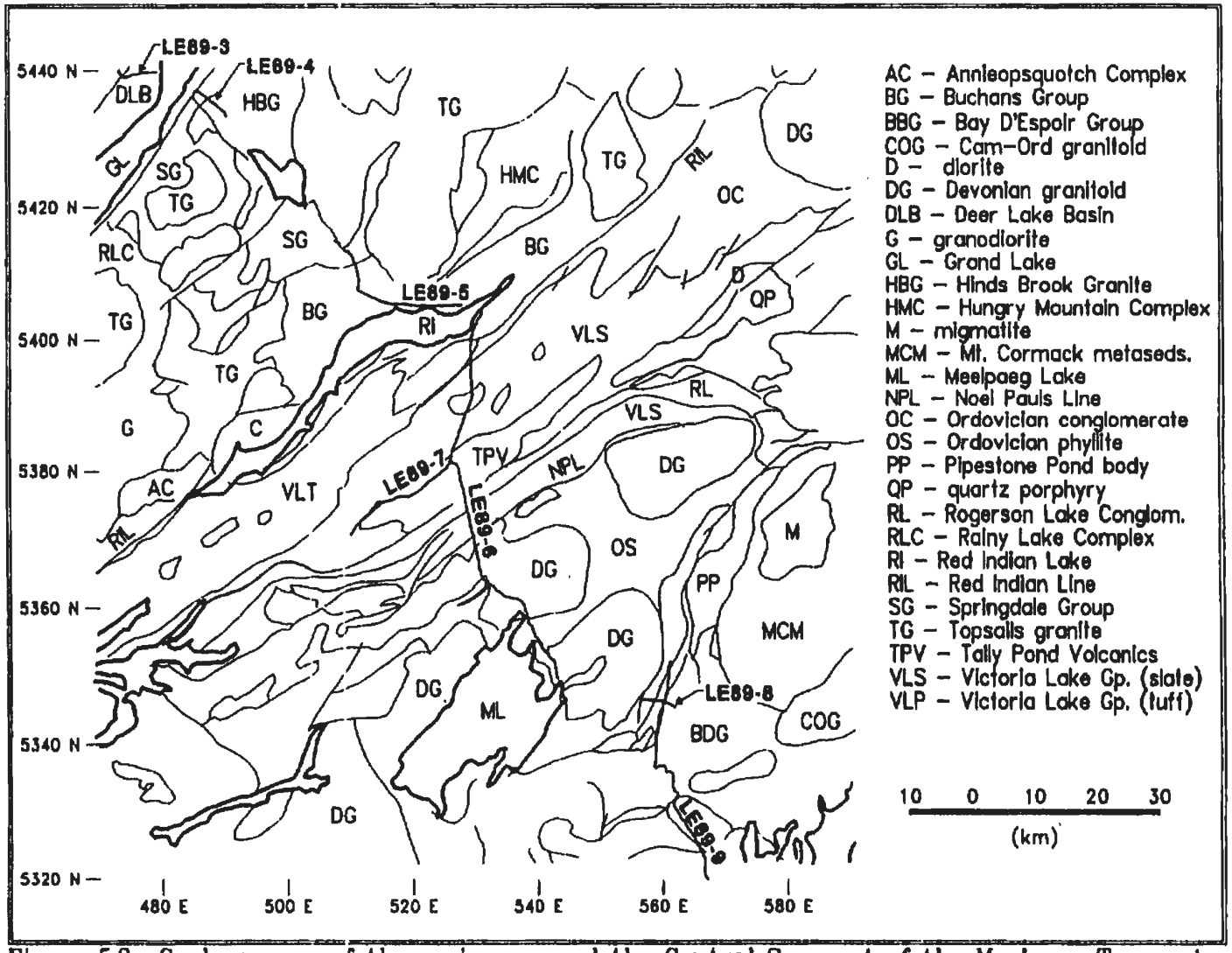

Figure 5.3: Geology map of the region around the Central Segment of the Meelpaeg Transect after Colman-Sadd et al. (1990). The coordinates are in UTM Zone 21 kilometers. The legend is presented at the right.

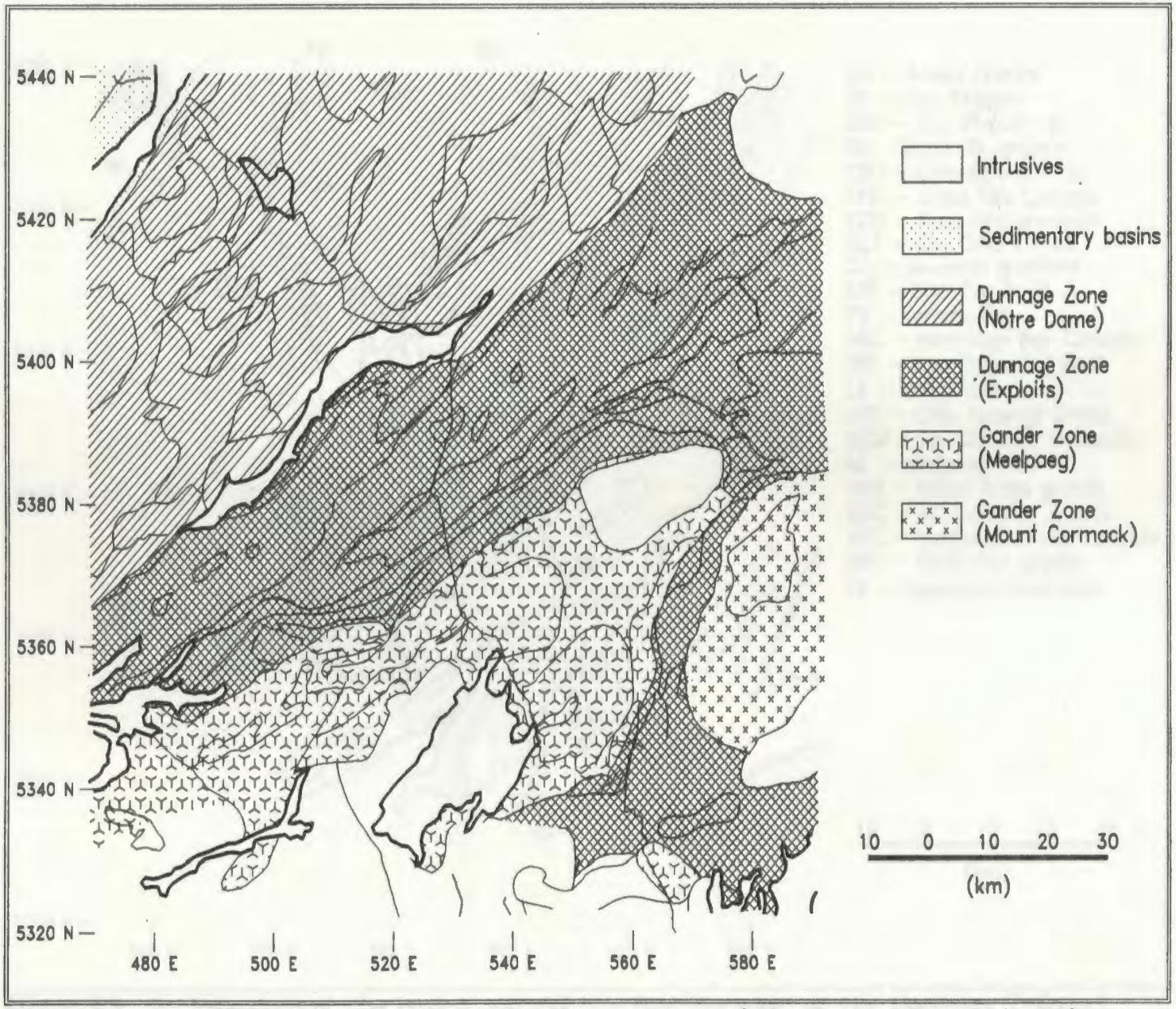

Figure 5.4: Tectono-stratigraphic zones for the area around the Central Segment of the Meelpaeg Transect.

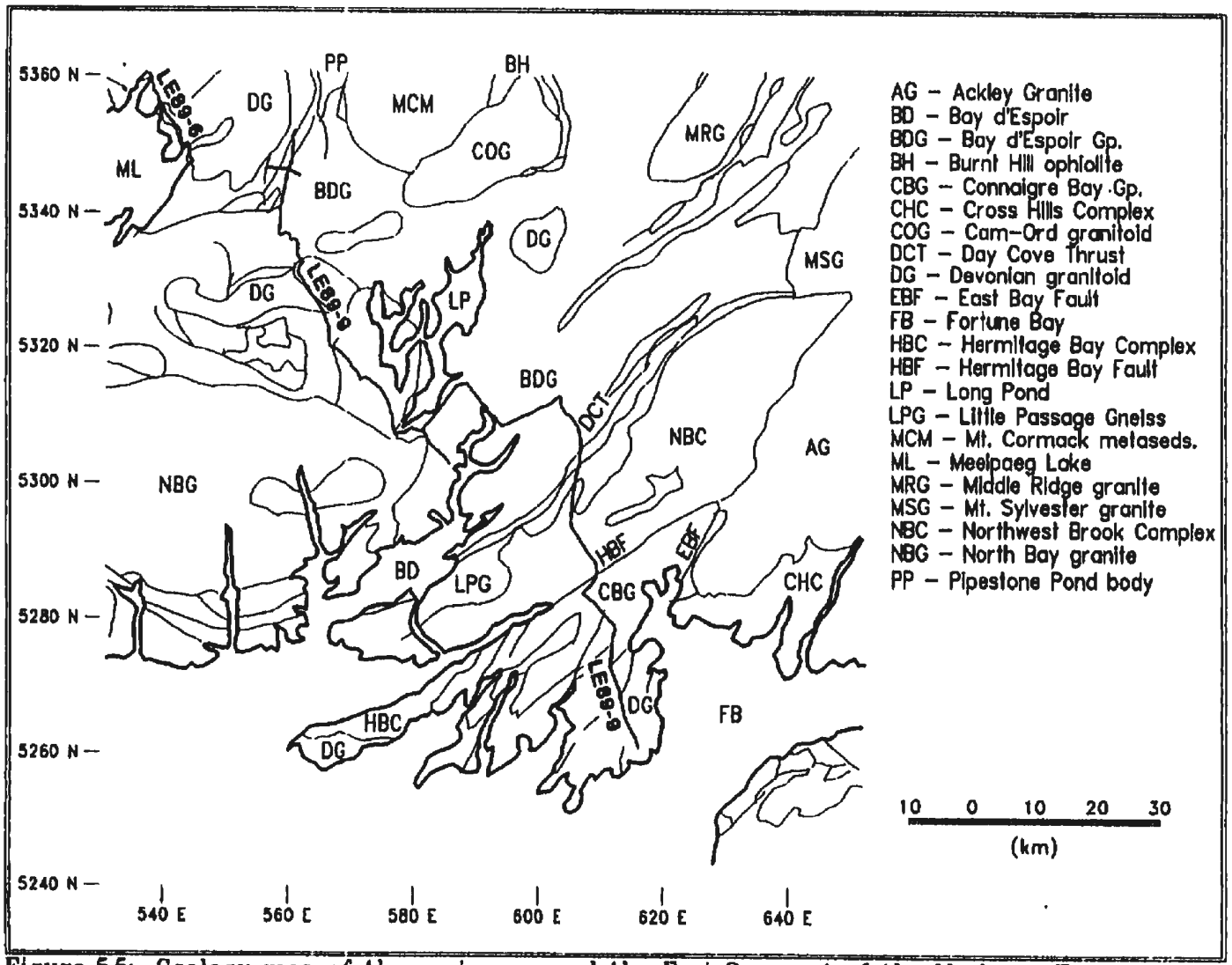

Figure 5.5: Geology map of the region around the East Segment of the Meelpaeg Transect after Colman–Sadd et al. (1990). The coordinates are in UTM Zone 21 kilometers. The legend is presented at the right.

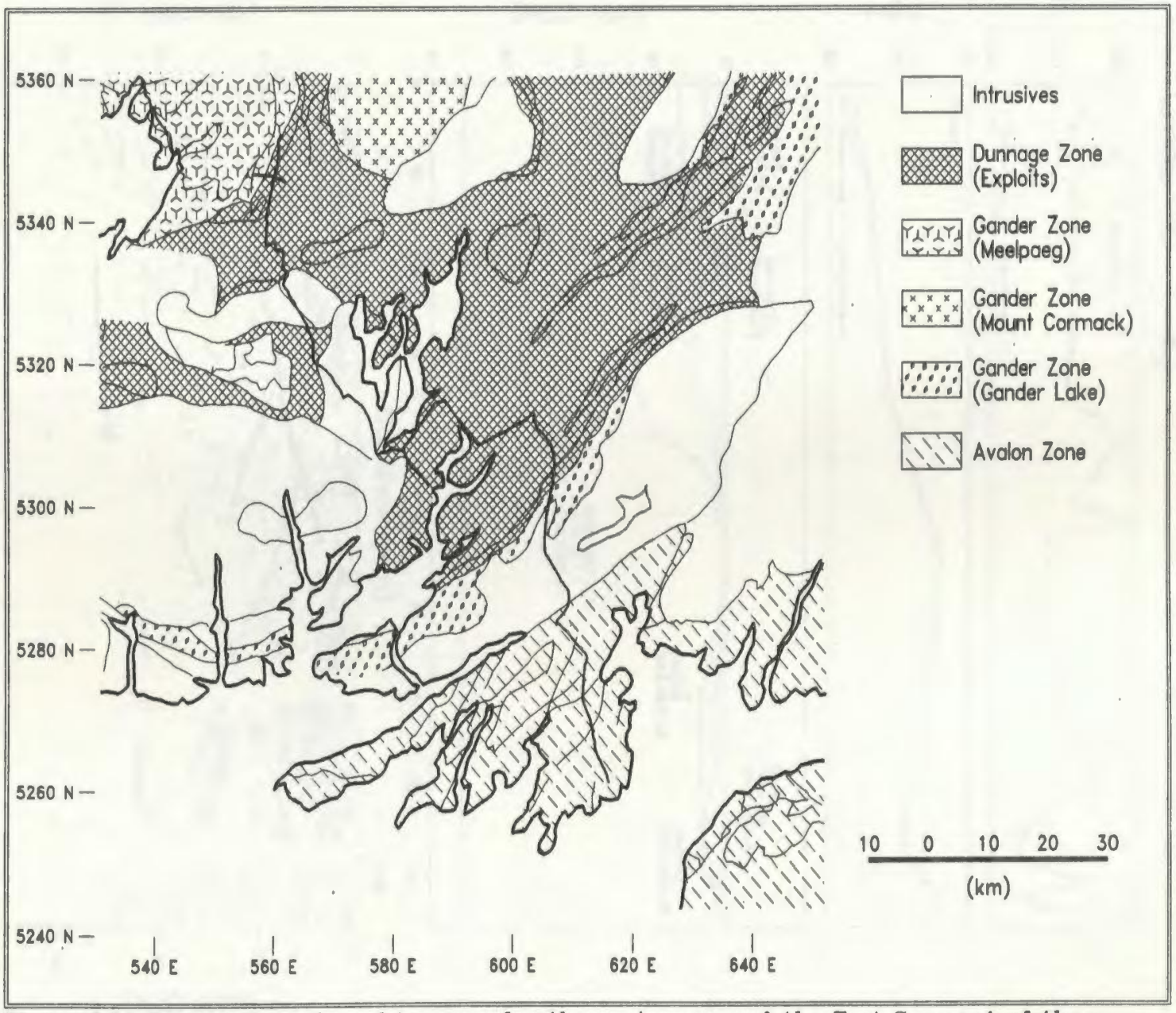

Figure 5.6: Tectono-stratigraphic zones for the region around the East Segment of the Meelpaeg Transect.

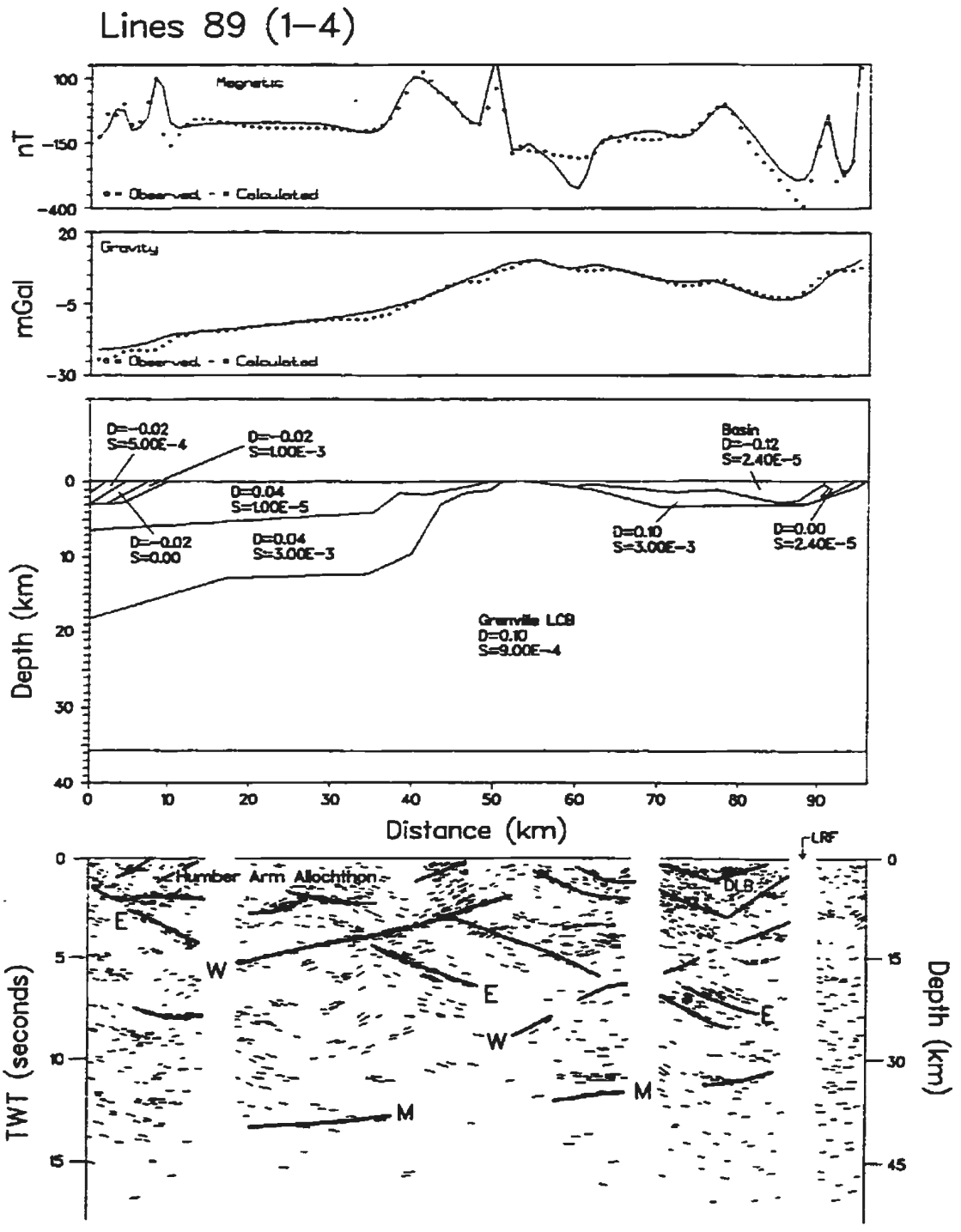

Figure 5.7: Seismic line drawing and 2 1/2–D gravity and magnetic model for the West Segment of the Meelpaeg Tansect. Legend: D – density contrast relative to 2.67 g/cc, DLB – Deer Lake Basin, E – east–dipping reflectors, LRF – Long Range Fault, M – Moho, S – magnetic susceptibility in c.g.s. units, W – west–dipping reflectors.

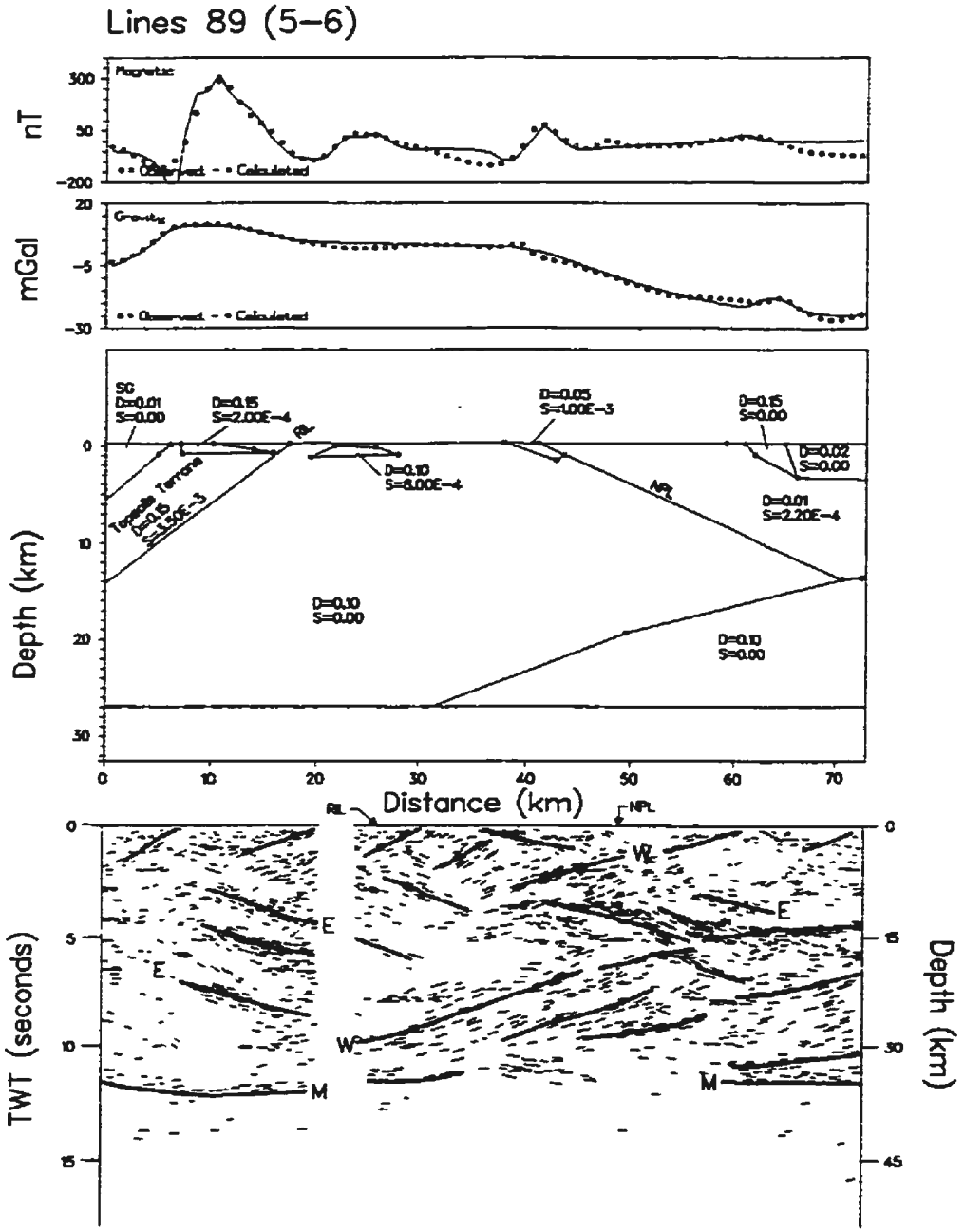

Figure 5.8: Seismic line drawing and 2 1/2–D gravity and magnetic model for the Central Segment of the Meelpaeg Transect. Legend: D – density contrast relative to 2.67 g/cc, E – east–dipping reflectors, M – Moho, NPL – Noel Pauls Line, RIL – Red Indian Line, S – magnetic susceptibility in c.g.s. units, SG – Springdale Group, W – west–dipping reflectors.

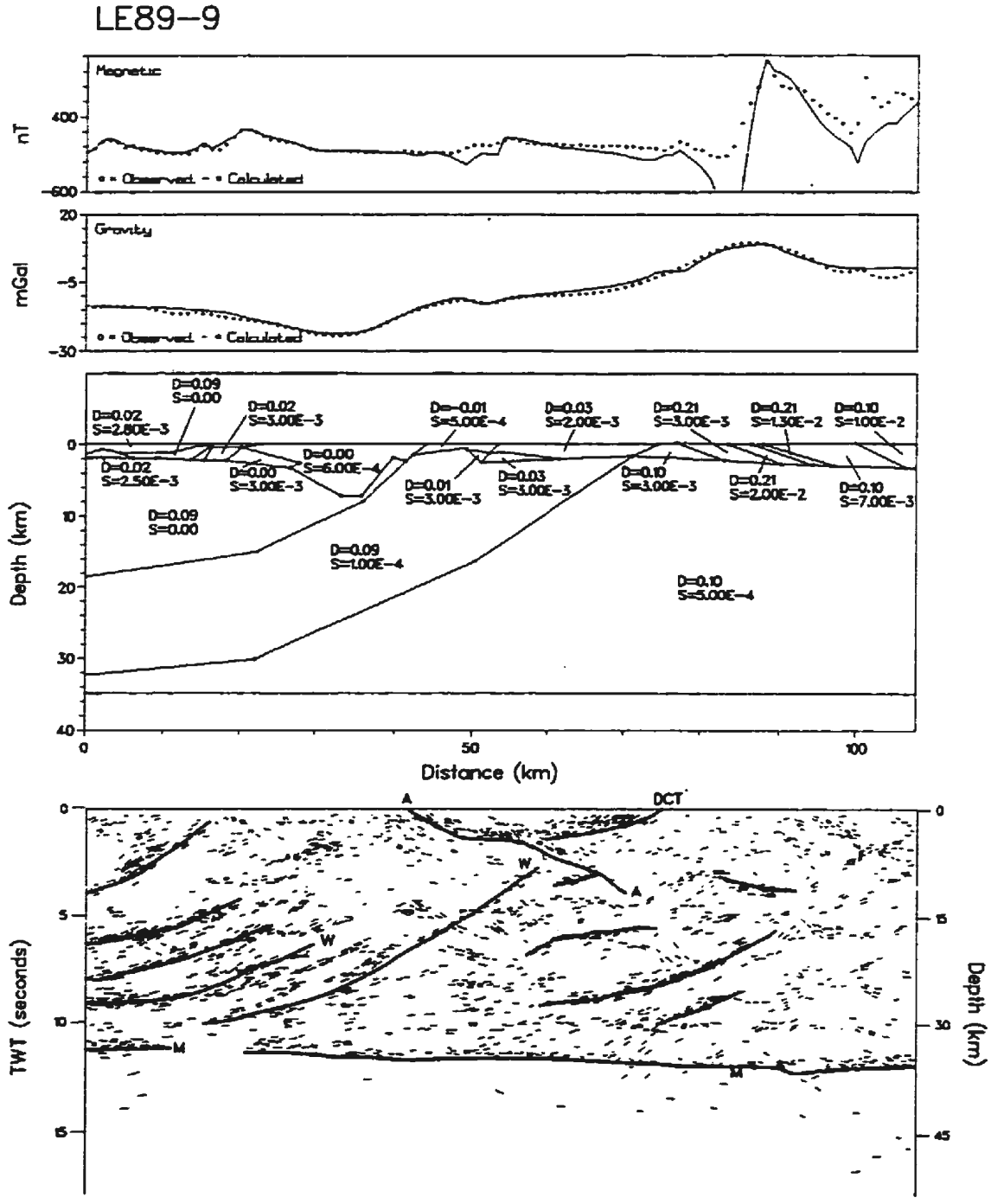

Figure 5.9: Seismic line drawing and 2 1/2-D gravity and magnetic model for the East Segment of the Meelpaeg Transect. Legend: A – reflector mentioned in the text, D – density contrast relative to 2.67 g/cc, DCT – Day Cove Thrust, M – Moho, S – magnetic susceptibility in c.g.s. units, W – west-dipping reflectors.

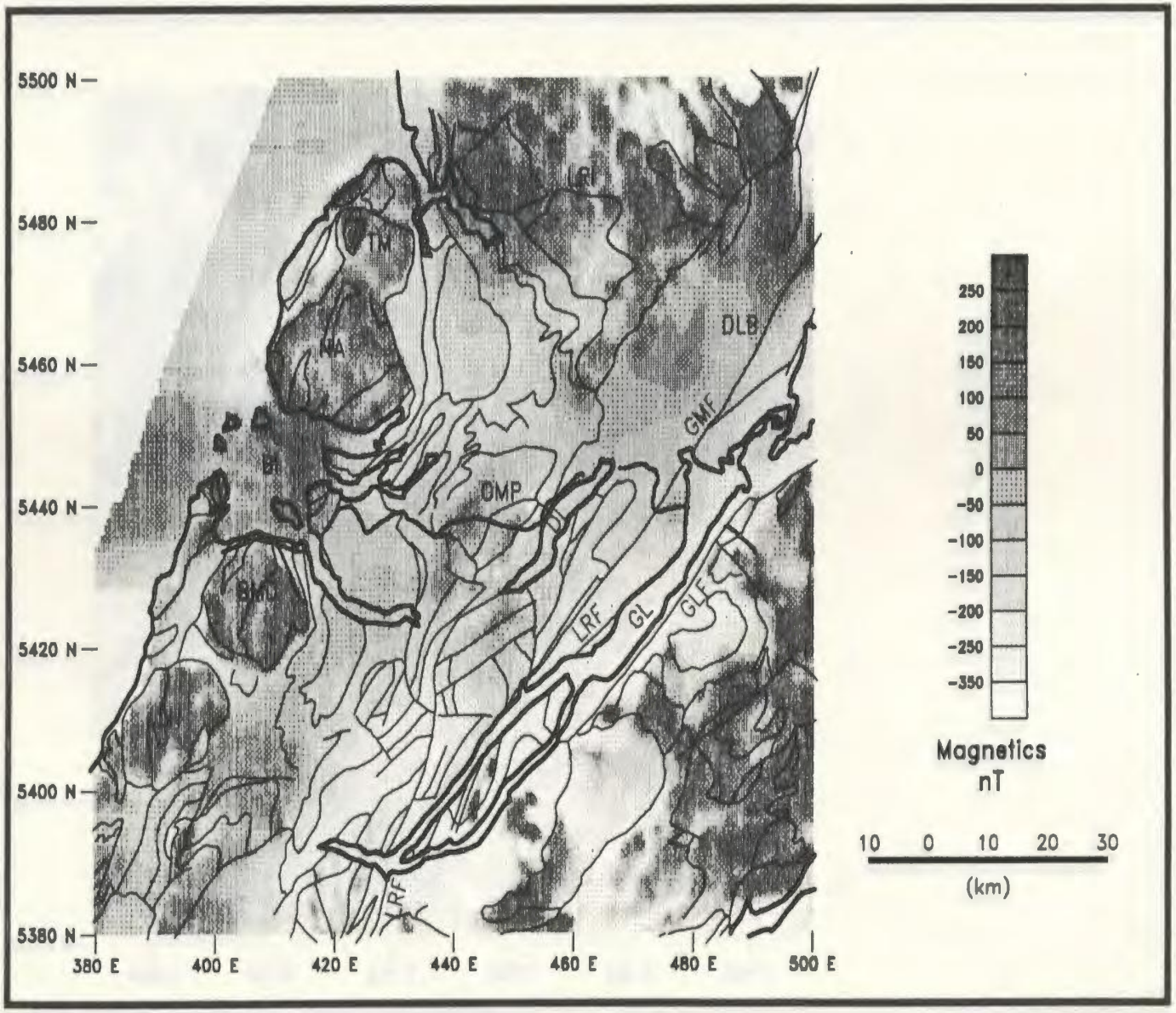

Figure 5.10: Total field aeromagnetic map of the region around the West Segment of the Meelpaeg Transect. Coordinates are in UTM Zone 21 kilometers. The legend follows that of Figure 5.1.

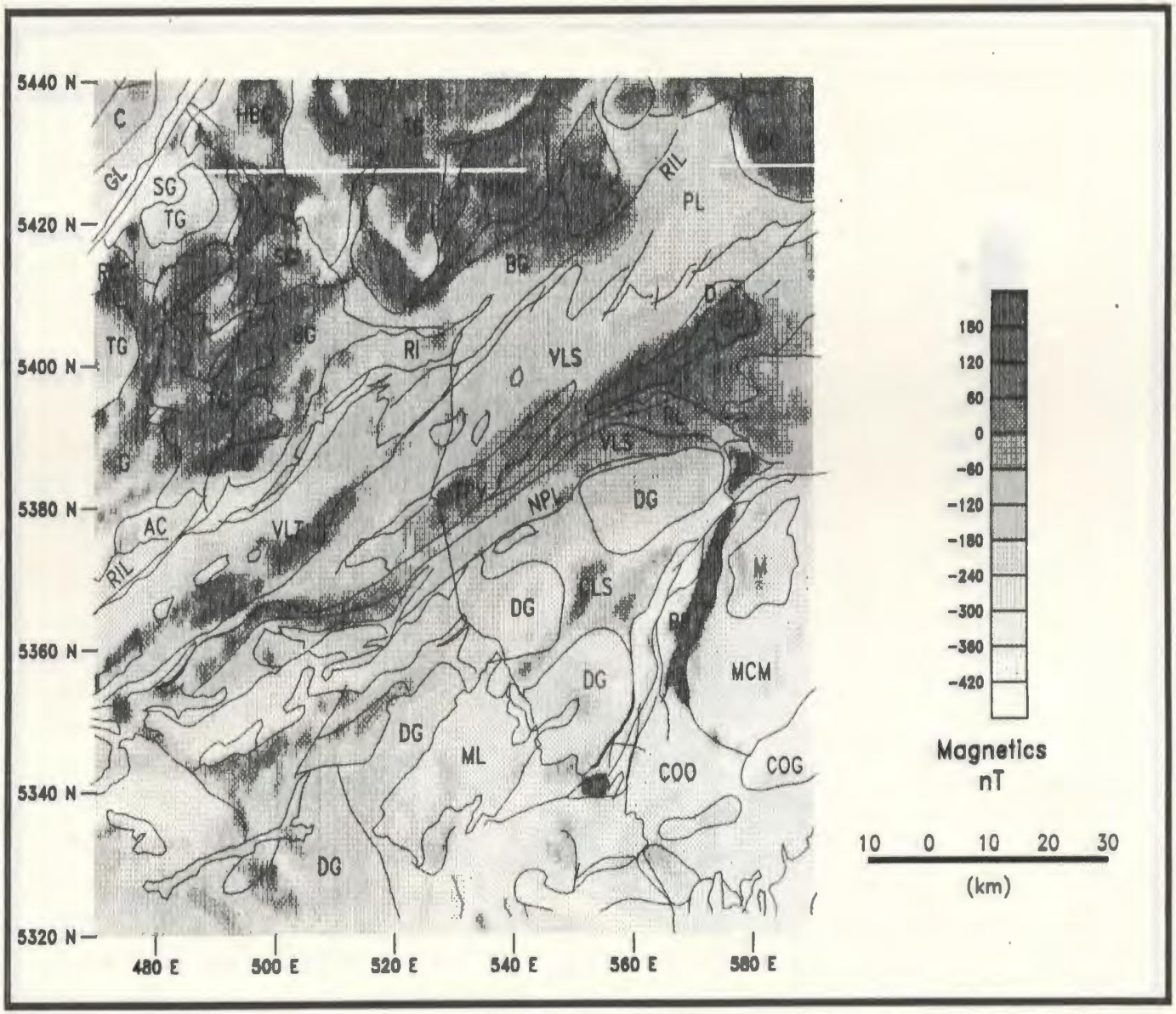

Figure 5.11: Total field aeromagnetic map of the region around the Central Segment of the Meelpaeg Transect. Coordinates are in UTM Zone 21 kilometers. The legend follows that of Figure 5.3.

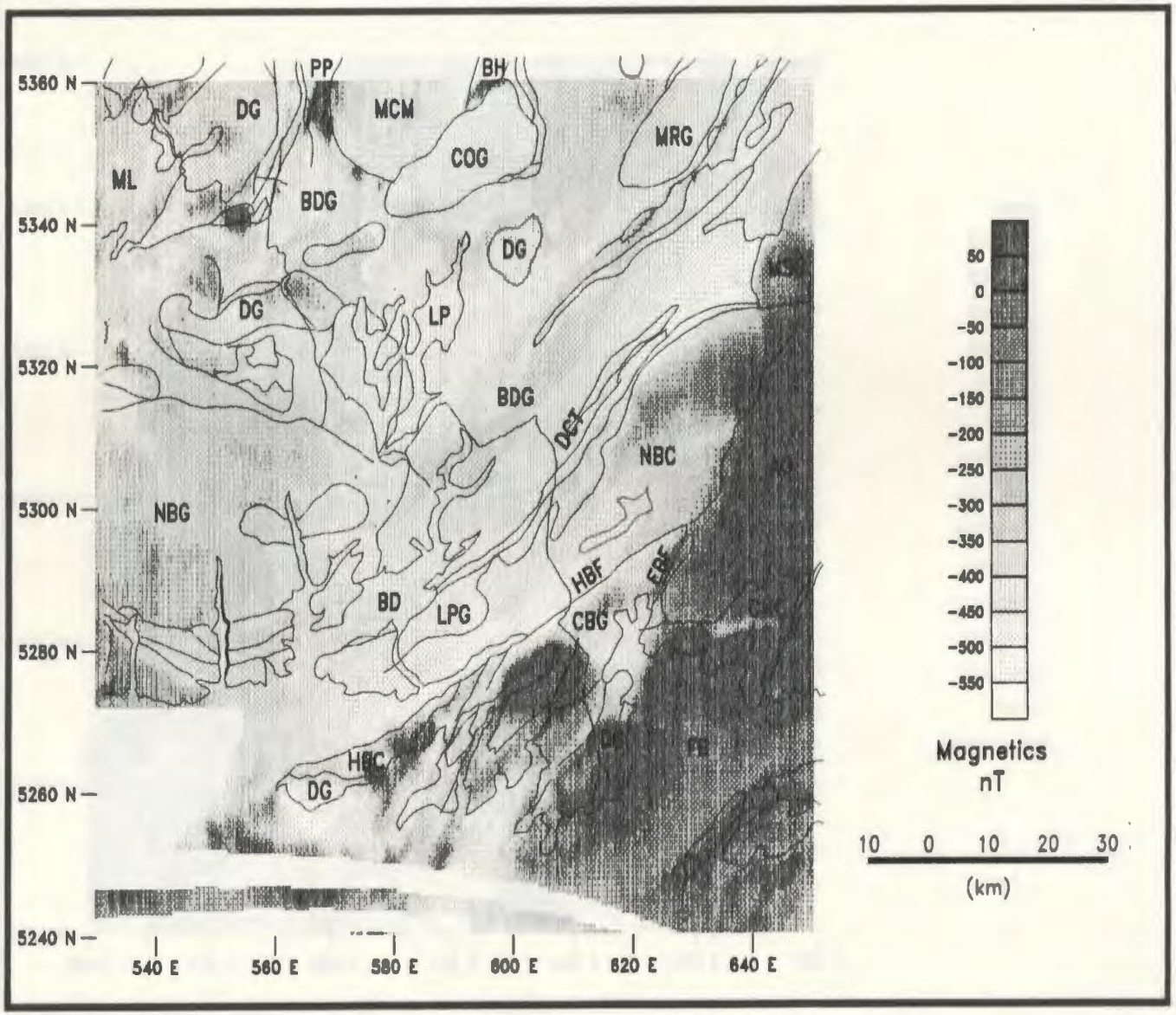

Figure 5.12: Total field aeromagnetic map of the region around the East Segment of the Meelpaeg Transect. Coordinates are in UTM Zone 21 kilometers. The legend follows that of Figure 5.5.

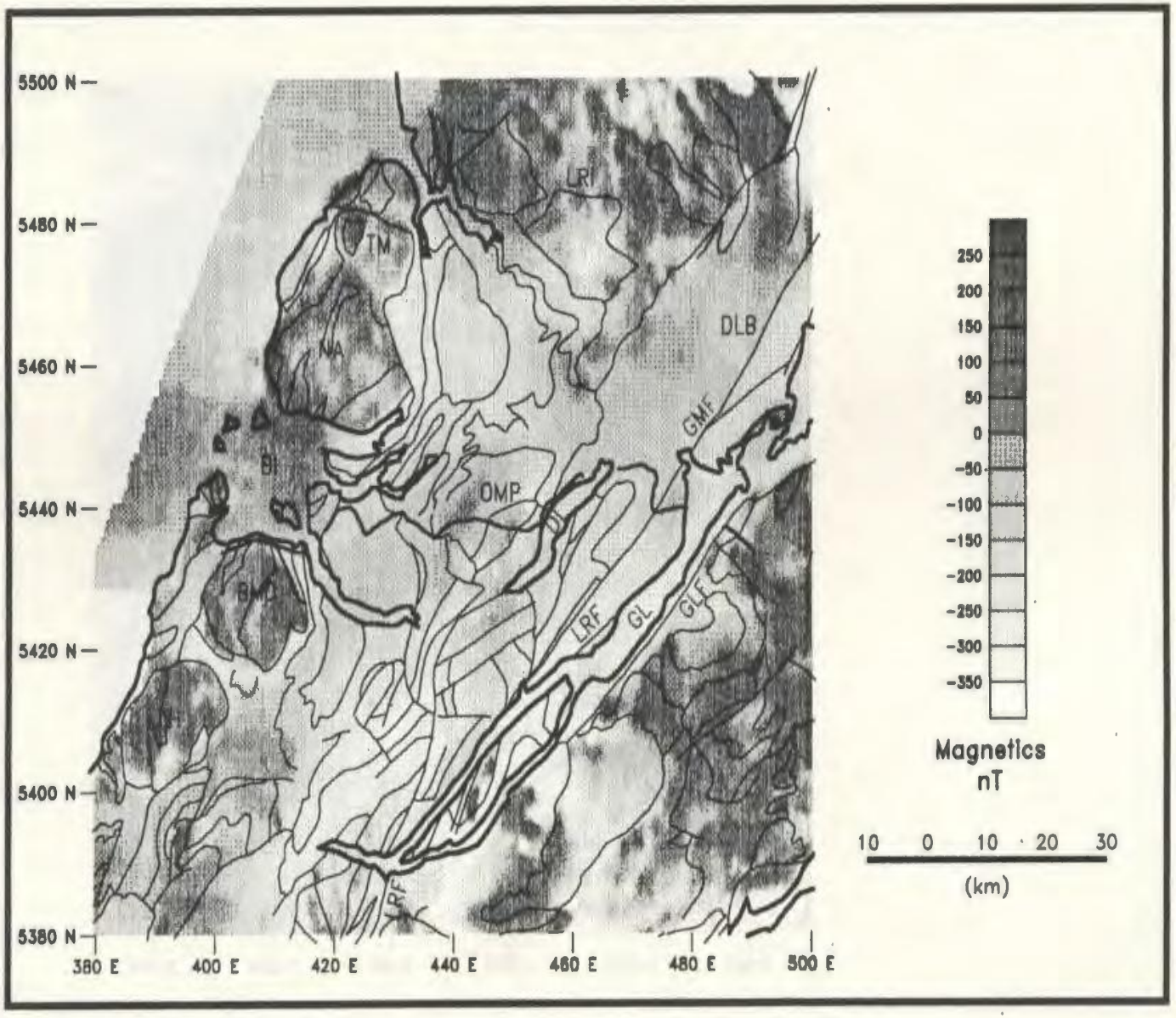

Figure 5.13: Total field aeromagnetic map of the region around the West Segment of the Meelpaeg Transect after rotation to the north magnetic pole. The legend follows that of Figure 5.1.

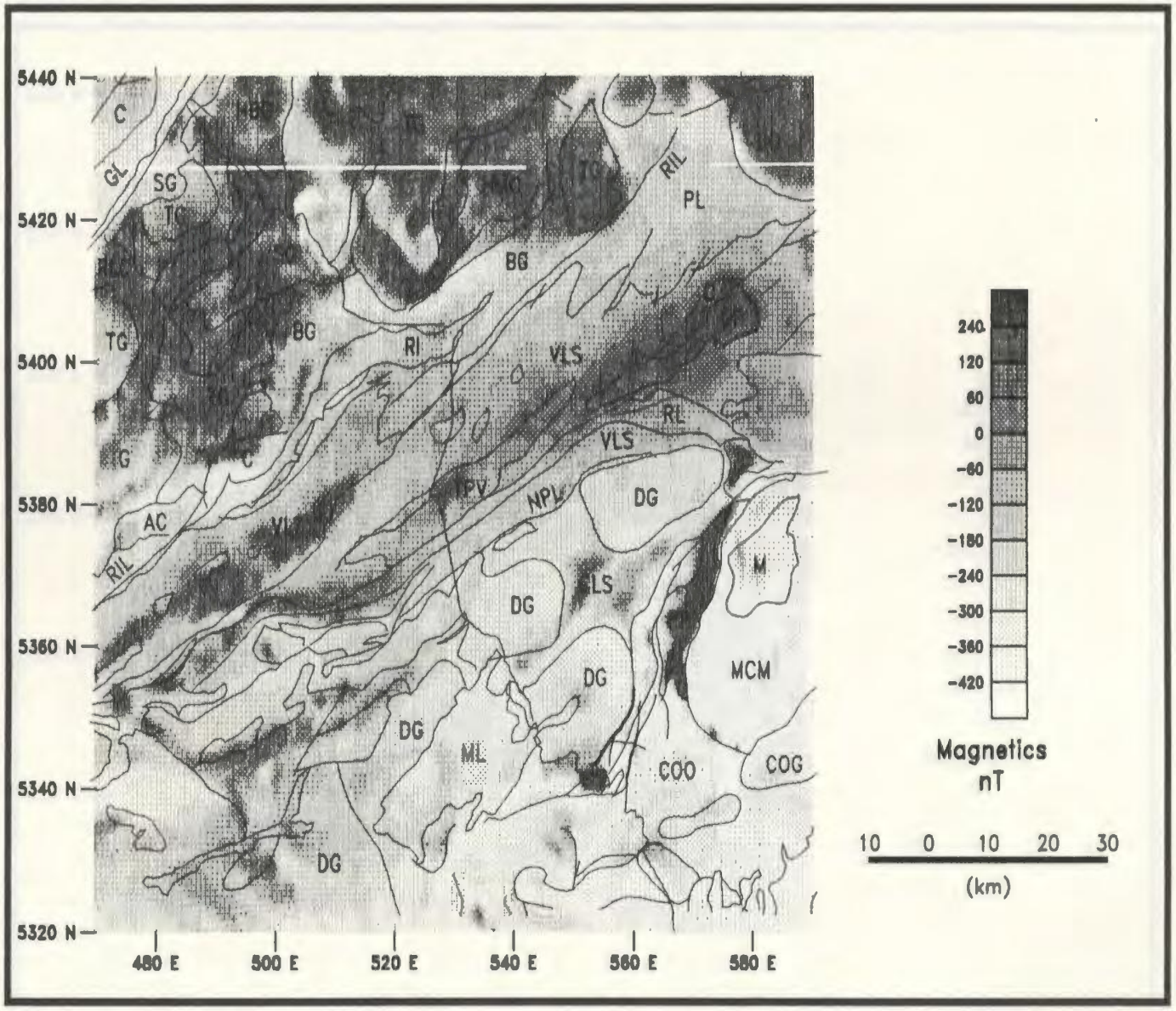

Figure 5.14: Total field aeromagnetic map of the region around the Central Segment of the Meelpaeg Transect after rotation to the north magnetic pole. The legend follows that of Figure 5.3.

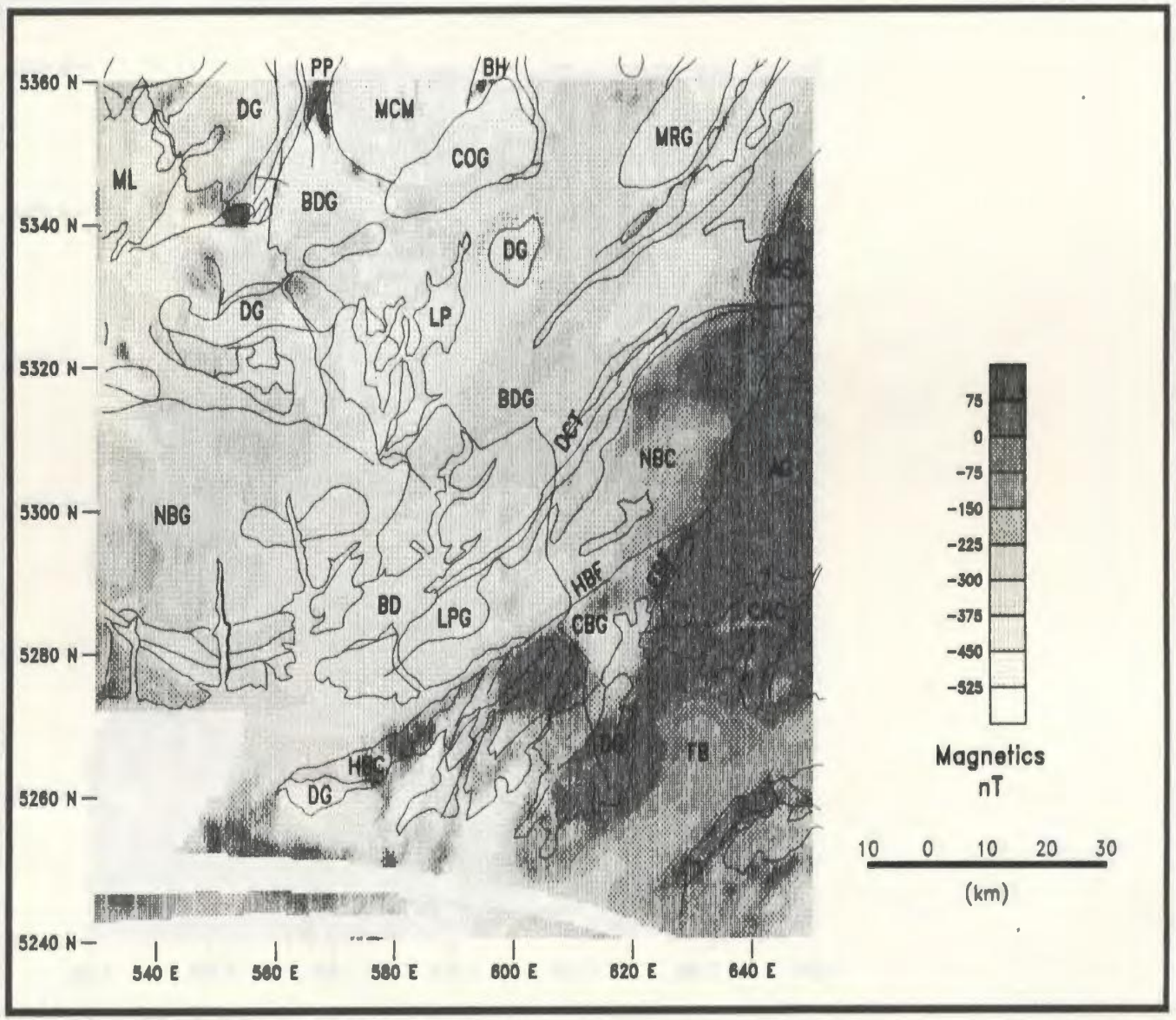

Figure 5.15: Total field aeromagnetic map of the region around the East Segment of the Meelpaeg Transect after rotation to the north magnetic pole. The legend follows that of Figure 5.5.

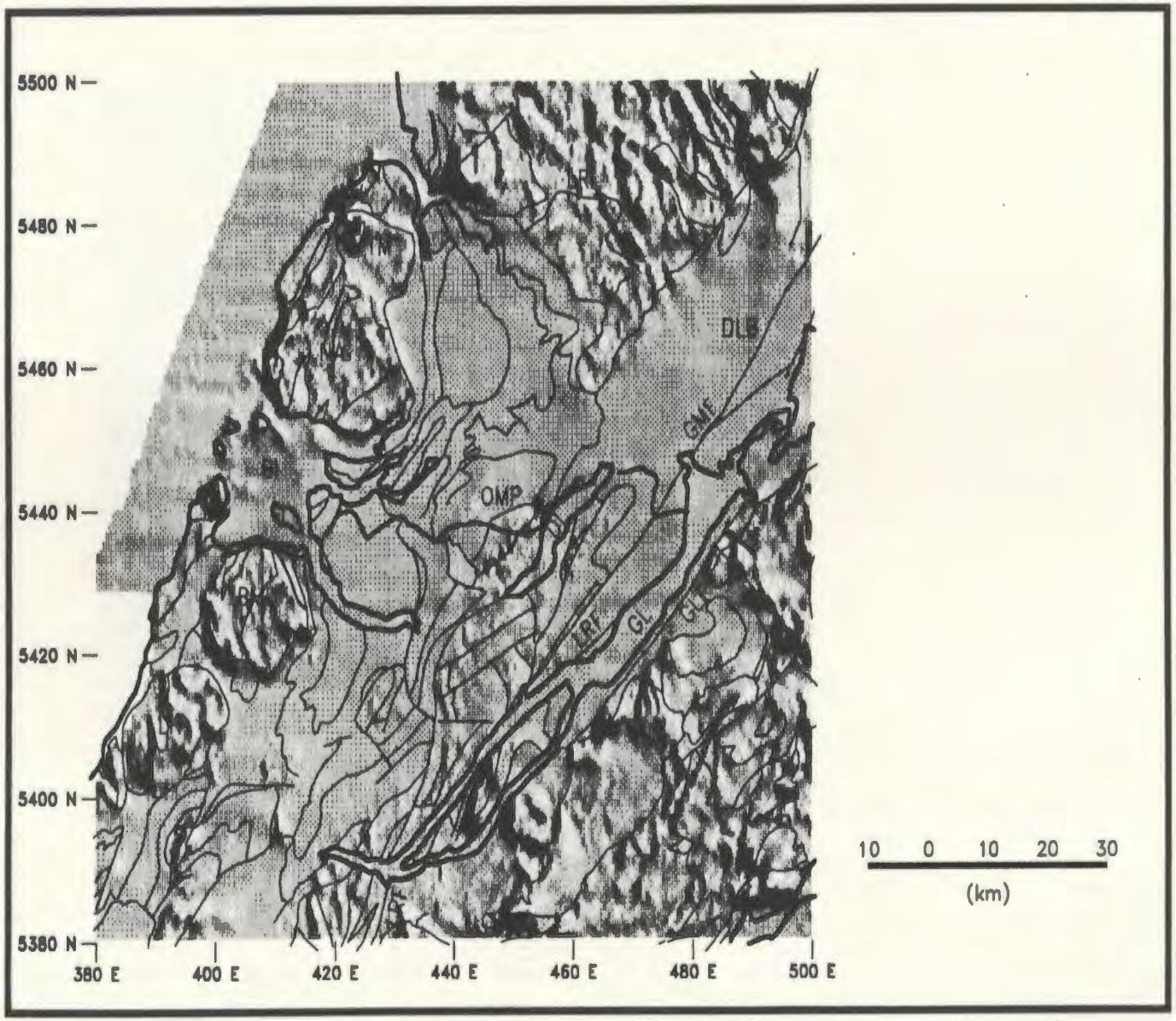

Figure 5.16a: Shaded relief image of the magnetic map for the region around the West Segment of the Meelpaeg Transect with illumination azimuth of 45° and declination of 45°. The legend follows that of Figure 5.1.

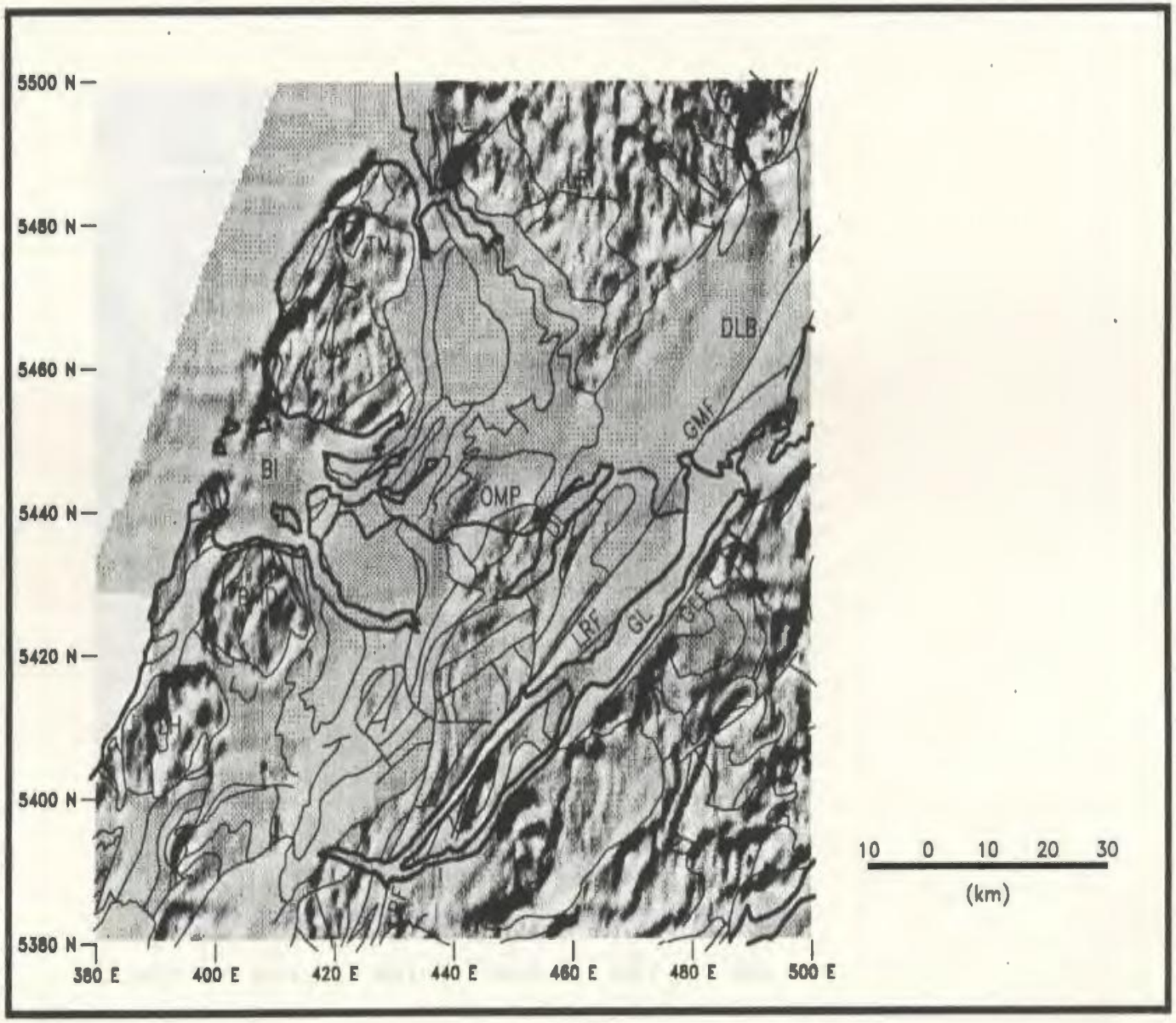

Figure 5.16b: Shaded relief image of the magnetic map for the region around the West Segment of the Meelpaeg Transect with illumination azimuth of 135° and declination of 45°. The legend follows that of Figure 5.1.

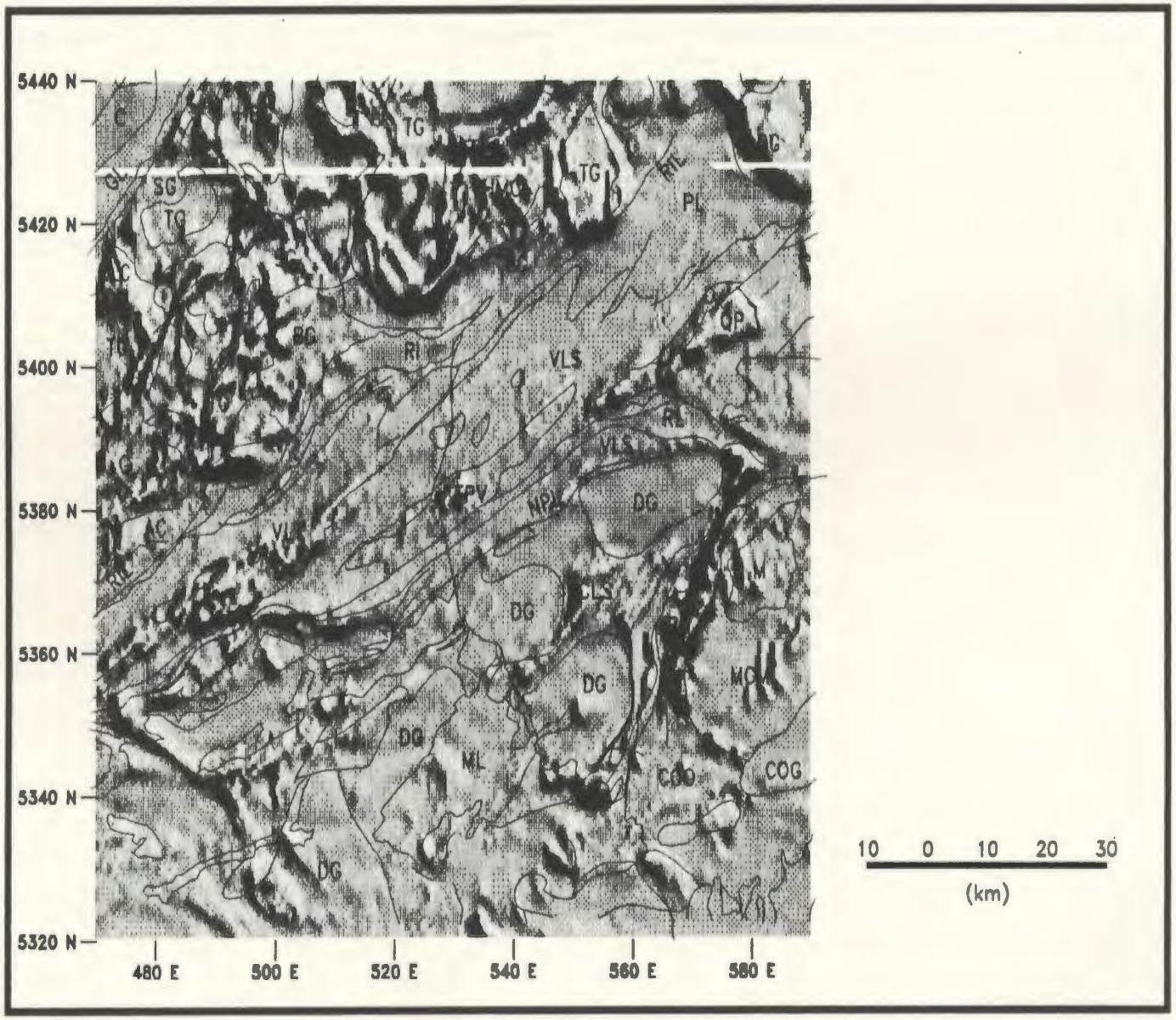

Figure 5.17a: Shaded relief image of the magnetic map for the region around the Central Segment of the Meelpaeg Transect with illumination azimuth of 45° and declination of 45°. The legend follows that of Figure 5.3.

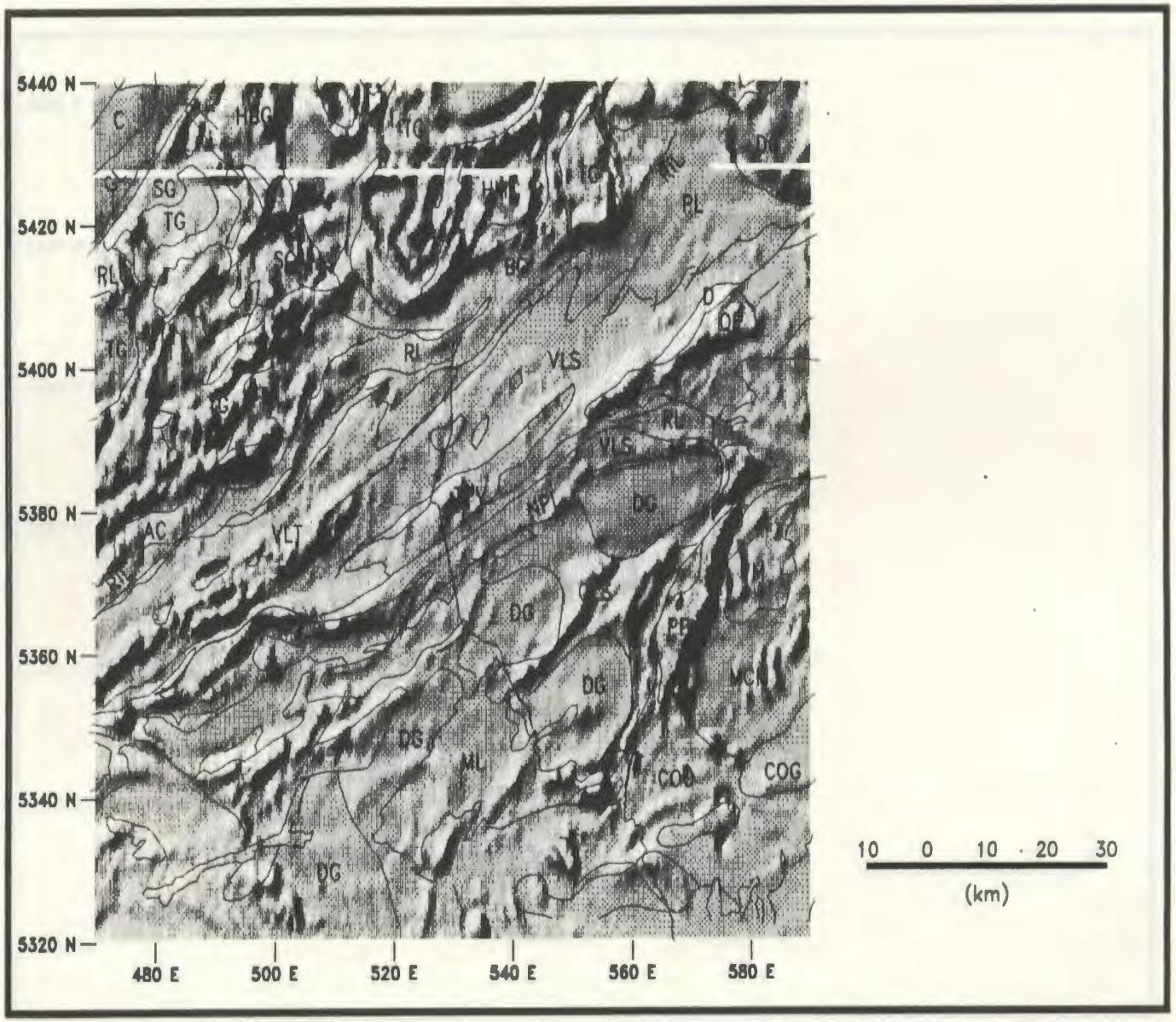

Figure 5.17b: Shaded relief image of the magnetic map for the region around the Central Segment of the Meelpaeg Transect with illumination azimuth of 315° and declination of 45°. The legend follows that of Figure 5.3.

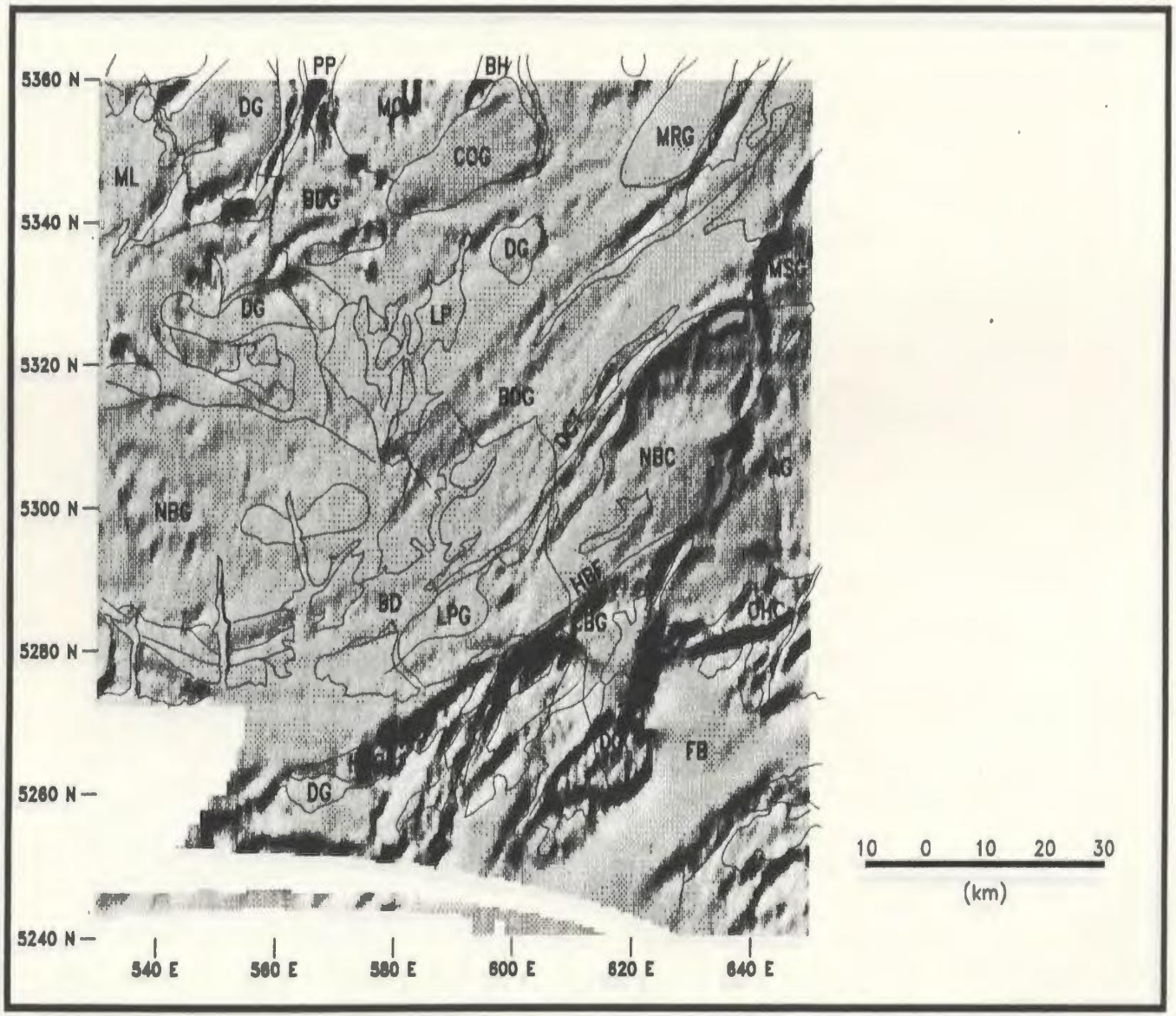

Figure 5.18a: Shaded relief image of the magnetic map for the region around the East Segment of the Meelpaeg Transect with illumination azimuth of 135° and declination of 45°. The legend follows that of Figure 5.5.

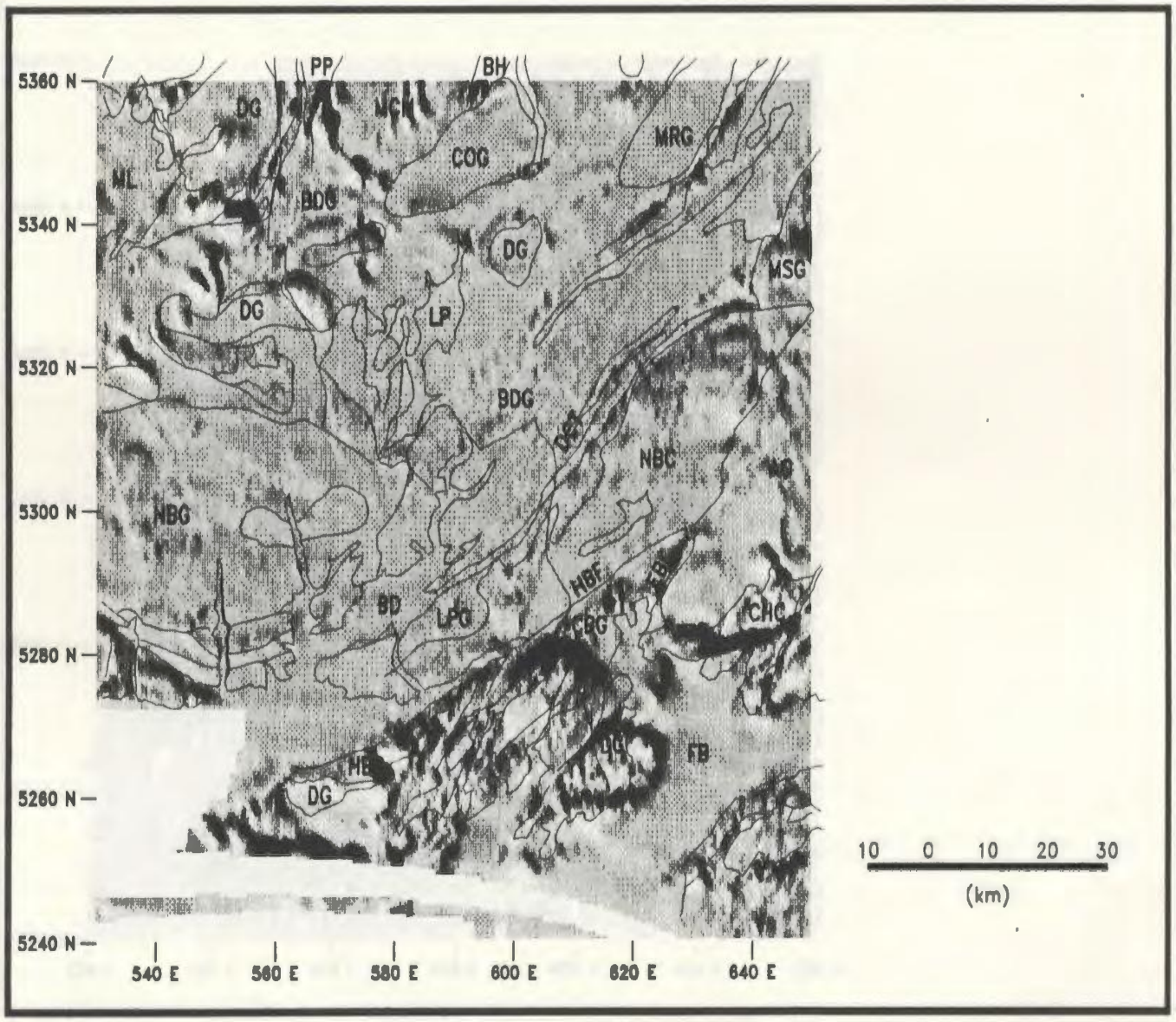

Figure 5.18b: Shaded relief image of the magnetic map for the region around the East Segment of the Meelpaeg Transect with illumination azimuth of 225° and declination of 45°. The legend follows that of Figure 5.5.

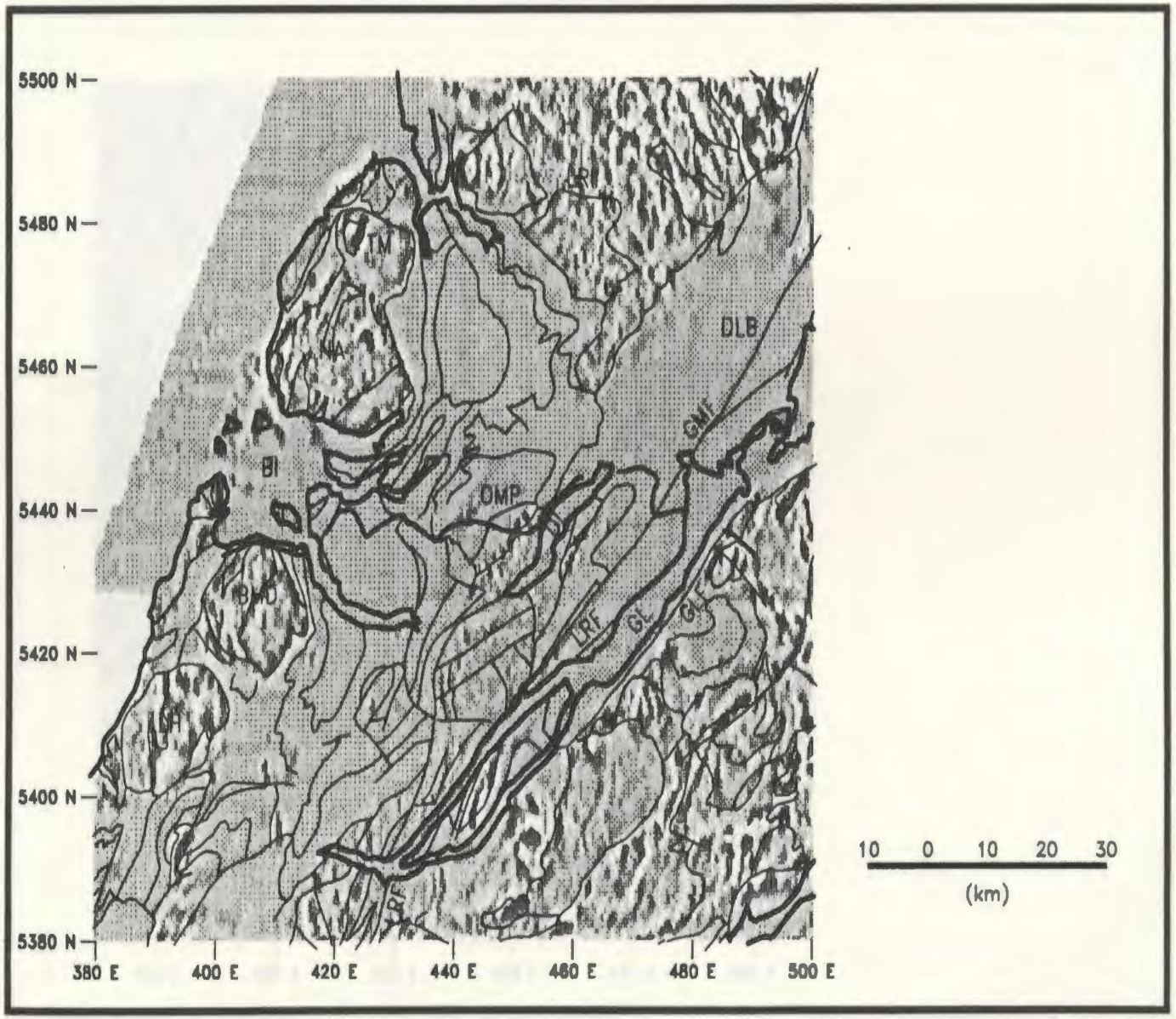

Figure 5.19: Second vertical derivative of the magnetic field for the region around the West Segment of the Meelpaeg Transect. The legend follows that of Figure 5.1.

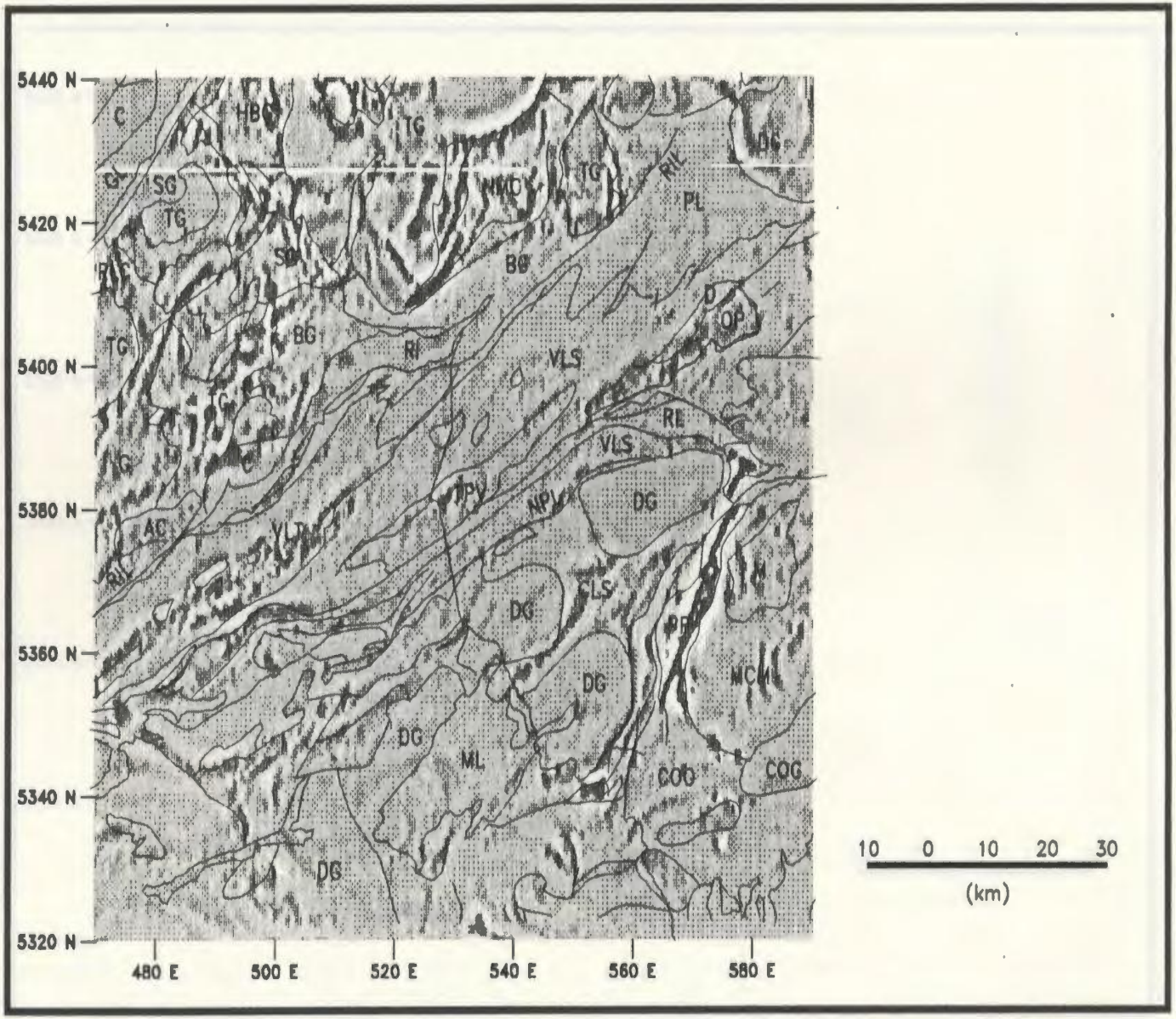

Figure 5.20: Second vertical derivative of the magnetic field for the region around the Central Segment of the Meelpaeg Transect. The legend follows that of Figure 5.3.

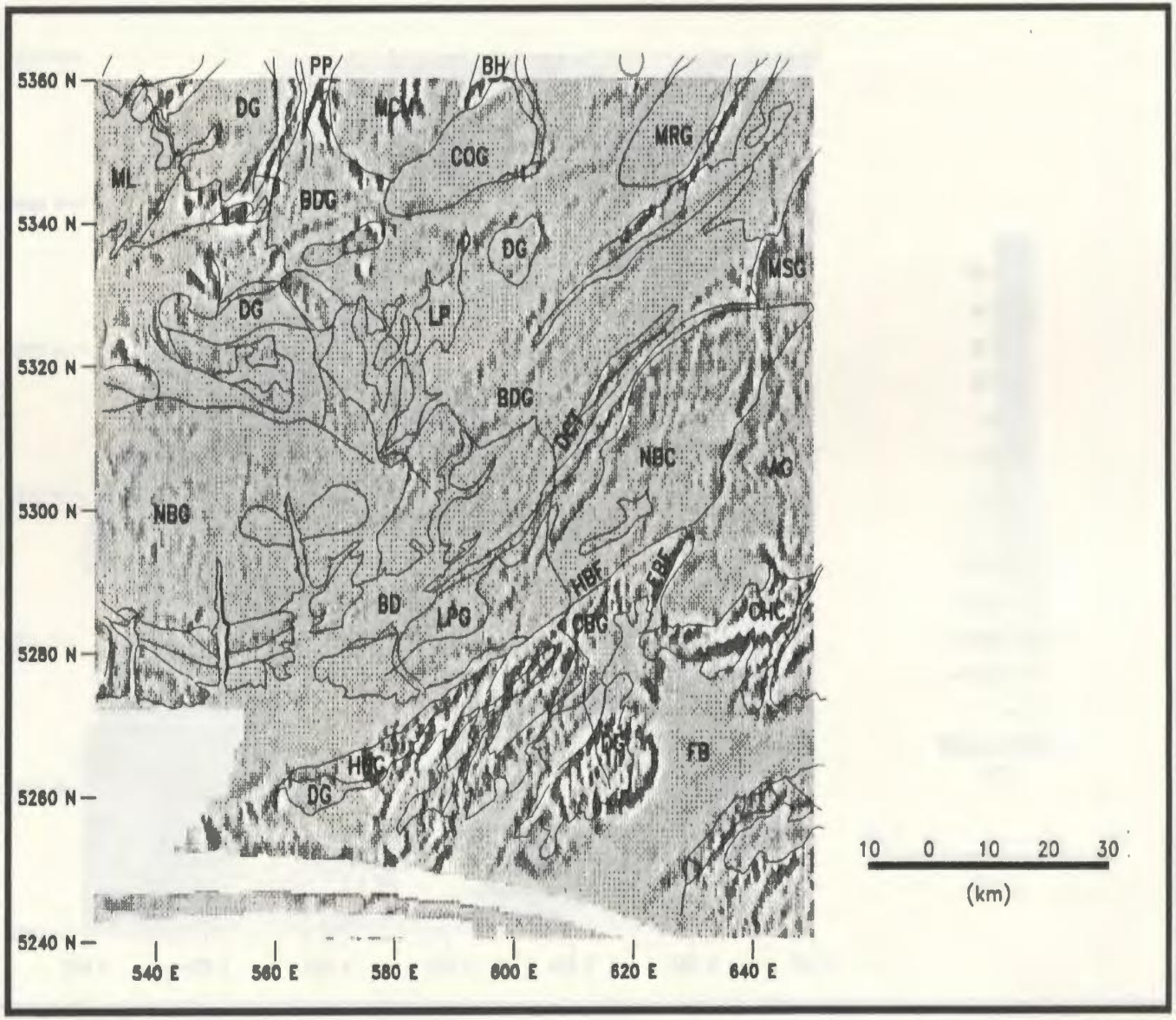

Figure 5.21: Second vertical derivative of the magnetic field for the region around the East Segment of the Meelpaeg Transect. The legend follows that of Figure 5.5.

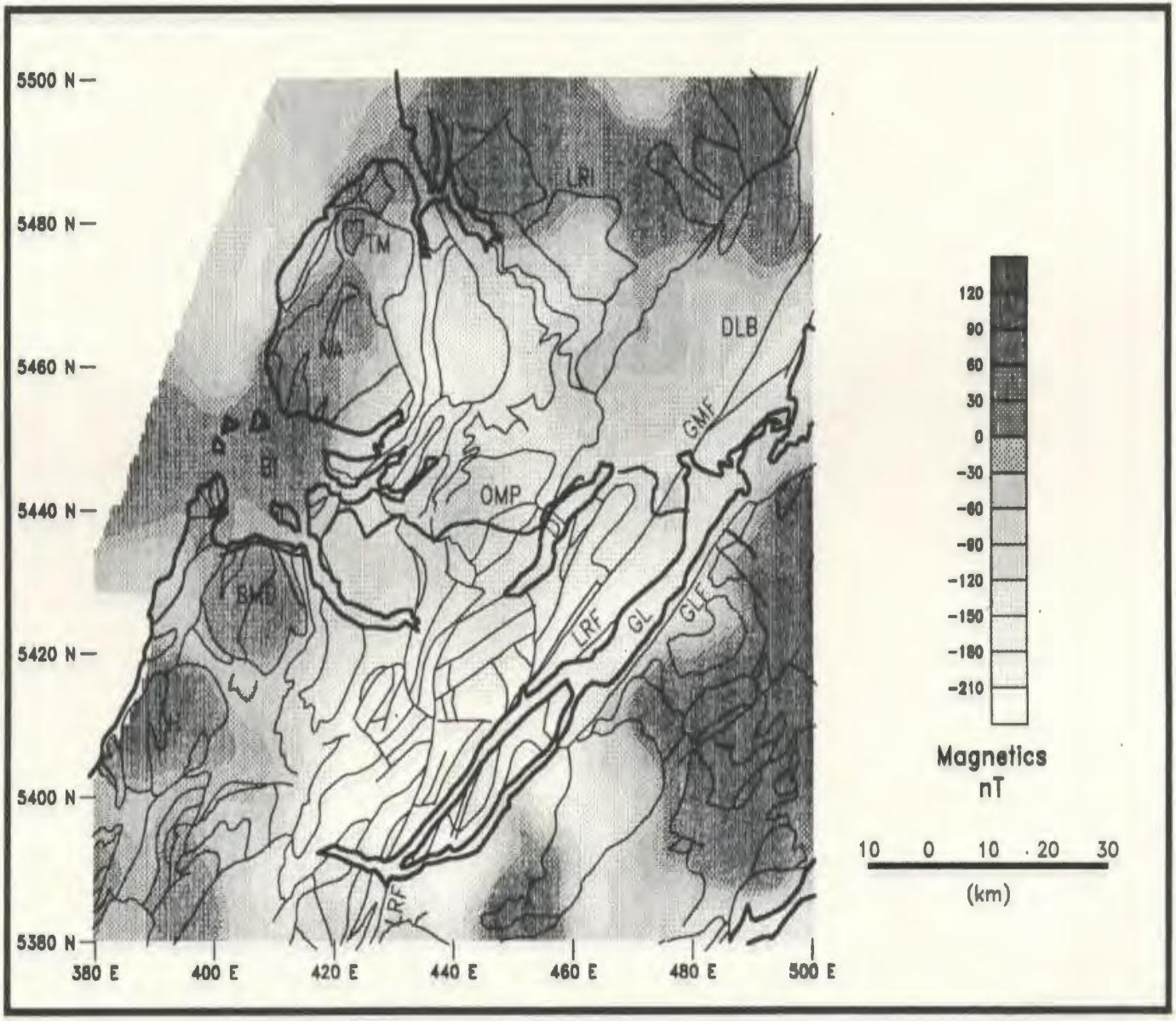

Figure 5.22a: Magnetic field for the area around the West Segment of the Meelpaeg Transect continued upward 3 km. The legend follows that of Figure 5.1.

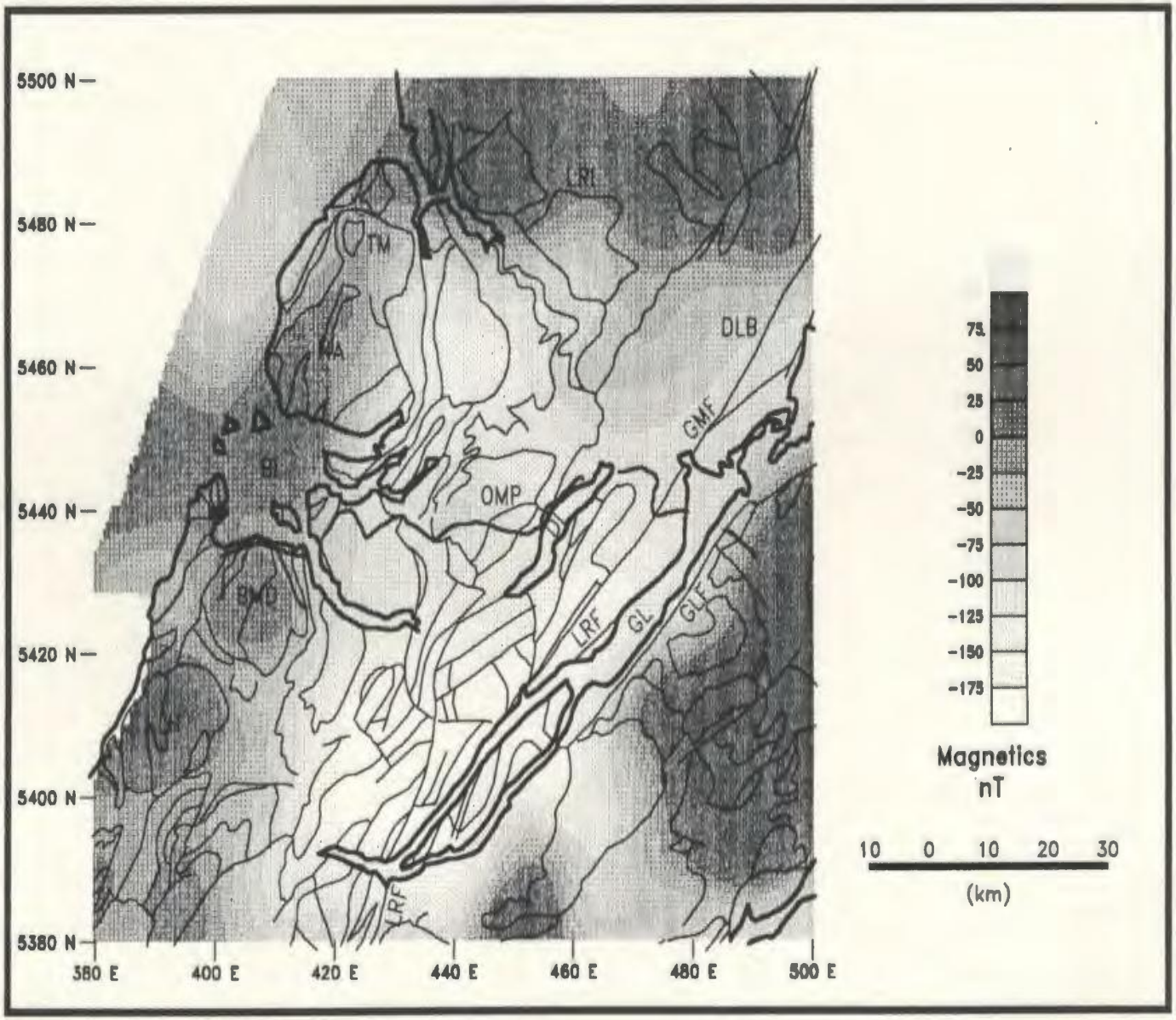

Figure 5.22b: Magnetic field for the area around the West Segment of the Meelpaeg Transect continued upward 6 km. The legend follows that of Figure 5.1.

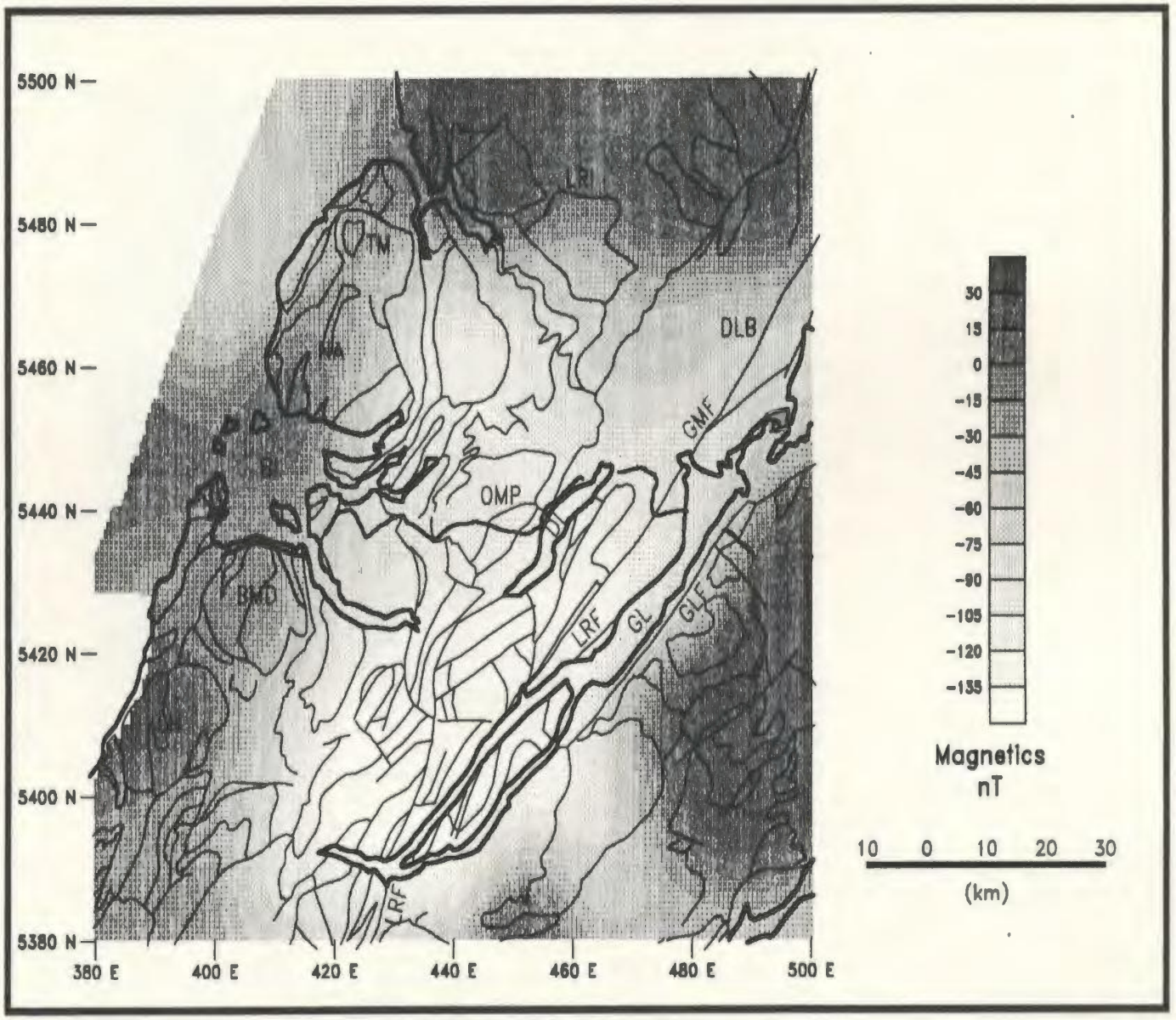

Figure 5.22c: Magnetic field for the area around the West Segment of the Meelpaeg Transect continued upward 10 km. The legend follows that of Figure 5.1.

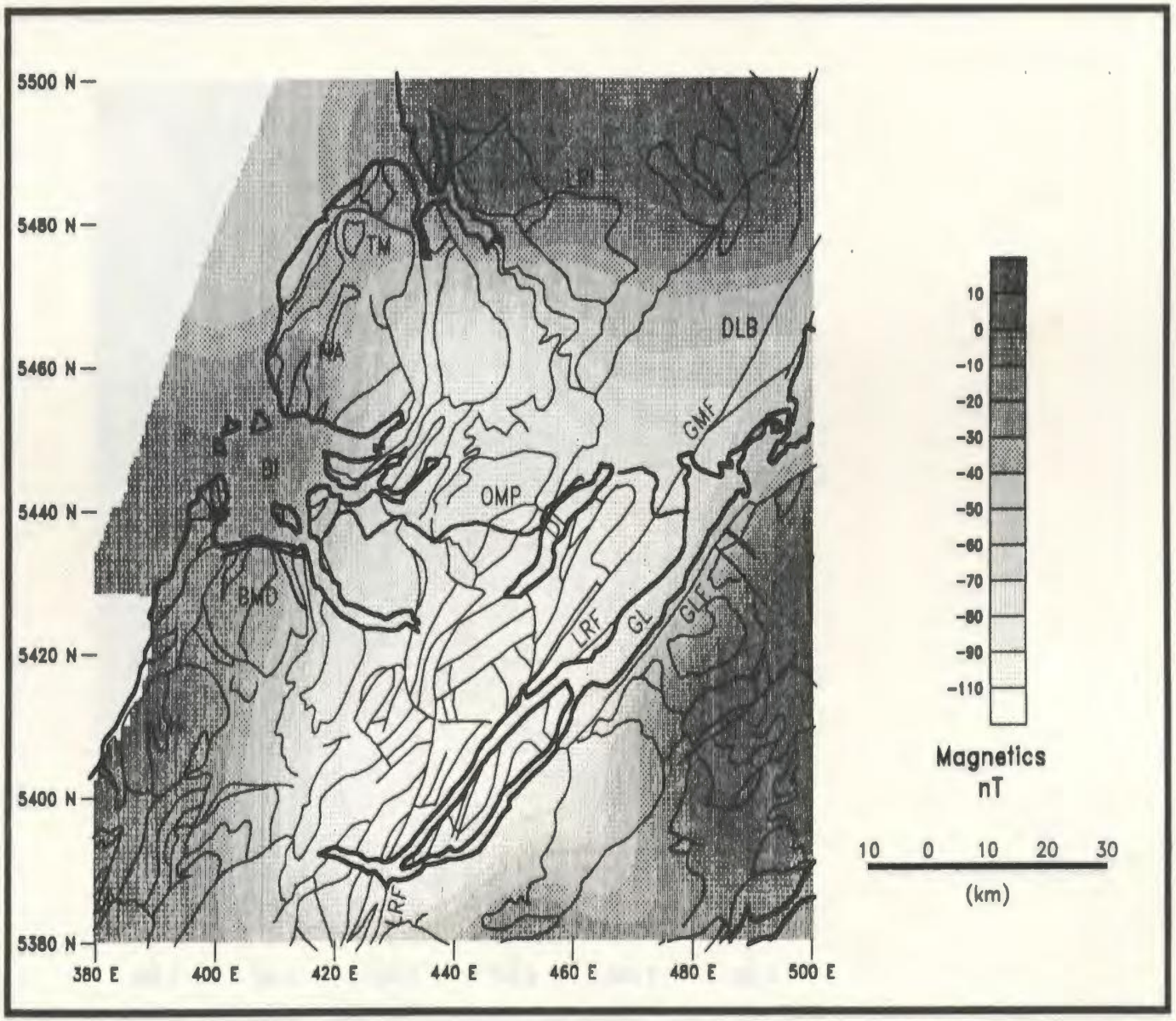

Figure 5.22d: Magnetic field for the area around the West Segment of the Meelpaeg Transect continued upward 15 km. The legend follows that of Figure 5.1.

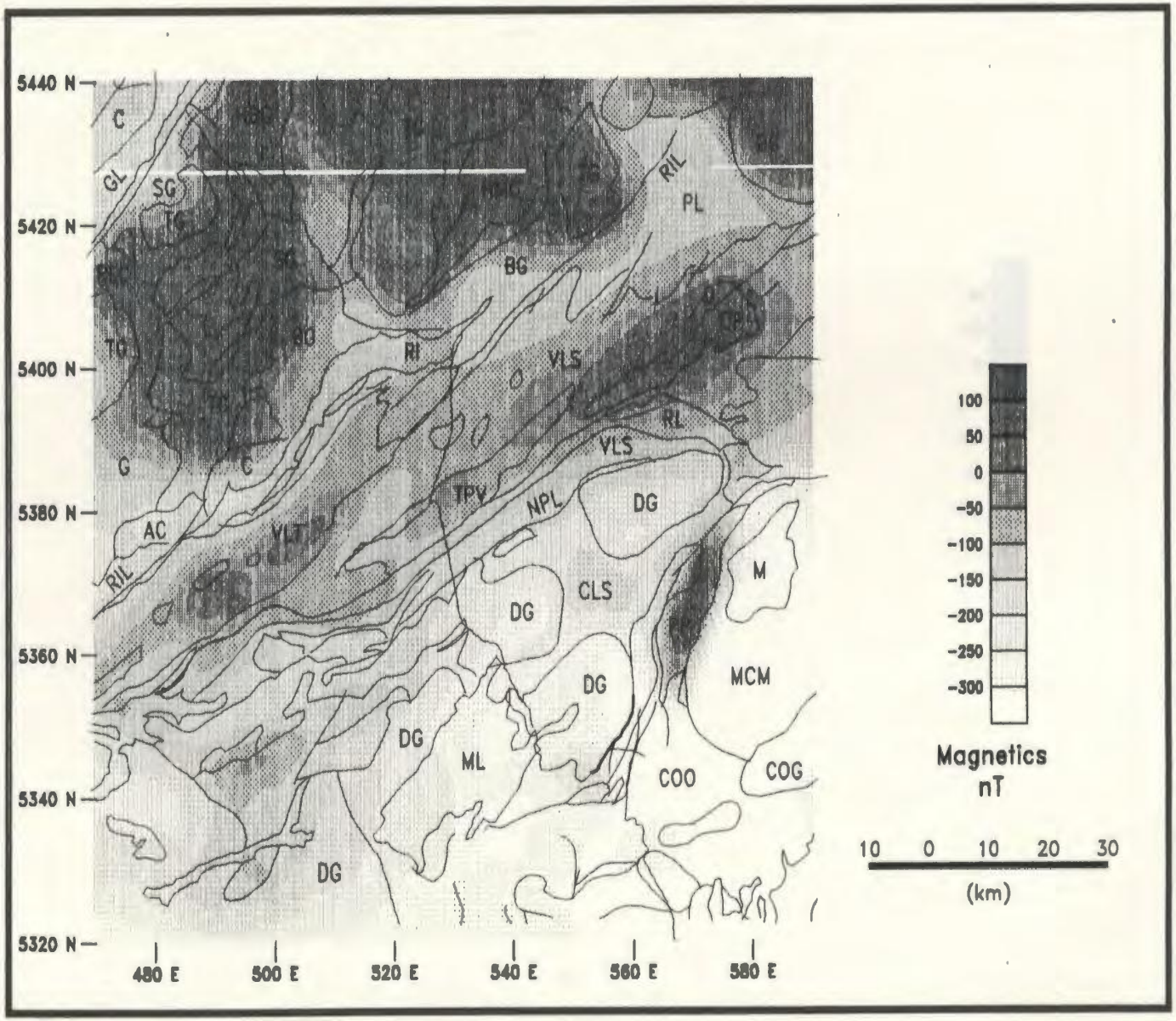

Figure 5.23a: Magnetic field for the area around the Central Segment of the Meelpaeg Transect continued upward 3 km. The legend follows that of Figure 5.3.

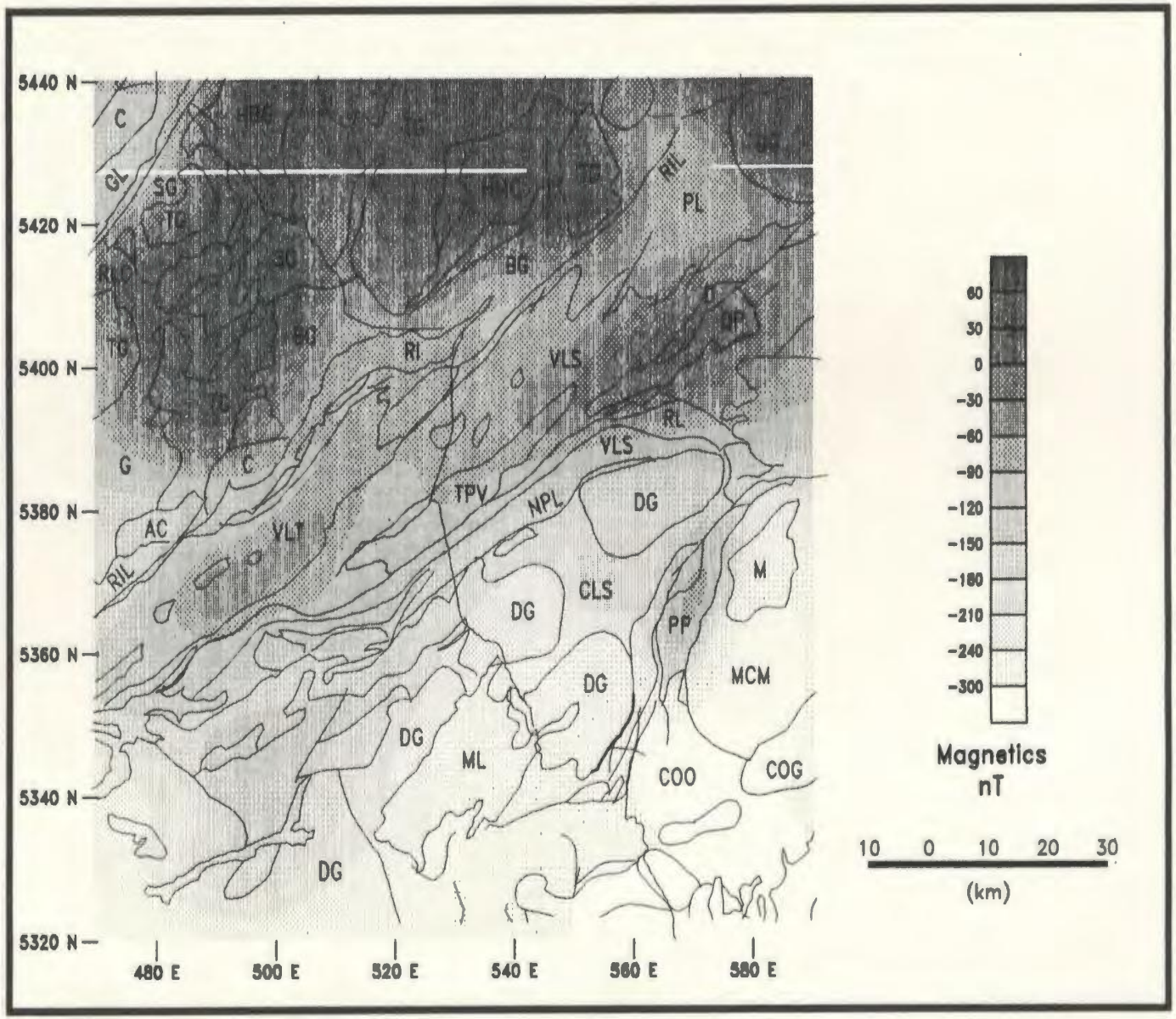

Figure 5.23b: Magnetic field for the area around the Central Segment of the Meelpaeg Transect continued upward 6 km. The legend follows that of Figure 5.3.

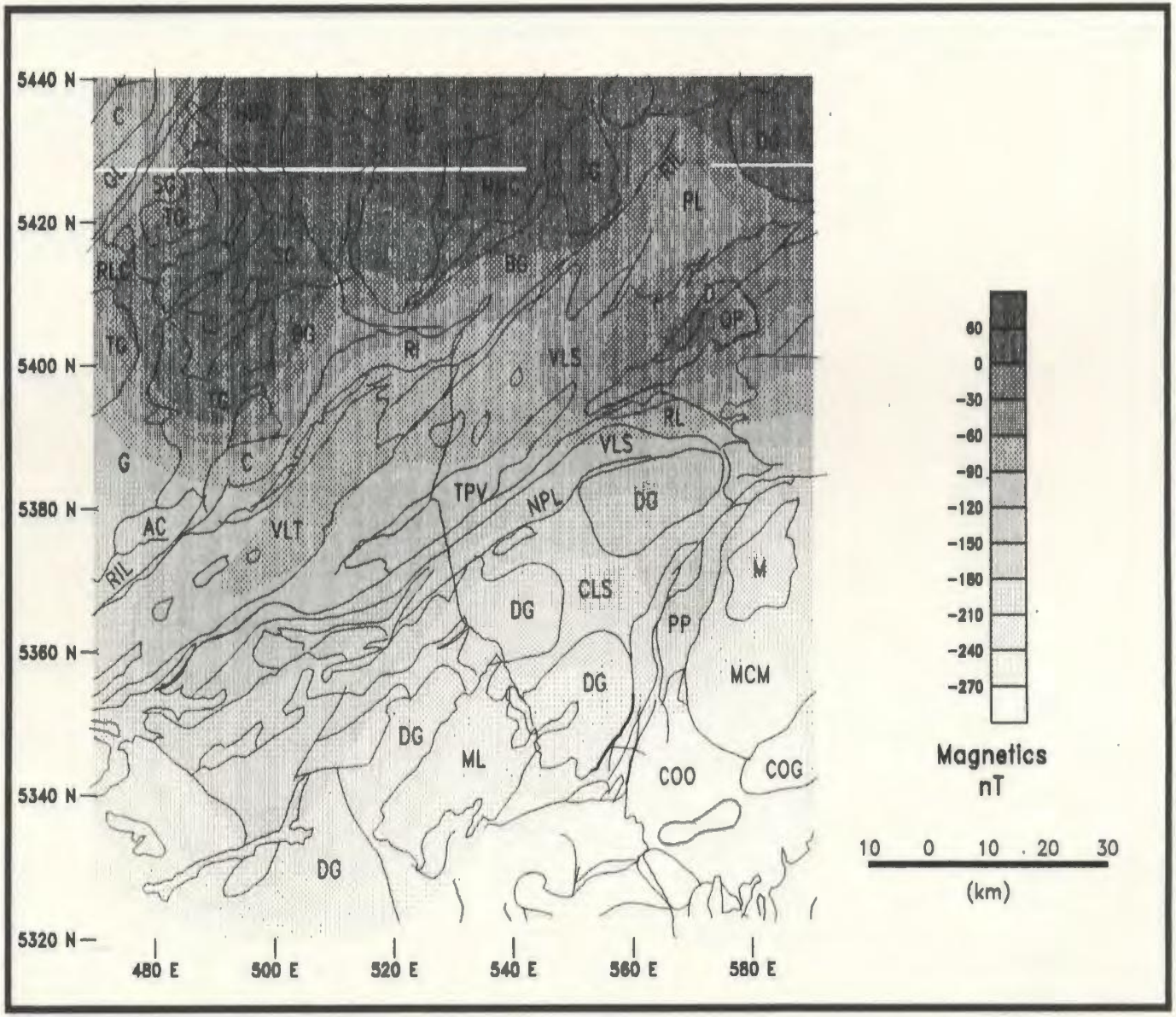

Figure 5.23c: Magnetic field for the area around the Central Segment of the Meelpaeg Transect continued upward 10 km. The legend follows that of Figure 5.3.

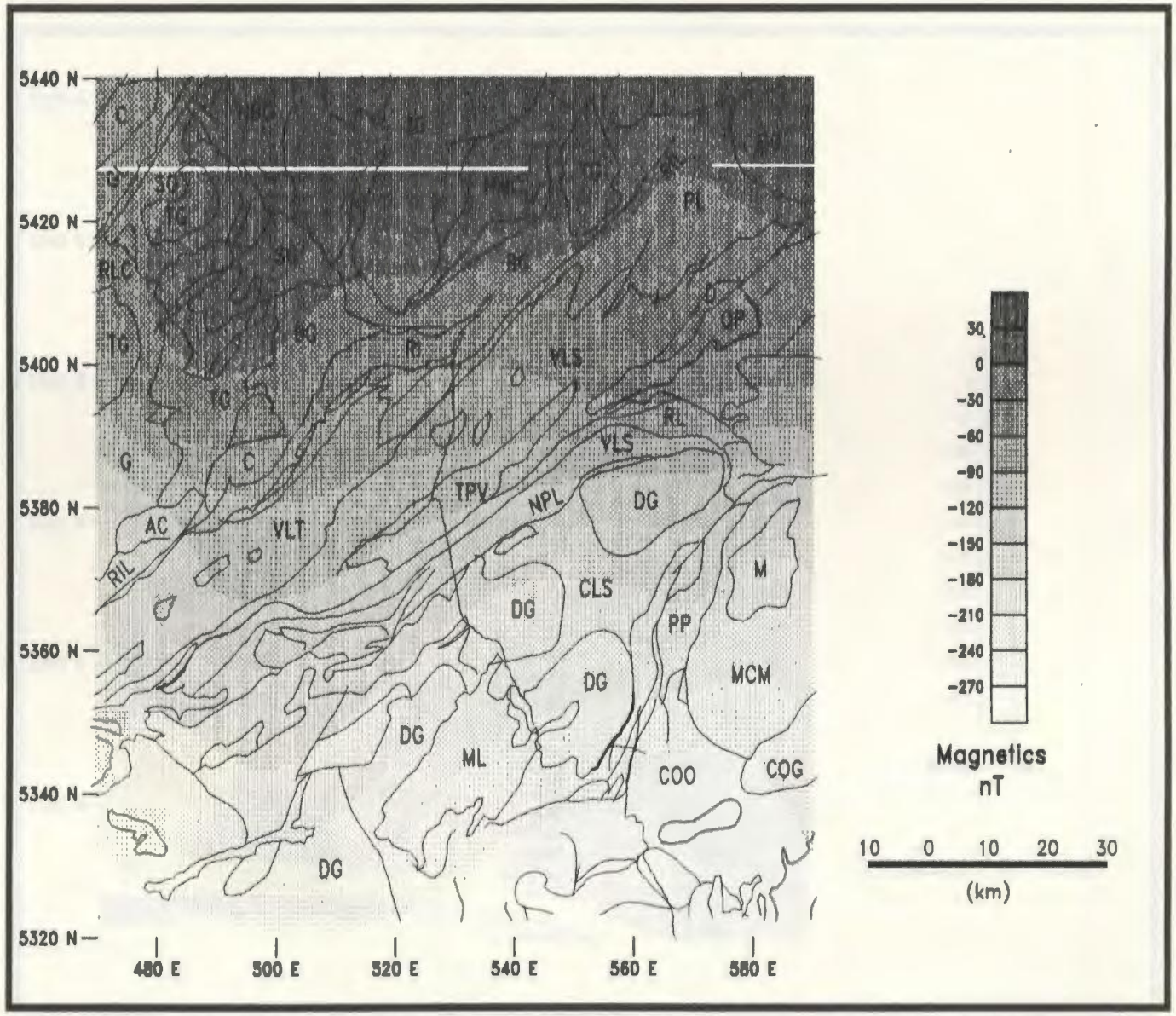

Figure 5.23d: Magnetic field for the area around the Central Segment of the Meelpaeg Transect continued upward 15 km. The legend follows that of Figure 5.3.

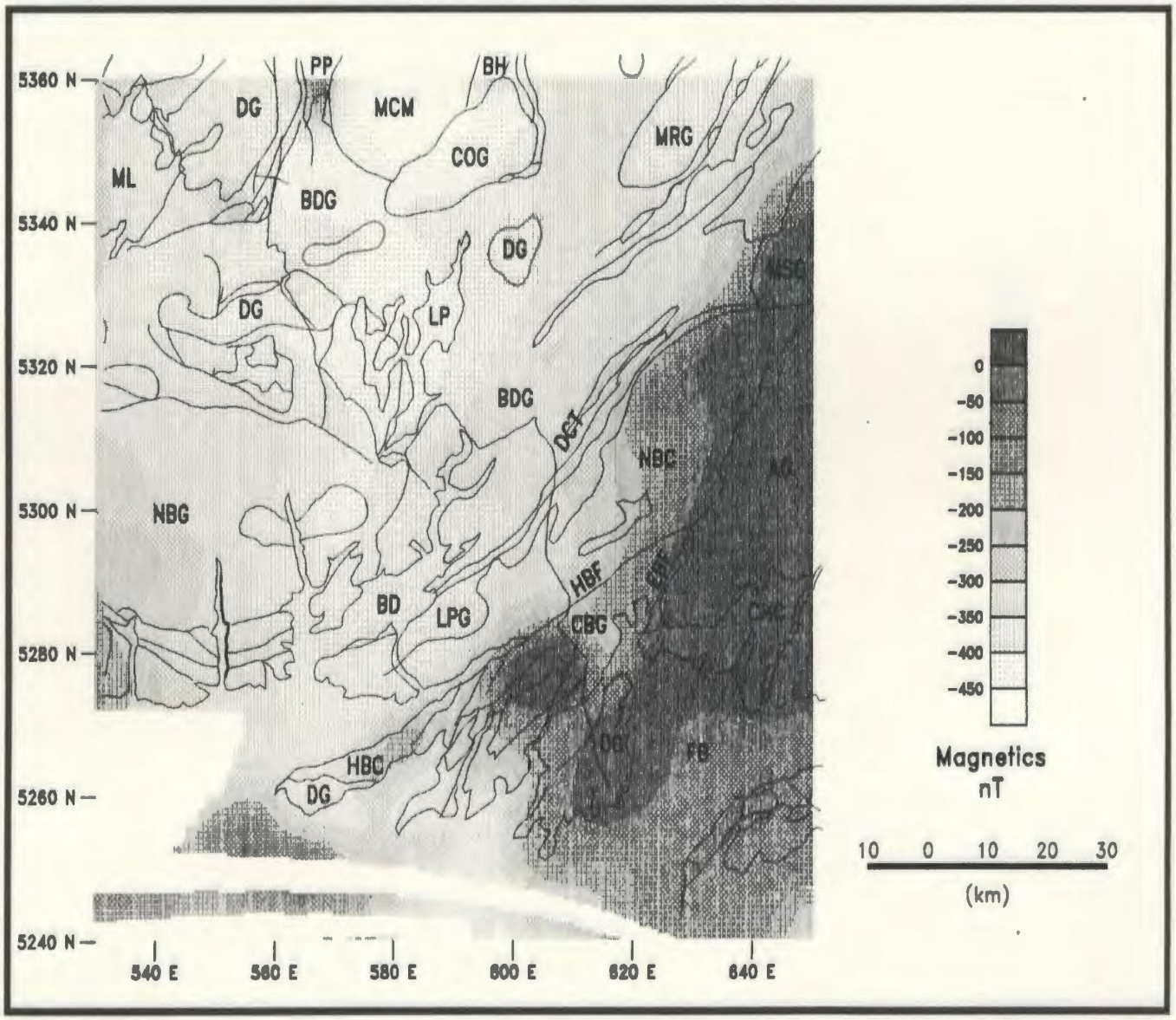

Figure 5.24a: Magnetic field for the area around the East Segment of the Meelpaeg Transect continued upward 3 km. The legend follows that of Figure 5.5.

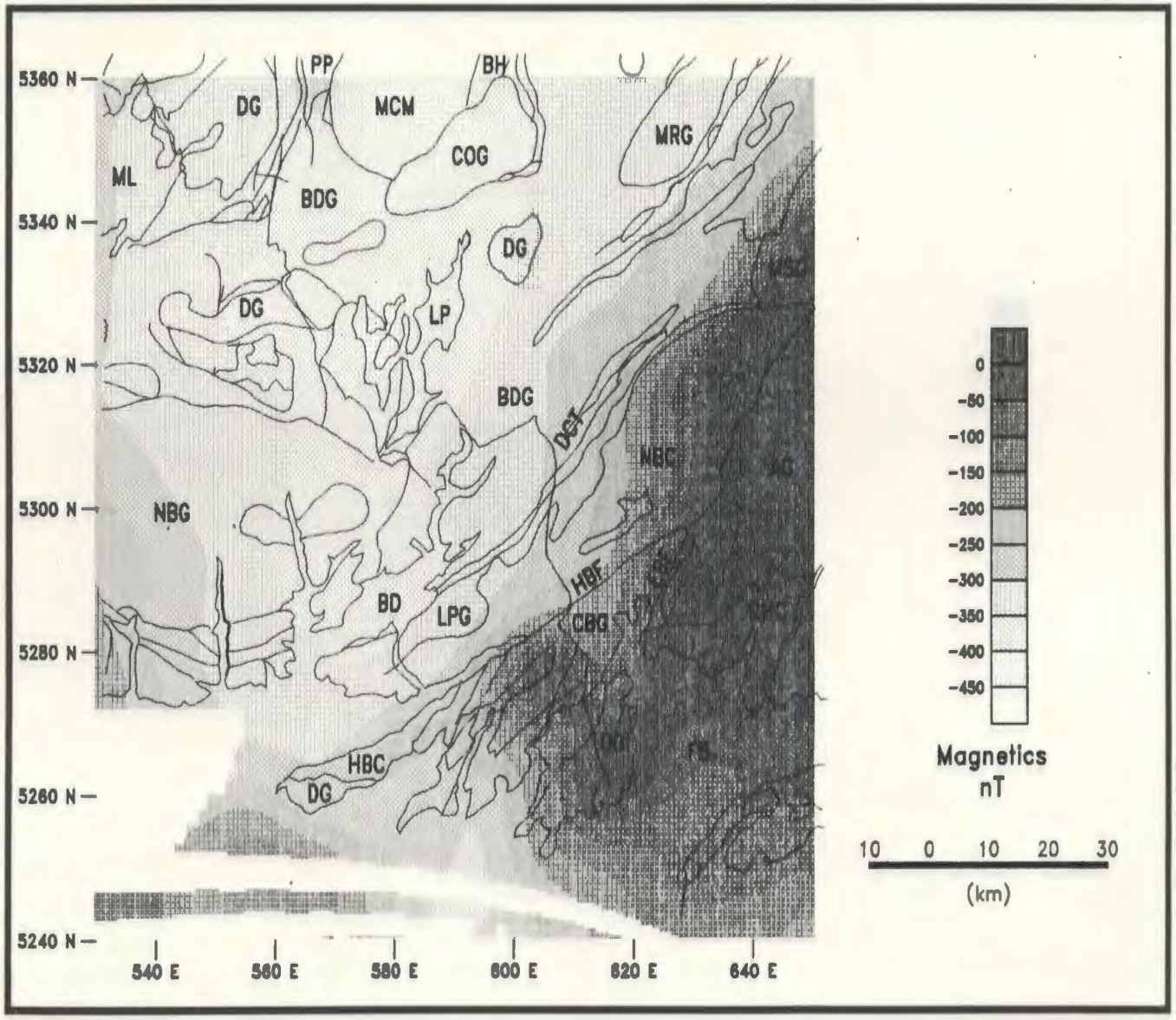

Figure 5.24b: Magnetic field for the area around the East Segment of the Meelpaeg Transect continued upward 6 km. The legend follows that of Figure 5.5.

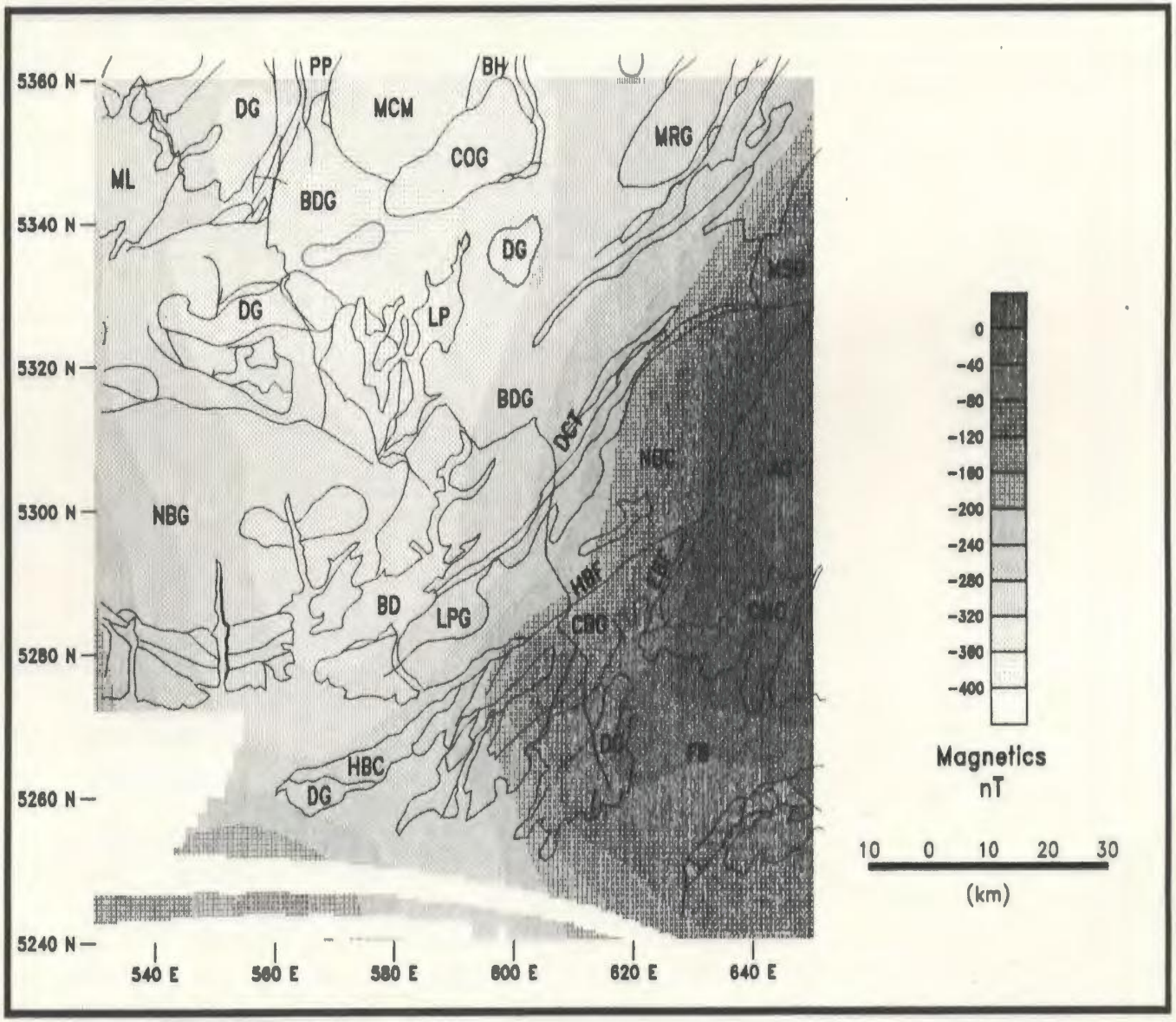

Figure 5.24c: Magnetic field for the area around the East Segment of the Meelpaeg Transect continued upward 10 km. The legend follows that of Figure 5.5.

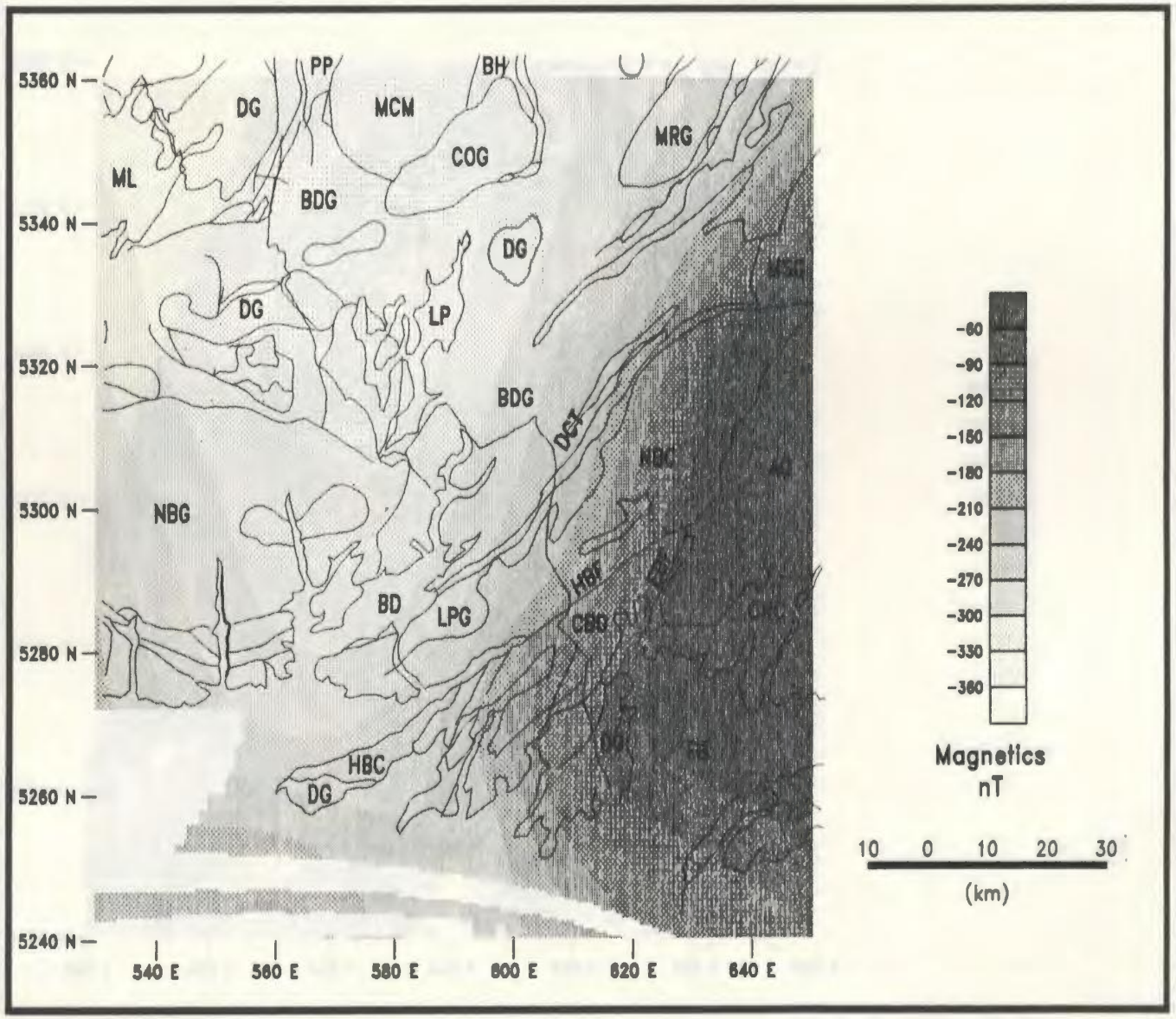

Figure 5.24d: Magnetic field for the area around the Central Segment of the Meelpaeg Transect continued upward 15 km. The legend follows that of Figure 5.5.

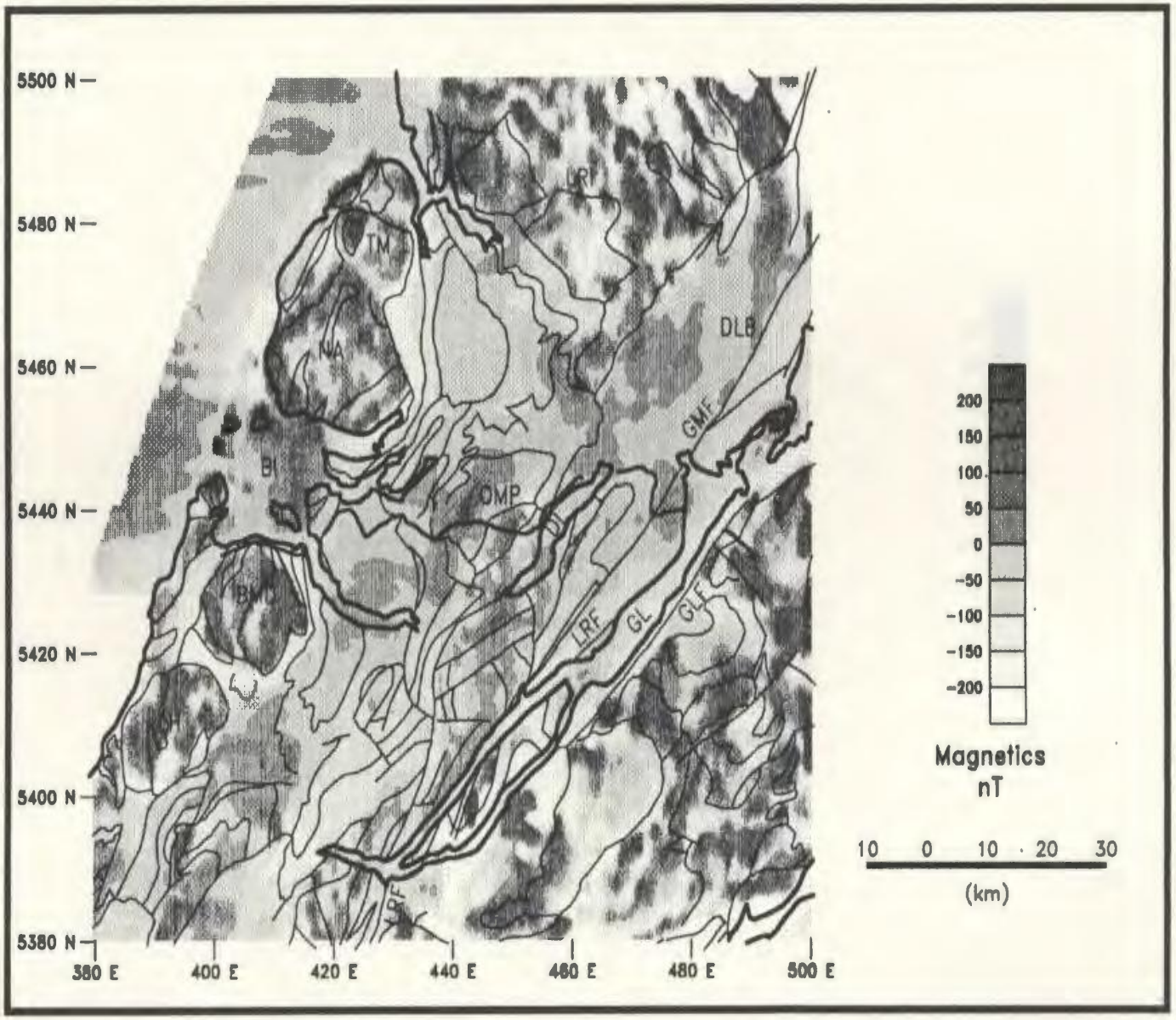

Figure 5.25a: Layer strip (Jacobson, 1987) map for sources around the West Segment of the Meelpaeg Transect within the upper 1.5 km. The legend follows that of Figure 5.1.

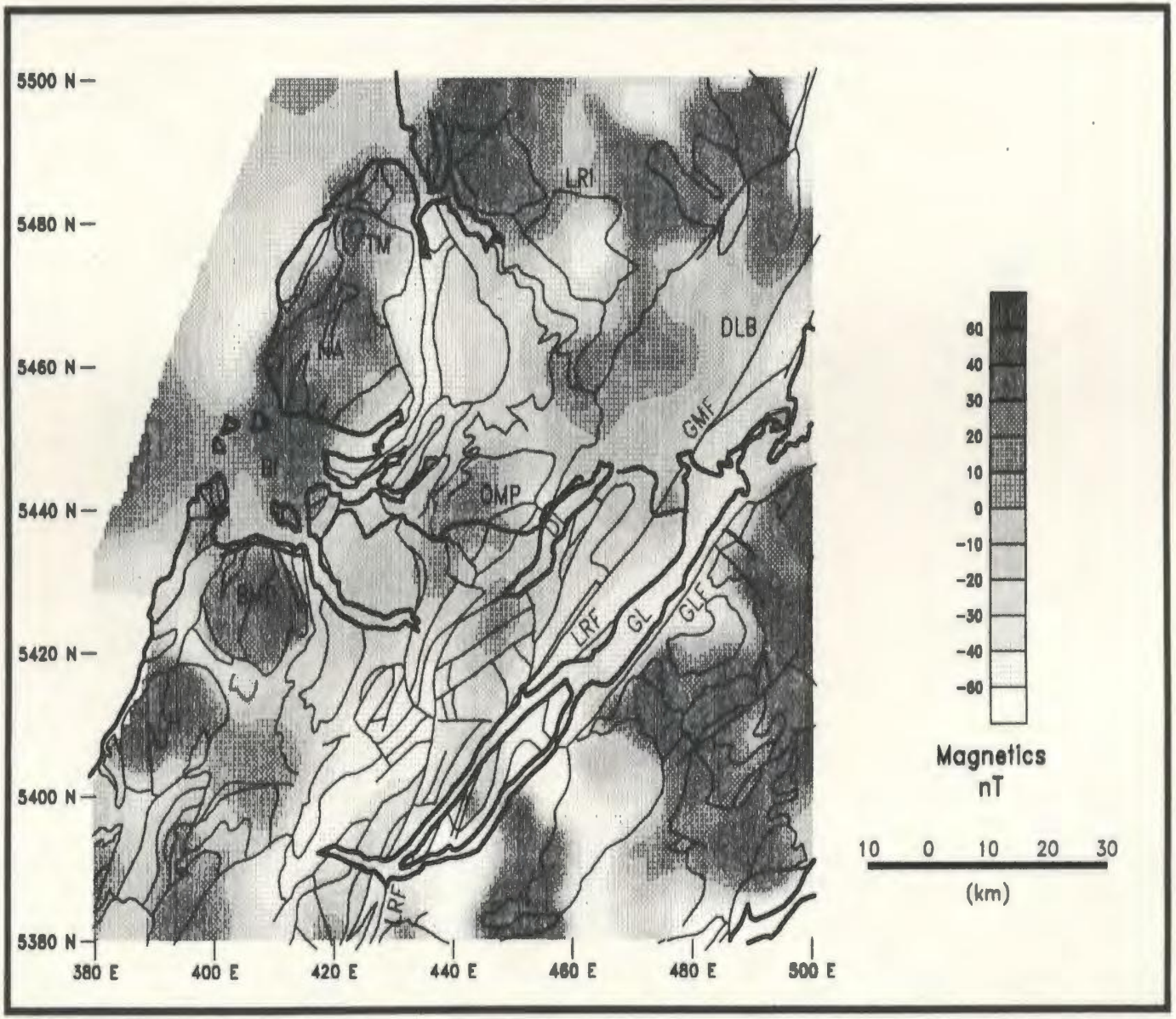

Figure 5.25b: Layer strip (Jacobson, 1987) map for sources around the West Segment of the Meelpaeg Transect between 1.5 and 3 km depths. The legend follows that of Figure 5.1.

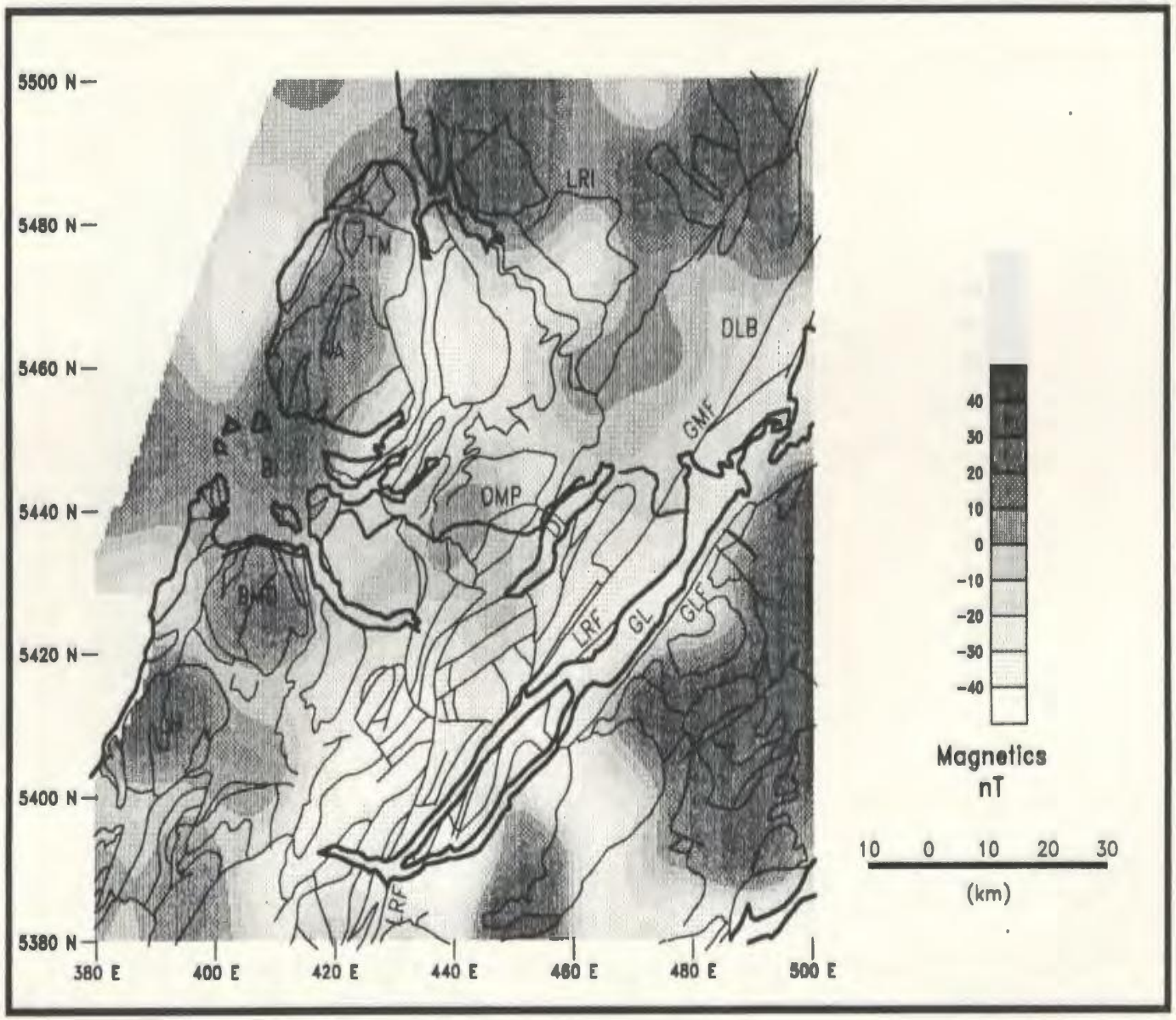

Figure 5.25c: Layer strip (Jacobson, 1987) map for sources around the West Segment of the Meelpaeg Transect between 3 and 5 km depths. The legend follows that of Figure 5.1.

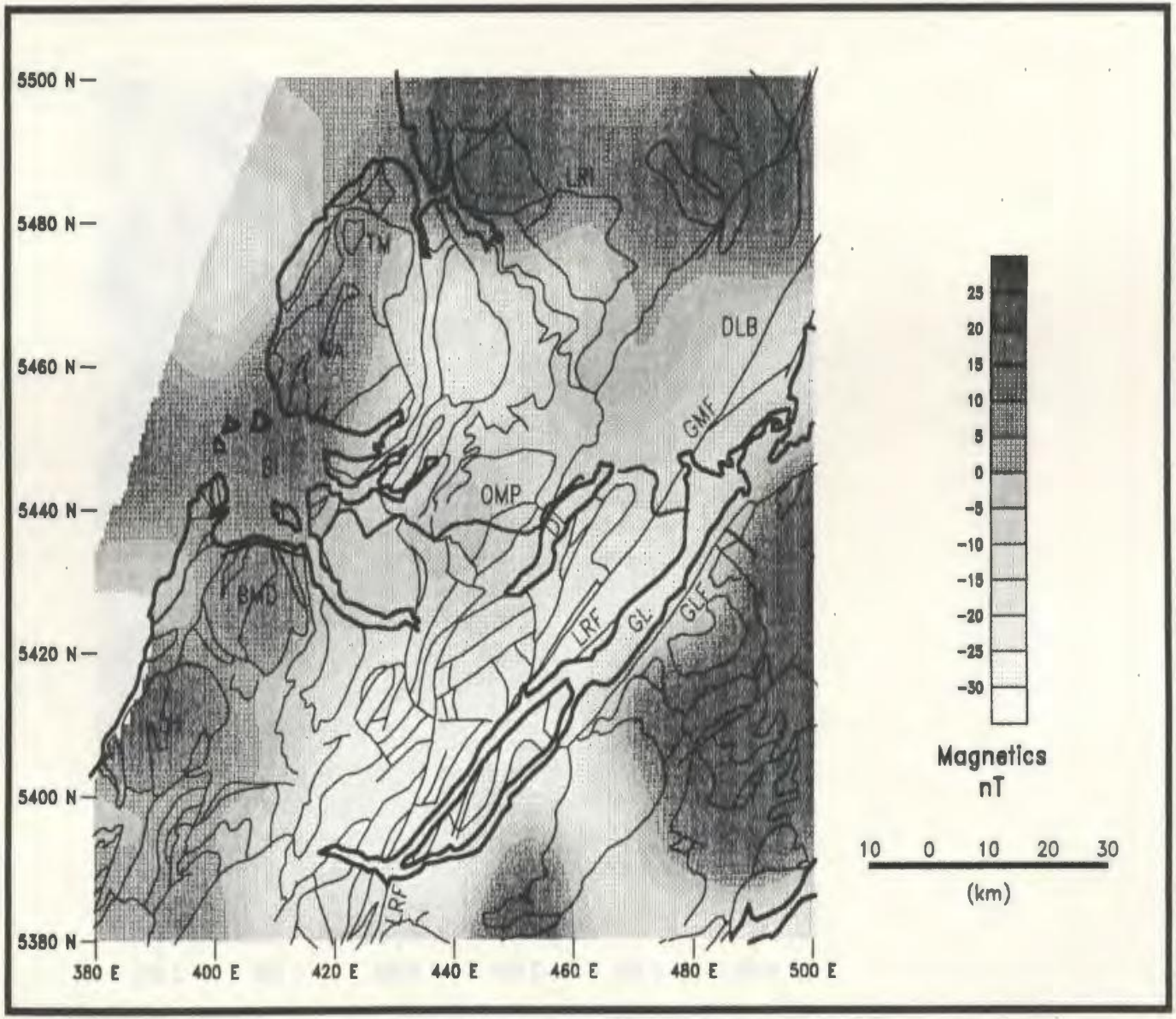

Figure 5.25d: Layer strip (Jacobson, 1987) map for sources around the West Segment of the Meelpaeg Transect between 5 and 7.5 km depths. The legend follows that of Figure 5.1.

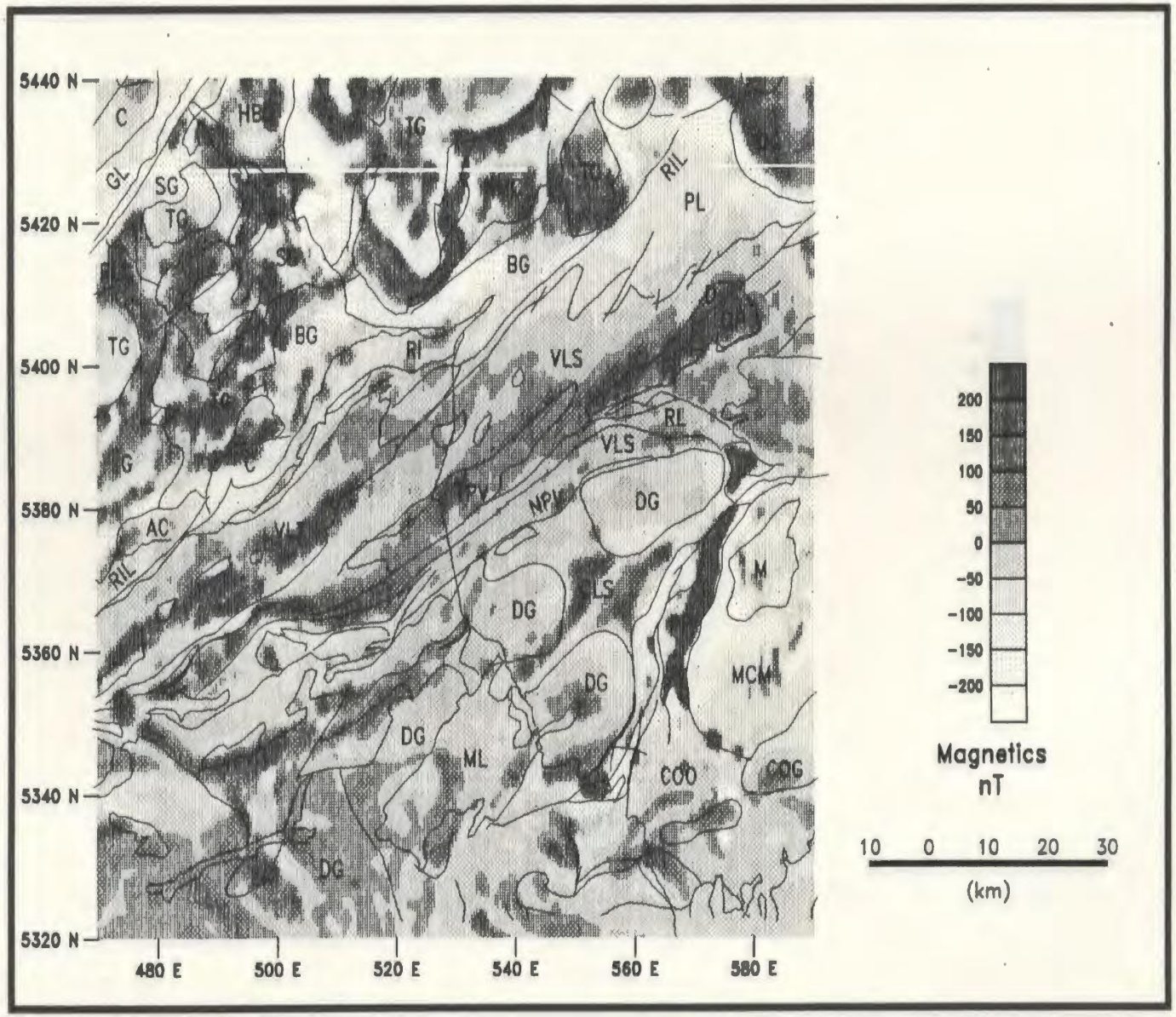

Figure 5.26a: Layer strip (Jacobson, 1987) map for sources around the Central Segment of the Meelpaeg Transect within the upper 1.5 km. The legend follows that of Figure 5.3.

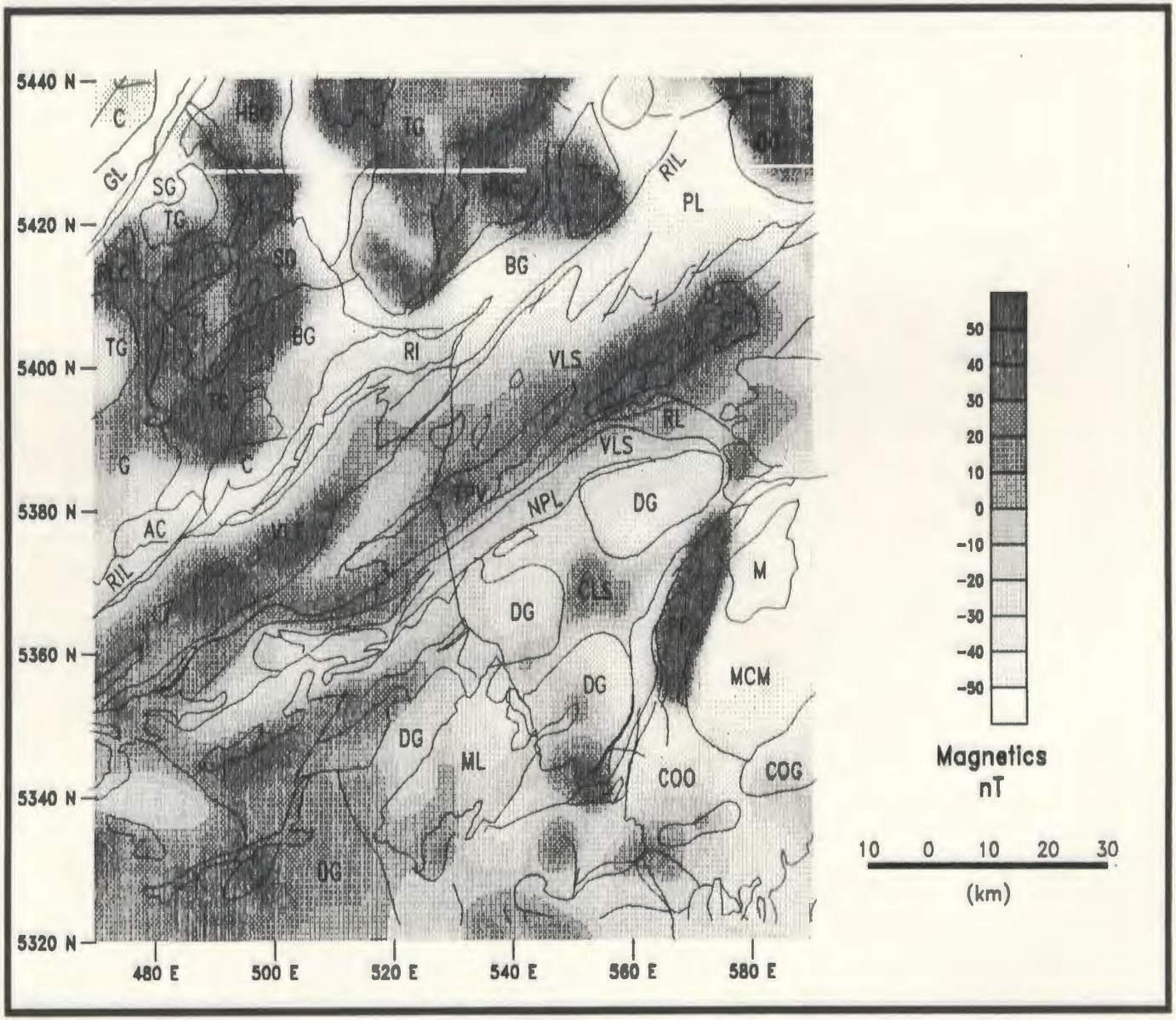

Figure 5.26b: Layer strip (Jacobson, 1987) map for sources around the Central Segment of the Meelpaeg Transect between 1.5 and 3 km depths. The legend follows that of Figure 5.3.

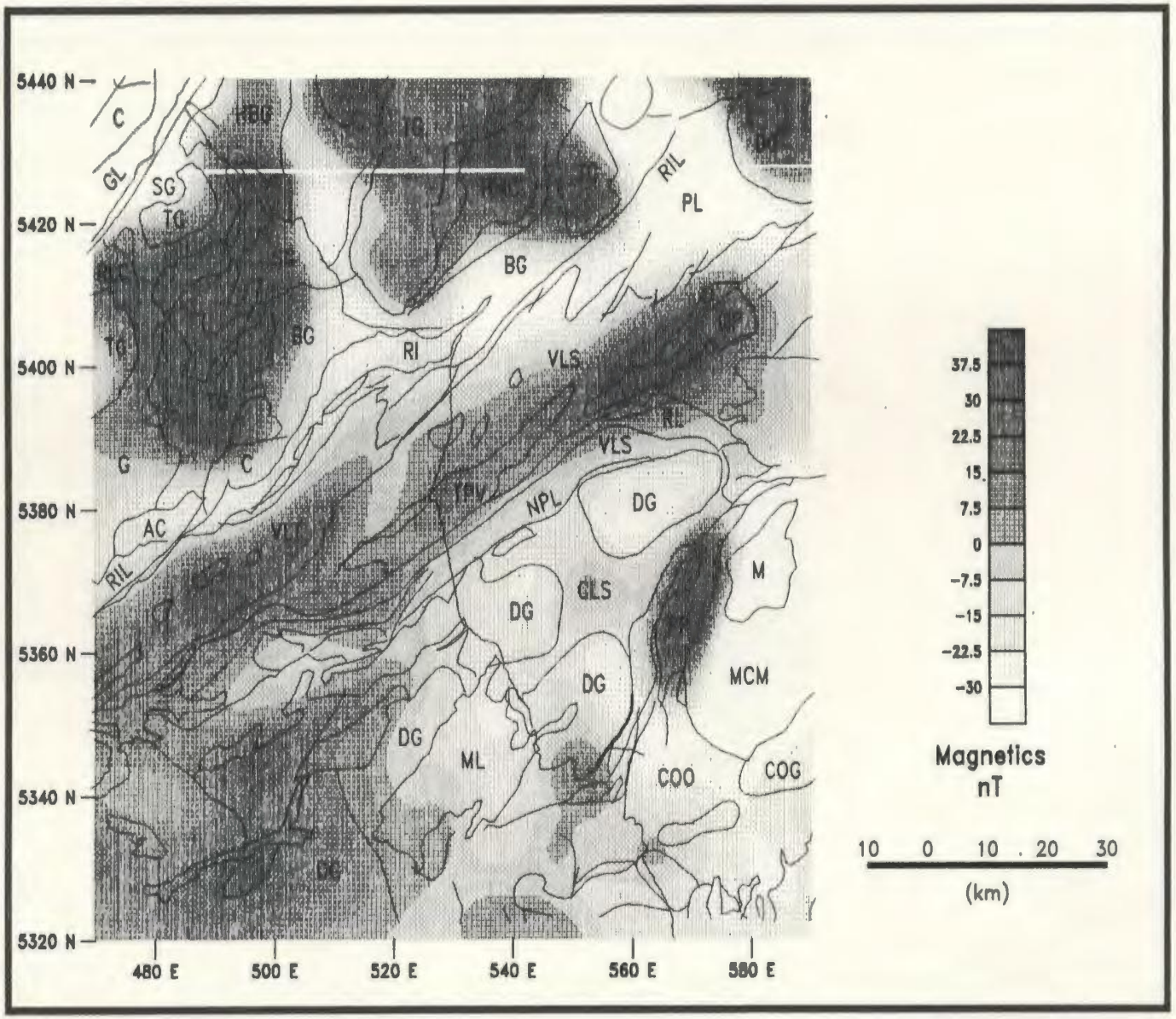

Figure 5.26c: Layer strip (Jacobson, 1987) map for sources around the Central Segment of the Meelpaeg Transect between 3 and 5 km depths. The legend follows that of Figure 5.3.

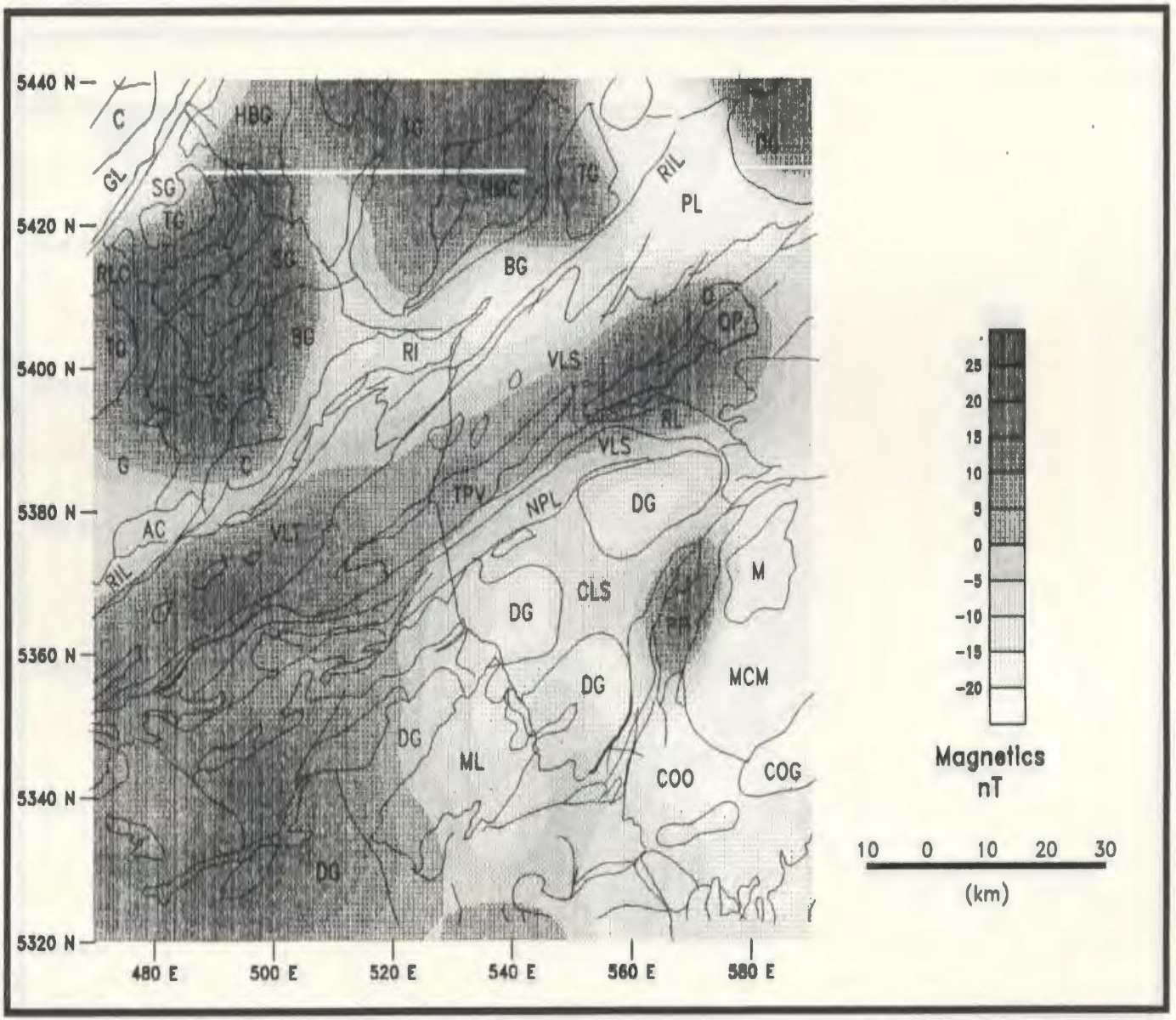

Figure 5.26d: Layer strip (Jacobson, 1987) map for sources around the Central Segment of the Meelpaeg Transect between 5 and 7.5 km depths. The legend follows that of Figure 5.3.

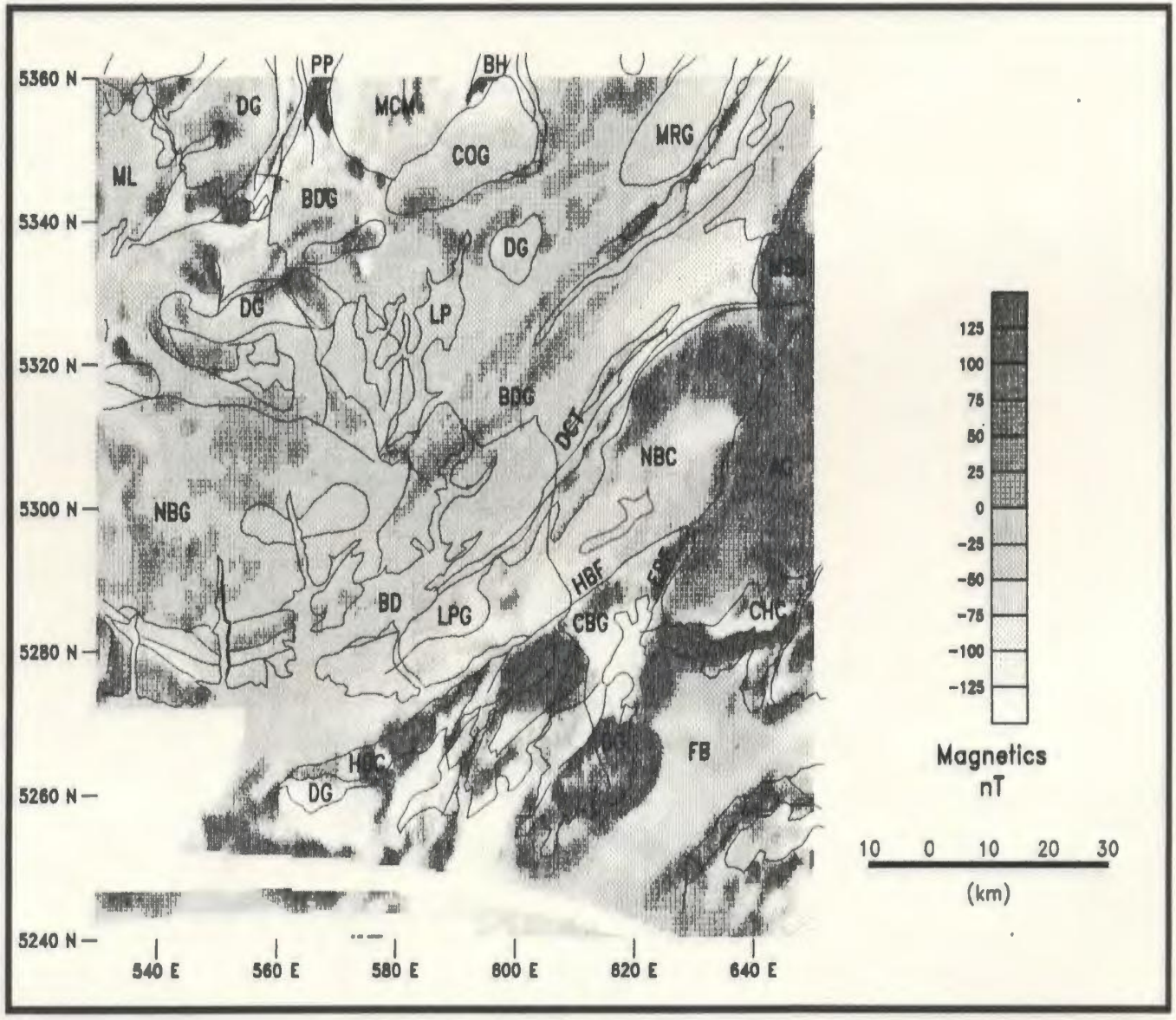

Figure 5.27a: Layer strip (Jacobson, 1987) map for sources around the East Segment of the Meelpaeg Transect within the upper 1.5 km. The legend follows that of Figure 5.5.

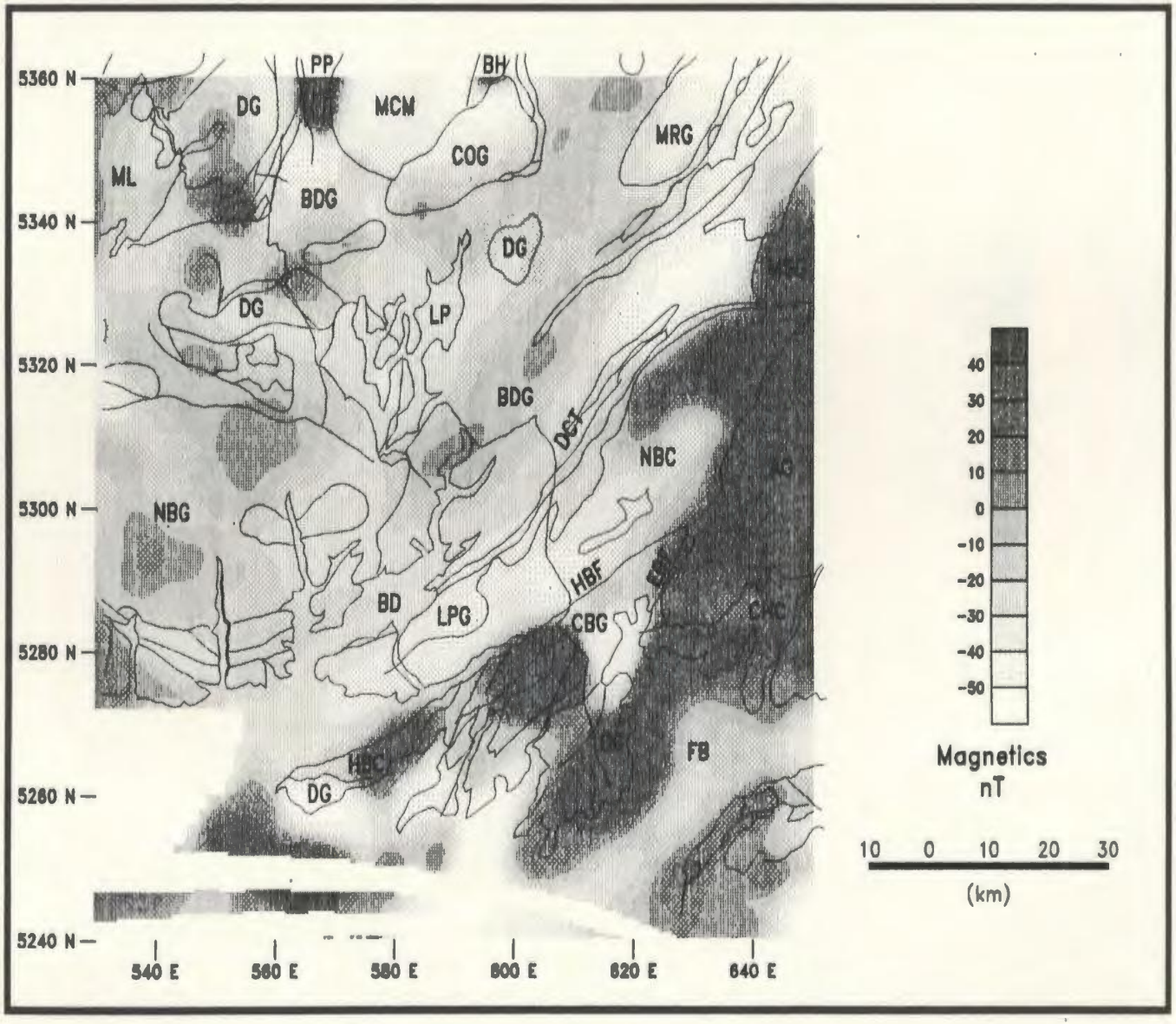

Figure 5.27b: Layer strip (Jacobson, 1987) map for sources around the East Segment of the Meelpaeg Transect between 1.5 and 3 km depths. The legend follows that of Figure 5.5.

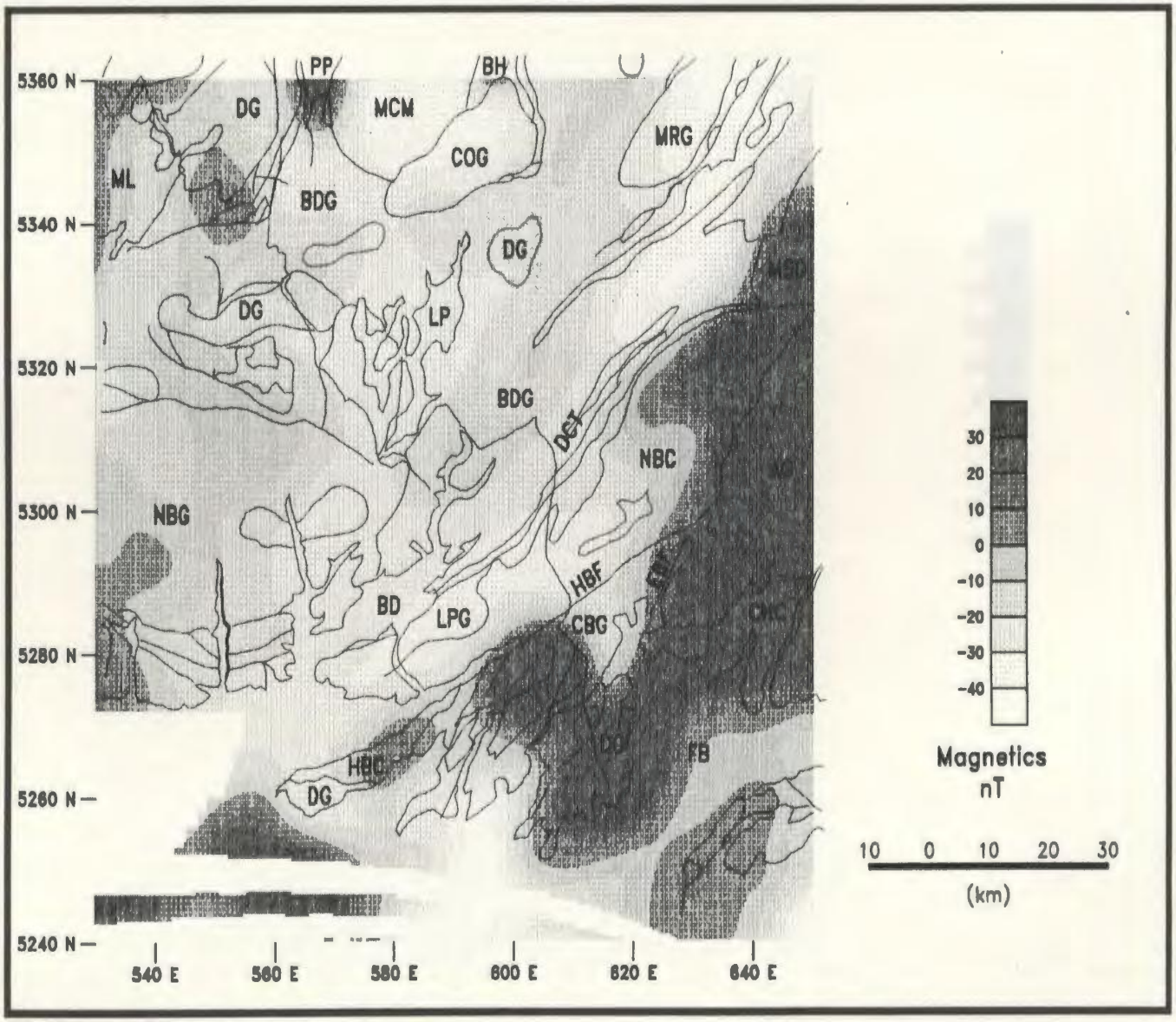

Figure 5.27c: Layer strip (Jacobson, 1987) map for sources around the East Segment of the Meelpaeg Transect between 3 and 5 km depths. The legend follows that of Figure 5.5.

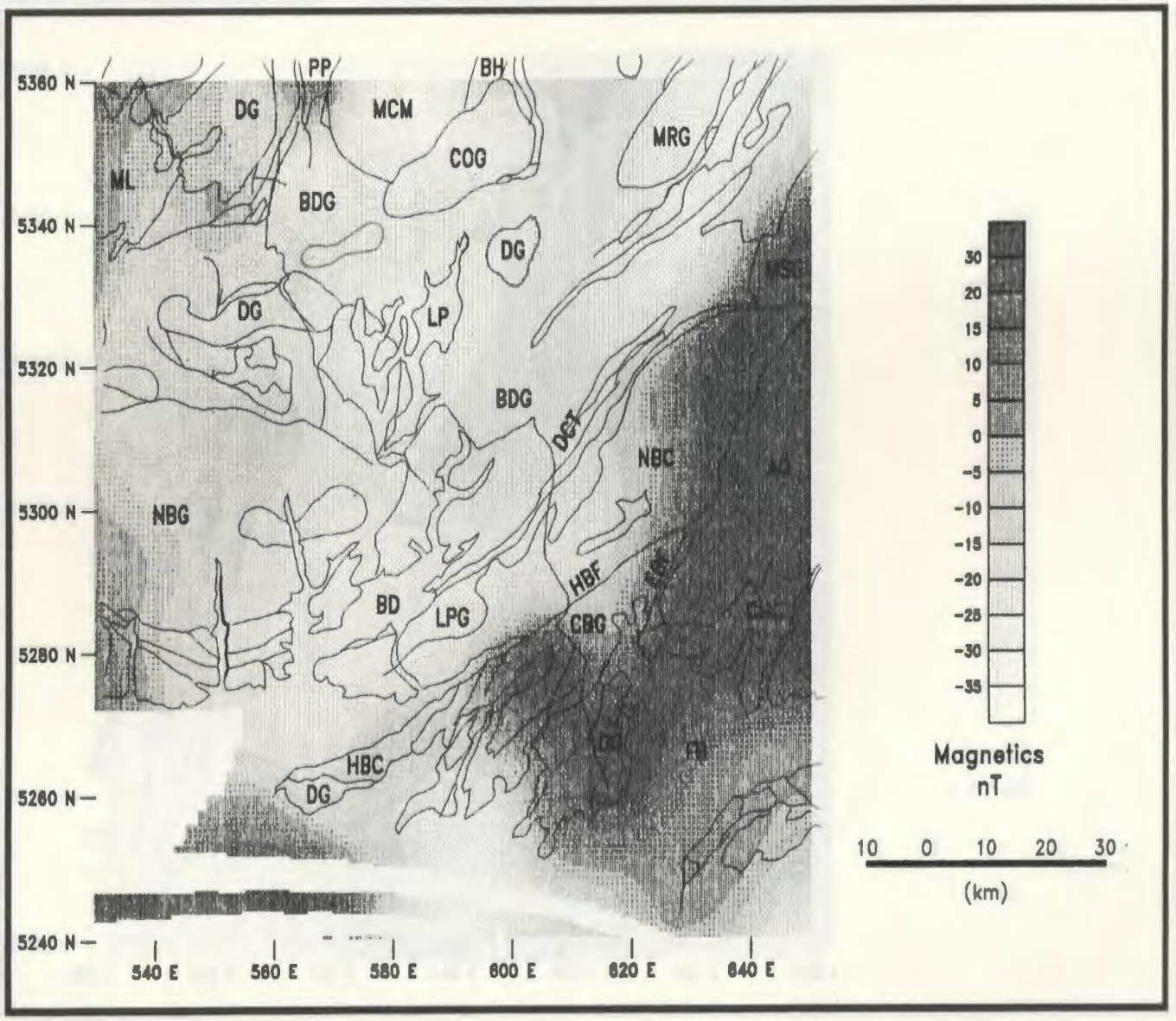

Figure 5.27d: Layer strip (Jacobson, 1987) map for sources around the East Segment of the Meelpaeg Transect between 5 and 7.5 km depths. The legend follows that of Figure 5.5.

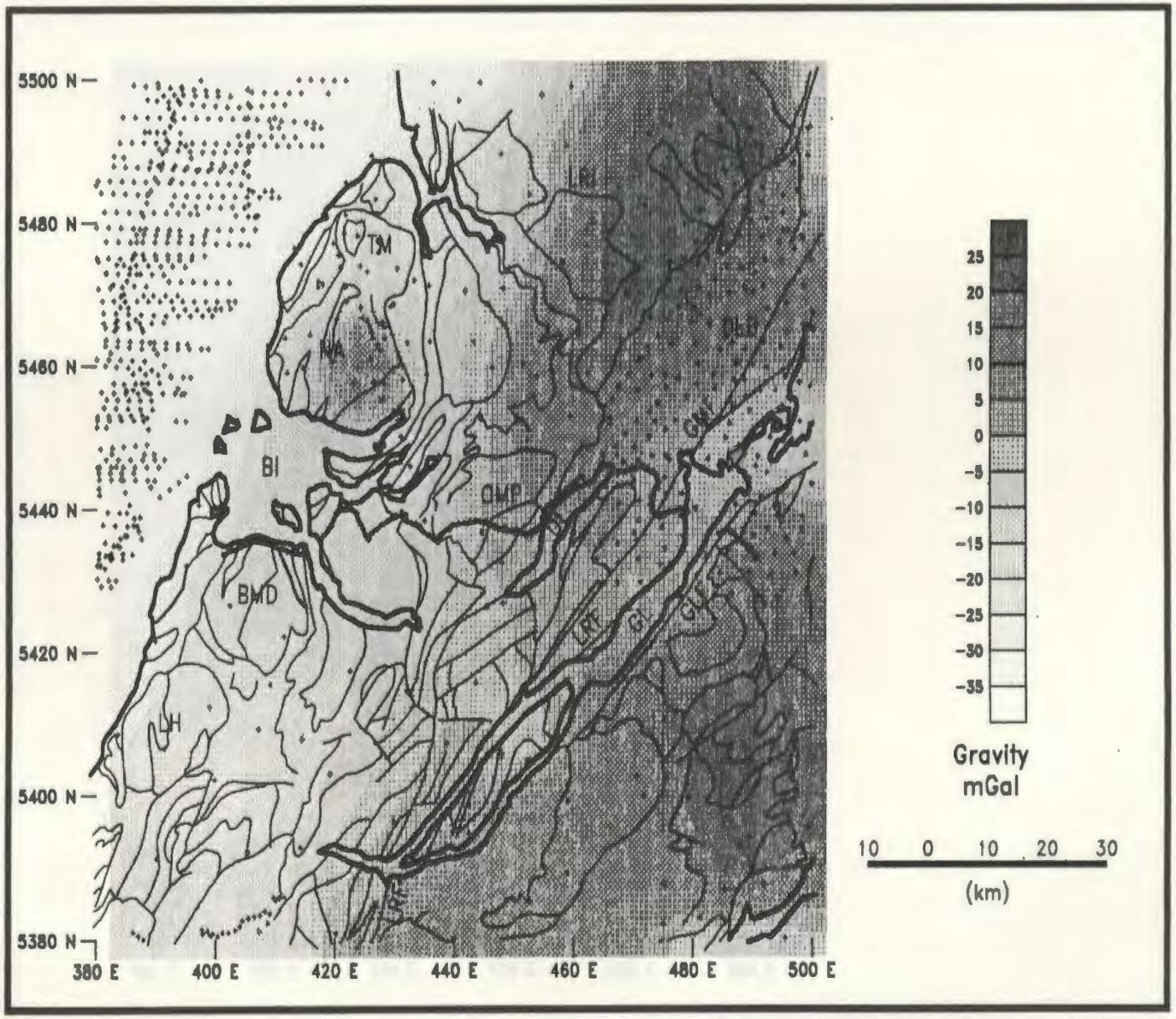

Figure 5.28: Bouguer gravity map for the region around the West Segment of the Meelpaeg Transect. The small plus symbols indicate gravity station locations. Otherwise the legend follows that of Figure 5.1.

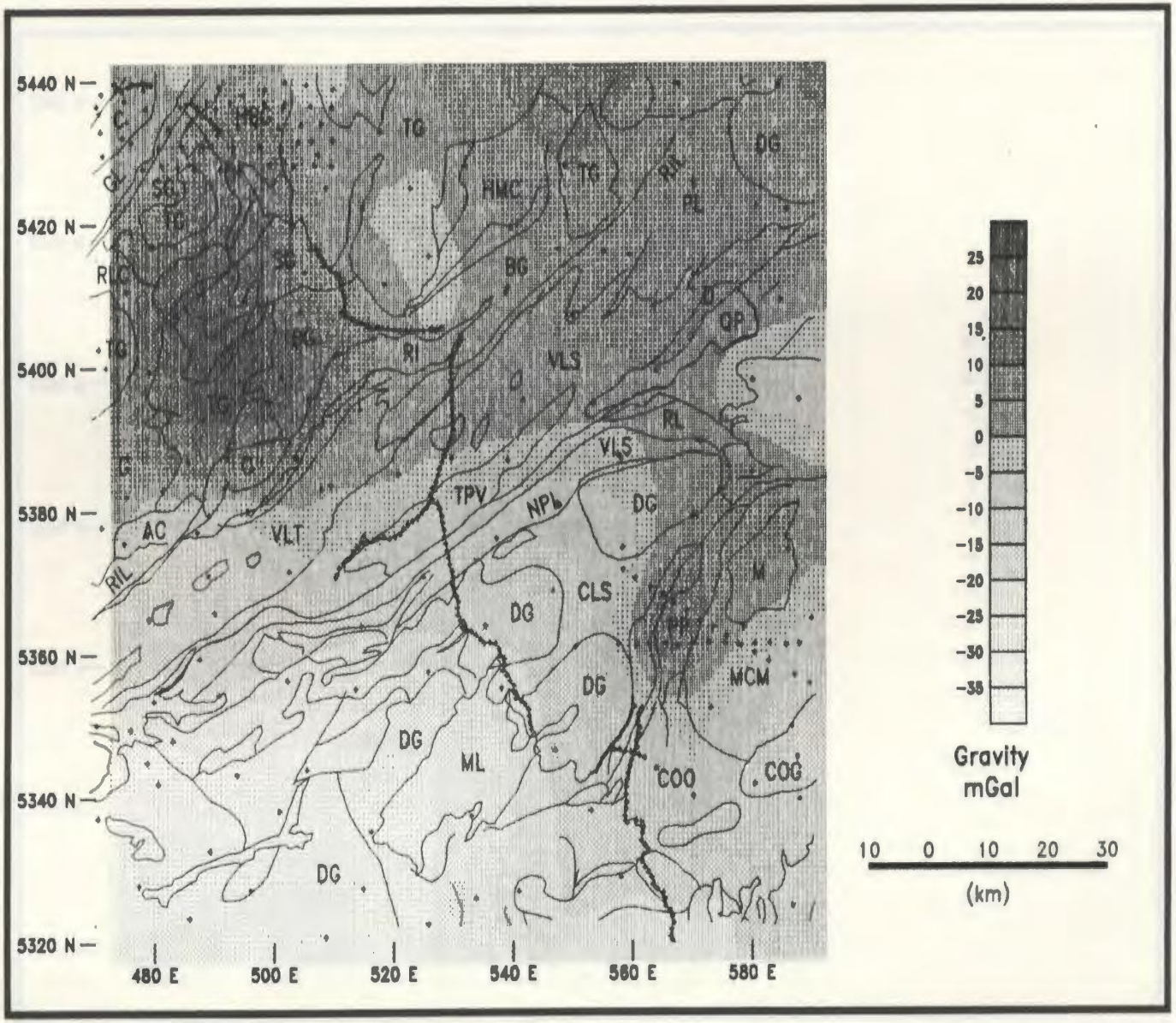

Figure 5.29: Bouguer gravity map for the region around the Central Segment of the Meelpaeg Transect. The small plus symbols indicate gravity station locations. Otherwise the legend follows that of Figure 5.3.

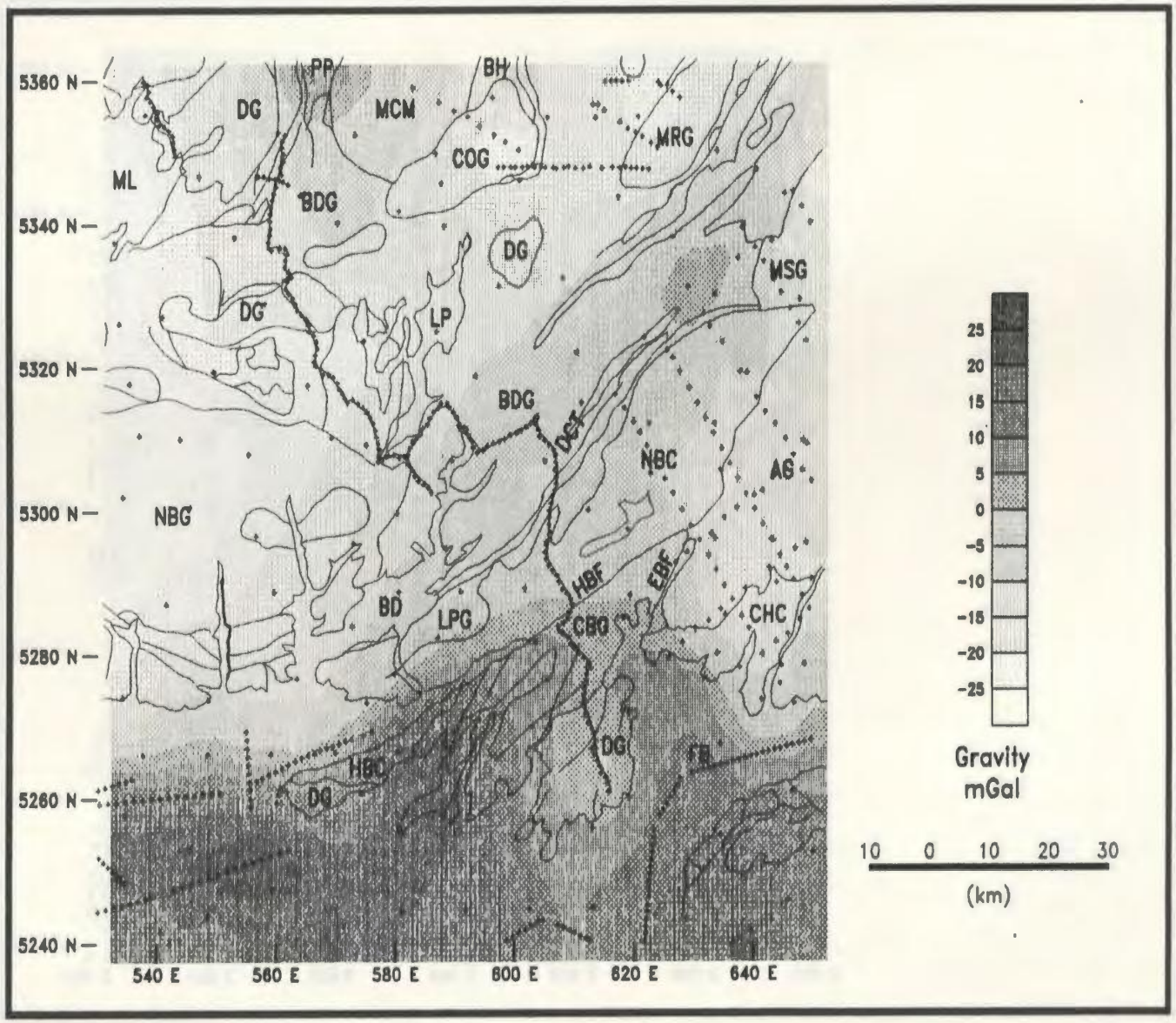

Figure 5.30: Bouguer gravity map for the region around the East Segment of the Meelpaeg Transect. The small plus symbols indicate gravity station locations. Otherwise the legend follows that of Figure 5.5.

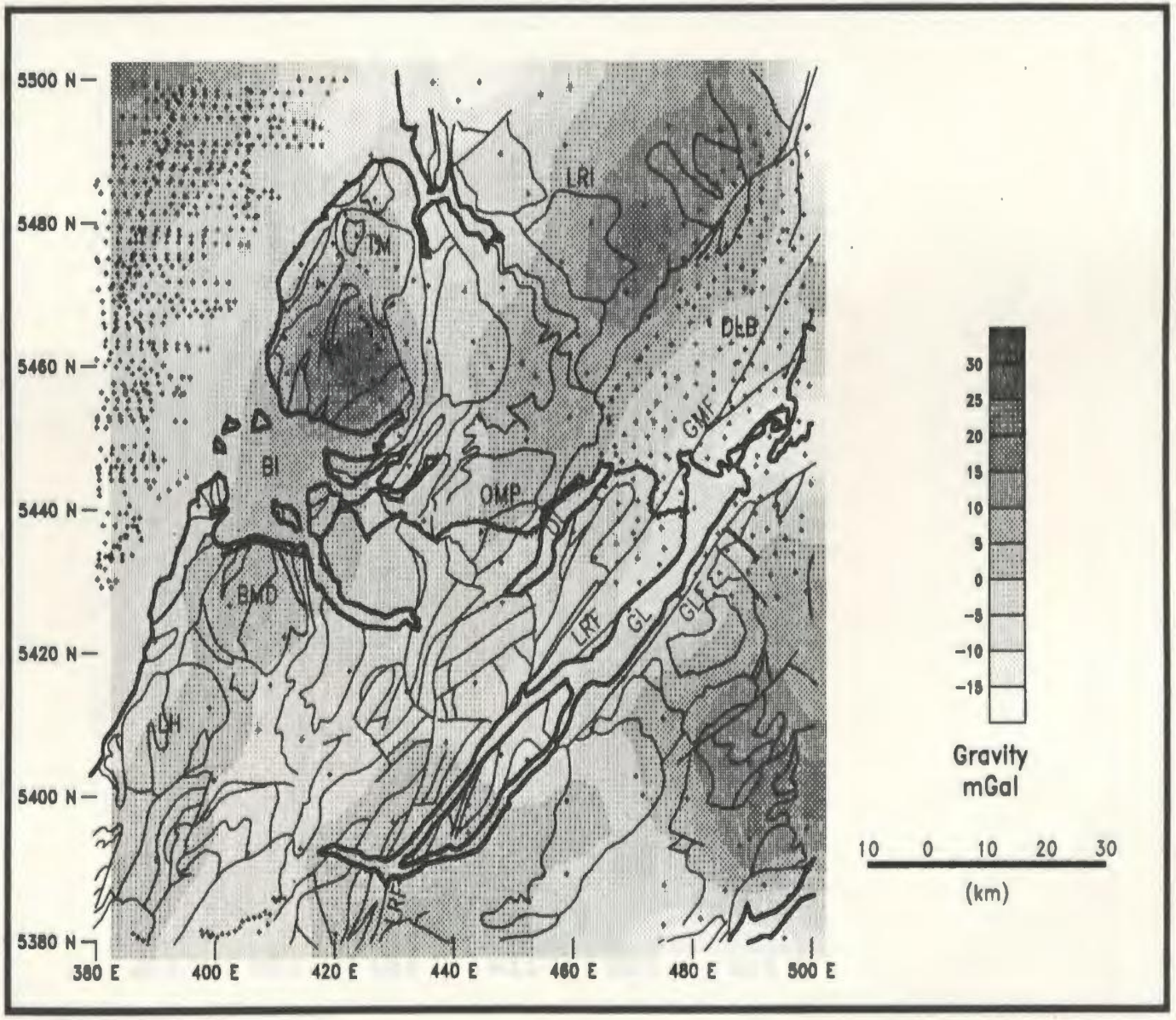

Figure 5.31: Residual gravity map for the region around the West Segment of the Meelpaeg Transect produced by removing a third order polynomial surface from the Bouguer gravity map. The legend follows that of Figure 5.28.

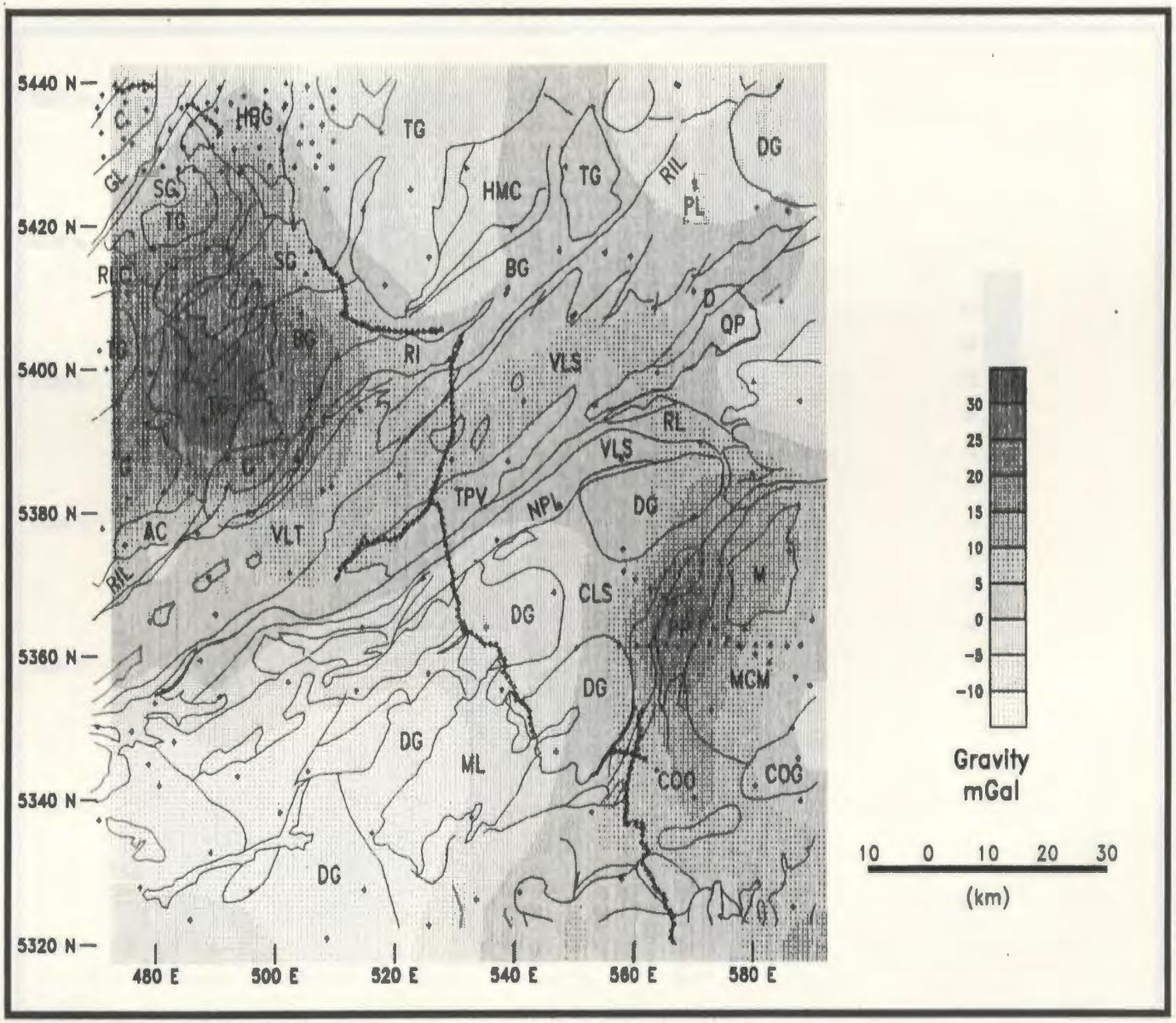

Figure 5.32: Residual gravity map for the region around the Central Segment of the Meelpaeg Transect produced by removing a first order polynomial surface from the Bouguer gravity map. The legend follows that of Figure 5.29.

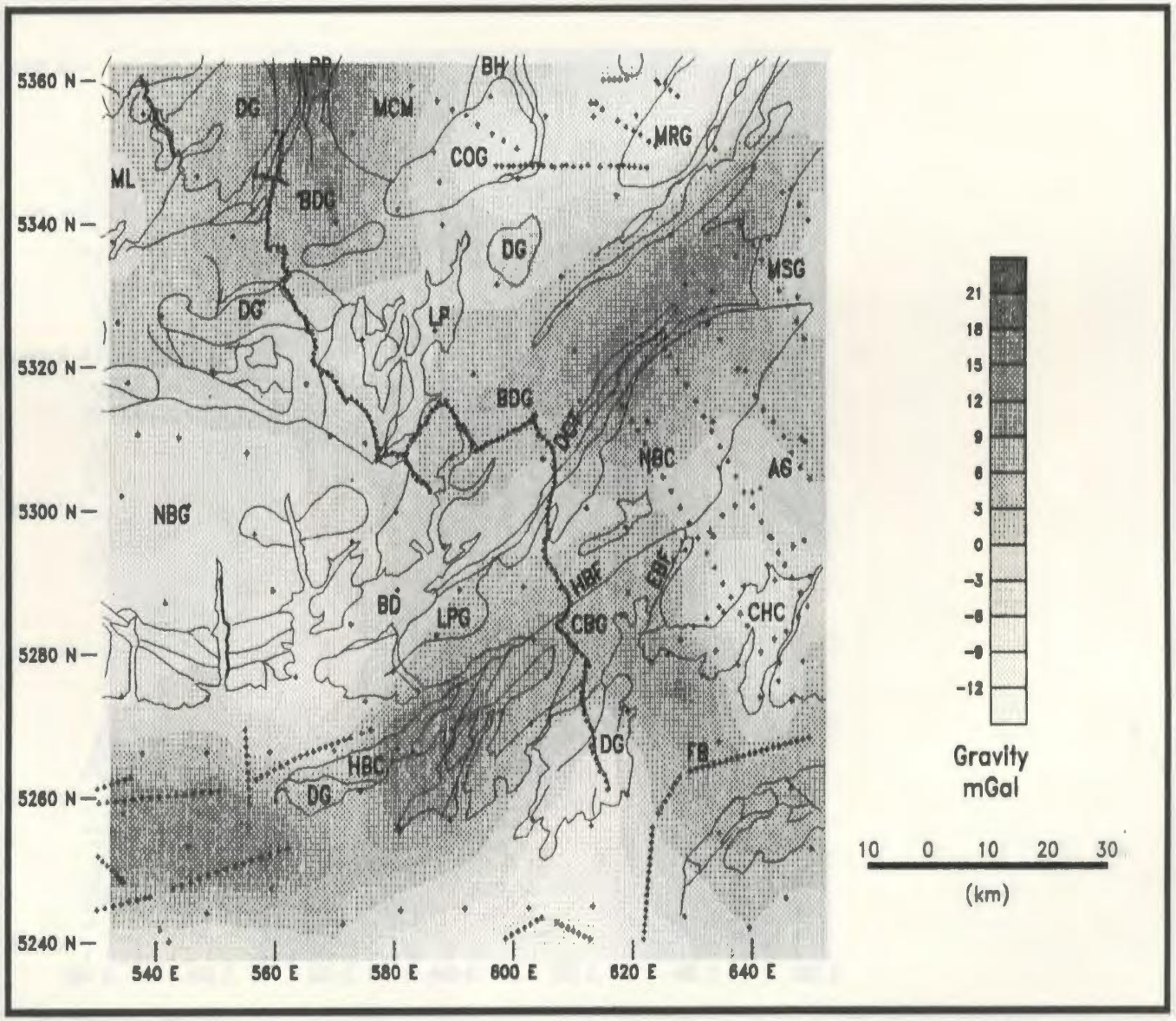

Figure 5.33: Residual gravity map for the region around the East Segment of the Meelpaeg Transect produced by removing a second order polynomial surface from the Bouguer gravity map. The legend follows that of Figure 5.30.

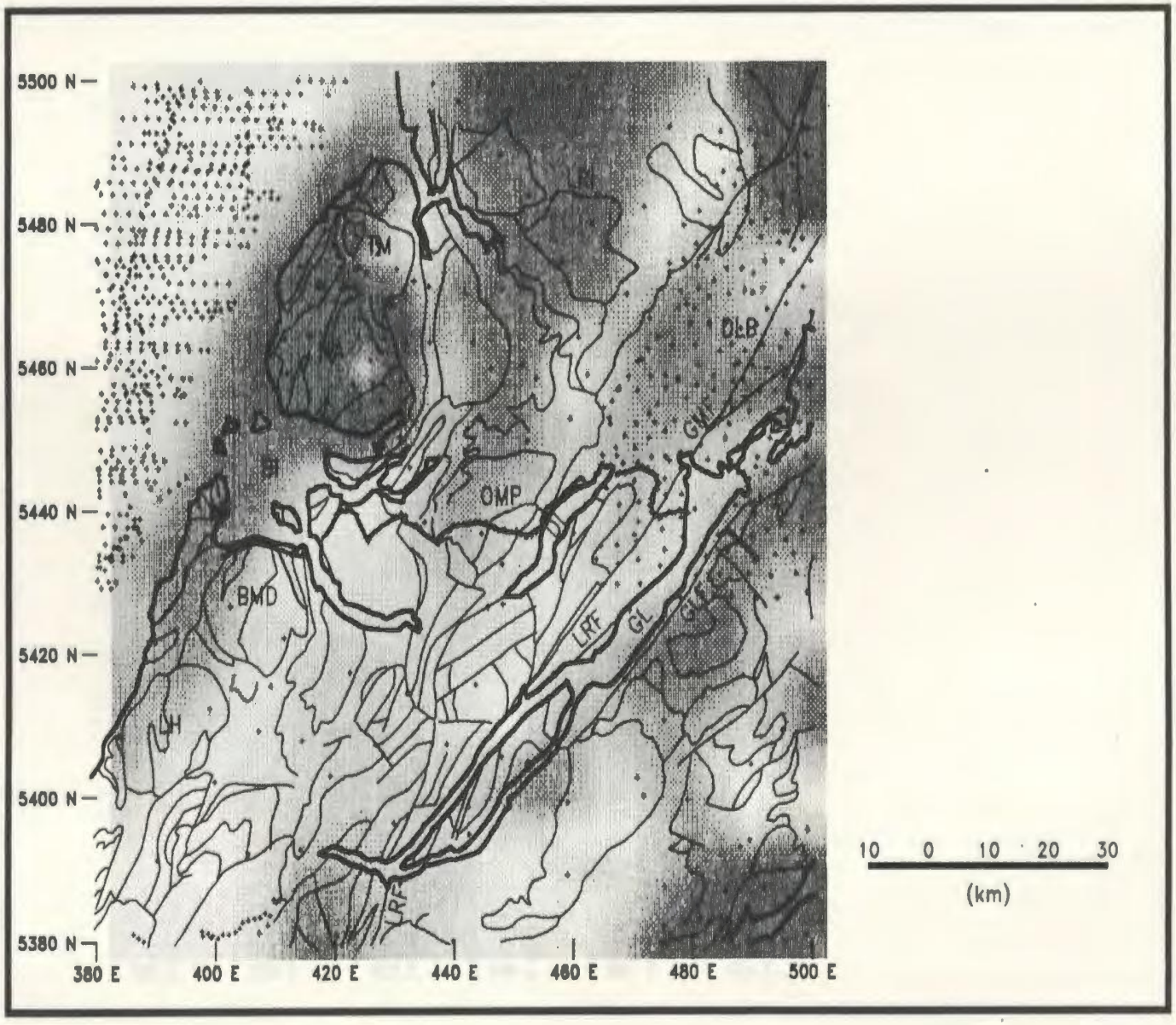

Figure 5.34: Horizontal gradient of the gravity field for the area around the West Segment of the Meelpaeg Transect. The legend follows that of Figure 5.28.

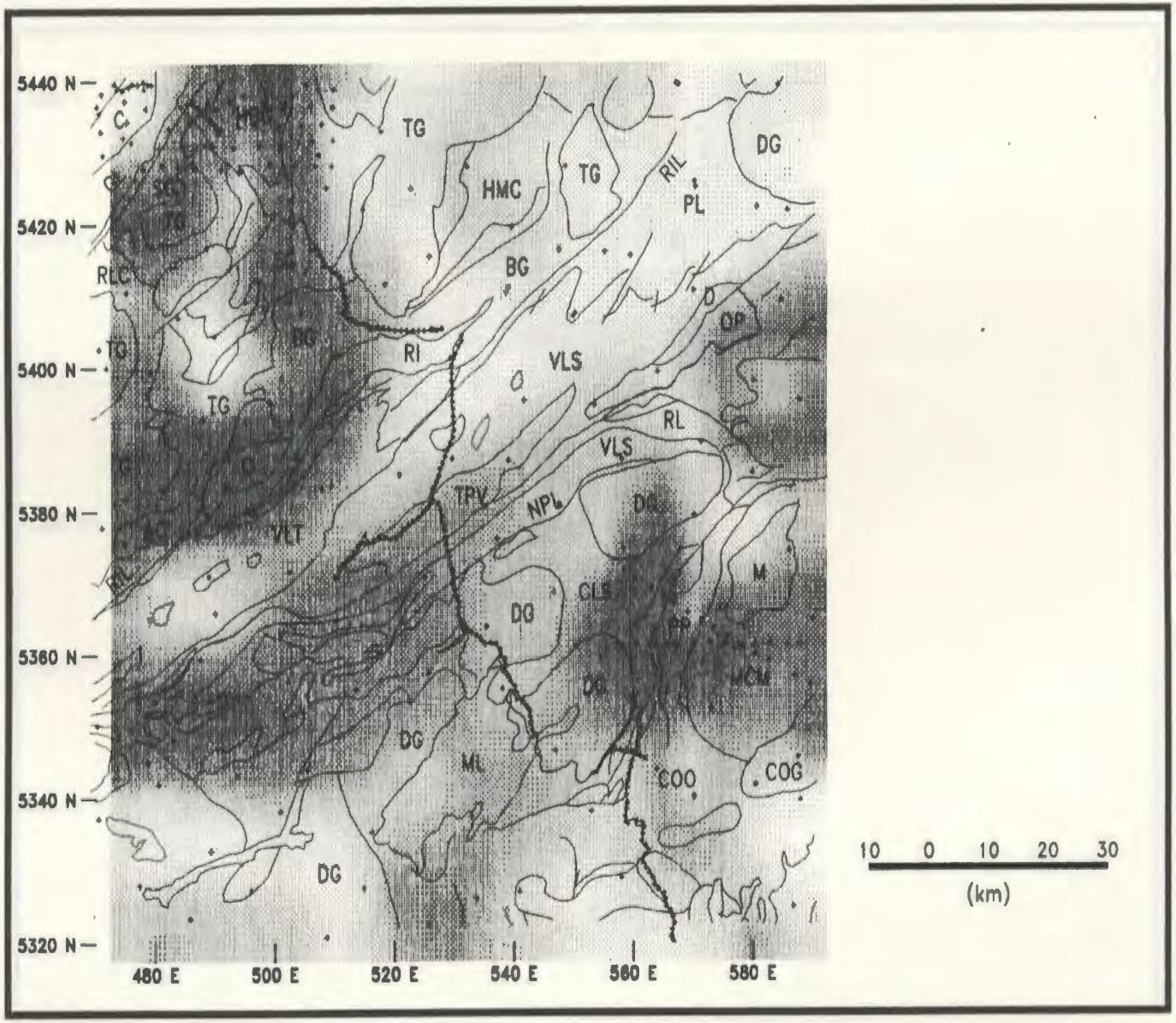

Figure 5.35: Horizontal gradient of the gravity field for the area around the Central Segment of the Meelpaeg Transect. The legend follows that of Figure 5.29.

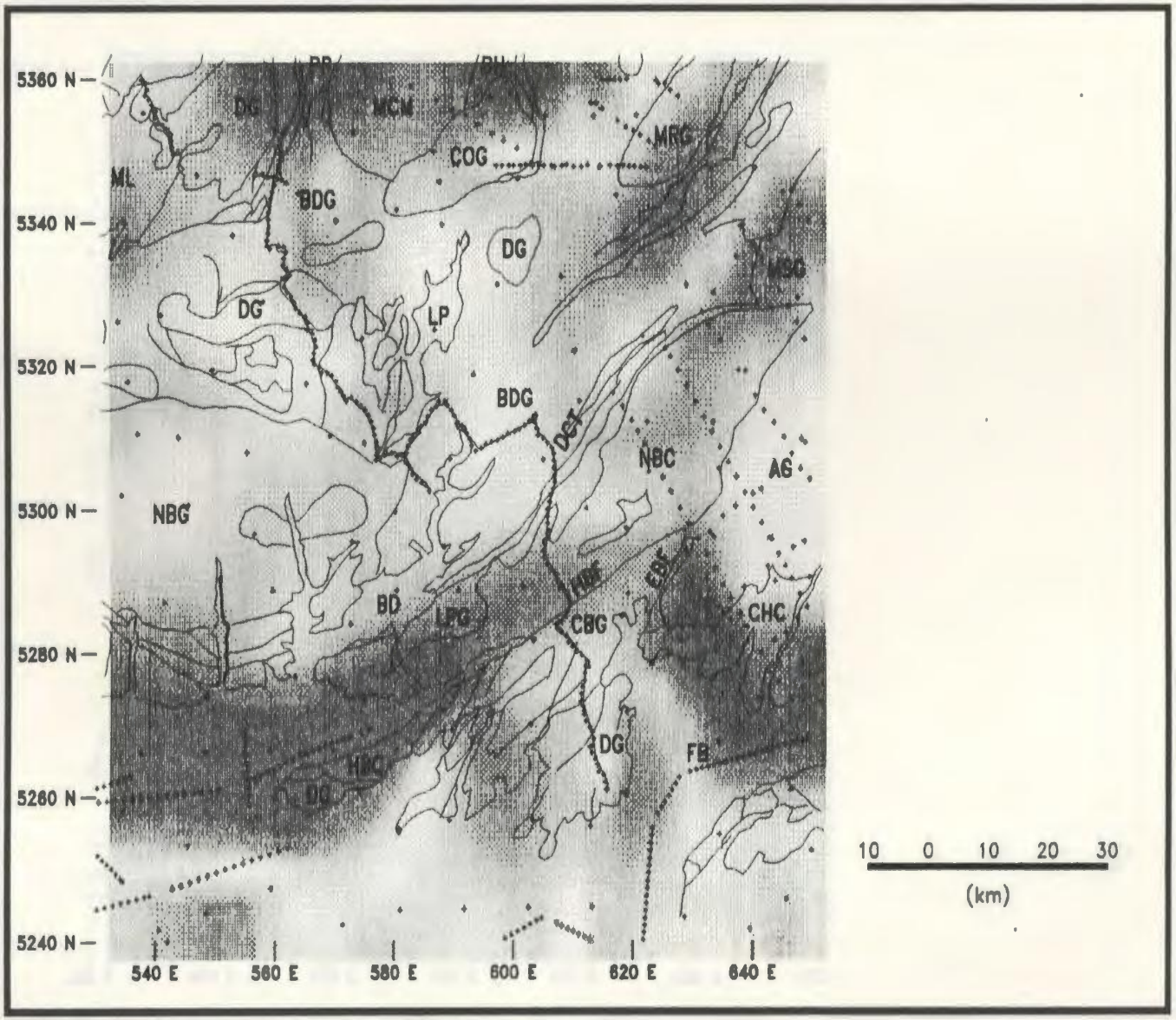

Figure 5.36: Horizontal gradient of the gravity field for the area around the East Segment of the Meelpaeg Transect. The legend follows that of Figure 5.30.

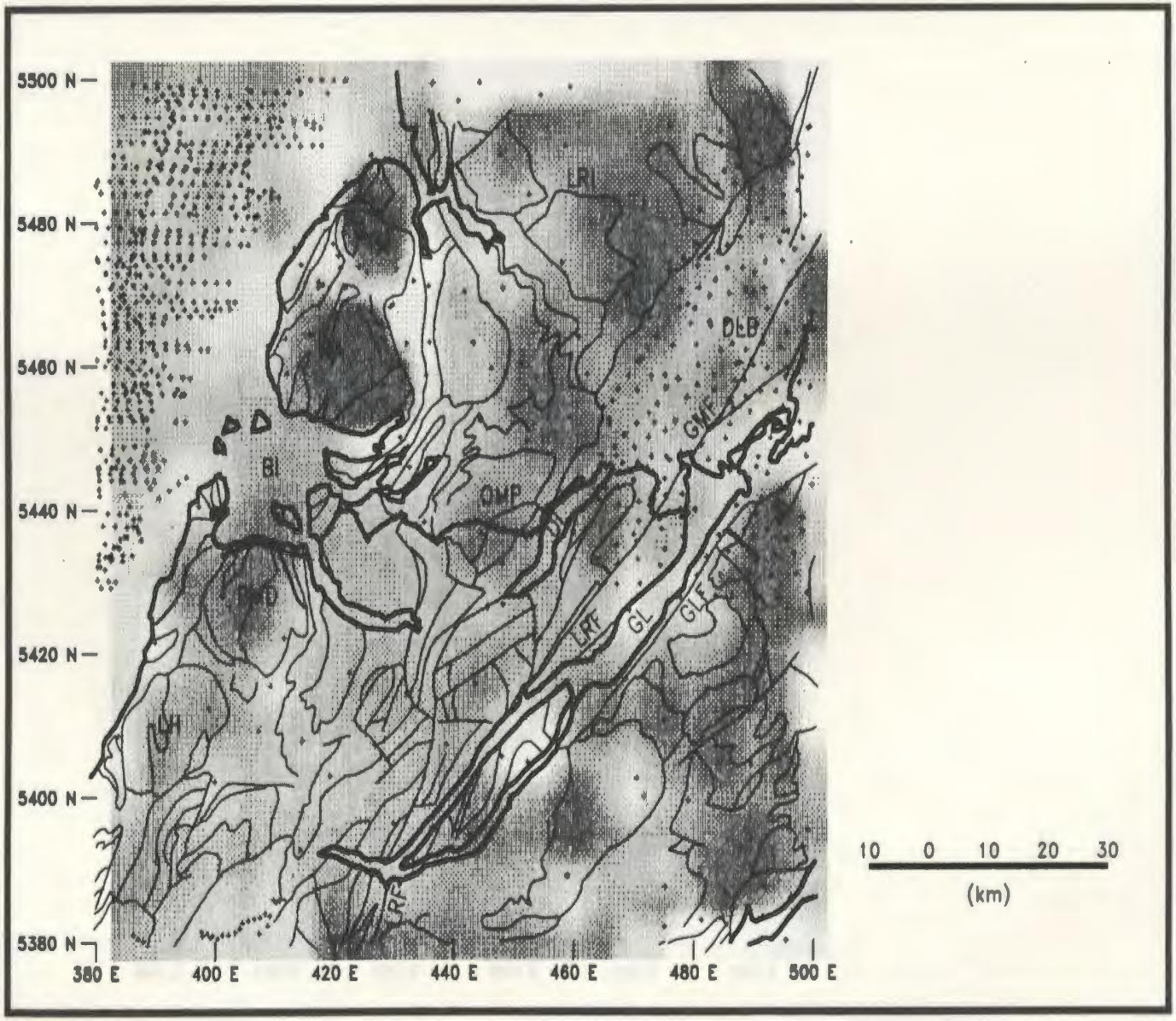

Figure 5.37: Second vertical derivative of the gravity field for the area around the West Segment of the Meelpaeg Transect. The legend follows that of Figure 5.28.

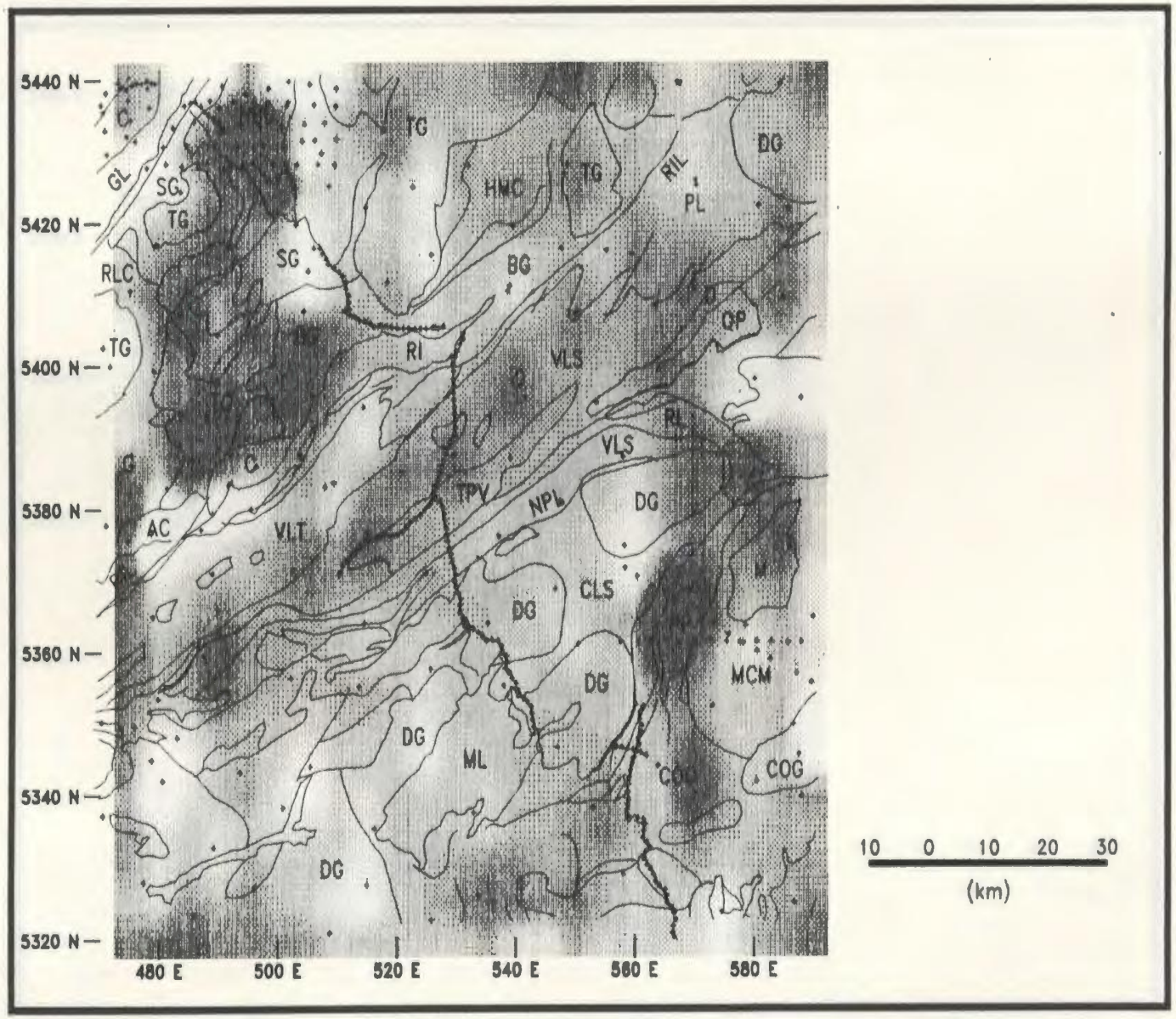

Figure 5.38: Second vertical derivative of the gravity field for the area around the Central Segment of the Meelpaeg Transect. The legend follows that of Figure 5.29.

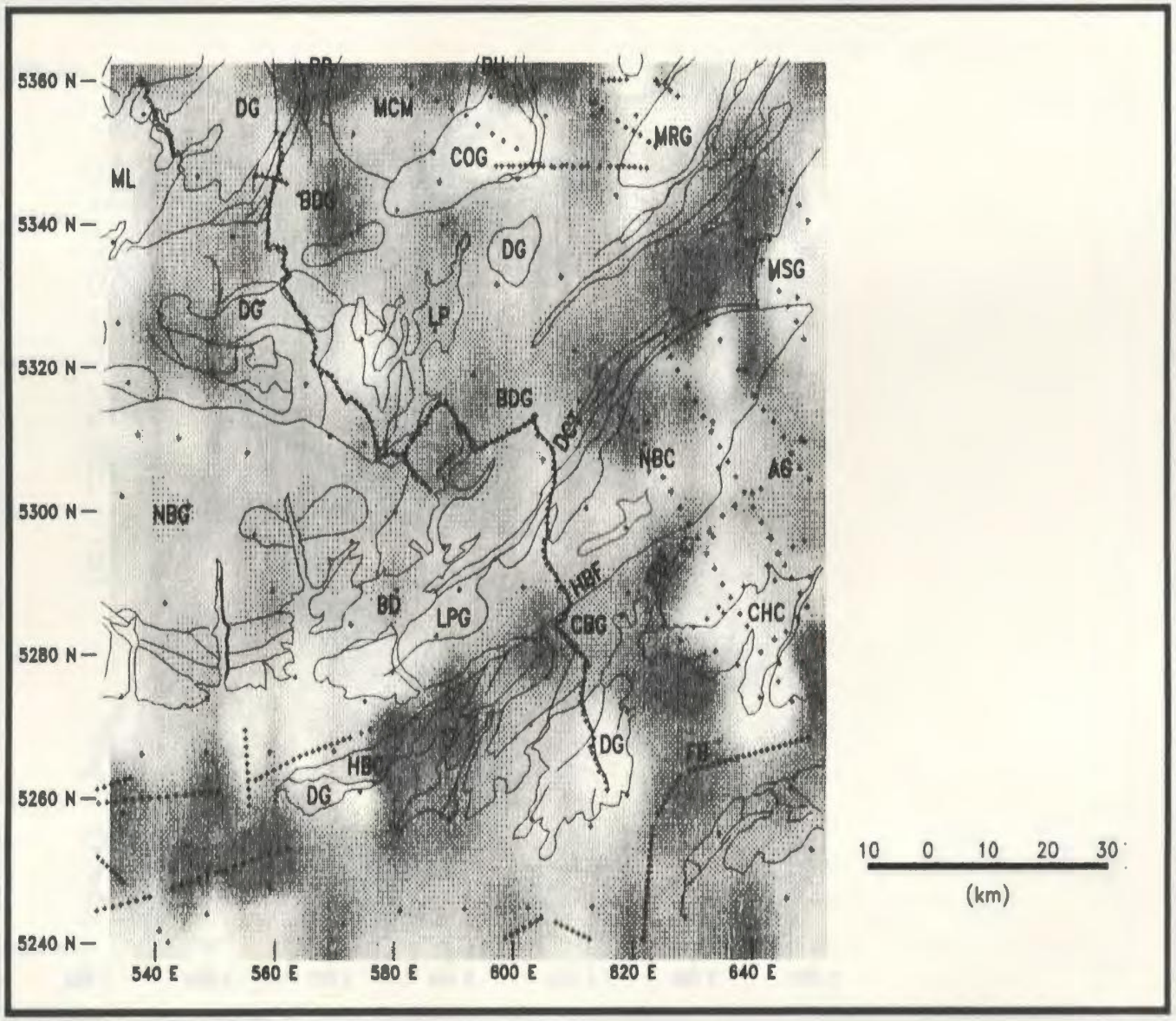

Figure 5.39: Second vertical derivative of the gravity field for the area around the East Segment of the Meelpaeg Transect. The legend follows that of Figure 5.30.

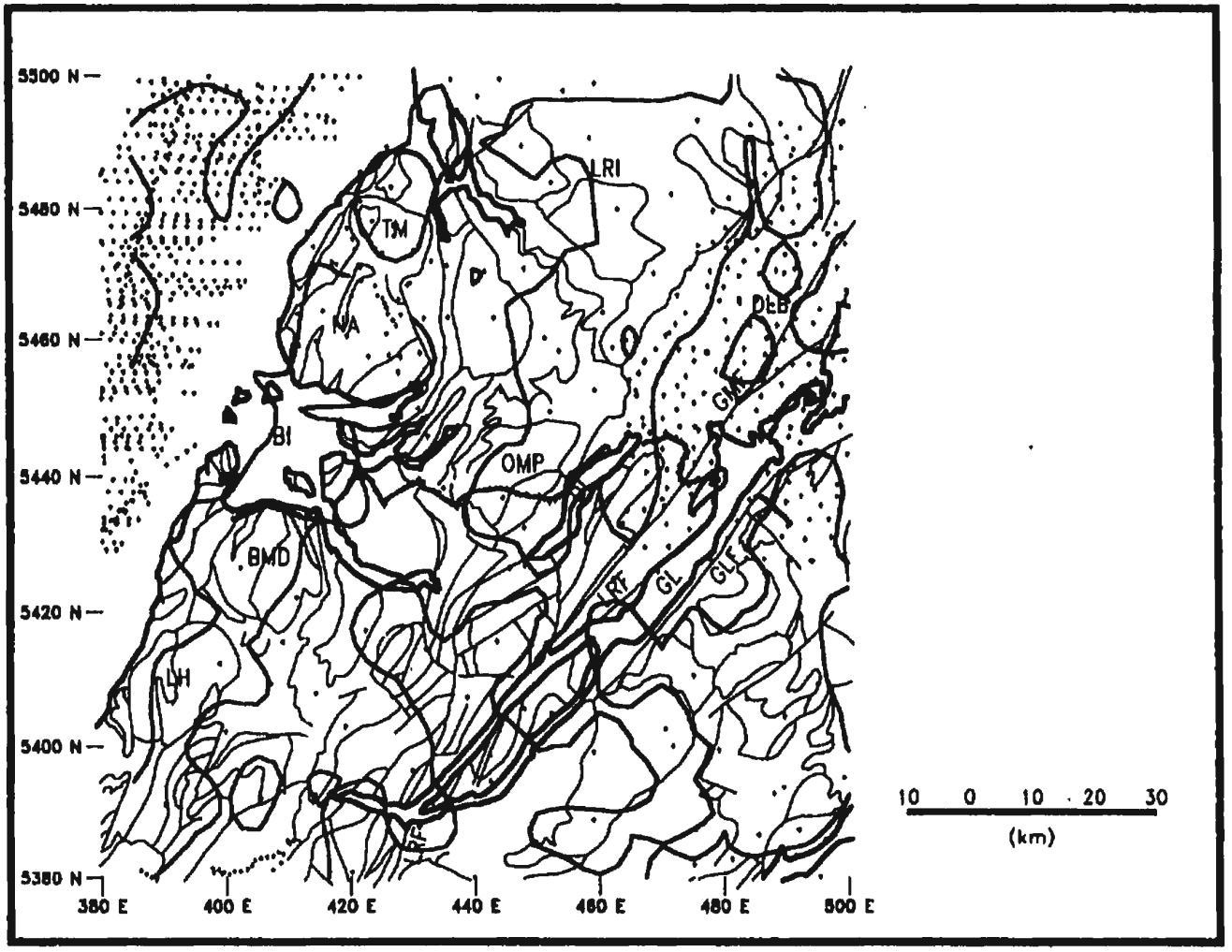

Figure 5.40: Zero level contour map of the second vertical derivative of the gravity field for the area around the West Segment of the Meelpaeg Transect. The legend follows that of Figure 5.28.

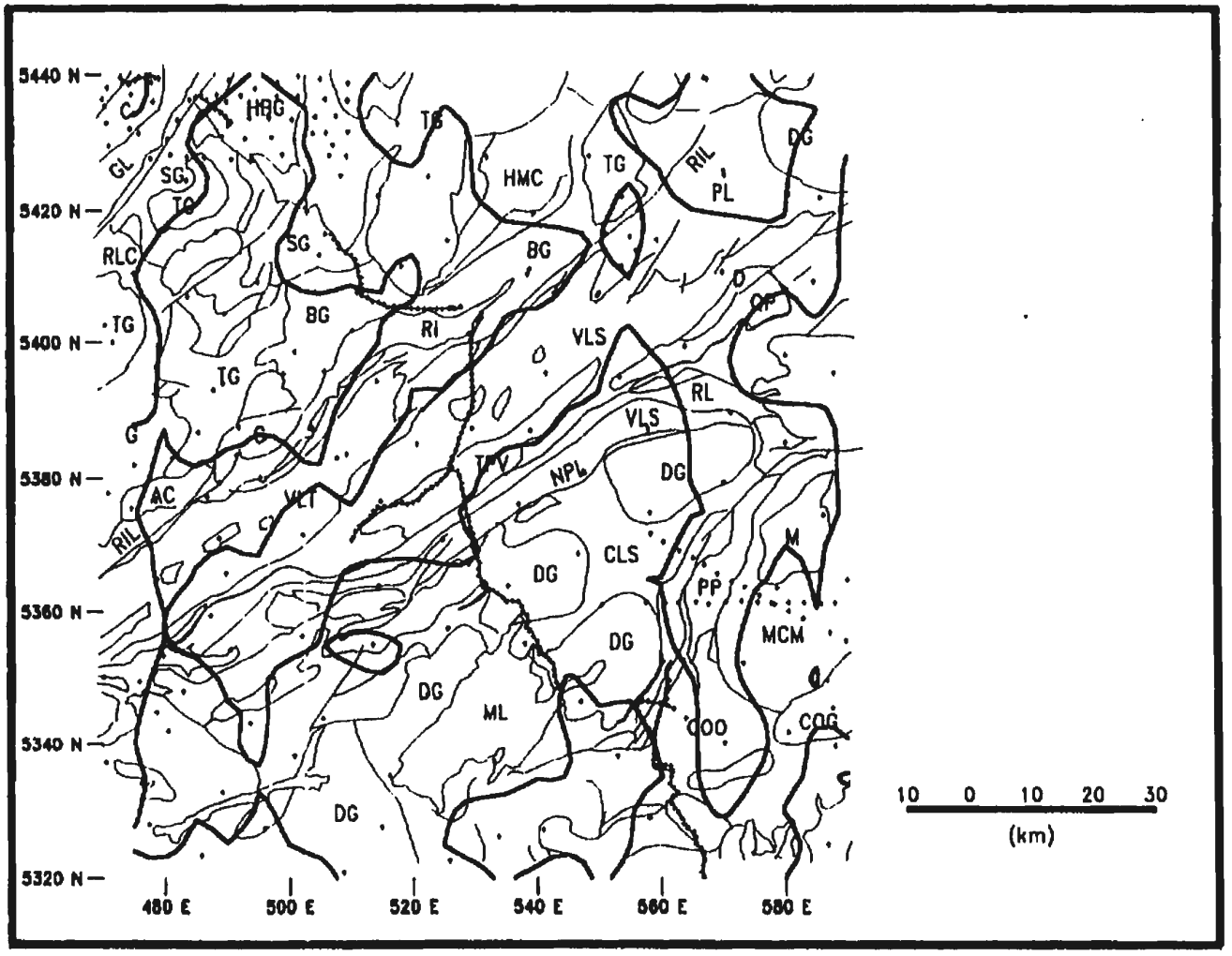

Figure 5.41: Zero level contour map of the second vertical derivative of the gravity field for the area around the Central Segment of the Meelpaeg Transect. The legend follows that of Figure 5.29.

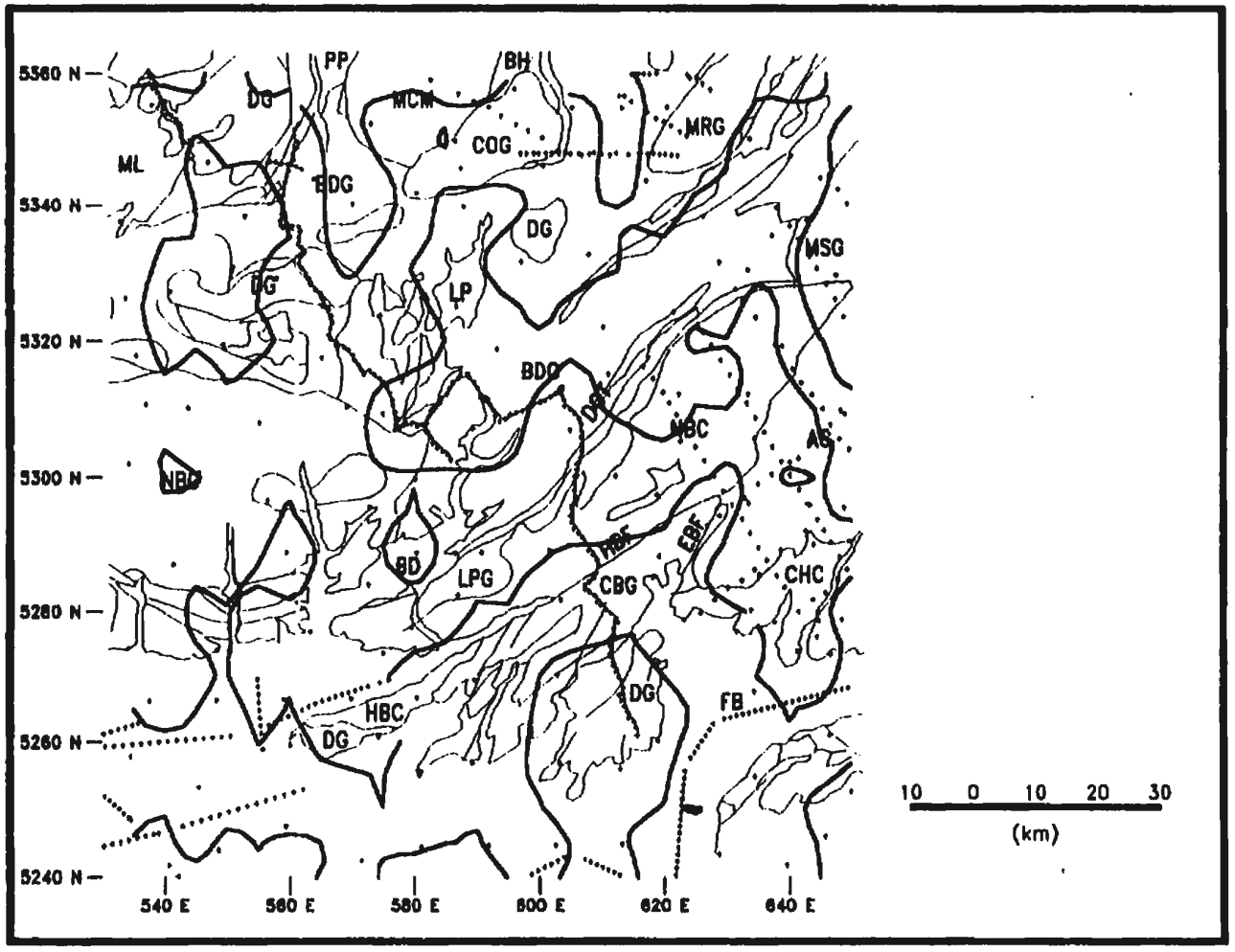

Figure 5.42: Zero level contour map of the second vertical derivative of the gravity field for the area around the East Segment of the Meelpaeg Transect. The legend follows that of Figure 5.30.

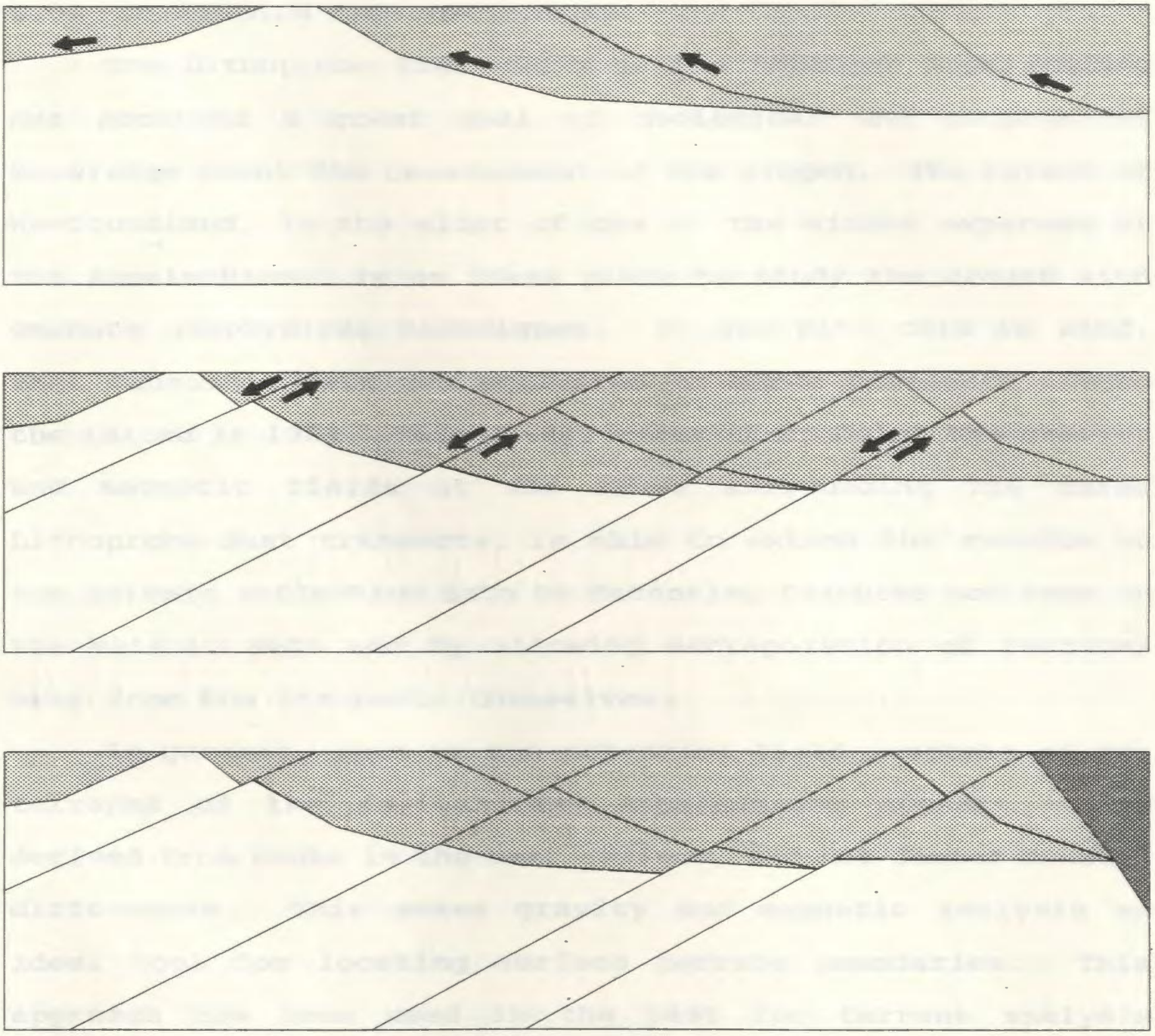

Figure 5.43: Geological evolution of the Meelpaeg Transect (LE89-1,2,3,4,5,6, & 9). The current structure can be explained by three stages: (A) thrusting of allochthonous units from the east, (B) a stage of crustal extension, and (C) emplacement of the Avalon Zone rocks presumably by strike-slip motion.

6.0. DISCUSSION AND CONCLUSIONS:

The Lithoprobe East study of the northern Appalachians has provided a great deal of geological and geophysical knowledge about the development of the orogen. The island of Newfoundland, in the midst of one of the widest expanses of the Appalachians, is an ideal place to study the orogen with onshore geophysical techniques. It was with this in mind, that Vibroseis data was collected on three transects across the island in 1989. This study, aimed at studying the gravity and magnetic fields of the areas surrounding the three Lithoprobe East transects, is able to extend the results of the seismic reflection data by detecting features not seen on the seismic data and by allowing extrapolation of features away from the transects themselves.

In general, much of the potential field response of the terranes of the Newfoundland Appalachians appears to be derived from rocks in the near surface, and not deeper crustal differences. This makes gravity and magnetic analysis an ideal tool for locating surface terrane boundaries. This approach has been used in the past for terrane analysis (Williams et al., 1988; Miller, 1990).

Most of the terranes of the Newfoundland Appalachians have differing gravity signatures, making gravity analysis and modelling a good method for determining the structure of terrane boundaries and the orogen as a whole.

On the Baie Verte Peninsula, both the Vibroseis data and potential field processing and modelling suggest that the Baie Verte Line, the Humber-Dunnage boundary, is a shallow east-dipping fault, not a near-vertical fault as was previously thought (Hibbard, 1983). Its equivalent, the Long Range Fault, is also observed to be east-dipping along the Burgeo Transect but may have a steeper dip in this location.

Along the Meelpaeg Transect, the Humber-Dunnage boundary occurs somewhere beneath the Deer Lake Basin and is not observed on the Vibroseis data. Masking from the sediments in the basin makes it difficult, if not impossible, to define the boundary by potential field methods. As it is, gravity and magnetic analysis identifies a boundary on the eastern edge of the Deer Lake Basin, but this is due to the contrast between the basin sediments and the Topsails Igneous Terrane. A detailed potential field study of the Deer Lake Basin may establish the location and orientation of the Humber-Dunnage boundary in this area.

Seismic reflection data and gravity modelling indicate that most terrane boundaries dip to the east, but the Red Indian Line and Day Cove Thrust appear to be exceptions.

The Red Indian Line, the boundary between the Notre Dame Subzone and the Exploits Subzone, is not identified as a reflector on the Vibroseis data, but there are a number of northwest-dipping reflectors in this area which are likely

genetically related to the Red Indian Line. It is identified on the basis of gravity anomalies.

The Day Cove Thrust, the Dunnage-Gander boundary, is observed to be a northwest-dipping reflector on the Vibroseis data. It shows a small gravity signature, but is not magnetically defined.

The nature of the crust beneath the Dunnage Zone has been a topic of debate. One theory has the Dunnage Zone oceanic material emplaced upon continental crust, while another has the crust of central Newfoundland consisting of an overthickened stack of oceanic material extending down to the mantle.

Gravity modelling suggests that the Dunnage Zone material is allochthonous upon continental type crust, as high density oceanic material throughout the whole crust is not required to produce the Bouguer gravity anomalies observed for the Dunnage Zone. This is consistent with recent results from a Lithoprobe East seismic refraction survey carried out in 1991 which detects only typical continental crust velocities in the crust beneath central Newfoundland (S. Hughes, pers. comm.).

In general, the structure of the Appalachian Orogen in Newfoundland can be explained in three major deformation stages. Initially, during the closing of the Iapetus ocean, oceanic material comprising the Dunnage Zone was thrust from the east upon the eastern miogeocline of North America.

Following this stage of crustal compression, extension with some strike-slip motion occurred throughout the Orogen. The next stage in the development of the Orogen was another period of crustal compression. It was during this stage that the Avalon Zone, and possibly the Meguma Zone, was accreted to the rest of the Appalachian Orogen. The accretion occurred by oblique thrusting with strike-slip motion.

REFERENCES

Barnett, C.T., 1976. Theoretical modeling of the magnetic and gravitational fields of an arbitrarily shaped three-dimensional body. Geophysics, 41, No. 6, pp. 1353-1364.

Bhattacharyya, B.K., 1965. Two-dimensional harmonic analysis as a tool for magnetic interpretation. Geophysics, 30, pp. 829-857.

Blackwood, R.F., 1985. Geology of the Facheux Bay area (11P/9), Newfoundland. Newfoundland Department of Mines and Energy, Report 85-4, 56 p.

Briggs, I., 1974. Machine contouring using minimum curvature. Geophysics, 39, No. 1, pp. 39-48.

Broome, J., 1986. Display and enhancement of aeromagnetic data with examples from Guysborough County, Nova Scotia. In: A.K. Goodacre (Ed.), **Interpretation of Gravity and Magnetic Anomalies for Non-specialists.** Notes for Canadian Geophysical Union Short Coarse, May 18, 1986, pp. 212-252.

Chorlton, L., 1980. Geology of the La Poile River Area (110/16), Newfoundland. Newfoundland Department of Mines and Energy, Report 80-3, 86 p.

Coggon, J.H., 1976. Magnetic and gravity anomalies of polyhedra. Geoexploration, 14, pp. 93-105.

Colman-Sadd, S.P., 1976. Geology of the St. Alban's map-area, Newfoundland (1M/13). Newfoundland Department of Mines and Energy, Report 76-4, 19 p.

Colman-Sadd, S.P., Greene, B.A., and O'Driscoll, C.F., 1979. Gaultois. Newfoundland Department of Mines and Energy, Map 79-104.

Colman-Sadd, S.P., Hayes, J.P., and Knight, I., 1990. Geology of the Island of Newfoundland. Newfoundland Department of Mines and Energy, Map 90-01.

Cordell, L. and Grauch, V.J.S., 1985. Mapping basement magnetization zones from aeromagnetic data in the San Juan basin, New Mexico. In: W.J. Hinze (Ed.), **The Utility of Regional Gravity and Magnetic Anomaly Maps.** Society of Exploration Geophysists, 1985.

Cordell, L. and Henderson, R.G., 1968. Iterative three-dimensional solution of gravity anomaly data using a digital computer. Geophysics, 33, pp. 596-602.

de Wit, M.J., 1972. The geology around Bear Cove, eastern White Bay, Newfoundland. Unpublished Ph.D. thesis, Cambridge University, England, 232 p.

de Wit, M.J., 1980. Structural and metamorphic relationships of pre-Fleur de Lys and Fleur de Lys rocks of the Baie Verte Peninsula, Newfoundland. Canadian Journal of Earth Sciences, 17, pp. 1559-1575.

Dickson, W.L., 1983. Geology, geochemistry and mineral potential of the Ackley Granite and parts of the North West Brook and Eastern Meelpaeg Complexes, southeast Newfoundland (Parts of map areas 1M/10,11,14,15,16; 2D/1,2,3 and 7). Newfoundland Department of Mines and Energy, Report 83-6, 129 p.

Dickson, W.L., 1990. Geology of the North Bay Granite Suite and metasedimentary rocks in southern Newfoundland (NTS 11P/15E, 11P/16, and 12A/2E). Newfoundland Department of Mines and Energy, Report 90-3, 101 p.

Dods, S.D., Teskey, D.J., and Hood, P.J., 1985. The new series of 1:1000000-scale magnetic anomaly maps of the Geological Survey of Canada: Compilation techniques and interpretation. In: W.J. Hinze (Ed.), The Utility of Regional Gravity and Magnetic Anomaly Maps. Society of Exploration Geophysists, 1985.

Dunning, G.R., 1981. The Annieopsquotch ophiolite belt, southwest Newfoundland. In: **Current Research**, Part B, Geological Survey of Canada, Paper 81-1B, pp. 11-15.

Dunning, G.R., and Chorlton, L.B., 1985. The Annieopsquotch ophiolite belt of southwest Newfoundland: geology and tectonic significance. Geological Society of America Bulletin, 96, pp. 1466-1476.

Dunning, G.R., and Herd, R.K., 1980. The Annieopsquotch ophiolite complex, southwest Newfoundland, and its regional relationships. In: **Current Research**, Part A, Geological Survey of Canada, Paper 80-1A, pp. 227-234.

Fuller, B.D., 1967. Two-dimensional frequency analysis and design of grid operators. In: **Mining Geophysics** 2, Society of Exploration Geophysicists, pp. 658-708.

Grauch, V.J.S. and Cordell, L., 1987. Limits of determining density or magnetic boundaries from the horizontal gradient of gravity or pseudogravity data. Geophysics, 52, No. 1, pp. 118-121.

Gupta, V.K. and Ramani, 1982. Optimum second vertical derivatives in geologic mapping and mineral exploration. Geophysics, 47, No.2, pp. 1706-1715.

Hibbard, J., 1983. Geology of the Baie Verte Peninsula, Newfoundland. Newfoundland Department of Mines and Energy, Memoir 2, 279 p.

Hildenbrand, T.G., 1985. Magnetic terranes in the central United States determined from the interpretation of digital data. In: W.J. Hinze (Ed.), **The Utility of Regional Gravity and Magnetic Anomaly Maps**, Society of Exploration Geophysicists, pp. 248-266.

Horn, B.K.P. and Bachman, B.L., 1978. Using synthetic images to register real images with surface models. Commun. Assoc. for Comput. Mach., 21, pp. 914-924.

Jacobson, B.H., 1987. A case for upward continuation as a standard separation filter for potential field maps. Geophysics, 52, No.8, pp. 1138-1148.

Jamieson, R.A., Anderson, S., and MacDonald, I., and Goodwin, L.B. 1993. Silurian extension along the Humber-Dunnage boundary zone, Baie Verte Peninsula, Newfoundland. Abstracts volume, Late Orogenic extension in mountain belts, Montpellier, France, Document du BRGM no 219.

Kean, B.F., Dean, P.L., and Strong, D.F., 1981. Regional geology of the Central Volcanic Belt of Newfoundland. In: E.A. Swanson, D.F. Strong, and J.G. Thurlow (Eds.), **The Buchans Orebodies: Fifty Years of Geology and Mining**, Geological Association of Canada, Special Paper 22, pp. 65-78.

Keen, C.E., Boutilier, R., De Voogd, B., Mudford, B., and Enachescu, M.E., 1987. Crustal geometry and extensional models for the Grand Banks, Eastern Canada: Constraints from deep seismic reflection data. In: C. Beaumont and A.J. Tankard (Eds.), **Sedimentary Basins and Basin-Forming Mechanics**. Canadian Society of Petroleum Geologists, Memoir 12, pp. 101-115.

Keen, C.E., Stockmal, G.S., Welsink, H., Quinlan, G., and Mudford, B., 1987. Deep crustal structure and evolution of the rifted margin northeast of Newfoundland: results from Lithoprobe East. Canadian Journal of Earth Sciences, 24, pp. 1537-1549.

Keppie, J.D., 1985. The Appalachian collage. In: D.G. Dee and B. Sturt (Eds.), **The Caledonide Orogen: Scandinavia and Related Areas.** Wiley, New York, pp. 1217-1226.

Keppie, J.D, Nance, R.D., Murphy, J.B., and Dostal, J., 1989. Northern Appalachians: Avalon and Meguma Terranes. In: R.D. Dallmeger and Lécorché (Eds.), **West African Orogens and Circum-Atlantic Correlations.** Springer, Berlin.

Kilfoil, G.J. and Bruce, P.A., 1991. Gridded aeromagnetic data, 200 m grid cell, Newfoundland by 1:250000 NTS map area. Newfoundland Department of Mines and Energy, Open File NFLD (2063).

Knight, 1983. Geology of the Carboniferous Bay St. George Subbasin, Western Newfoundland. Newfoundland Department of Mines and Energy, Memoir 1, 358 p.

Marillier, F., Keen, C.E., Stockmal, G.S., Quinlan, G., Williams, H., Colman-Sadd, S.P., O'Brien, S.J., 1989. Crustal structure and surface zonation of the Canadian Appalachians: implications of deep seismic reflection data. Canadian Journal of Earth Sciences, 26, pp. 305-321.

Marillier, F. and Louden, K., 1991. The 1991 marine refraction experiment: A first look at the data. In: Quinlan (Ed.), **Lithoprobe East Report of Transect Meeting**, November 29-30, 1991, Memorial University of Newfoundland, St. John's, Newfoundland. Lithoprobe Report No. 23., 120 p.

Miller, H.G., 1988. Geophysical studies of the Ackley Intrusive Suite and the northeastern Gander Zone, NNewfoundlannd. Newfoundland Department of Mines and Energy, Report 88-3, 44 p.

Miller, H.G., 1990. A synthesis of the geophysical characteristics of terranes in eastern Canada. Tectonophysics, 177, pp. 171-191.

Miller, H.G. and Deutsch, E.R., 1976. New gravitational evidence for the subsurface extent of oceanic crust in north-central Newfoundland. Canadian Journal of Earth Sciences, 13, pp. 459-469.

Miller, H.G., Kilfoil, G.J, and Peavy, S.T., 1990. An integrated geophysical interpretation of the Carboniferous Bay St. George Subbasin, western Newfoundland. Bulletin of Canadian Petroleum Geology, 38, No.3, pp. 320-331.

Mufti, I.R., 1975. Iterative gravity modeling by using cubical blocks. Geophysical Prospecting, 23, pp. 163-198.

Nagy, D., 1966. The gravitational attraction of a right rectangular prism. Geophysics, 31, pp. 362-371.

O'Brien, B.H. and O'Brien, S.J., 1989. Geology of the western Hermitage Flexure: Bay D'Est fault and south (parts of 110/9, 110/16, 11P/12, and 11P/13), southwest Newfoundland. Newfoundland Department of Mines and Energy, Map 89-133 (1:100000).

Paul, M.K., 1974. The gravity effect of a homogeneous polyhedron for three-dimensional interpretation. Pageoph, 112, III, pp. 553-561.

Pederson, L.B., 1991. Relations between potential fields and some equivalent sources. Geophysics, 56, No.7, pp. 961-971.

Quinlan, G.M., Hall, J., Williams, H., Wright, J.A., Colman-Sadd, S.P., O'Brien, S.J., Stockmal, G.S., Marillier, F., 1992. Lithoprobe onshore reflection transects across the Newfoundland Appalachians. Canadian Journal of Earth Sciences, 29, pp. 1865-1877.

Quinlan, G.M., Hall, J., Williams, H., Wright, J.A., Colman-Sadd, S.P., O'Brien, S.J., Stockmal, G.S., Marillier, F., 1991. Onshore seismic reflection transects across the Newfoundland Appalachians. In: Quinlan (Ed.), **Lithoprobe East Report of Transect Meeting**, November 29-30, 1991, Memorial University of Newfoundland, St. John's, Newfoundland. Lithoprobe Report No. 23., 120 p.

Rasmussen, R. and Pedersen, L.B., 1979. End corrections in potential field modeling. Geophysical Prospecting, 27, pp. 749-760.

Roberts, B., Hall, J., Lu, H., Quinlan, G., and Wright, J., 1991. Delineating crustal blocks in the northern Appalachians: Results from the onland part of Lithoprobe East's seismic refraction / wide-angle reflection experiment in Newfoundland. In: Quinlan (Ed.), **Lithoprobe East Report of Transect Meeting**, November 29-30, 1991, Memorial University of Newfoundland, St. John's, Newfoundland. Lithoprobe Report No. 23., 120 p.

Smith, W.H.F. and Wessel, P., 1990. Gridding with continuous curvature splines in tension. Geophysics, 55, No. 3, pp. 293-305.

Spector, A. and Grant, F.S., 1970. Statistical models for interpreting aeromagnetic data. Geophysics, 35, pp. 293-302.

St. Julian, P. and Béland, J., 1982 (Eds). **Major Structural Zones and Faults of the Northern Appalachians.** Geological Association of Canada, Special Paper 24, 280 p.

St. Julian, P., Hubert, C., and Williams, H., 1976. The Baie Verte - Brompton line and its possible tectonic significance in the northern Applachians. Geological Society of America, Program with Abstracts, 8, No.2, pp. 259-260.

Stockmal, G.S. and Waldron, J.W.H., 1991. Interpretations of western Newfoundland Lithoprobe East lines: problems and possibilities for Humber Zone tectonics. In: Quinlan (Ed.), **Lithoprobe East Report of Transect Meeting**, November 29-30, 1991, Memorial University of Newfoundland, St. John's, Newfoundland. Lithoprobe Report No. 23., 120 p.

Talwani, M., 1965. Computation with the help of a digital computer of magnetic anomalies caused by bodies of arbitrary shape. Geophysics, 30, pp. 797-817.

Talwani, M. and Ewing, M., 1960. Rapid computation of gravitational attraction of three-dimensional bodies of arbitrary shape. Geophysics, 25, pp. 203-225.

Talwani, M. and Heirtzler, J.R., 1964. Computation of magnetic anomalies caused by two-dimensional bodies of arbitrary shape. In: G.A. Parks (Ed.), **Computers in the Mineral Industries**, Part 1. Stanford University Publications, Geological Sciences, 9, pp. 464-480.

Talwani, M., Worzel, J.L., and Landisman, M., 1959. Rapid gravity computations for two-dimensional bodies with application to the Mendicino submarine fracture zone. Journal of Geophysical Research, 64, pp.49-59.

Telford, W.M., Geldart, L.P., Sheriff, R.E., and Keys, D.A., 1976. **Applied Geophysics**, Cambridge University Press, 860 p.

Thorarinsson, F., Magnusson, S.G., and Bjornsson, A., 1988. Directional spectral analysis and filtering of geophysical maps. Geophysics, 53, No. 12, pp. 1587-1591.

van Berkil, J.T., and Currie, K.L., 1986. Geology of the southern Long Range, southwest Newfoundland (12B/1, 12B/8, 12B/9E, 12A/4, 12A/5, 12A/12). Geological Survey of Canada, Open File Report 0000 (1:100000 map with marginal notes).

van Berkil, J.T., Currie, K.L., 1989?. Descriptive notes to the preliminary map of the southern Long Range, southwest Newfoundland. In prog.

van Berkil, J.T., Johnston, P., and Currie, K.L., ?. A preliminary report on the geology of the southern Long Range, southwest Newfoundland. Geological Survey of Canada, Project 850017, 22 p.

Whalen, J.B., and Currie, K.L., 1988. Geology: Topsails igneous terrane, Newfoundland. Geological Survey of Canada, Map 1680A (1:200000).

Williams, 1979. Appalachian Orogen in Canada. Canadian Journal of Earth Sciences, 16, pp. 792-807.

Williams, H. and Cawood, P.A., 1989. Geology: Humber Arm Allochthon, Newfoundland. Geological Survey of Canada, Map 1678A (1:250000).

Williams, H., Colman-Sadd, S.P., Swinden, H.S., 1988. Tectonic-stratigraphic subdivisions of central Newfoundland. In: **Current Research**, Part B, Geological Survey of Canada, Paper 88-1B, pp. 91-98.

Williams, H. and Hatcher, R.D., 1982. Suspect terranes and accretionary history of the Appalachian Orogen. Geology, 10, pp. 530-536.

Williams, H. and St. Julian, P., 1978. The Baie Verte - Brompton Line in Newfoundland and regional correlations in the Canadian Appalachians. Geological Survey of Canada, Paper 78-1A, pp. 225-229.

Wiseman, 1991. A mineralogical and magnetic study of altered ophiolitic ultramafic rocks on the Baie Verte Peninsula, Newfoundland. Unpublished B.Sc. thesis, Memorial University of Newfoundland, 85 p.

Wright, J.A., McNeice, G., Korja, T., Jones, A.G., Craven, J. and Ellis, R., 1991. Electromagnetic studies in the Lithoprobe East Transect. In: Quinlan (Ed.), **Lithoprobe East Report of Transect Meeting**, November 29-30, 1991, Memorial University of Newfoundland, St. John's, Newfoundland. Lithoprobe Report No. 23., 120 p.

APPENDIX A: PHYSICAL PROPERTY DATA

Physical property data used for potential field modelling was collected from various sources. Tables summarizing the physical property data for each region of interest follow, along with notes indicating the origin of the data. Where data was unavailable, tables of physical property data versus rock type published in Telford et al. (1976) were used.

Table I: Physical property data for the Baie Verte Peninsula

	D g/cc	Std. Dev.	N	k c.g.s.	Std. Dev.	N
Burlington Granodiorite[1]	2.69	0.04	6	1.88e-05	1.05e-05	24
Cape Brule Poprhyry[1]	2.65	0.02	4	3.40e-04	4.32e-04	16
East Pond Metamorphic Suite[1]	2.72	0.04	3	2.50e-05	2.50e-05	12
Flat Water Pond[2]	2.74	0.13	46	2.46e-03	2.11e-03	48
Garden Cove Fm.[1]	2.75		1	7.50e-06	8.29e-06	4
Middle Arm Metaconglomerate[1]	2.67	0.02	2	3.63e-05	4.00e-05	8
Old House Cove Gp.[1]	2.81	0.09	5	4.17e-04	6.02e-04	20
Pigeon Island Fm.[1]	2.72		1	6.00e-05	1.87e-05	4
White Bay Gp.[1]	2.71		1	1.25e-05	8.29e-06	4

Table II: Physical property data for the Burgeo Road region

	D g/cc	Std. Dev.	N	k c.g.s.	Std. Dev.	N
Bay du Nord Group[3]	2.64	0.04	7	2.00e-04	4.50e-04	7
Buck Lake Granite[3]	2.60	0.02	3	3.33e-05	4.71e-05	3
Burgeo Intrusive Suite[3]	2.62	0.07	19	1.34e-03	8.09e-04	18
Carboniferous sediments[4]	2.55	0.08		0.00		
Chetwynd Granite[3]	2.50	0.02	2	2.00e-04	2.00e-04	2
Indian Head Inlier[4]	2.68	0.07		1.78e-04		
Lapoile Group[3]	2.67	0.01	3	1.67e-04	9.43e-05	3
Sandbanks Migmatite[3]	2.68	0.11	7	1.51e-03	2.04e-03	7
Steel Mountain Anorthosite[4]	2.83	0.34		1.78e-04		
Top Pond Tonalite[3]	2.76	0.04	5	2.20e-04	1.47e-04	5
Wolf Hills Migmatite[3]	2.75	0.12	5	2.65e-03	1.10e-03	4

Table III: Physical property data for the West Segment of the Meelpaeg Transect

	D g/cc	Std. Dev.	N	k c.g.s.	Std. Dev.	N
Bay of Islands Complex[5]	2.76	0.10	10	3.21e-04	7.21e-04	10
Blow Me Down Brook Fm.[5]	2.65	0.03	7	8.57e-06	9.90e-06	7
Companion Melange[5]	2.71	0.08	5	1.80e-05	7.48e-06	5
Cooks Brook Fm.[5]	2.67	0.06	6	1.00e-05	8.16e-06	6
Deer Lake Group[5]	2.55	0.07	6	1.67e-05	9.43e-06	6
Irishtown Fm.[5]	2.64	0.05	8	1.13e-05	7.81e-06	8
Old Mans Pond Group[5]	2.73	0.05	20	1.40e-05	8.60e-06	20
Springdale Group[5]	2.70	0.01	3	2.67e-04	3.42e-04	3
Summerside Fm.[5]	2.68	0.08	3	1.00e-05	0.00	3
Table Head Group[5]	2.69	0.14	8	3.75e-06	4.84e-06	8

Table IV: Physical proberty data for the Central Segment of the Meelpaeg Transect

	D g/cc	Std. Dev.	N	k c.g.s.	Std. Dev.	N
Buchans Group[5]	2.62	0.08	5	3.60e-05	4.84e-05	5
North Bay Granite eq.[5]	2.68	0.07	14	1.20e-04	1.73e-04	14
Spruce Brook Fm.[5]	2.80	0.14	6	2.35e-03	5.59e-03	6
Tally Pond Volcanics[5]	2.76	0.03	2	3.00e-05	1.00e-05	2
Tulks Hill Volcanics[5]	2.76	0.13	7	8.57e-06	4.00e-06	7
Victoria Lake Group[5]	2.70	0.03	2	2.00e-05	0.00	2

Table V: Physical property data for the East Segment of the Meelpaeg Transect

	D g/cc	Std. Dev.	N	k c.g.s.	Std. Dev.	N
Bay D'Espoir Group[5]	2.74	0.10	13	1.07e-04	1.07e-05	13
Cold Spring Pond Fm.[5]	2.73	0.15	14	1.08e-04	3.85e-04	14
Connaigre Bay Group[5]	2.60	0.10	2	6.50e-05	6.50e-05	2
Hermitage Bay Complex[5]	2.89	0.01	2	2.80e-04	2.20e-04	2
North Bay Granite[5]	2.66	0.05	8	6.75e-05	1.96e-04	8
Salmon River Dam Fm.[5]	2.74	0.07	13	7.69e-05	2.98e-04	13

1: data measured from rock samples collected by R. Wiseman
2: data presented in Wiseman (1991)
3: data from the Newfoundland Department of Mines and Energy physical property archives
4: data published in Miller et al. (1990)
5: data collected as part of the Lithoprobe East physical property study